Investigating the role of dual specificity phosphatases in neuroblastoma

Elliott Thompson

University College London

Great Ormond Street Institute of Child Health

A thesis submitted for the degree of Doctor of Philosophy

Declaration

I, Elliott Thompson, confirm that the work presented in this thesis is my own. Where information has been derived from other sources, I confirm that this has been indicated in the thesis.

[redacted]

London, March 2022

Abstract

Neuroblastoma (NB) is a cancer of the developing neural crest that accounts for 7-10% of paediatric malignancies worldwide. Phosphotyrosine signalling is an integral aspect to neural crest cell development and the progression of NB. Protein tyrosine phosphatases (PTPs) are important regulators of these pathways and therefore their dysregulation can perturb NB cell survival and neuronal differentiation. The dual specificity phosphatases (DUSPs) are a subgroup of PTPs increasingly linked to tumorigenesis. Hence, the aim of this project was to understand the molecular function of DUSPs in NB and whether they can promote NB cell growth. I hoped this would reveal phosphatase enzymes that could serve as novel molecular targets in NB.

An initial loss-of-function siRNA screen was performed to identify growth-promoting DUSPs in NB cells. Various candidate DUSPs were investigated further using CRISPR/Cas9 technology. Although in many cases CRISPR/Cas9-mediated genetic depletion did not reproduce siRNA knockdown findings, loss of DUSP6 or DUSP3 did suppress NB cell growth. However, the molecular function of DUSPs in NB cells remained elusive as individually, they did not appear to affect the MAP kinase or AKT pathways. In parallel, the therapeutic potential of a dual DUSP1/6 inhibitor, BCI, was investigated in NB. As in other cancer models, BCI demonstrated potent cytotoxicity in multiple NB cell lines. However, depletion of DUSP1 and DUSP6 did not influence BCI cytotoxicity, therefore we concluded BCI was hampered by multiple off-target effects. Lastly, I investigated whether DUSPs are important to oncogenic ALK signalling in ALK-mutated NB cells. Promisingly, removal of DUSP6 sensitised NB cells to ALK inhibition, however this effect was not rescued by re-introduction of exogenous DUSP6. A phosphoproteomic screen demonstrated ALK-mutated NB cells may have a biochemical co-dependency on ALK and DUSP6. Elucidating the DUSP6/ALK relationship further could identify novel pathways that could be therapeutically targeted alongside ALK.

Impact statement

Neuroblastoma (NB) is the most prevalent extra-cranial cancer in children, affecting approximately 100 children a year in the UK. Phosphotyrosine signalling is integral to NB cell growth, driven by the cooperative nature of protein tyrosine kinases and protein tyrosine phosphatases (PTPs). The dual specificity phosphatases (DUSPs) are a subgroup of PTPs that display oncogenic and tumour-suppressing roles in various cancer models. A subset of NB tumours are driven by hyperactive ERK signalling via the ALK oncogene, which is predominantly regulated by DUSPs. Hence, this research explored the role(s) of DUSPs in NB cells and whether they can be therapeutically targeted to prevent NB cell growth.

I employed three loss-of-function approaches to targeting DUSPs: siRNA gene knockdown, chemical inhibition using a dual DUSP1/6 inhibitor, and CRISPR/Cas9 gene-deletion. These studied revealed potent off-target toxicities inherent to many siRNAs. Similarly, BCI remained potent in NB cells depleted of DUSP1 and DUSP6 protein. These data highlighted the importance of generating cells depleted of the target to rule out false-positive results. Furthermore, as many studies use BCI as a specific DUSP1/6 inhibitor, these studies also revealed potential non-specific effects of BCI in cancer cells.

A wide range of DUSP genes were investigated using CRISPR/Cas9 technology to determine whether they influence NB cell growth. The *DUSP3* and *DUSP6* genes appeared to promote the survival or proliferation of NB cells. Considering the lack of targetable aberrations in NB, this is a beneficial finding and suggests these genes are worthy of further research in NB cells. Additional studies *in vivo* or in 3D models would reveal whether these DUSP genes could be of clinical importance.

There is a higher frequency of RAS/ERK pathway mutations in relapsed NB patients suggesting ERK signalling could promote NB relapse. Hence, it is imperative we understand the mechanisms at play regulating ERK signalling in NB cells. Surprisingly, none of the other DUSPs appeared to significantly

regulate ERK signalling. This is an important finding for the field as it suggests either a high degree of DUSP redundancy or alternative mechanisms are present to restrain ERK signalling in NB cells.

Chemical inhibition of the ALK oncogene has been extensively explored as a treatment option for ALK-driven NB. As resistance has emerged to conventional ALK inhibitors, I sought to determine whether manipulation of DUSP expression could improve ALK inhibitor efficacy. Promisingly, complete loss of DUSP6 appeared to sensitise NB cells to ALK inhibition. Although this effect was not rescued by DUSP6 re-expression, it would be beneficial to explore these findings further in other NB models. I also identified diverse biochemical changes caused by ALK inhibition specifically in DUSP6-depleted cells compared to wild type cells. Several of the affected pathways are known regulators of cancer cell behaviour. This is a novel finding that suggests that DUSP6 does significantly influence ALK signalling in these tumour cells. Further insight into how ALK and DUSP6 co-regulate these pathways may reveal proteins that could be targeted alongside ALK to improve the treatment options for patients suffering with NB.

Acknowledgements

There are so many people who I would like to thank for their help and support throughout my PhD. I would like to begin by thanking Andy Stoker for all his guidance and patience. Especially when there has been an insurmountable amount of work to do, your calm and understanding attitude has always made me feel free to have fun with experiments. I also don't know quite how you found the time to help me with all my problems and read through my multitude of drafts but your generosity has been incredible.

There are numerous people within the ICH that have supported me throughout the past four years and have made my time in the lab so much more enjoyable. Within Andy's group I would like to thank Elsa, Vruti, Tina and Enzo, we have had so many lab meetings together that I have taken so much away from. Especially, Tina and Vruti, you have both given me so much time to show me different techniques which have been extremely helpful at different parts of the PhD. There are also numerous people within the ICH that have taught me various useful techniques and given me much needed reagents; a special mention must go to Sandra who has always somehow been in the right place at the right time to help me when there is something I need!

I would also like to thank all of my friends and family, those nearby and those further afield, who have supported me throughout. Each group of friends have kept me sane (just) when I felt like work was too tough or all-consuming. I would also like to thank all of the church families I have been a part of during the PhD. Especially to Enfield Town Community Church, during COVID-19 you helped me feel close to Jesus regardless of the situation in the world around us. I would like to thank my family at home who had to deal with all of the ups and downs first hand everyday. Thank you mum and dad for all of your love, support and encouragement at each step of this journey. Thank you Jonny for always being there to help me relax when not at work and for continually distracting me with sport. And thank

you Arsenal, after the highs and lows we have been through I do wonder who has had a harder four years with the state of our team sometimes.

Lastly, I would like to thank my wife, Naomi. You have been an absolute rock throughout the last four years, continually supporting and encouraging me at each step of the PhD. As you plan to embark on a PHD in September I can only hope I am half as supportive to you as you have been for me.

Table of Contents

Abstract 3

Impact statement 4

Acknowledgements 6

List of figures 13

List of tables 18

Abbreviations 19

Chapter 1. General introduction 22

1.1. Neuroblastoma (NB) 23

1.1.1. Clinical presentation and patient prognosis 23

1.1.2. Cell of origin 25

1.1.3. Diagnosis, patient stratification and treatment 27

1.1.4. Molecular and genetic alterations 31

1.1.5. Molecular-targeted therapies 36

1.2. Phosphotyrosine signalling 38

1.2.1. Protein tyrosine phosphatases (PTPs) 38

1.2.2. Dual specificity phosphatases (DUSPs) 41

1.3. Protein tyrosine phosphatases (PTPs) in cancer 47

1.3.1. Phosphotyrosine signalling in cancer 47

1.3.2. Dual specificity phosphatases (DUSPs) in cancer 52

1.4. Phosphotyrosine signalling in NB 59

1.4.1. Phosphotyrosine signalling can drive NB cell growth 59

1.4.2. Protein tyrosine phosphatases in NB 60

1.5. Project overview 63

1.5.1. Project aims 65

Chapter 2. Materials and methods 66

2.1. Cell culture techniques 67

2.1.1. Mammalian cell lines 67
2.1.2. Cell passage 69
2.1.3. Chemical treatments 69
2.2. DNA-based assays 71
2.2.1. CRISPR-Cas9 gRNA design and generation 71
2.2.2. Genomic DNA extraction 75
2.2.3. Determination of indels within a population 75
2.3. RNA-based assays 78
2.3.1. RNA extraction 78
2.3.2. cDNA synthesis 79
2.3.3. Quantitative real-time PCR 79
2.4. Protein assays 81
2.4.1. Protein extraction 81
2.4.2. Bradford Assay 82
2.4.3. Western blotting 82
2.4.4. Phosphoproteomics 85
2.4.5. Immunofluorescence 86
2.5. Cell-based assays 88
2.5.1. Transient cell transfection with plasmid DNA 88
2.5.2. Transient cell transfection with siRNA 89
2.5.3. Generation of inducible CRISPR/Cas9 system 90
2.5.4. Generation of DUSP-null cells 90
2.5.5. DUSP6 overexpression 92
2.5.6. Resazurin assay 92
2.5.7. MCB assay 93
2.5.8. Colony forming assays 93
2.5.9. Microscopy 94

2.6. Bioinformatic analysis 94
2.6.1. Cox regression analysis 94
2.6.2. Phosphoproteomic data analysis..... 95
2.7. Statistical analysis 97
Chapter 3. Identifying growth-promoting DUSP genes in NB 98
3.1. Introduction 99
3.2. Results 104
3.2.1. Identification of growth-promoting DUSPs..... 104
3.2.2. Survival analysis with DUSP gene expression 108
3.2.3. Knockdown of DUSP6 suppresses KELLY cell viability 116
3.2.4. DUSP6 siRNAs display potent off-target effects in KELLY cells 120
3.2.5. Generation of DUSP6-null KELLY and IMR-32 cells 122
3.2.6. Genetic deletion of DUSP6 reduces KELLY cell growth..... 133
3.3. Discussion 137
Chapter 4. Investigating the therapeutic potential of BCI and BCI-215.. 146
4.1. Introduction 147
4.2. Results 150
4.2.1. BCI and BCI-215 are cytotoxic in NB cell lines..... 150
4.2.2. MAPK or AKT inhibition does not antagonise BCI cytotoxicity 155
4.2.3. BCI and BCI-215 do not induce ROS but trigger cleavage of PARP and caspase 3 160
4.2.4. BCI perturbs the JNK and mTOR signalling pathways 164
4.2.5. Complete loss of DUSP6 and partial loss of DUSP1 do not affect BCI cytotoxicity..... 169
4.3. Discussion 171
Chapter 5. Broadening the search for growth-promoting DUSPs in NB 178

5.1. Introduction 179
DUSP4 179
DUSP10 180
DUSP3 182
DUSP26 183
DUSP12 184
5.2. Results 185
5.2.1. Deconvolution of candidate DUSP siRNA pools 185
5.2.2. Generation and characterisation of DUSP-null NB cells 188
5.2.3. DUSP5 promotes IMR-32 cell growth in a DUSP6-dependent mechanism 197
5.2.4. Acute loss of a single MAP kinase phosphatase is not sufficient to alter MAPK or AKT signalling 201
5.3. Discussion 204
Chapter 6. Characterising the role of DUSP6 in ALK-mutated NB 213
6.1. Introduction 214
6.2. Results 221
6.2.1. DUSP6 is regulated by ALK independently of ERK 221
6.2.2. Complete loss of DUSP6 sensitises KELLY cells to ALK inhibition 232
6.2.3. Re-introduction of DUSP6 does not rescue cell viability in response to ALK inhibition 243
6.2.4. Phosphoproteomic screen identifies potential roles of DUSP6 in ALK-mutated NB 247
6.3. Discussion 263
Chapter 7. Concluding remarks 273
7.1. Summary of key findings 274
7.2. Final discussion points 277

7.2.1. Comparing loss of function approaches 277
7.2.2. The collective role of DUSPs in NB cells 279
7.2.3. The function of DUSP6 in ALK-driven NB 282
Appendices 287
Appendix 1 – Individual siRNA oligonucleotide sequences 287
Appendix 2 – Phosphoproteomic analysis output 290
Appendix 3 – DUSP27 expression across NB cell lines 292
Appendix 4 – Cell populations that derive from NB cell lines 293
Appendix 5 – Synergy maps for Bliss and Loewe models 295
Appendix 6 – Indels present in candidate DUSP-null subclones 297
Appendix 7 – Inverse correlations of pERK levels and DUSP6 expression in SK-N-AS cells 298
Appendix 8 – PI3K/AKT canonical pathway from IPA analysis 299
References 300

List of figures

Figure 1.1 – Clinical presentation of NB and sites of tumour dissemination. 24
Figure 1.2 – Overall survival of high-risk patients NB patients diagnosed between 1990 - 2010 25
Figure 1.3 – INRG classification criteria 29
Figure 1.4 – Primary treatment options for NB 30
Figure 1.5 – MYCN regulates multiple downstream targets which influence NB malignancy 33
Figure 1.6 – Catalytic mechanism of action of a PTP on a phospho-tyrosine substrate 40
Figure 1.7 – The PTP family 41
Figure 1.8 – Tumour-suppressive actions of PTEN 50
Figure 1.9 – Negative feedback of Ras/ERK signalling cascade by MKPs 53
Figure 1.10 – Roles of DUSP3 in cancer 57
Figure 1.11 – Therapeutic potential of inhibiting PTPs in NB 61
Figure 2.1 – Plasmids used to introduce gRNA's 74
Figure 2.2 – Methods used to determine CRISPR/Cas9 efficiency 78
Figure 2.3 – Counting cells with high cCas3 using ImageJ 88
Figure 2.4 – ImageJ analysis of crystal violet staining 94
Figure 3.1 – Change in DUSP mRNA expression in response to RA treatment in NB cells 100
Figure 3.2 – Identifying growth-promoting or -suppressing DUSPs in NB cells 106
Figure 3.3 – Efficiency of DUSP siRNA pools 108
Figure 3.4 – Overall survival of NB patients dichotomised by *DUSP4*, *DUSP6* and *DUSP26* gene expression 116
Figure 3.5 – Knockdown of *DUSP6* suppresses KELLY cell viability 117
Figure 3.6 – MAPK signalling appears unaffected in KELLY cells after knockdown of *DUSP6* and minor suppression of *DUSP1* 119
Figure 3.7 – Deconvolution of DUSP6 siRNAs 121

Figure 3.8 – Loss of DUSP6 using gRNA 3 124
Figure 3.9 – Partial loss of *DUSP6* does not affect cell growth or response to DUSP6 siRNA 126
Figure 3.10 – Designing gRNA 1 and gRNA 4..... 128
Figure 3.11 – Depletion of DUSP6 using gRNA 1 130
Figure 3.12 – Generating DUSP6-null subclones using gRNA 4 132
Figure 3.13 – Sequences of KELLY and IMR-32 DUSP6-null subclones 133
Figure 3.14 – Loss of DUSP6 reduces KELLY cell growth 134
Figure 3.15 – Loss of DUSP6 has no apparent effect on the MAPK or AKT signalling pathways 136
Figure 3.16 – Generating DUSP6 loss-of-function phenotypes 141
Figure 3.17 – Loss of ERK negative feedback regulation triggers apoptotic signalling 143
Figure 4.1 – Chemical inhibitors of DUSP6 148
Figure 4.2 – Effect of dual DUSP1/6 inhibition by BCI and BCI-215..... 149
Figure 4.3 – Cytotoxicity of BCI and BCI-215 in NB cell lines..... 152
Figure 4.4 – Effect of BCI and BCI-215 on MAPK and AKT signalling pathways 154
Figure 4.5 – Identifying synergy and antagonism between BCI and MAPK or AKT inhibitors in KELLY cells..... 157
Figure 4.6 – Intracellular effect of combining MAPK and AKT inhibitors with BCI in KELLY cells 159
Figure 4.7 – BCI and BCI-215 do not activate ROS in KELLY cells 162
Figure 4.8 – BCI-215 increases cleavage of PARP in KELLY cells..... 162
Figure 4.9 – BCI and BCI-215 increase cleavage of Cas3 163
Figure 4.10 – Phosphoproteomic analysis of BCI treatment in KELLY and IMR-32 cells 165
Figure 4.11 – Biological pathway enrichment of the phosphoproteomic dataset 167
Figure 4.12 – KSEA reveals JNK and mTOR pathway enrichment 168
Figure 4.13 – Cytotoxicity of BCI and BCI-215 after DUSP1 and DUSP6 depletion..... 170

Figure 4.14 – Speculated mechanism of BCI-induced cell death in NB cells 175
Figure 5.1 – DUSP10 is transcriptionally regulated by a wide range of stimuli..... 181
Figure 5.2 – *DUSP3* gene expression is associated to overall survival of NB patients 183
Figure 5.3 – Deconvolution of siRNA pools for candidate DUSPs 187
Figure 5.4 – Design of candidate DUSP gRNA sequences..... 189
Figure 5.5 – Characterisation of indels in mixed populations 191
Figure 5.6 – DUSP candidates do not promote KELLY cell growth..... 194
Figure 5.7 – Loss of DUSP3 suppresses KELLY clonogenicity..... 195
Figure 5.8 – DUSP siRNA pools cause significant off-target toxicities .. 197
Figure 5.9 – Investigating compensatory mechanisms between DUSP proteins 199
Figure 5.10 – DUSP5 promotes IMR-32 cell growth via DUSP6 201
Figure 5.11 – Individual MKPs do not have tight control of MAPK or AKT signalling 203
Figure 5.12 – Correlation of *DUSP1*, *DUSP5* and *DUSP6* gene expression in NB patients..... 210
Figure 6.1 – Summary of the ALK aberrations in ALK-positive cancer.. 215
Figure 6.2 – ALK signalling pathways in NB 218
Figure 6.3 – Transcriptional regulation of the DUSP family by ALK 220
Figure 6.4 – ALK suppresses DUSP6 gene expression in ALK-mutated NB cells..... 224
Figure 6.5 – Stimulating the ALK receptor in NB cell lines 225
Figure 6.6 – ALK regulates DUSP6 independently of ERK in KELLY and LAN-5 cells..... 227
Figure 6.7 – Working model of DUSP6 transcriptional regulation by ALK in NB cell lines 228
Figure 6.8 – ALK can regulate DUSP6 in a transcriptional and post-translational manner 231
Figure 6.9 – Loss of DUSP6 sensitised KELLY cells to ALK inhibition.. 234

Figure 6.10 – Acute depletion of DUSP6 does not affect sensitivity to ALK inhibition 235
Figure 6.11 – ALK does not regulate DUSP6 via the MAPKs or AKT pathways 238
Figure 6.12 – Loss of other DUSP genes does not sensitise KELLY cells to ALK inhibition 240
Figure 6.13 – ALK inhibition has a cytostatic effect on KELLY and LAN-5 cells 243
Figure 6.14 – Generation of KELLY cells expressing exogenous DUSP6 protein 245
Figure 6.15 – Validation of DUSP6 overexpression 246
Figure 6.16 – Overexpression of DUSP6 does not rescue the incapacity to proliferate driven by the ALK inhibitor 247
Figure 6.17 – Overview of phosphoproteomic screen 249
Figure 6.18 – Significant phosphopeptides after lorlatinib treatment and DUSP6 depletion 252
Figure 6.19 – There is a minor overlap in significant phosphopeptides between treatment comparisons 253
Figure 6.20 – KSEA heatmap of significantly enriched kinases 256
Figure 6.21 – Log2-Fold Changes for kinase-related phosphosites 257
Figure 6.22 – IPA analysis reveals differentially regulated canonical pathways 261
Figure 6.23 – ERK and RhoA signalling pathways are downregulated in DUSP6 KO cells 262
Figure 6.24 – HIPPO signalling is downregulated by lorlatinib in DUSP6-null cells 263
Figure 6.25 – Working model for how ALK regulates DUSP6 expression in KELLY and LAN-5 cells 266
Figure 6.26 – Model speculating how DUSP6 could regulate RhoA signalling pathway 269
Figure 6.27 – Model speculating how loss of DUSP6 could promote ALK-HIPPO signalling 271

Figure 7.1 – Perturbation effect of *DUSP6* gene in a CRISPR/Cas9 or RNAi screen in NB cell lines..... 278
Figure 7.2 – Redundancy and cooperation of ALK and DUSP6 signalling promotes NB cell survival 285
Figure A1 – MRNA expression of *DUSP27* across NB cell lines..... 292
Figure A2 – A 2D synergy map using the Loewe and Bliss reference models 296
Figure A3 – Sequence alignment of the gRNA region of KELLY cells and the DUSP-null subclones 297
Figure A4 – Quantification of pERK levels and DUSP6 expression in SK-N-AS cells after CHX and MG132 treatment 298
Figure A5 – PI3K/AKT signalling is downregulated by lorlatinib in DUSP6-null cells 299

List of tables

Table 1.1 – MKPs and atypical DUSPs sub-families..... 44
Table 2.1 – Cell lines used in project 68
Table 2.2 – Genetic lesions in NB cell lines 68
Table 2.3 – Chemicals used in cell-based assays and for antibiotic selection 70
Table 2.4 – GRNA sequences used to target DUSP genes 72
Table 2.5 – Primers used to introduce gRNA sequence into the PU6 plasmid 74
Table 2.6 – Primers designed to amplify a gRNA target region 76
Table 2.7 – Primers deigned for qPCR of the DUSP family 80
Table 2.8 – Antibodies used for western blotting 84
Table 3.1 – Univariate cox regression of DUSP family genes and clinical variables in SEQC database 109
Table 3.2 – Univariate cox regression of DUSP family genes and clinical variables in NRC database..... 111
Table 3.3 – Multivariate cox regression of DUSP family genes and clinical variables in SEQC database 113
Table 3.4 – Multivariate cox regression of DUSP family genes and clinical variables in NRC database..... 115
Table 3.5 – DUSP6-null subclones generated from the 2E11g3 mixed population..... 125
Table 5.1 – Single cell clones generated from the DUSP mixed population 192
Table 5.2 – Common siRNA off-target effects and the strategies employed to minimise them 206
Table 6.1 – Comparisons used for data analysis 251
Table A1 – Each individual siRNA sequence, its target name and source 287
Table A2 – Peptide intensities for the ERK1 Tyr204 phosphopeptide ... 290
Table A3 – Log2-Fold Change and p-value for peptide p03928 291

Abbreviations

aDUSP	Atypical dual-specificity phosphatase
ALCL	Anaplastic large cell lymphoma
ALK	Anaplastic lymphoma kinase
ALKAL1	ALK activating ligand 1
ALL	Acute lymphoblastic leukaemia
ANOVA	Analysis of variance
BMOV	Bismaltolato oxovanadium
BSA	Bovine serum albumin
BSO	Buthionine sulfoximine
cCas3	Cleaved caspase 3
CHX	Cyclohexamide
CI	Confidence interval
cPARP	Cleaved PARP-1
CRC	Colorectal cancer
CRISPR	Clustered regularly interspaced short palindromic repeats
CRIZ	Crizotinib
CSC	Cancer stem cell
C_t	Threshold cycle
CTD	C-terminal domain
DLBCL	Diffuse large B cell lymphoma
DMSO	Dimethyl sulfoxide
Dox	Doxycycline
DPBS	Dulbecco's phosphate-buffered saline
DUSP	Dual-specificity phosphatase
EC50	Half maximal effective concentration
EGF	Epidermal growth factor
EMT	Epithelial to mesenchymal transition
ER	Endoplasmic reticulum
ERK	Extracellular signal-regulated kinase
FAK	Focal adhesion kinase
FGF	Fibroblast growth factor
GBC	Gallbladder cancer
GFP	Green fluorescent protein
GN	Ganglioneuroma
GNB	Ganglioneuroblastoma
gRNA	Guide RNA
GSH	Reduced glutathione
HEPES	N-2-Hydroxyethylpiperazine-N'-2-Ethanesulfonic Acid
HR	Hazard ratio
HVA	Homovanillic acid
IDRF	Image-defined risk factors
Indel	Insertions and deletions
INPC	International Neuroblastoma Pathology Committee
INRG	International Neuroblastoma Risk Group
INSS	International Neuroblastoma Staging System
IPA	Ingenuity pathway analysis

JNK	c-Jun N-terminal Kinase
KIM	Kinase-interacting motif
KO	Knockout
KSEA	Kinase substrate enrichment analysis
LB	Luria Broth Base
LOF	Loss of function
LOR	Lorlatinib
MAPK	MAP kinase
MCB	Monochlorobimane
MKP	MAP kinase phosphatase
MIBG	Metaiodobenzylguanidine
MNA	MYCN amplification
MQ	Milli-Q water
MS	Mass spectrometry
NC	Neural crest
NES	Nuclear export signal
NLS	Nuclear localisation signal
NSCLC	Non-small-cell lung carcinoma
NTD	N-terminal domain
PNS	Peripheral nervous system
RA	Retinoic acid
RNAi	RNA interference
ROS	Reactive oxygen species
SCP	Schwann cell precursor
SCR	non-targeting siRNA
SD	Standard deviation
SDS	Sodium dodecyl sulfate
SEM	Standard error of mean
SHP2	Src homology-2 domain-containing protein tyrosine phosphatase-2
shRNA	short hairpin RNA
siRNA	Small interfering RNA
SNP	Single nucleotide polymorphism
SPECT	Single-photon emission computed tomography
PAM	Protospacer adjacent motif
PBS	Phosphate buffered saline
PC	Prostate cancer
PCR	Polymerase chain reaction
PDBu	Phorbol 12,13-dibutyrate
PFA	Para-formaldehyde
PIP3	Phosphatidylinositol 3,4,5-trisphosphate
PTEN	Phosphatase and tensin homolog
PTP	Protein tyrosine phosphatase
PTP1b	Protein tyrosine phosphatase 1B
PVDF	Polyvinylidene fluoride
qPCR	Quantitative real-time polymerase chain reaction
RPMI	Roswell Park Memorial Institute
RTK	Receptor tyrosine kinase
TBS	Tris-buffered saline
TBST	TBS tween

TKI	Tyrosine kinase inhibitors
Tm	Melting temperature
T7E1	T7 endonuclease 1
Unt	Untreated
VMA	Vanillylmandelic acid
WT	Wild type

Chapter 1. General introduction

1.1. Neuroblastoma (NB)

1.1.1. Clinical presentation and patient prognosis

Neuroblastoma (NB) is the most common extracranial cancer diagnosed in childhood and accounts for 7-10% of paediatric malignancies worldwide (Brodeur, 2003). Each year, there are approximately 100 new cases of NB in the UK with a 5-year survival rate of 67% (Children with Cancer UK). The median age for onset of NB is 18 months but only 2% of patients are diagnosed in adulthood (Brodeur, 2003).

NB tumours arise from progenitor cells of the sympathoadrenal lineage in the neural crest and can therefore manifest anywhere in the sympathetic nervous system (Kholodenko et al., 2018) (**Fig. 1.1, left panel**). NB symptomology depends on where the primary tumour forms (Vo et al., 2014). In a retrospective analysis of 8369 cases, 71% of tumours were located in the abdomen; 47% in the adrenal region and 24% in other abdominal/retroperitoneal regions, and they displayed the poorest survival probability (Vo et al., 2014). As cells of the sympathetic ganglia travel to other paraspinal areas, NB primary tumours were also located in the thorax (15%), neck (3%), pelvis (3%) and other sites (8%) (Vo et al., 2014). Tumours of the neck can disrupt the oculosympathetic tract. In such patients, NB manifests concurrently to Horner's syndrome which classically presents as miosis, ptosis and anhidrosis (Smith et al., 2010). In a minority of cases, large tumour masses of sympathetic ganglia put pressure on the spinal cord causing neurologic symptoms such as motor deficits, sphincteric deficits or sensory loss (De Bernardi et al., 2001).

NB displays a large degree of tumour heterogeneity with diverse clinical outcomes. In some cases, tumours spontaneously regress without the need for treatment, but in others there is persistent tumour progression and widespread metastasis (Maris et al., 2007, DuBois et al., 1999). Over 50% of infants that present with NB already display metastatic disease which presents a major treatment challenge (DuBois et al., 1999). Dissemination

to different sites varies depending on stage group and age at diagnosis. The most common metastasis occur in the bone marrow, bone, lymph node and liver, with rare cases in the skin, central nervous system and lung (**Fig. 1.1, right panel**). Unfortunately, the additional tumour burden of metastasis often leads to further complications. Tumours presenting in the bone can cause severe bone pain, leaving patients with a limp (Parmar et al., 2013, Chu et al., 2011). Bone marrow involvement can cause anaemia and thrombocytopenia and dissemination to the liver frequently leads to coagulopathy (Tolbert and Matthay, 2018). On the other hand, spontaneous regression is most prevalent in younger children with alterations in tumour cell ploidy (Brodeur and Bagatell, 2014). It is unclear what drives tumour regression, although various mechanisms have been proposed including TrkA-mediated apoptosis, loss of telomerase activity and a NB cell-specific immunological response (Brodeur and Bagatell, 2014).

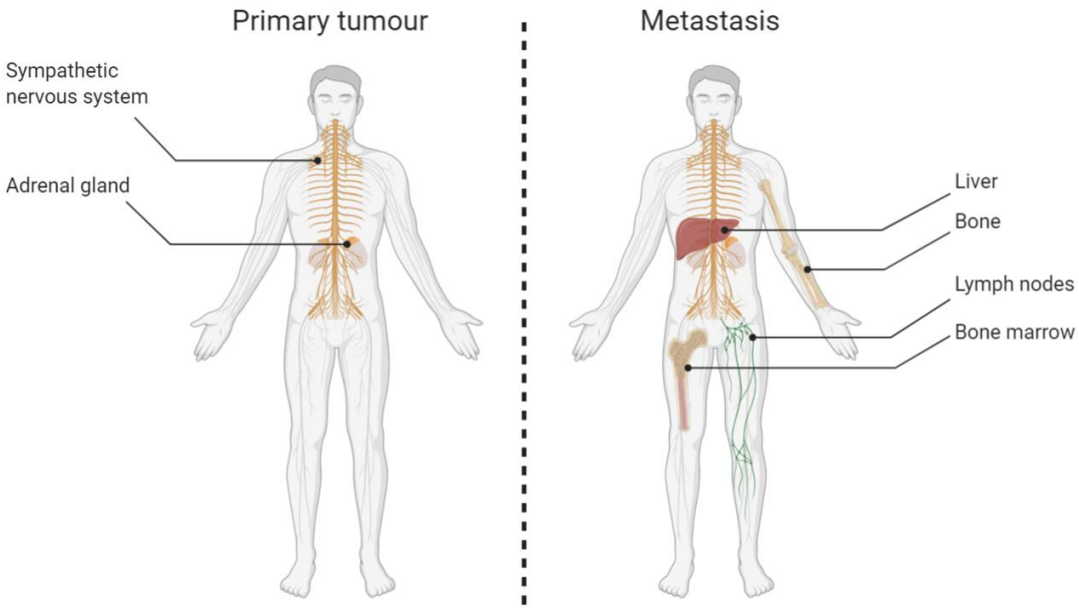

Figure 1.1 – Clinical presentation of NB and sites of tumour dissemination. Primary tumours are located predominantly in adrenal medulla and along sympathetic nerve ganglia of the peripheral nervous system. Most common metastasis are located in the liver, bone, bone marrow and lymph nodes (DuBois et al., 1999).

There is a strong association between disease prognosis and age of onset (Matthay et al., 2016). To date, a cut-off separating old and young patients has not been defined, however NB that manifests in adulthood displays a

unique tumour biology (Castel et al., 2010, Mossé et al., 2014). Somewhat contradictively, such patients show an indolent phenotype but also high-risk prognostic features and a worse overall survival. Patients are stratified into low-, intermediate- and high-risk groups. For the younger patients, the 5-year event-free survival is promising in the low-and intermediate-risk groups at >90% (Park et al., 2013, Cohn et al., 2009). However, for 'high-risk' patients, despite an increase in therapeutic options, survival rates have not surpassed 50% (Pinto et al., 2015) (**Fig. 1.2**). Due to this poor response to therapy and unrelenting aggressiveness of high-risk NB, significant effort has been exerted to improve our understanding of disease aetiology and progression.

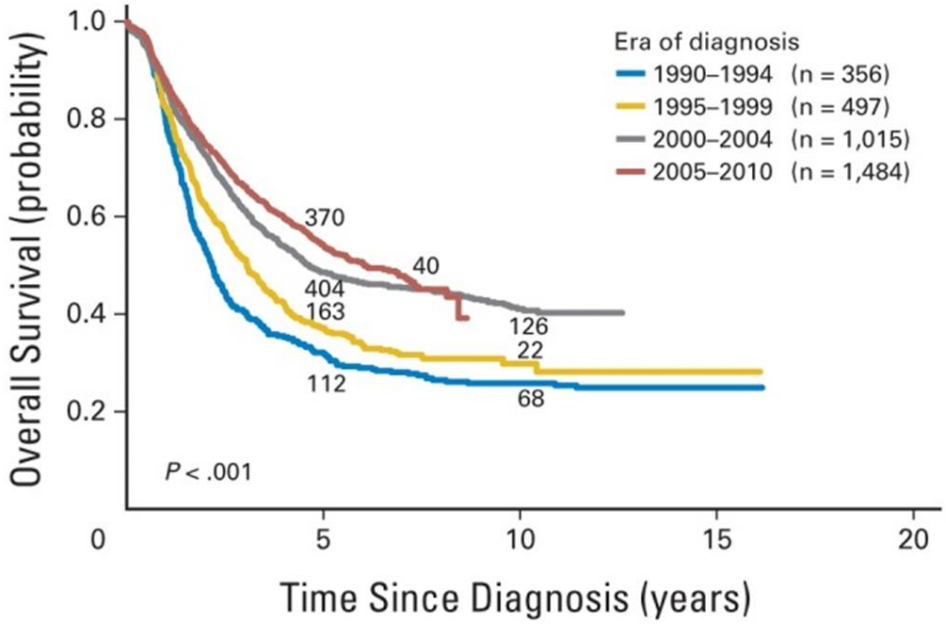

Figure 1.2 – Overall survival of high-risk patients NB patients diagnosed between 1990 - 2010. Patients diagnosed with NB in the COG ANBL00B1 study split into 5-year time periods. Overall survival has improved for high-risk patients diagnosed after the year 2000. Taken from Pinto et al. (2015).

1.1.2. Cell of origin

The neural crest (NC) is a multipotent stem cell population induced during neurulation at the neural plate border (Mayor and Theveneau, 2013). NC cells undergo epithelial to mesenchymal transition (EMT) to allow widespread migration throughout the developing embryo. Depending on

where they migrate to, NC cells can give rise to a huge variety of derivative cell types broadly split into five functional types: vagal, sacral, cranial, cardiac and trunk cells (Kholodenko et al., 2018). Trunk NC cells migrate to the dorsal aorta where they differentiate down the sympathoadrenal lineage to form part of the peripheral nervous system (PNS) (Vega-Lopez et al., 2017). It is here, in the adrenal chromaffin cells and sympathetic ganglia of the PNS, where NB tumorigenesis occurs (**Fig. 1.1**) (Matthay et al., 2016). As NC cells can differentiate into a wide range of tissues, tumorigenesis of NC progenitor cells has caused various cancers, including NB, melanomas, paragangliomas and schwannomas (Zage et al., 2017). Interestingly, adult cells that derived from the NC retain the stem cell properties attributed to embryonic stem cells and NC progenitor cells (Kholodenko et al., 2018). Although it is challenging to identify tumour-initialling cells due to the heterogeneity of the NB microenvironment, cancerous stem cell populations have been identified in NB tumours and bone marrow metastases (Hansford et al., 2007). Such cells are distinguished from other cells by their cell surface markers and intracellular proteins that are associated to normal stem cells (Garner and Beierle, 2016).

Until recently, it was believed NB tumours derive solely from cells of the direct sympathoadrenal lineage (Matthay et al., 2016). This is supported by the fact that i) NB cell lines function in accord to NC progenitor cells and ii) the transcriptome profile in NB is akin to that in NC progenitor cells (Kholodenko et al., 2018). However, a recent study demonstrates that adrenal chromaffin cells originate not from NC cell progenitors with sympathoadrenal cell fate but from a population of peripheral glial stem cells, termed Schwann cell precursors (SCPs) (Furlan et al., 2017). SCPs travel to the adrenal gland via the preganglionic motor and are essential for assembly of the adrenal medulla (Adameyko and Ernfors, 2014). Using lineage tracing experiments, Furlan et al. (2017) demonstrated that after NC migration, there is an early lineage split into SCPs and sympathetic neurons. A ‘bridge’ transition state including multiple intermediate cell types were identified where SCPs markers were downregulated, and adrenal chromaffin cell markers upregulated. Crucially, this ‘bridge’ stage was not

identified between the sympathetic neurons and adrenal chromaffin cells or SCPs. Further studies are required to reveal whether this transition is important in NB aetiology and whether it is a route for therapeutic intervention.

1.1.3. Diagnosis, patient stratification and treatment

Diagnostic evaluation of NB involves a broad spectrum of assays including biochemical and radiological tests, tumour biopsies and molecular characterisation. The gold-standard method for biochemical diagnosis is abnormally high levels of catecholamine metabolites, secreted by chromaffin cells in the adrenal medulla, in patient urine. As catecholamines are broken down into homovanillic acid (HVA) and vanillylmandelic acid (VMA), urinary levels of HVA and VMA are increased in over 90% of NB patients (Matthay et al., 2016). Alongside this, blood tests are performed to evaluate liver function as well as determine the concentrations of serum ferritin and lactate dehydrogenase, both of which are elevated in patients with poor prognosis (Hann et al., 1985, Shuster et al., 1992). As 50% of NB cases have bone marrow involvement, it is also routine to perform a bilateral bone marrow biopsy and aspirate smear (Rastogi et al., 2015). If patients undergo myeloablative therapy, peripheral blood samples and bone marrow biopsies are taken during and after treatment to monitor the presence of residual disease (Beiske et al., 2009). Fluorescence-based immunocytology and quantitative RT-PCR are used to accurately determine the quantity of tumour cells in both the bone marrow and peripheral blood cells.

Tumour biopsy ultimately determines whether the tumour mass should be classified as a NB, ganglioneuroma (GN) or ganglioneuroblastoma (nodular or intermixed) (GNB) (Tolbert and Matthay, 2018). NB, GN and GNB are distinguished by their amount of Schwannian stroma cells and degree of cellular maturation. The International Neuroblastoma Pathology Committee (INPC) created a classification of such tumours whereby: NB is Schwannian stroma-poor; GN is Schwannian stroma-dominant; GNB intermixed is Schwannian stroma-rich; and GNB nodular is a mix of Schwannian stroma-

rich and -poor (Shimada et al., 2001). Generally speaking, maturation increases from NB < GNB < GN and a mature phenotype correlates with patient age and prognosis.

Radiology is essential for diagnostic evaluation of the tumour. Due to its ease of use, ultrasound is often the first line investigative tool used for paediatric cancers (Dumba et al., 2015). However, either cross-section CT or MRI imaging is required to evaluate the primary tumour mass in more detail and the degree of dissemination. Furthermore, nuclear medicine imaging is often used to diagnose occult disease and assess patient response to therapy (Bar-Sever et al., 2018). Various radioactive tracers have been evaluated for NB diagnosis and currently, the preferred technique is Metaiodobenzylguanidine (mIBG) scintigraphy (Gauguet et al., 2017, Bleeker et al., 2015). As mIBG is analogous to norepinephrine, it is readily taken up by neuroendocrine tumours and is therefore highly specific for NB. In patients treated with mIBG, single-photon emission computed tomography (SPECT) has been used to estimate the levels of mIBG uptake (Bar-Sever et al., 2018, Tolbert and Matthay, 2018). This combination has allowed the accurate tracking of NB dissemination in 3D.

During diagnosis, patients are stratified into risk groups by evaluating a range of pathological and biochemical features (Cohn et al., 2009). To generate a global consensus on NB patient stratification, an international criteria was established in 1988, termed the International Neuroblastoma Staging System (INSS) (Brodeur et al., 1993). This system is based on tumour localisation, surgical operability and dissemination to other sites, in particular the lymph nodes and bone marrow. Although widely accepted and still used in the literature, the INSS requires surgical resection and sampling of the lymph nodes and does not consider the molecular characteristics of NB that have since been discovered (Monclair et al., 2009). Consequently, a new staging system termed the International Neuroblastoma Risk Group (INRG) was created, based solely on pre-treatment molecular characteristics of the tumour (Cohn et al., 2009) (**Fig. 1.3**). The imaging studies previously described are used to define the patients' image-defined risk factors (IDRFs) which determines the INRG stage (Monclair et al.,

2009). Histologic analysis of tumour tissue determines the aforementioned INPC classification (NB, GNB nodular, GNB intermixed or GN) and the degree of tumour differentiation (Shimada et al., 2001). Also considered are genetic features of the tumour including MYCN amplification (MNA), 11q aberration and tumour ploidy (discussed below). Once each characteristic has been evaluated, patients are stratified into one of sixteen pre-treatment groups (A-R) which is split into low-, intermediate- and high-risk NB (**Fig. 1.3**).

INRG Stage	Age (months)	Histologic Category	Grade of Tumor Differentiation	*MYCN*	11q Aberration	Ploidy	Pretreatment Risk Group
L1/L2		GN maturing; GNB intermixed					A Very low
L1		Any, except GN maturing or GNB intermixed		NA			B Very low
				Amp			K High
L2	< 18	Any, except GN maturing or GNB intermixed		NA	No		D Low
					Yes		G Intermediate
	≥ 18	GNB nodular; neuroblastoma	Differentiating	NA	No		E Low
					Yes		H Intermediate
			Poorly differentiated or undifferentiated	NA			
				Amp			N High
M	< 18			NA		Hyperdiploid	F Low
	< 12			NA		Diploid	I Intermediate
	12 to < 18			NA		Diploid	J Intermediate
	< 18			Amp			O High
	≥ 18						P High
MS	< 18			NA	No		C Very low
					Yes		Q High
				Amp			R High

Figure 1.3 – INRG classification criteria. Patients are stratified based on the criteria presented into low, intermediate, and high pretreatment risk groups which is further subdivide into sixteen lettered designations. Taken from Cohn et al. (2009).

The INRG risk classification has been extremely valuable for evaluating patient prognosis and determining which treatment regime is best suited. Generally, the treatment approach to NB is split into three phases: induction, consolidation and maintenance (**Fig. 1.4**) (Tolbert and Matthay, 2018). For low-risk patients, treatment decisions aim to reduce invasiveness but maintain high patient survival. Therefore, in cases where patients are under 1 year old with an adrenal mass less than 5cm in diameter, expectant observation alone is used (Tolbert and Matthay, 2018). Although surprising, the 3-year overall survival of low-risk patients treated by observation alone compared to surgical resection are very comparable (Nuchtern et al., 2012).

In cases where unfavourable IDRFs have been identified or patients are above 1 years old, surgical resection is recommended. This may also be combined with limited chemotherapy if clinical symptoms are also present (Matthay et al., 2016). For patients with intermediate classification, a combination of chemotherapy and surgery are used (Baker et al., 2010, Kohler et al., 2013). Patients will undergo surgery if the primary tumour can be resected without complications. Furthermore, patients undergo 4 - 8 cycles of chemotherapy dependent on the ploidy and differentiation status of the tumour (Baker et al., 2010, Kohler et al., 2013). Unfortunately, a minority of older patients considered intermediate-risk present with unresectable tumours which require more intensive therapies (Pinto et al., 2015).

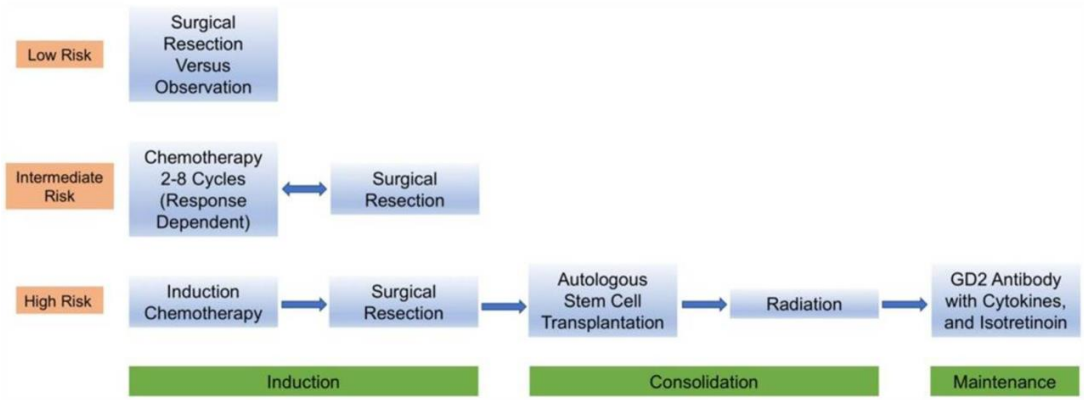

Figure 1.4 – Primary treatment options for NB. Low-risk and intermediate-risk patients are treated in the induction phase predominantly with surgical resection. In contrast, high-risk patients undergo an extensive treatment regime of multimodal therapy across all three phases: induction, consolidation and maintenance. Taken from Tolbert and Matthay (2018).

In the case of high-risk NB, accounting for ~50% of cases, an extended period of multi-modal therapy is required, typically lasting 18 months (Tolbert and Matthay, 2018). Initially, to decrease tumour burden the patient undergoes multiple cycles of combination chemotherapy, during which, primary tumour resection is performed. Following this, the consolidation phase comprises myeloablative chemotherapy and autologous stem cell transplantation alongside radiotherapy directed at the primary tumour site. Stem cells are harvested during or immediately after induction

chemotherapy as tumour cell contamination does not affect treatment responses (Tolbert and Matthay, 2018). Following this, targeted differentiation therapy and immunotherapy are used. It is well known that isotretinoin (13-*cis*-retinoic acid) reduces tumour cell growth by inducing cell differentiation which, when delivered in the maintenance phase, increases patient event-free survival (Matthay et al., 1999). Isotretinoin is concurrently administered with the anti-GD2 monoclonal antibody (mAb) that binds specifically to GD2, a disialoganglioside ubiquitously expressed on the surface of neuroblastic cells (Wu et al., 1986). The anti-GD2 mAb is combined with granulocyte–macrophage colony-stimulating factor and Interlukin-2 to form an immunotherapy regimen that significantly improves patient survival (Cheung et al., 2012a, Yu et al., 2010). Over the past 20 years, overall patient survival has improved for high-risk patients owed to the increased intensity of treatments and introduction of the immunotherapies, although **Figure 1.2** demonstrates far more work is needed (Pinto et al., 2015). There are also a range of molecular targeted therapies in clinical trials which target, among others, the ALK receptor and MYCN (Discussed below).

1.1.4. Molecular and genetic alterations

MYCN amplification (MNA)

The human MYC family consists of three transcription factors; MYC, MYCL and MYCN which are all proto-oncogenes involved in human malignancy (Mathsyaraja and Eisenman, 2016, Brodeur et al., 1984, Gabay et al., 2014, Nau et al., 1985). MNA is the best-characterised genetic biomarker for NB, affecting approximately 20% of NB patients (Brodeur et al., 1984, Seeger et al., 1985). As MNA is highly associated to poor prognosis and metastasis, it is included in the INRG classification schema (**Fig. 1.3**). MYCN is activated by hetero-dimerisation with the MYC-associated protein MAX which permits binding to the E-box element of DNA (Gherardi et al., 2013). The role of MYCN as a transcriptional activator has been well described as MYCN recruits a range of acetyltransferase complexes (Ruiz-Pérez et al., 2017).

MYCN can also function as a transcriptional repressor but the mechanisms behind this remain far more elusive (Gherardi et al., 2013).

A comprehensive review by Huang and Weiss (2013) describe the myriad of roles displayed by MYCN to maintain a malignant state in NB (**Fig. 1.5**). Firstly, MYCN can enhance cell migration and invasion whilst decreasing cell adhesion. *MYCN* expression is inversely correlated to *Integrin α1* and *Integrin β1*, two cell surface receptors that bind the extracellular matrix (Tanaka and Fukuzawa, 2008, van Golen et al., 2003). In NB cell lines, knockdown of MYCN led to an increase in *Integrin α1* expression and enhanced cell adhesion, whereas exogenous expression of MYCN had the opposite effect. MNA tumours also display high levels of Focal adhesion kinase (FAK), a cytoplasmic kinase that promotes cell motility via integrin-mediated intracellular signalling (Beierle et al., 2008). In one *in vitro* study, both siRNA and chemical inhibition of FAK decrease cell migration, invasion and survival. Importantly, this effect was more exaggerated in MNA NB cells compared to non-MNA cells (Megison et al., 2013). Secondly, MNA tumours have increased propensity to vascularise as MYCN promotes the secretion of pro-angiogenic factors whilst also inhibiting anti-angiogenic factors (Huang and Weiss, 2013, Ribatti et al., 2002). As MCYN-driven angiogenesis was driven through PI3K signalling, chemical inhibition of PI3K destabilised MYCN in TH-MYCN transgenic mice and prevented MYCN-mediated secretion of VEGF *in vitro* (Chanthery et al., 2012).

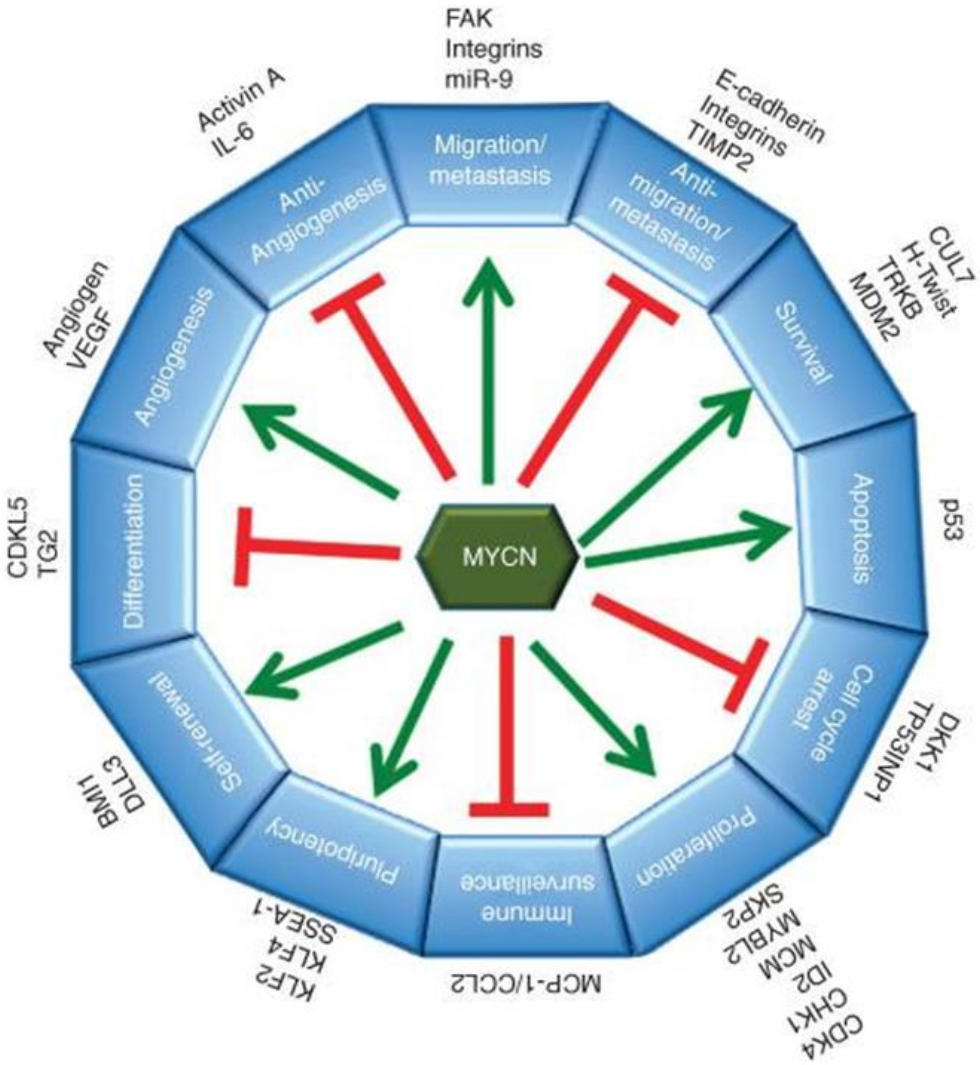

Figure 1.5 – MYCN regulates multiple downstream targets which influence NB malignancy. The outer circle displays the direct targets of MYCN and in blue boxes are the cellular processes affected. Taken from Huang and Weiss (2013).

MYCN expressed during NC cell development is downregulated during differentiation, suggesting MYCN could promote a ‘stem-cell like’ phenotype in NB. MYCN displays a positive feedback loop with OCT4 which enhances the self-renewal capabilities of undifferentiated NB cells (Yoshida, 2018). Also, MYCN transcriptionally upregulates a broad spectrum of pluripotency genes. In TET21N cells, MYCN-induced upregulation of *KLF2*, *KLF4*, and *LIN28B* promoted a stem cell-like phenotype (Cotterman and Knoepfler, 2009). In another study, MYCN directly upregulated *BMI1A*, a polycomb-group protein required for neural stem cell maintenance, which prevented NB cell differentiation (Ochiai et al., 2010). In accord with the cancer stem

cell (CSC) concept, MNA NB cells display greater symmetric cell division than non-MNA NB cells allowing retention of stem cell pools in the tumour niche (Izumi and Kaneko, 2012).

MYCN also promotes tumour cell growth by driving cell-cycle progression and cell proliferation whilst inhibiting apoptosis. *In vitro*, MNA NB cells fail to undergo G1-arrest in response to DNA damage (Bell et al., 2006). This is potentially due to MYCN-mediated downregulation of p21 as p21 normally induces G1 arrest (Bell et al., 2007). Cell cycle progression could also be due to MYCN-mediated upregulation of CDK4 as MNA tumours display elevated *CDK4* expression (Westermann et al., 2008). Alternatively, MYCN can promote cell cycle progression by upregulation of ID-2, an inhibitor of retinoblastoma (Lasorella et al., 2000). *ID2* correlates with *MYCN in vitro* and *in vivo* and ID2 expression is an indicator of poor survival in NB patients (Lasorella et al., 2002). MYCN can also promote cell proliferation via upregulation of *MDM2* which subsequently suppresses p53-depednent oncogenic apoptotic signalling (Chesler et al., 2008, Chen et al., 2009b). Curiously, p53 is inactivated to a significantly greater extent at relapse than at primary tumour (Carr-Wilkinson et al., 2010). As MYCN sensitises NB cells to MDM2 antagonists (Gamble et al., 2012), inhibiting MDM2 could be a therapeutic route to targeting MNA tumours. Paradoxically, MYCN can also induce a developmentally-timed apoptotic response in a transgenic zebrafish model demonstrating MYCN can both promote and suppress apoptosis (Zhu et al., 2012).

ALK mutation

In rare familial cases, highly penetrant germline mutations have been identified in the *ALK* and *PHOX2B* genes (Mosse et al., 2004, Mossé et al., 2008, Trochet et al., 2004). In sporadic NB, genome-wide studies have identified a range of DNA polymorphisms in NB tumour samples (Molenaar et al., 2012, Pugh et al., 2013, Sausen et al., 2013, Cheung et al., 2012b). Molenaar et al. (2012) performed whole-genome paired-end sequencing on 87 primary NB tumours and identified 12 somatic mutations per tumour. ALK mutations occurred most frequently, but in only 7% of tumours, highlighting

the degree of tumour heterogeneity. Similarly, Pugh et al. (2013) used whole exome and whole genome sequencing on blood leukocytes from 240 patients to reveal mutations at a significant frequency in six genes: *ALK*, *PTPN11*, *ATRX*, *OR5T1*, *MYCN* and *NRAS*. Interestingly, relapsed NBs demonstrate a much larger mutational burden than that at initial diagnosis (Fletcher et al., 2018). Although this leads to more targetable aberrations, relapse remains the largest cause of death for stage 4 NBs.

ALK is aberrantly activated in NB by both genomic amplification (2-3%) and point mutations (8-10%) (Mossé et al., 2008, Janoueix-Lerosey et al., 2008, Carén et al., 2008). Small interfering RNA (siRNA) treatment and chemical inhibition of ALK decrease proliferation of NB cell lines harbouring *ALK* mutations and the data indicate that the key downstream signalling is through the AKT pathway (Janoueix-Lerosey et al., 2008). Due to their proximal locations on chromosome 2p, *ALK* is almost exclusively amplified in MNA tumours. It has been speculated that the ALK-MYCN axis drives NB progression as ALK is also more frequently mutated in MNA tumours (De Brouwer et al., 2010, Chang et al., 2019). In NB cell lines, exogenous expression of ALK (wild type (WT) or mutated) upregulated MYCN expression which was reversed upon addition of an ALK inhibitor (Schönherr et al., 2012). Transfection of mutated ALK led to a robust transformation in NIH3T3 cells, but, co-transfection of mutant ALK with MYCN increased the transformation threefold. Also, in a transgenic zebrafish model, MYCN-induced apoptosis was prevented by co-expression with ALK (Zhu et al., 2012). Overall, these results demonstrate the potential synergism of ALK and MYCN in the more aggressive and malignant NB phenotype.

Numerical and segmental chromosome alterations

A diploid tumour has long been recognised as a prognostic indicator for poor prognosis in NB as it occurs more frequently in high-risk patients (Eckschlager et al., 1996, Kaneko et al., 1987). Hyperdiploid tumours are present in 65% of NB patients, the majority of which are non-MNA (Look et al., 1991). In a study analysing MNA tumours at stage 1, 2 or 4s,

hyperdiploid tumours displayed a greater overall survival than diploid tumours (Schneiderman et al., 2008). In patients presenting with metastasis, tumour ploidy has an age-dependent correlation with prognosis. In infants below 18 months old, hyperdiploidy is highly associated to a favourable outcome, however, in patients older than 24 months the DNA index becomes irrelevant (Look et al., 1991, George et al., 2005). As mentioned previously, the only segmental chromosome change in the INRG classification system is 11q deletion (Cohn et al., 2009). However, there are a range of other chromosomal changes which have been identified in NB, notably loss of 1p and gain of 17q (Attiyeh et al., 2005, Spitz et al., 2003, Maris et al., 1995, Bown et al., 1999). Loss of heterozygosity at 11q and 1p and gain of 17q occurs in 34%, 23% and 54% of cases, respectively (Attiyeh et al., 2005, Bown et al., 1999). All three aberrations are significantly associated with high-risk NB and 1p and 17q are also associated to MNA. A significant proportion of NB tumours have no recognised oncogenic driver. Therefore these changes, as well as alteration in tumour ploidy, are especially important when characterising non-MNA tumours. It has been demonstrated that analysing overall pattern of segmental chromosome alterations, rather than individual chromosome changes, adds valuable prognostic information as it predicts patient relapse and overall survival probabilities (Janoueix-Lerosey et al., 2008, Schleiermacher et al., 2011). These data suggest NB is predominantly a disease of chromosomal copy number changes and chromosome instability. The precise mechanisms behind chromosome instability in NB are unclear, but are likely due to either impaired mitosis, DNA damage or defective replicative fork progression (Fusco et al., 2018). This theory is supported by evidence that NB patients have an increased susceptibility to chromothripsis (Molenaar et al., 2012).

1.1.5. Molecular-targeted therapies

The majority of treatment options for NB are relatively non-specific (**Fig. 1.4**). This is predominantly due to the lack of recognised molecular aberrations in NB. Nonetheless, a range of targeted therapies are under investigation. Unsurprisingly, many of these seek to perturb MYCN or ALK

function, either directly or indirectly (Greengard, 2018). With regards to MYCN, studies have tried to prevent MYCN expression, stabilisation, activation and downstream activity, each with varying degrees of success. Preventing MYCN expression has been achieved by targeting the BET bromodomain epigenetic modifiers. A pharmacogenomic screen revealed that BET bromodomain inhibition reduced the MYCN transcriptional program and decreased MNA tumour growth *in vivo* (Puissant et al., 2013). There are currently many BET inhibitors in clinical trials, some of which include MNA NB (Zafar et al., 2021). Alternatively, MYCN activity has been targeted by preventing interactions to MAX or Aurora kinase A as these interactions stabilise MYCN protein and promote its activity (Gherardi et al., 2013, Richards et al., 2016). Promisingly, aurora kinase inhibition appears efficacious in NB cells, however the mechanism of action still remains unclear (DuBois et al., 2018). Alternatively, pathways that interact with MYCN have been targeted such as mTOR and MDM2. The PI3K/AKT/mTOR pathway functions downstream of ALK as is able to drive MYCN signalling (Chesler et al., 2006, Vaughan et al., 2016). Furthermore, as demonstrated previously, MYCN can upregulate MDM2 activity thereby suppressing p53-mediated apoptosis (Slack and Shohet, 2005). Inhibitors have been generated targeting both mTOR and MDM2 which appear promising in *in vivo* models (Wang et al., 2020, Johnsen et al., 2008). Aside from MYCN, ALK signalling via the RAS/ERK pathway has also been identified as a targetable pathway. There are mutations in many signalling components of this pathway (Pugh et al., 2013, Eleveld et al., 2015) but targeted therapies have seen most success targeting ALK directly (Hallberg and Palmer, 2016). Unfortunately, many of these inhibitors are hampered by resistance mechanisms therefore many newly-optimised ALK inhibitors are in clinical trials (Brenner and Gunnes, 2021). There are also a plethora of other proteins and pathways that have been studied less extensively, reviewed in Zafar et al. (2021) and Greengard (2018).

1.2. Phosphotyrosine signalling

Protein phosphorylation is a post-translational modification widely regarded as a global regulatory mechanism modulating protein function. Due to its size and negative charge, the addition of a phosphate ion induces large topological and electrostatic effects. Consequently, during a cellular response to internal or external stimuli, alterations in protein phosphorylation can dictate the downstream signalling pathways. In eukaryotes, proteins are phosphorylated on three residues: Serine, Threonine and Tyrosine. The intracellular abundance of the three phospho-Serine (pSer), phospho-Threonine (pThr) and phospho-Tyrosine (pTyr) are 86.4%, 11.8% and 1.8%, respectively (Olsen et al., 2006). However, tyrosine phosphorylation plays a disproportionately large role in cell signalling systems. Hunter (2014) speculates pTyr has become more specialised than pSer/Thr due to its phenolic ring spacer. The phosphoryl moiety is bound to the para- position further away from the peptide backbone and therefore adds a degree of specificity not present in pSer/Thr. The tyrosine residue is phosphorylated and dephosphorylated by protein tyrosine kinases and phosphatases, respectively.

1.2.1. Protein tyrosine phosphatases (PTPs)

A subset of protein tyrosine kinases, the receptor tyrosine kinase (RTK) family, have been researched significantly more than protein tyrosine phosphatases (PTPs) for various reasons. Firstly, the RTK family was discovered in the early 1980's, a decade before that of the PTPs, therefore more research has been performed into their structure and function (Schlessinger, 2014). Secondly, less research was geared towards PTPs as there was previously the belief that PTPs merely "switch off" proteins fairly non-specifically, whereas phosphate addition increases oncogenic signals and is more therapeutically valuable. Thirdly, PTPs are notoriously difficult to target. High target specificity is difficult to achieve as they contain a catalytic HCX_5R 'PTP motif' that is structurally conserved across the enzyme family, therefore a phospho-mimetic inhibitor will bind multiple PTP

substrates. Additionally, the multi-charged nature and hydrophilicity of the phospho-amino acid results in inhibitors with similar properties. Although these inhibitors may appear promising *in vitro*, they lack cell permeability *in vivo* (Barr, 2010, Tautz et al., 2006).

PTPs are highly modular as ~75% contain an additional domain or motif alongside the core catalytic domain, providing more diverse function and regulation (Alonso et al., 2004). PTPs are also highly regulated transcriptionally through alternative promoters, translationally through splicing variants and post-translationally through interacting partners, dimerisation and post-translational modifications (Tonks, 2006, Hertog et al., 2008). The only module present in all PTPs is a conserved catalytic domain which carries out dephosphorylation. The active site region is formed by a well-defined PTP-loop, where the HCX_5R motif resides, and a WPD loop (**Fig. 1.6**). The catalytic mechanism proceeds via acid/base catalysis in a two-step mechanism (Denu and Dixon, 1998, Zhang, 2002). Initially, the electronegative phosphate group, stabilised by several hydrogen bonds, is attacked by the cysteine thiolate as the substrate is protonated by the aspartate in the WPD loop. Following this, re-protonation of the aspartate generates an activated water molecule that hydrolyses the resulting phospho-cysteine complex (Kim and Ryu, 2012). As demonstrated in **Figure 1.6**, the invariant arginine coordinates the phosphoryl moiety which stabilises transition state formation. Also crucial to enzymatic activity is the orientation of the surrounding PTP loop residues which lowers the pka of the cysteine residue, promoting nucleophilic attack (Zhang, 2002). Mutational studies have demonstrated the structural role of many active site residues. As expected, mutation of the catalytic cysteine is the most significant as it abolishes enzymatic activity completely (Zhang, 2002).

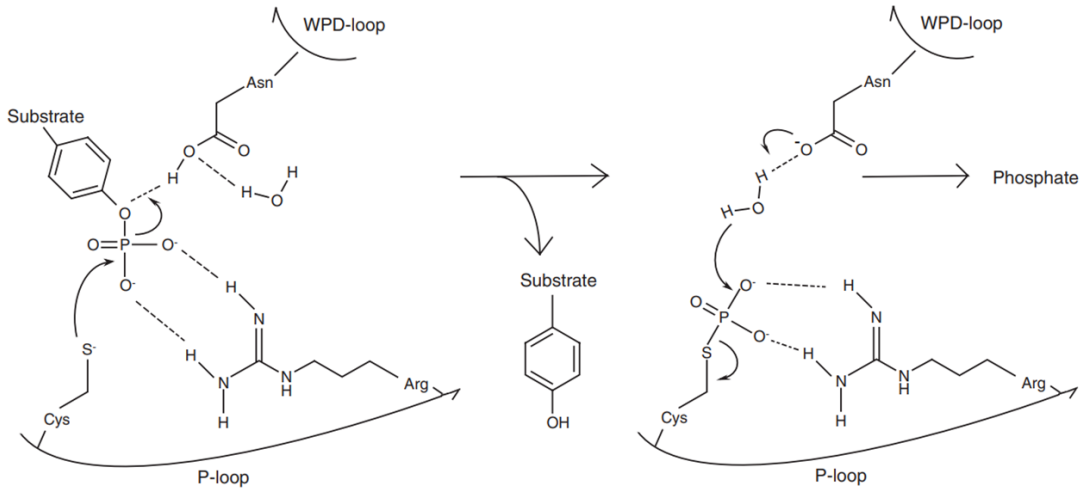

Figure 1.6 – Catalytic mechanism of action of a PTP on a phospho-tyrosine substrate. The 2-step sequential process begins with nucleophilic attack of the phosphoryl moiety by the catalytic Cysteine which leads to the formation of the phospho-cysteine complex. Following this, the aspartic acid activates a water molecule which subsequently hydrolyses the phospho-cysteine complex. Taken from Tautz et al. (2006).

Over 100 PTP superfamily genes have been identified (**Fig. 1.7**). These can be divided into 4 classes. Classes 1 - 3 contain a Cys-based active site whereas class 4 contains an Asp-based active site (Alonso et al., 2004). Class 1 constitutes the majority of these genes (99/107) and can be further sub-divided into the 'classical' PTPs, containing the receptor and non-receptor PTPs, and the 'VH1-like' dual-specificity phosphatases (DUSPs). A broad spectrum of Class 1 PTPs spanning both sub-classes have been well-studied and help modulate various cellular and biochemical processes (Tonks, 2006, Patterson et al., 2009, Xu and Fisher, 2012). The degree of substrate specificity is also extremely varied across the PTP family. For example, DUSP5 displays absolute substrate specificity for ERK due to specific DUSP5-ERK contacts which are required to activate DUSP5 (Mandl et al., 2005). On the other hand, PTP1b displays a high degree of active site plasticity and can therefore dephosphorylate a range of intracellular substrates (Yip et al., 2010). It is worth mentioning that there are also catalytically dead PTPs, termed pseudophosphatases, that appear as

integral to cellular physiology as the classical PTPs (Reiterer et al., 2014). Such phosphatases are thought to have many non-enzymatic functions, including scaffolding, molecular anchoring and signal integrating roles. With this knowledge, it is unsurprising that PTP malfunction is increasingly observed in a range of diseases including cancer and diabetes (Tonks, 2006, Alonso et al., 2004). Consequently, PTPs have emerged as major therapeutic targets.

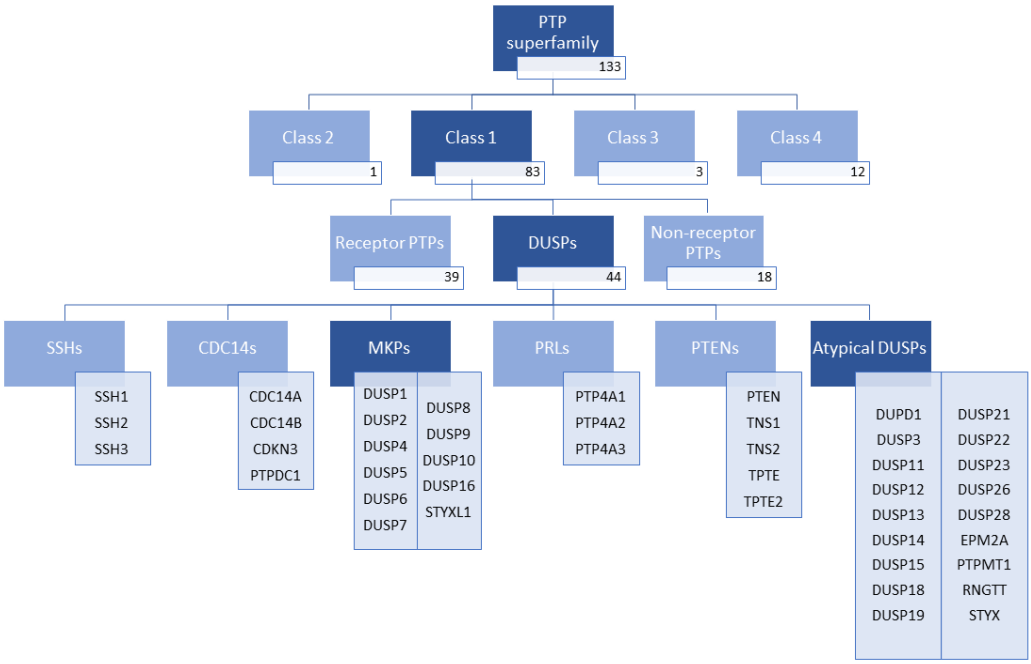

Figure 1.7 – The PTP family. The darker shade of blue represents the sup-groups of interest in this report and each DUSP is denoted by its gene name as documented in the HUGO Gene Nomenclature Committee.

1.2.2. Dual specificity phosphatases (DUSPs)

Although initial literature surrounding the importance of PTPs in cell physiology involved non-receptor PTPs such as SHP2, PTP1b and PTEN, there is growing evidence that the DUSPs are also integral regulators of intracellular signalling (Patterson et al., 2009, Caunt and Keyse, 2013). Unlike the classical PTPs, DUSPs can dephosphorylate both tyrosine and

serine/threonine residues. This is owed to a wider and shallower substrate binding region than the ‘classical’ PTPs (Denu et al., 1996). The first DUSP identified was VH1 from the vaccina virus (Guan et al., 1991). Since then, 61 human DUSP genes have been identified which are broadly divided into 6 classes: the MAP kinase phosphatases (MKPs), slingshot phosphatases, atypical DUSPs (aDUSPs), PTENs, CDC14s and myotubularins (Patterson et al., 2009). Interestingly, not all DUSPs dephosphorylate amino acids. The physiological substrates of PTEN and myotubularins are inositol phospholipids. In addition, certain aDUSPs can dephosphorylate glycogen and the 5’ CAP structure of mRNA (Wishart and Dixon, 2002, Bayón and Alonso, 2010). Nonetheless, all DUSPs demonstrate the same catalytic mechanism (Denu and Dixon, 1998). The emerging roles of DUSPs is exemplified by DUSP26. When discovered, DUSP26 was considered an MKP as it was able to dephosphorylate p38 and ERK (Vasudevan et al., 2005, Hu and Mivechi, 2006). However, DUSP26 was subsequently classed as an aDUSP as an increasing number of non-MAP kinase substrates were identified whereby it influences a range of intracellular signalling pathways (Shang et al., 2010, Kim et al., 2014, Tanuma et al., 2009, Yang et al., 2017). This demonstrates there is much still to learn about the function and regulation of DUSPs. Each member of the DUSP family has various synonyms, including names of other DUSPs in the same subgroup. To avoid confusion, I will use their gene name as documented in the HUGO Gene Nomenclature Committee.

MAP kinase phosphatases (MKPs)

The best characterised subgroup of DUSPs is the MAP Kinase phosphatases (MKPs). The MAP kinase (MAPK) pathways are a conserved set of signalling cascades essential for responding to extracellular stimuli. Such pathways are intricately regulated by scaffolding proteins and MAPK phosphatases (MKPs) which fine-tune the biological response generated (Imajo et al., 2006). To date, eleven MKPs have been discovered, one of which is a pseudophosphatase (Dickinson and Keyse, 2006). MKPs are grouped based on their most prominent sub-cellular location which is in

accord with their highest sequence homology and MAPK substrate (**Table 1.1**). Although the pseudophosphatase STYXL1 does not conform to the MKP rules on substrate specificity or localisation, it is classed as an MKP due to its sequence similarity, in particular with DUSP1 (Wishart and Dixon, 1998). Structurally, the MKPs subfamily contain an N-terminal domain (NTD) which governs substrate specificity and a catalytic C-terminal domain (CTD). The NTD contains a kinase-interacting motif (KIM) responsible for MAPK binding which is flanked by two cdc25/rhodenase homology regions commonly found in eukaryotic phosphatases (Dickinson and Keyse, 2006). Intracellular localisation of MKPs is also tightly regulated by nuclear localisation/export signals (NLS and NES) present in the NTD. In terms of their catalytic CTD, the secondary structures formed are very conserved and contain a well-defined PTP loop where the HCX_5R motif resides.

On the surface, MKPs appear as 'simple' negative feedback regulators, dephosphorylating MAPKs to prevent further signalling. However, the MAPK-MKP relationship is now considered very complex as MKPs display varying substrate specificities, redundancy and spatiotemporal regulation of their target (Caunt and Keyse, 2013). Also, MKPs are not ubiquitously expressed and must be transcriptionally upregulated to inactivate MAPK signalling. Tight regulation of the MAPKs is best explained through the cooperative function of DUSP5 and DUSP6 in controlling ERK localisation and function. After ERK pathway stimulation, dually phosphorylated ERK translocates to the nucleus and interacts with a broad spectrum of substrates. Due to the NLS present at its N-terminal region, DUSP5 resides in the nucleus whereas DUSP6, along with other cytoplasmic MKPs, contain a leucine-rich NES which permits translocation from nucleus to the cytoplasm (Caunt and Keyse, 2013). DUSP5 and DUSP6 act as part of a spatiotemporal model with two functions: ERK dephosphorylation and anchoring ERK in their vicinity (Karlsson et al., 2004, Mandl et al., 2005). In both cases, a functional NES or NLS and KIM region were required for ERK binding. However, ERK anchoring appears independent of catalytic activity as nuclear accumulation of ERK was unaffected by a catalytically dead DUSP5 (Mandl et al., 2005). There are a host of proteins, including ERK,

that regulate DUSP5 and DUSP6 transcriptionally. Both appear to be targeted by p53, and p53-mediated regulation of DUSP6 alters the expression of Bcl2-related proteins (Ueda et al., 2003, Piya et al., 2012). ERK is thought to mediate DUSP5 and DUSP6 expression via the ETS family of proteins, such as ETS1, ETS2 and ELK-1, as ETS-binding sites have been identified in both DUSP5 and DUSP6 promoters (Buffet et al., 2015, Zhang et al., 2010, Ekerot et al., 2008). As well as directly upregulating DUSP5 and 6 transcriptionally, ERK phosphorylates DUSP5 and DUSP6 at disparate locations. DUSP6 is phosphorylated at Ser159 and Ser197, distant from DUSP6-ERK interface, and induces proteasomal degradation in an ERK2 and MEK dependent manner (Marchetti et al., 2005). Phosphorylation of DUSP5 occurs proximal to the KIM region, at Thr321, Ser346 and Ser376, but has no immediate effect on DUSP5 stability (Kucharska et al., 2009). To add further complexity, a range of other DUSP6 post-translational modifications have been identified (Marchetti et al., 2005, Wu et al., 2021, Ma et al., 2020), which most likely occur to DUSP5 as well. Overall, this serves as an example of how there is much still to learn about how the network of DUSPs collectively regulate MAPK signalling.

Table 1.1 – MKPs and atypical DUSPs sub-families. The first 11 DUSPs are MKPs and the subsequent 20 are aDUSPs. Modified from Thompson and Stoker (2021).

Gene name	Synonyms	Chromosome location	Protein size	Substrates
DUSP1	CL100, HVH1, MKP-1, MKP1, PTPN10	5q35.1	367	JNK, p38, ERK
DUSP2	PAC-1, PAC1	2q11.2	314	ERK, p38
DUSP4	TYP; HVH2; MKP2; MKP-2	8p12	394	ERK, JNK, p38
DUSP5	DUSP; HVH3	10q25.2	384	ERK
DUSP6	HH19; MKP3; PYST1	12q21.33	381	ERK

DUSP7	MKPX; PYST2	3p21.2	419	ERK
DUSP8	C11orf81, HB5, HVH-5, HVH8	11p15.5	625	JNK, p38
DUSP9	MKP4; MKP-4	Xq28	384	ERK, p38
DUSP10	MKP-5, MKP5	1q41	482	JNK, p38
DUSP16	MKP7; MKP-7	12p13.2	665	JNK, p38
STYXL1	DUSP24; MKSTYX; MK-STYX	7q11.23	313	-
DUPD1	FMDSP; DUSP27	10q22.2	220	-
DUSP3	VHZ; LDP3; MOSP; LDP-3; DUSP25	1q23.2	185	ERK, JNK, p38, STAT5, FAK, EGFR, NPM1, NUCL, NBS1, HNRNPC
DUSP11	PIR1	2p13.1	377	5′-phosphorylated RNA CAP
DUSP12	YVH1; DUSP1	1q23.3	340	Glukokinase, ASK1, ERK, JNK, p38
DUSP13A	BEDP; MDSP; TMDP; SKRP4; DUSP13B	10q22.2	188	-
DUSP13B	BEDP; MDSP; TMDP; SKRP4; DUSP13A	10q22.2	198	JNK, p38, ERK
DUSP14	MKP6; MKP-L	17q12	198	ERK, JNK, p38, Otulin, TAK1, TAB1
DUSP15	VHY; C20orf57	20q11.21	295	Unknown
DUSP18	DSP18; DUSP20; LMWDSP20	22q12.2	188	JNK, SHP2

DUSP19	SKRP1; DUSP17; LMWDSP3; TS-DSP1	2q32.1	217	JNK
DUSP21	LMWDSP21	Xp11.3	190	-
DUSP22	VHX; JKAP; JSP1; MKPX; JSP-1; MKP-x; LMWDSP2; LMW-DSP2	6p25.3	184	ERK, JNK, p38, STAT3, Erα, FAK, Lck
DUSP23	VHZ; LDP3; MOSP; LDP-3; DUSP25	1q23.2	150	GCM1, p38, β-catenin
DUSP26	LDP4; MKP8; NEAP; DSP-4; LDP-4; MKP-8; NATA1; SKRP3; DUSP24	8p12	211	EGF, p38, FADD, TrkA, FGFR1, TAK1, KAP3, Kif3a
DUSP27	-	1q24.1	1158	-
DUSP28	VHP; DUSP26	2q37.3	176	-
EPM2A	EPM2; MELF	6q24.3	331	GSK3β, Glucans
PTPMT1	MOSP; PLIP; DUSP23; PNAS-129	11p11.2	201	SDHA, PI(3,5)P2, PI5P, PGP
RNGTT	HCE; HCE1; hCAP; CAP1A	6q15	597	5′-phosphorylated RNA Cap
STYX	-	14q22.1	223	-

Atypical phosphatases

The aDUSPs are a heterogenous group of 20 DUSPs which dephosphorylate a range of different substrates (**Table 1.1**). The aDUSPs are separated from the MKPs as they do not contain the KIM which governs MKP specificity. However, as demonstrated in **Table 1.1** some aDUSPs are still able to dephosphorylate the MAPKs. Due to this confusion, DUSP14 and DUSP26 were originally classified as MKPs and later switched to aDUSPs. With the KIM absent and such a broad range of substrates, this raises the question as to what mechanisms are in place to regulate aDUSP activity? A subset of aDUSPs which are analogous; DUSP26, DUSP13a, DUSP13b and DUPD1, all display restricted expression to certain tissues suggesting they are heavily regulated transcriptionally (Friedberg et al., 2007, Vasudevan et al., 2005, Chen et al., 2004). Studies on DUSP3, the most characterised aDUSP, have identified Tyr138 as a regulatory site which when phosphorylated, increases catalytic activity significantly (Hoyt et al., 2007, Alonso et al., 2003). Furthermore, homo-dimerization of DUSP3 driven by residues Phe68 and Met69 decreases catalytic activity *in vivo* against ERK (Pavic et al., 2014). It is likely that mechanisms such as post-translational modification and dimerisation apply to other aDUSPs, especially in cases where there is a diverse range of substrates.

1.3. Protein tyrosine phosphatases (PTPs) in cancer

1.3.1. Phosphotyrosine signalling in cancer

Phosphotyrosine signalling plays a significant role in many cellular processes such as differentiation, proliferation, apoptosis and migration (Soulsby and Bennett, 2009). It is therefore unsurprising that when deregulated, PTPs and RTKs are implicated in cancer progression. Once discovered, aberrant activation of RTKs was identified in an array of human malignancies and RTKs formed the largest group of dominant oncogenes

(Blume-Jensen and Hunter, 2001). This is exemplified by EGFR-mediated activation of the RAS/ERK, PI3K/AKT and PLC-γ1/PKC pathways. As these pathways mediate a wide range of physiological responses, constitutive activation of EGFR significantly disrupts intracellular homeostasis. Hence, somatic mutation, deletion or amplification of *EGFR* is frequently observed in glioblastoma, breast cancer and non-small cell lung cancer (Yarden and Pines, 2012). Consequently, a broad spectrum of antibodies and small molecules have been developed to inhibit different components of the RTK signalling pathways (Regad, 2015, Yarden and Pines, 2012).

Logically, if RTKs are bona fide oncogenes which drive tumorigenesis, this implies PTPs would largely function as tumour suppressors, hindering oncogenic RTK signalling. Indeed, the loss of tumour suppressive PTPs is well documented, either genetically via gene deletions or mutations, or epigenetically via promoter methylation or transcriptional repression (Bollu et al., 2017). This subsequently releases the restraint of oncogenic signalling pathways, leading to malignant transformation. However, it has become apparent that PTPs can also promote intracellular signalling thus enhancing cell survival. For example, the Src kinase family are known to drive tumorigenesis in a myriad of cancers (Irby and Yeatman, 2000), and to be activated they require dephosphorylation of their CTD, driven by various PTPs (Abdollahi et al., 2017, Zheng et al., 1992). Furthermore, PTP loss of function (LOF) can trigger excess oncogenic signalling resulting in cancer cell death (Li et al., 2011). Consequently, via gene amplification, translocations and activating mutations, an upregulation of PTP activity can also result in malignancy (Elson, 2018, Bollu et al., 2017). Depending on the cancer type, it is now believed a complex network of PTPs are involved in both promoting and suppressing tumorigenesis. The first implications of PTPs in cancer were demonstrated by SHP2 and PTEN, two non-receptor PTPs which demonstrate contrasting pro- and anti-survival roles in tumorigenesis (Steck et al., 1997, Östman et al., 2006, Li et al., 1997). Summarised below are the regulatory roles of PTEN and SHP2 in tumorigenesis and how they can be targeted therapeutically.

PTEN and SHP2 as putative tumour-suppressors and promoters

Initial studies demonstrated PTEN is frequently lost across a wide range of cancers and functions as a tumour suppressor (Li et al., 1997, Steck et al., 1997). Loss of PTEN predominantly occurs via somatic mutations which result in protein truncation (Bonneau and Longy, 2000). However, promoter methylation and loss of heterozygosity have been observed in a broad spectrum of cancers (Milella et al., 2015). PTEN can function in both a PI3K-dependent and -independent manner (**Fig. 1.8**) (Song et al., 2012). As PI3K phosphorylates phosphatidylinositol 4,5-bisphosphate to phosphatidylinositol 3,4,5-trisphosphate (PIP3), PTEN dephosphorylates PIP3 thus counteracting the function of PI3K. Loss of PTEN leads to accumulation of PIP3 at the plasma membrane and downstream activation of AKT/mTOR which drive a plethora of oncogenic processes (Song et al., 2012, Milella et al., 2015). PTEN can translocate to the nucleus where it has an essential role in chromosome stability by binding to CENP-C, and DNA-damage repair by upregulating RAD51 transcriptionally (Shen et al., 2007). Additionally, nuclear PTEN promotes formation of the APC-CDH1 complex, a putative tumour suppressor that regulates a range of cell cycle-associated proteins (Song et al., 2011).

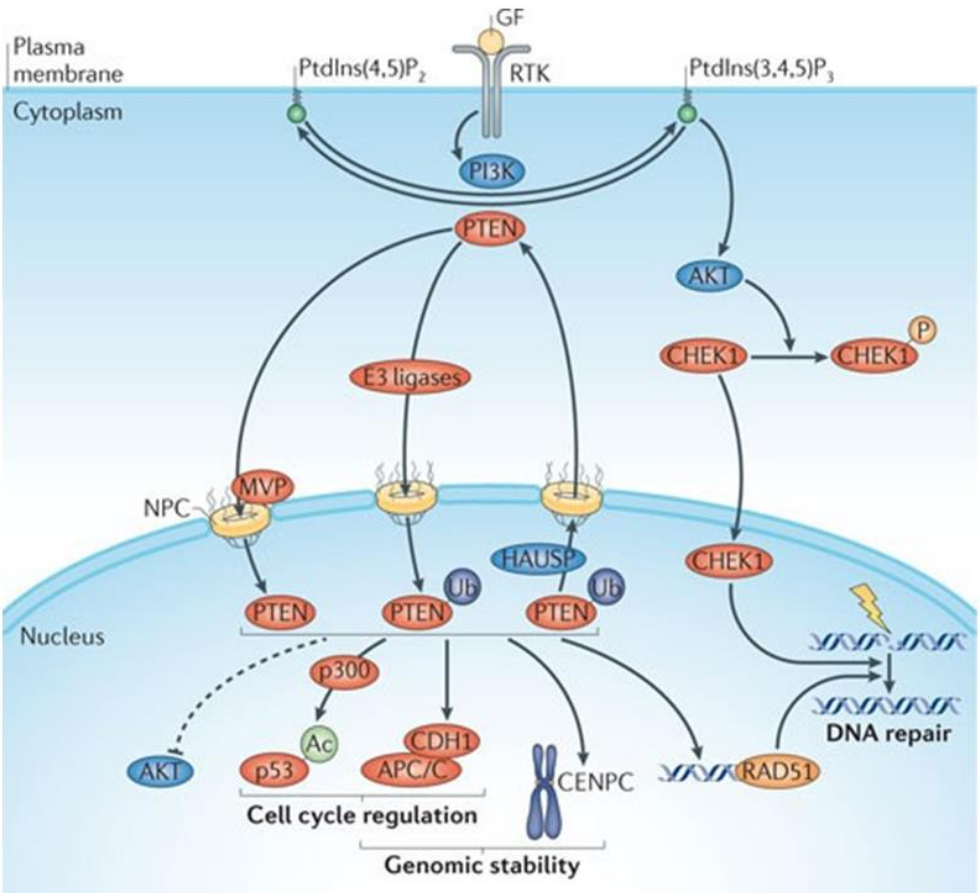

Figure 1.8 – Tumour-suppressive actions of PTEN. In both a PI3K-dependent and independent manner, PTEN can downregulate a range of intracellular pathways involved in oncogenesis. PTEN functions in the cytoplasm as a regulator of PIP3 signalling but also in the nucleus affecting genomic stability, DNA repair and cell cycle regulation. Taken from Song et al. (2012).

In contrast to PTEN, a range of tumour-promoting roles have been identified by SHP2 (Zhang et al., 2015, Östman et al., 2006). Gain-of-function mutations in SHP2 have been identified in ~30% of Juvenile myelomonocytic leukaemia tumours and at lower frequencies in other cancers (Chen et al., 2006, Paulsson et al., 2008, Tartaglia et al., 2003, Miyamoto et al., 2008). Furthermore, oncogenic activity of SHP2 has been identified in breast, lung, gastric cancer and NB (Jiang et al., 2013, Schneeberger et al., 2014, Zhou et al., 2008). Once recruited to the cell surface, SHP2 interacts with both Gab1 and Grb2 in the Gab1/Grb2 complex (Ahmed et al., 2013, Furcht et al., 2015). Such interactions can promote oncogenic signalling of the RAS/ERK and PI3K/AKT pathways,

depending on the extracellular stimuli and RTK activated (Zhang et al., 2015). These pathways have a wide range of downstream effects, therefore SHP2 is associated with EMT, tumour cell proliferation and apoptosis. Interestingly, SHP2 plays a fundamental role in promoting RTK-driven drug resistance (Prahallad et al., 2015). Once identified as a synthetically lethal gene in BRAF-mutant colon cancer cells, subsequent studies demonstrated loss of SHP2 abrogates RTK-mediated cell growth and suppressed drug resistance in melanoma cells.

As a central node of oncogenic signalling, SHP2 is an ideal drug target. Although chemical inhibition of PTPs is extremely difficult, more recently, significant efforts have been employed to develop novel orthosteric, allosteric, and oligomerization-inhibiting PTP inhibitors (Zhang, 2017, Stanford and Bottini, 2017). Two inhibitors have recently been developed against SHP2 which appear promising. Firstly, a competitive inhibitor 11a-1 was identified in a structure-guided fragment-based library approach using a precursor inhibitor termed II-B08 (Zeng et al., 2014). 11-a is cytotoxic across a range of cancer cell lines and suppressed tumour growth in a melanoma xenograft model (Zeng et al., 2014, Zhang et al., 2016). However, 11a-1, along with other SHP2 inhibitors, demonstrated off-target effects by suppressing PDGFRβ phosphorylation independent of SHP2 activity (Tsutsumi et al., 2018). A second allosteric inhibitor, SHP099, was identified by in an *in vivo* small molecule screen prioritising compounds that did not inhibit the PTP catalytic domain (Chen et al., 2016c, Garcia Fortanet et al., 2016). SHP099 did not inhibit 21 other phosphatases and demonstrated a potent inhibition of SHP2 *in vivo*. Further work is required to demonstrate whether the selectivity and potency of these inhibitors are sufficient for clinical trials.

1.3.2. Dual specificity phosphatases (DUSPs) in cancer

As demonstrated above, the roles of PTPs in cancer can be complex and far reaching as they modulate a range of intracellular pathways. This remains true for the MKPs as they target each of the MAPKs which in turn each have varying intracellular roles depending on the context. It is therefore unsurprising that both oncogenic and tumour-suppressive roles of MKPs have been identified (Low and Zhang, 2016, Keyse, 2008, Nunes-Xavier et al., 2011). Although less well studied than the MKPs, a range of aDUSPs have also been implicated in tumorigenesis, both through MAPK and non-MAPK signalling pathways (Nunes-Xavier et al., 2011, Cain and Beeser, 2013). As the potential roles of DUSPs in cancer are vast, discussed below are the best-characterised DUSPs with a particular focus on the intracellular pathways they affect.

MAP kinase phosphatases (MKPs) in tumorigenesis

I will predominantly focus on DUSP1 and DUSP6 as these appear the most implicated in tumorigenesis, however other MKPs are also mentioned throughout. In accord with the classical negative feedback loop, DUSP1, DUSP5 and DUSP6 can restrain oncogenic Ras/ERK signalling, preventing tumour growth (**Fig. 1.9**) (Nunes-Xavier et al., 2011). *DUSP6* is frequently hypermethylated in pancreatic cancer at a CpG island identified in intron 1 (Xu et al., 2005). Silencing of *DUSP6* occurs almost exclusively in cases with *KRas* mutations, suggesting DUSP6 can no longer restrain hyperactive ERK signalling (Furukawa et al., 2005). Similarly, loss of *DUSP6* via methylation and proteasomal degradation has been observed in lung and ovarian cancer respectively, which both resulted in hyperactive ERK1/2 signalling and increased tumorgenicity (Chan et al., 2008, Okudela et al., 2009). In another study, *DUSP5* knockout (KO) mice were used to determine the involvement of DUSP5 in skin cancer (Rushworth et al., 2014). Loss of *DUSP5* led to an increase in tumour incidence and a deregulation of ERK signalling which was further exacerbated by

exogenous expression of HRas^{Q61L}. Interestingly, loss of *DUSP5* also led to a significant increase in the ERK target gene *SerpinB2* which was requisite for tumorigenesis, however the downstream mechanism causing cell transformation was unclear. Removal of *DUSP1* is associated with tumorigenesis in gallbladder cancer (GBC) via the ERK-MMP2/VEGF pathway (Shen et al., 2017). In a xenograft model subcutaneously injected with GBC cells, exogenous *DUSP1* inhibited cell proliferation and suppressed ERK phosphorylation. Further analysis in the same xenograft model demonstrated *DUSP1* overexpression reduced liver and mesenteric metastasis and down-regulated *MMP2* and *VEGF*.

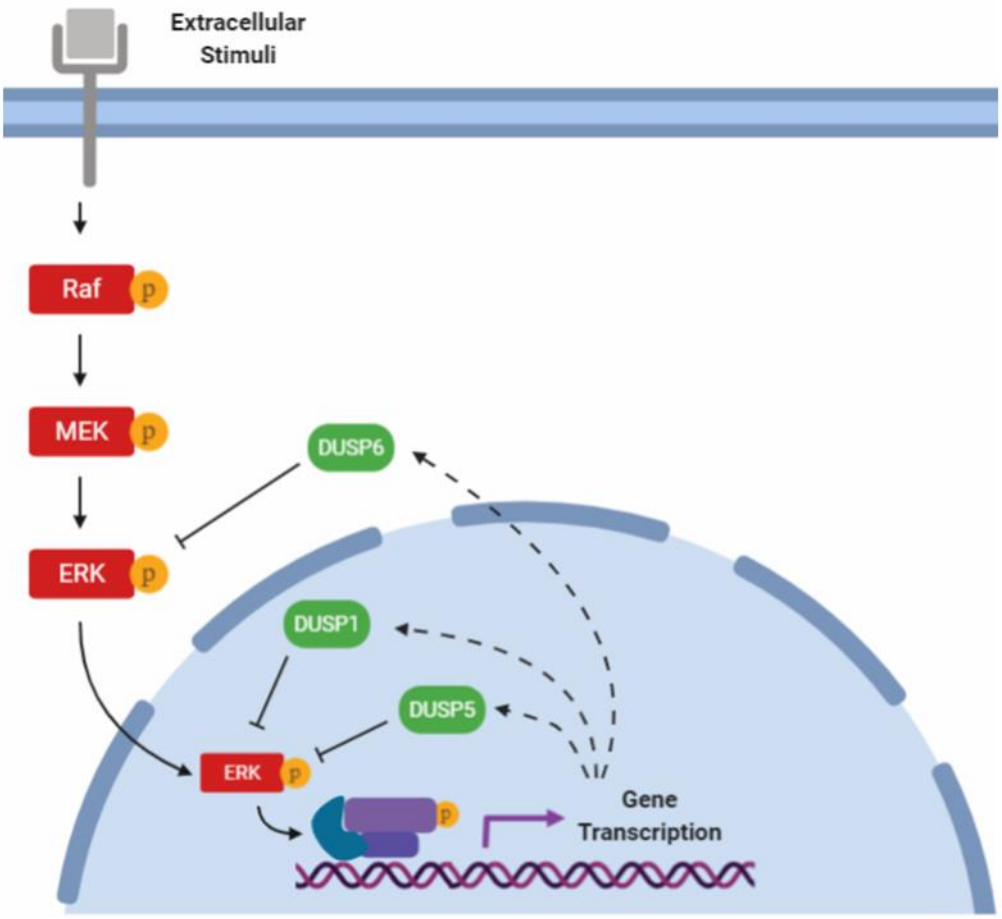

Figure 1.9 – Negative feedback of Ras/ERK signalling cascade by MKPs. A range of external stimuli will trigger the three-tiered Ras/ERK cascade via activation of a cell surface receptor. ERK signalling leads to transcriptional upregulation of various MKPs that subsequently suppress ERK signalling.

In contrast, there are a myriad of DUSPs that are overexpressed/amplified in cancer and display tumorigenic properties. DUSP1 is overexpressed in low-grade prostate cancer (PC) and its expression is inversely correlated to JNK expression (Magi-Galluzzi et al., 1997). Interestingly, androgen-treated PC specimens displayed a reduction in DUSP1 and up-regulation of JNK suggesting DUSP1-mediated inhibition of JNK drives PC progression. A similar mechanism is employed by DUSP1 to increase chemoresistance in a range of cancers (Nunes-Xavier et al., 2011). This is most clearly documented in breast cancer where DUSP1 led to resistance to cisplatin, paclitaxel, proteasome inhibitors and H_2O_2-induced cell death (Haagenson and Wu, 2010). DUSP1 aids chemoresistance predominantly via inhibition of JNK-mediated apoptosis, however alterations in p38 and ERK activity have also been identified. Similarly, DUSP6 is able to promote tumorgenicity and chemoresistance in glioblastoma (Messina et al., 2011). In a panel of human glioblastomas, DUSP6 was overexpressed compared to healthy astrocytes. Although exogenous expression of DUSP6 did not alter glioblastoma cell viability, it exacerbated the malignant phenotype and increased resistance to cisplatin. Interestingly, it appears resistance was generated via ERK inhibition, however the downstream effect of ERK was not identified. DUSP6 is also implicated in breast cancer carcinogenesis. In MCF-7 cells treated with phorbol myristate acetate, exogenous expression of DUSP6 promoted cell proliferation and anchorage independent cell growth (Nunes-Xavier et al., 2010). *DUSP6* was regulated by the ETS2 transcription factor in an ERK-dependent manner. In accord, another study demonstrated *DUSP6* knockdown in MDA-MB-231 cells suppressed cell migration and invasiveness and promoted cell cycle arrest (Song et al., 2015). Similar results were found in another study investigating the role of DUSP1, DUSP4 and DUSP6 in EMT and CSC maintenance in breast cancer (Boulding et al., 2016). Interestingly, all three genes were upregulated during phorbol myristate acetate-induced EMT and DUSP1 and DUSP4 bound to the promoter of mesenchymal-related genes suggesting they actively promoted the migratory phenotype. Following this, *DUSP1* knockdown, but not that of *DUSP4* and *DUSP6*, promoted the breast cancer

CSC maintenance as the proportion of $CD44^{hi}/CD24^{lo}/EpCAM^{+}$ cells post-transfection increased.

There is evidently a complex picture where depending on their substrate and the cancer subtype, DUSPs can have contrasting roles in cancer. For example, DUSP1 appears tumour-promoting or -suppressing depending on whether JNK or ERK is the predominant substrate, respectively. Whereas DUSP6, through ERK modulation alone, can have different physiological roles solely depending on the cancer type. Interestingly, there have been indications that DUSPs can compensate for each other, further complicating matters (Buffet et al., 2017, Caunt et al., 2008a). In HeLa cells, knockdown of *DUSP2* led to an upregulation of PDBu-mediated *DUSP1* mRNA (Caunt et al., 2008a). Furthermore, in thyroid cancer, where DUSP5 and DUSP6 suppress oncogenic ERK signalling, knockdown of *DUSP5* leads to an upregulation of *DUSP6* mRNA (Buffet et al., 2017). Although concomitant knockdown of DUSP5 and DUSP6 did not affect cell viability, these results suggest MAPK signalling is modulated by a network of DUSPs rather than individual drivers.

It is worth noting, the nature of MKP signalling in cancer progression can differ depending on tumour grade (Loda et al., 1996, Li et al., 2012). For example, *DUSP1* expression was inversely correlated to histological grade and metastasis in colon, prostate and bladder cancers, but correlated with tumour severity in breast carcinomas (Loda et al., 1996). As DUSP1 can dephosphorylate JNK, p38 and ERK, a change in DUSP1 localisation or substrate during tumour progression could reflect its switch from tumour suppressor to promoter. A similar phenomenon is observed by DUSP6 in malignant melanoma subtypes. In a mouse melanocyte model, Li et al. (2012) overexpressed DUSP6 that led to increased tumorigenicity of the cells, whereas in human A375 melanoma cells, DUSP6 overexpression led to a decrease in tumorigenicity.

Atypical dual specificity phosphatases (aDUSPs) in tumorigenesis

The aDUSPs are relatively understudied compared to the MKPs, however many of these are also implicated in tumorigenesis. The prototypical DUSP3 is the best characterised aDUSP, including its relation to human malignancy (**Fig. 1.10**)(Monteiro et al., 2018). In both cervical cancer cell lines and primary cervical carcinoma specimens, *DUSP3* is overexpressed (Henkens et al., 2008). DUSP3 is also overexpressed in human prostate cancer specimens (Arnoldussen et al., 2008). Treatment of LNCaP cells with 12-O-tetradecanoylphorbol-13-acetate and thapsigargin promoted JNK-mediated apoptosis, however, exogenous expression of DUSP3 reversed this effect suggesting an oncogenic role of DUSP3 in prostate cancer (Arnoldussen et al., 2008, Engedal et al., 2002). In accordance, DUSP3 is thought to upregulate angiogenesis. DUSP3 was required for tubulogenesis in endothelial cells and *DUSP3* deficiency abrogated *in vivo* and *ex vivo* angiogenesis in a murine model (Amand et al., 2014). In contrast to this, *DUSP3* expression is decreased in primary non-small-cell lung carcinoma (NSCLC) tissues and in H1299 cells, exogenous DUSP3 expression decreased tumour formation (Wang et al., 2011). EGFR and ErbB2 were the bona fide substrates of DUSP3 and DUSP3 activity decreased cellular sensitivity to EGF treatment. Surprisingly, DUSP3 overexpression had no effect on MAPK activation which suggests, similar to DUSP1, the change in DUSP3 target can significantly alter its physiological role. DUSP3 is also implicated in BRCA1-IRIS-overexpressed breast cancer (Hao and ElShamy, 2007). In breast cancer cells, BRCA1-IRIS/EGFR/ErbB2 signalling suppresses *DUSP3* expression which results in JNK activation and Cyclin D upregulation (Hao and ElShamy, 2007). As DUSP3 overexpression overcame BRCA1-IRIS signalling and suppressed Cyclin D activation, unlike in cervical cancer, DUSP3 suppressed cell cycle progression via indirect Cyclin D inhibition.

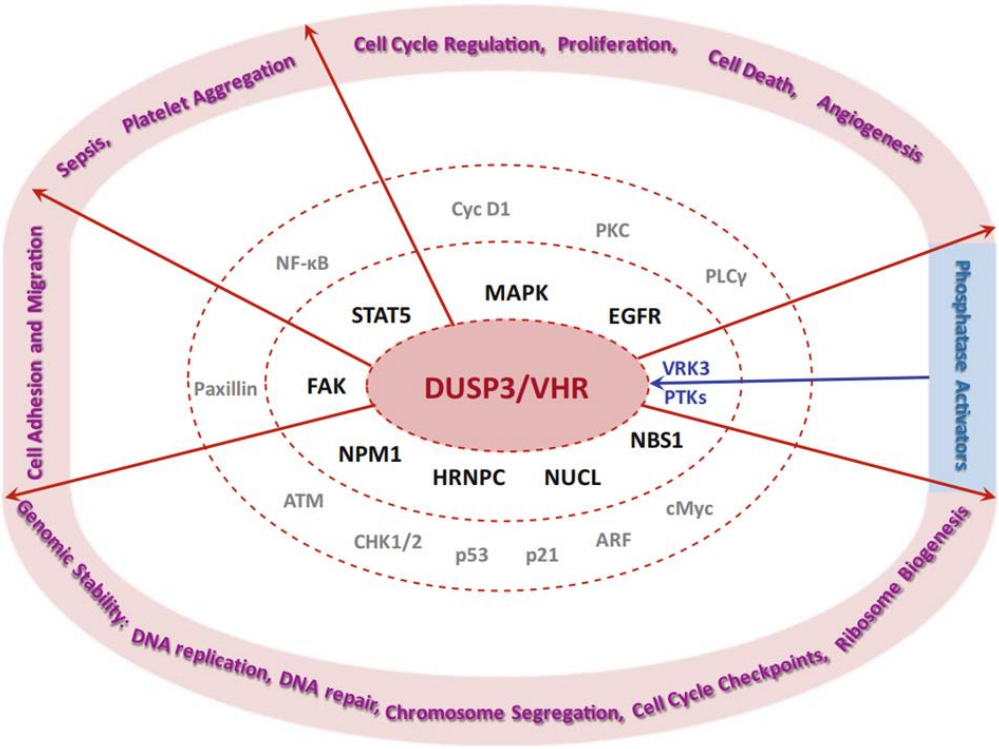

Figure 1.10 – Roles of DUSP3 in cancer. The most inner circle represents direct substrates of DUSP3 that have been validated *in vivo* and/or *in vitro*. The second layer contains substrates identified *in vitro* or predicted *in silico*. The text in magenta represents all the cellular functions affected by DUSP3 function and in blue are the phosphatase activators that bind and upregulate DUSP3 activity. Taken from Monteiro et al. (2018).

Similar to DUSP3, the phosphatases DUSP22, DUSP23 and DUSP26 are implicated in cancer by regulating non-MAPK substrates. In breast cancer, both loss and gain of *DUSP26* has been observed (Moelans et al., 2018, Kim et al., 2014). In this setting, DUSP26 dephosphorylates FADD by interacting with AK2, a phosphotransferase enzyme (Kim et al., 2014). Loss of *AK2* increased tumorgenicity in a mouse xenograft and in breast cancer specimens there is a correlation between *DUSP26* and *AK2* expression. DUSP26-mediated regulation of FADD has also be observed in T-cell lymphoblastic lymphoma (T-LBL). In T-LBL, *FADD* expression is downregulated (Villa-Morales et al., 2014). Marín-Rubio et al. (2016) demonstrated that *DUSP26* was overexpressed in a subset of T-LBL tumours and chemical inhibition of DUSP26 resulted in an increase of p-FADD expression. Therefore, AK2/DUSP26 modulation of FADD appears an active pathway involved in tumorigenesis.

Immunohistochemical analysis demonstrated *DUSP23* is overexpressed in a wide range of cancers (Tang et al., 2010). Further investigation in MCF-7 cells demonstrated DUSP23 was required for cell cycle progression. A large affinity and proximity-based proteomic screen identified PLK4, a critical regulator of centriole duplication, as a bona fide substrate of DUSP23 (St-Denis et al., 2016). Treatment with DUSP23 siRNA led to defective mitosis and inhibition of Myc-PLK4-mediaed centriole overduplication. Interestingly, DUSP23 possesses a unique phosphotransferase ability and both dephosphorylation and transphosphorylation functions of DUSP3 on PLK4 were necessary for unperturbed cell cycle (St-Denis et al., 2016).

DUSP22 is a putative tumour suppressor in breast and prostate cancer via downregulation of intracellular hormone signalling. In ERα-positive breast cancer cells, estrogen-mediated upregulation of *DUSP22* led to dephosphorylation of ERα which decreased the ERα transcriptional response and DNA-binding activity (Sekine et al., 2007). A subsequent study demonstrated that *DUSP22* mRNA is upregulated when *PPAPDC1B*, a candidate driver gene in breast cancer, is knocked down, suggesting the oncogenic activity of PPAPDC1B is driven by increasing endoplasmic reticulum (ER) activity (Bernard-Pierrot et al., 2008). *DUSP22* expression is also inversely correlated with progression-free survival of prostate cancer (Lin et al., 2019b). In LNCaP and C4-2B cells, exogenous expression of DUSP22 downregulated both the EGFR/ERK and EGFR/AR axis and suppressed cell growth. Consequently, it appears DUSP22 displays potent anti-tumorigenic activity by restraining hormone receptor signalling. Together, these results demonstrate that the DUSP family influences tumour progression in a wide range of cancers and via both MAPK and non-MAPK related targets.

1.4. Phosphotyrosine signalling in NB

1.4.1. Phosphotyrosine signalling can drive NB cell growth

Phosphotyrosine signalling is pivotal during development of the NC. It has been shown that RTK sub-families have specific functions in subpopulations of NC cells to regulate their development and activity during embryogenesis (Fantauzzo and Soriano, 2015). As mentioned previously, RTKs are able to drive tumorigenesis via amplification, mutation, chromosomal rearrangement or autocrine activation (Du and Lovly, 2018). Interestingly, in NB the expression of many RTKs is associated to NB patient survival suggesting aberrant activation of RTKs can promote NB progression (Trigg and Turner, 2018, Rozen and Shohet, 2021). Furthermore, in a phosphoproteomic screen spanning 21 NB cell lines, a wide range of functional RTK signalling pathways were identified (Palacios-Moreno et al., 2015). In this study, clustering of phosphorylation patterns revealed RTK sub-groups were functionally compartmentalised to regulate distinct cellular activities. This further suggests RTKs are integral signalling components to NB cell function.

Unsurprisingly, the RTK with the greatest link to NB progression is ALK. As mentioned in **Chapter 1.1**, ALK is both mutated and amplified in a subset of NB which leads to its constitutive activation. ALK is believed to drive tumorigenesis in NB predominantly via the RAS/ERK, PI3K/AKT and JAK/STAT signalling pathway (Trigg and Turner, 2018) (Discussed in **Chapter 6**). There are a handful of other RTKs, such as KIT, MET, and RET, which also have a significant correlation with worse patient survival (Rozen and Shohet, 2021). RET appears to cooperate with both ALK and MYCN to drive NB progression (Lopez-Delisle et al., 2018, Cazes et al., 2014). Interestingly, MYCN/Alk^{R1279Q} mice were acutely sensitive to RET inhibition suggesting the MYCN/ALK axis is somewhat dependent on RET function. However, RET is also important to retinoic acid (RA)-induced neuronal

differentiation, a response that is deemed tumour-suppressive in NB (Bunone et al., 1995, Esposito et al., 2008). Hence, the consequence of RET signalling in NB is highly dependent on the cellular context. Alternatively, the Trk family of RTKs are also implicated in NB tumorigenesis. The Trk family consists of TrkA, B and C and are often associated with p75, a member of the TGFR family, as the four receptors exclusively bind neurotrophic growth factors. Interestingly, the expression of different Trk receptors and their isoforms is highly predictive of NB aggressiveness. High expression of *TrkA*, TrkC and truncated TrkB are detected in the lower stage, more differentiated NB tumours (Nakagawara et al., 1993, Nakagawara et al., 1994, Yamashiro et al., 1996). In contrast, the full length TrkB receptor is predominantly expressed in aggressive MNA NBs, suggesting their physiological functions are critical in mediating NB cell differentiation (Nakagawara et al., 1994). Unfortunately, the specific downstream effects of Trk signalling in NB are not clear-cut, most likely due to the high degree of NB heterogeneity (Ngan, 2015) and different Trk expression profiles. Collectively, these examples demonstrate how phospho-tyrosine signalling is integral to various aspects of NB progression.

1.4.2. Protein tyrosine phosphatases in NB

Considering the importance of phosphotyrosine signalling to NB, our group has had a long-standing interest in the role of PTPs in NB. We and others have previously used vanadium-based compounds as pan-PTP inhibitors to investigate how PTPs influence intracellular signalling and NB cell survival (Clark et al., 2015, Clark et al., 2013, Boutterin et al., 2013, Tian et al., 2016). In NB cell lines, the vanadium-based compound bismaltolato oxovanadium (BMOV) enhanced RA-induced differentiation and led to sustained activation of the AKT and ERK pathways (Clark et al., 2013). Similarly, treatment of NIH3T3 cells with orthovanadate led to a significant upregulation of ALK signalling, demonstrating PTPs help restrain ALK downstream activity (Boutterin et al., 2013). As longer treatments of combined RA and BMOV led to irreversible differentiation and senescence of NB cells (**Fig. 1.11A**), there is therapeutic potential in targeting PTPs.

BMOV is also extremely cytotoxic in a range of NB cell lines, further suggesting NB cell dependence on PTP function (Clark et al., 2015) (**Fig. 1.11B**).

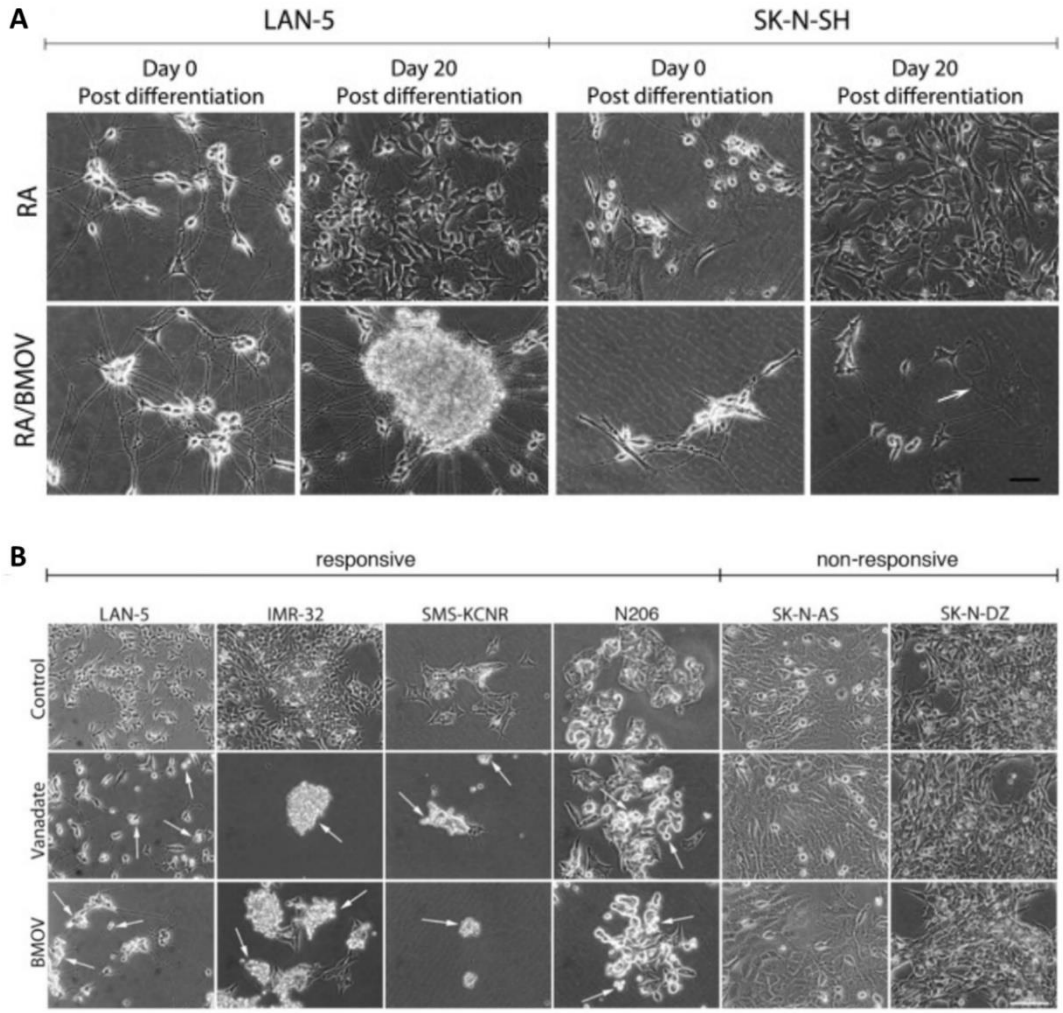

Figure 1.11 – Therapeutic potential of inhibiting PTPs in NB. (A) Sustained treatment with bismaltolato oxovanadium (BMOV) is able to augment RA-induced differentiation in NB cells. Arrow indicates formation of pseudoganglia. Taken from Clark et al. (2013). (B) Pan-inhibition of PTPs using vanadate or BMOV caused significant cellular toxicity in a range of NB cell lines. Arrows indicate dead or dying cell. Taken from Clark et al. (2015). Scale bars = 50 µm (A), 10 µm (B).

SHP2 and PTP1b remain the best characterised PTPs in terms of NB progression and function downstream of RTK signalling. Gain-of-function mutations in the SHP2 gene, *PTPN11*, occur in approximately 3% of NB cases, over half of which are also MNA (Bentires-Alj et al., 2004, Pugh et

al., 2013). SHP2 is requisite for NC cell development as SHP2-KO mice display severely impaired embryonic development (Grossmann et al., 2009). Further analysis in SHP2-mutant Schwann precursor cells revealed SHP2 is required for transduction of Ngr1 signalling via the ErbB receptors. In NB cells, SHP2 also regulates TrkB signalling. BDNF-mediated activation of TrkB signalling induced SHP2 phosphorylation and activation which led to sustained activation of the Ras/ERK pathway (Easton et al., 2006). Subsequent studies in SH-SY5Y cells demonstrated SHP2 dephosphorylated TrkB which leads to neuronal ER stress (Chitranshi et al., 2017). Also, SHP2 overexpression induced apoptosis via RAS/ERK activation whereas knockdown of SHP2 induced neuritogenesis. Consequently, neuronal cell survival and death is modulated by SHP2 expression. In a zebrafish model, constitutively active SHP2 synergised with MYCN to induce NB tumorigenesis via RAS/ERK signalling (Zhang et al., 2017). Constitutively active SHP2 promoted MYCN-induced hyperplasia by suppressing a developmentally-timed apoptotic pathway. Simultaneous inhibition of the ERK pathway and MYCN expression significantly reduced NB tumour size demonstrating the therapeutic potential of concurrent inhibition of these pathways. Overall, although only a minority of NB tumours contain SHP2 mutations, perturbed SHP2 expression and/or activity appears detrimental to NC cell development and this can potentially promote NB progression.

As mentioned, PTP1B is also implicated in NB progression. In primary NB specimens, high expression of *PTPN1* was associated to poor prognosis and metastatic disease (Nunes-Xavier et al., 2019a). However, knockdown of PTP1B increased NB cell growth *in vitro* demonstrating the role of PTP1b is more complex than a simple tumour promoter or suppressor. Similar to SHP2, TrkB is a putative target of PTP1b in SH-SY5Y cells (Ozek et al., 2014). Ozek et al. (2014) demonstrated inhibition of PTP1b resulted in TrkB-mediated activation of AKT and ERK signalling and increased BDNF-induced neurite outgrowth. A neuroprotective role of PTP1b inhibition was also demonstrated in SH-SY5Y cells after induced neuronal ER stress. PTP1b inhibition ameliorated the effects of ER stress inducers by

suppressing the PERK-eIF2α pathway, potentially via TrkB activation (Jeon et al., 2017). Furthermore, PTP1b dephosphorylates intracellular pools of ALK in murine fibroblast cells (Boutterin et al., 2013). If the same is true in NB then promoting PTP1b activation is a potential therapeutic route in suppressing oncogenic ALK activation.

A previous post doc in the lab performed a loss of function short hairpin (shRNA) screen against the PTP function (Dr. Ann Cichon, unpublished data). This identified a range of PTPs that appeared 'oncogenic-like' in IMR-32 cells. Interestingly, a handful of these PTPs were DUSPs, including DUSP6, a DUSP heavily implicated in a wide range of other cancers (Ahmad et al., 2018). A recent review by Nunes-Xavier et al. (2019b) demonstrated many DUSPs may be involved in neuronal differentiation and in the progression of NB. Considering ERK signalling is known to drive a subset of NB tumours, it is unsurprising that the majority of this literature surrounds the ERK-targeting DUSPs (Nunes-Xavier et al., 2019b). Especially downstream of ALK-ERK signalling in ALK-mutated NB, one would expect DUSPs to be particularly important in fine-tuning ERK function. Moreover, as there is a higher frequency of RAS-ERK mutations at relapse (Eleveld et al., 2015), it is of clinical importance to determine how ERK is regulated by DUSPs in NB cells. It is worth noting that JNK and p38 signalling can also influence NB (Chen et al., 2016a, Marengo et al., 2013), therefore other DUSPs may also be functionally important. Nonetheless, there is a dearth of studies that identify how DUSPs may function biochemically in NB cells and whether they could be manipulated to suppress NB cell growth.

1.5. Project overview

The importance of PTP function in NB is unequivocal as we and others have shown broader PTP inhibition is detrimental to NB cell survival or can promote neuronal differentiation (Clark et al., 2013, Clark et al., 2015, Boutterin et al., 2013, Tian et al., 2016). From what is described in **Chapter 1.3**, DUSPs can contribute to tumorigenesis in numerous tumour types in

both a tumour-promoting and -suppressing manner depending on the context. Furthermore, the previous PTP shRNA screen highlighted a subset of DUSPs that may promote NB cell survival. Taken together, the overarching aim of this thesis was to determine the function of DUSPs in NB cells and whether loss of function of one or more DUSPs could be proven detrimental NB cell growth or survival.

Initially, I performed an siRNA screen across the DUSP family across 4 NB cell lines to identify DUSPs that appeared to promote NB cell growth (**Chapter 3**). A handful of DUSPs were identified, including DUSP6. As DUSP6 has been implicated in a myriad of other cancers (reviewed in (Ahmad et al., 2018)), the role of DUSP6 in NB was characterised further using siRNAs and CRISPR/Cas9 (**Chapter 3**). Following this, although chemically targeting DUSPs has been hampered with specificity issues, an allosteric dual DUSP1/6 inhibitor, BCI, has been identified and demonstrates cytotoxicity in many cancer models (Wu et al., 2018, Ramkissoon et al., 2019, Kaltenmeier et al., 2017). Therefore, I then investigated whether BCI could be used to therapeutically target NB (**Chapter 4**). A key goal of the study was to determine which DUSPs drive NB cell growth and whether they do this independently or redundantly. To this end, the other DUSP candidates from the siRNA screen were then characterised further using CRISPR/Cas9 (**Chapter 5**). Furthermore, the redundant nature of DUSPs was investigated by targeting multiple DUSPs concurrently. Lastly, ALK is a potent oncogene that can drive an aggressive NB phenotype via the RAS/ERK, PI3K/AKT and JAK/STAT3 pathway (Trigg and Turner, 2018). DUSPs appear critical regulators of ERK signalling and can influence the AKT and STAT3 pathways in a range of cancer cell types, therefore we investigated whether DUSPs were regulated downstream of ALK (**Chapter 6**). Considering DUSP6 appeared to be tightly regulated by ALK, we finally investigated whether knockout of DUSP6 could improve molecular therapies targeting ALK and performed a phosphoproteomic screen to characterise the ALK-DUSP6 relationship and to identify regulatory pathway downstream of DUSP6 (**Chapter 6**).

1.5.1. Project aims

Aim 1: Use RNA interference (RNAi) and gene editing to identify DUSPs that promote NB cell growth (**Chapter 3** and **Chapter 5**)

Aim 2: Determine whether the dual DUSP1/6 inhibitor BCI could be used to therapeutically target NB cells (**Chapter 4**)

Aim 3: Understand the functional role of DUSPs downstream of oncogenic ALK signalling in NB cells (**Chapter 6**)

Chapter 2. Materials and methods

2.1. Cell culture techniques

2.1.1. Mammalian cell lines

Over the past few decades numerous patient-derived NB cell lines have become available as models for NB *in vitro*. The biological features of many of these cell lines have been well characterised (Thiele, 1998) and a subset of these established NB cell lines are used here (**Table 2.1**). KELLY, IMR-32 and SK-N-AS cells were a gift from Prof. Frank Speleman, University of Ghent. LAN-5 and SK-N-BE(2) were obtained from the Children's Oncology Group Cell Culture and Xenograft Repository, Texas Tech University Health Sciences Center, USA. NB1 cells were a gift from Prof. Ruth Palmer, University of Gothenburg. SH-SY5Y and HEK293T were purchased from ATCC and LAN-1 cells were a gift from Prof. John Anderson, UCL, London. The majority of the cell lines derive from a metastatic site rather than a primary site. Considering the heterogeneity of NB tumours (Ngan, 2015), it was important to include cells with both neuronal and Schwannian characteristics. Consequently, LAN-5 and SH-SY5Y cell lines, displaying neuronal morphology, were compared to the others that appear Schwannian. HEK293T cells were included as a non-NB control cell line for chemical treatments performed with a dual DUSP1/6 inhibitor, BCI (**Chapter 4**). The genetic lesions present in each of the cell lines are displayed in **Table 2.2**. An important aspect of this study was the role of ALK signalling therefore it was important that the ALK status of the cell lines used was variable.

Table 2.1 – Cell lines used in project. Brief description indicates cancer type and origin of sample.

Cell line	Brief description
IMR-32	Neuroblastoma - Abdominal metastases
KELLY	Neuroblastoma
LAN-1	Neuroblastoma - Bone marrow metastases
LAN-5	Neuroblastoma - Bone marrow metastases
NB1	Neuroblastoma - Cervical lymph node metastasis
SH-SY5Y	Neuroblastoma - Bone marrow metastases
SK-N-AS	Neuroblastoma - Bone marrow metastases
SK-N-BE(2)	Neuroblastoma - Bone marrow metastases
HEK293T	Human embryonic kidney - Fetal kidney

Table 2.2 – Genetic lesions in NB cell lines. Displayed are the hallmark genetic lesions, including chromosomal aberrations and sequence variations, for NB cell lines used in this study.

Cell line	MYCN status	ALK status	p53 status	1p36 deletion	11q deletion
IMR-32	Yes	WT	WT	Yes	Yes
KELLY	Yes	F1174L	P117T	Yes	Yes
LAN-1	Yes	F1174L	C182 Stop	Yes	-
LAN-5	Yes	R1275Q	WT	Yes	No
NB1	Yes	Amplified	WT	Yes	Yes
SH-SY5Y	No	F1174L	WT	No	Yes

SK-N-AS	No	WT	H168R	Yes	Yes
SK-N-BE(2)	Yes	WT	C135F	Yes	Yes

2.1.2. Cell passage

Cells were incubated at 37°C and 5% CO_2 in a humidified incubator. All cells were cultured in RPMI medium + Glutamax (Gibco) containing 10% FBS (Gibco), 100 U/ml Penicillin, 0.1 mg/ml Streptomycin (Sigma-Aldrich) and 25 mM HEPES (Fisher Scientific). When cells reached 70-90% confluency they were passaged. Briefly, cells were rinsed gently in Dulbecco's phosphate-buffered saline (DPBS) (Gibco) then incubated with 1x Trypsin-EDTA (Sigma-Aldrich). Once cells had detached, fresh media was added and cells were re-plated at low density in a new flask. For long-term storage, cells were aliquoted in cryovials (Thermo Fisher Scientific) and kept in liquid nitrogen. Fresh media containing 10% dimethyl sulfoxide (DMSO) (Sigma-Aldrich) was used as the freezing media for all cell lines.

To seed cells into multi-well plates (6-well or 12-well Corning™ Costar™ cell culture plates, Fisher Scientific; Nunc™ MicroWell™ 96-Well Microplate, Thermo Fisher Scientific), 10 µl of the cell suspension was pipetted onto a haemocytometer and cells were counted and averaged across three fields (each 10^{-4} mm^3).

2.1.3. Chemical treatments

Cells were treated with a wide range of chemicals (**Table 2.3**). In cell-based assays, unless stated otherwise, cells were treated 24 hours after seeding.

Table 2.3 – Chemicals used in cell-based assays and for antibiotic selection. Included are the function of the chemical, its solvent and the source. DMSO, dimethyl sulfoxide; BSO, L-Buthionine-(S,R)- sulfoximine; H20, Water; EGFR, Epidermal Growth Factor Receptor; FGFR, Fibroblast Growth Factor Receptor; MCB, Monochlorobimane; ALKAL1, ALK-activating ligand 1; GSH, glutathione.

Chemical	Function in assays	Buffer	Source
BCI	DUSP1/6 inhibitor	DMSO	Prof. A Vogt, University of Pittsburgh, USA
BCI-215	DUSP1/6 inhibitor	DMSO	Prof. A Vogt, University of Pittsburgh, USA
Doxycycline	Antibiotic selection marker	Water	Sigma-Aldrich, Dorset, UK
G418	Antibiotic selection marker	Water	Sigma-Aldrich, Dorset, UK
Puromycin	Antibiotic selection marker	Water	Merck, Gillingham, UK
EGF	Activation of EGFR	Water	Sigma-Aldrich, Dorset, UK
FGF	Activation of FGFR	Water	Peprotech, London, UK
BSO	Reduction of GSH levels	Water	Acros Organics, Belgium
SP600125	JNK inhibitor	DMSO	Insight Biotechnology, Middlesex, UK
SB202190	P38 inhibitor	DMSO	Insight Biotechnology, Middlesex, UK
MK-2206	AKT inhibitor	DMSO	Cayman chemical, Michigan, USA
U0126	MEK1/2 inhibitor	DMSO	Cell guidance systems, Cambridge, UK
MCB	Detection of GSH	PBS	Sigma-Aldrich, Dorset, UK

	production		
ALKAL1	ALK agonist	Water	Prof. R. Palmer, University of Gothenburg, Sweden
Crizotinib	ALK inhibitor	DMSO	Merck, Gillingham, UK
Lorlatinib	ALK inhibitor	DMSO	Sigma-Aldrich, Dorset, UK
Cyclohexamide	Protein synthesis inhibitor	DMSO	Prof. Owen Williams
MG132	Proteosome inhibitor	DMSO	Merck, Gillingham, UK

2.2. DNA-based assays

2.2.1. CRISPR-Cas9 gRNA design and generation

GRNA design

In a CRISPR-Cas9 system, a guide RNA (gRNA) directs a Cas9 endonuclease to the site of editing. In this project, gRNA design was performed using a combination of the Benchling online platform (https://www.benchling.com/) and the SNAP2 software (Hecht et al., 2015). The Benching platform generated a list of gRNAs, ranked by on- and off-target scores (Doench et al., 2016), for each DUSP gene. A subset of gRNA's were selected based on two criteria:

- Downstream from the DUSP start codon and any potential alternative start codons
- Upstream from the DUSP catalytic site and any other regions of known functional importance.

Out-of-frame indels generated in these positions should therefore lead to very truncated and hence dysfunctional protein. Following this, I used the

SNAP2 software which predicts the functional effect of each amino acid variant within a protein sequence (Hecht et al., 2015). GRNAs were selected that were within regions predicted to be of functional importance to the protein. This should then result in any in-frame mutation also leading to dysfunctional protein, an important consideration when later using any pooled, indel-containing cell populations. All gRNAs used in this project are presented in **Table 2.4**. The Benchling software also identified regions likely to exhibit off-target effects. The three regions with the highest off-target score for DUSP6 gRNA 3 also presented in **Table 2.4** (last three rows).

Table 2.4 – GRNA sequences used to target DUSP genes. Also included are the potential off-target sites (OTS) for DUSP6 gRNA 3 (last three rows).

Target gene	Guide RNA sequence (PAM sequence)
DUSP1	CGTTGACAGAGCCGGCGATGTGG
DUSP3	GTTGCCCACGTAGATCCGCGGGG
DUSP4	AGCGCACGTTGACCGAACCTAGG
DUSP6 (gRNA 1)	CGTGCCCTTCGCGTCGGAAATGG
DUSP6 (gRNA 3)	GTTCGGCTCCGATCGCCAACCCC
DUSP6 (gRNA 4)	CATCGAGTCGGCCATCAACGTGG
DUSP10	ACGTATATGCCCTCATCCAGCGG
DUSP12	ACCAGTGCACCAACACCGCACGG
DUSP26	AGCCTGTAACCATGCCGACGAGG
DUSP6 gRNA 3 OTS1	TGGGCGATCGGAACGGAAAC
DUSP6 gRNA 3 OTS2	TTGGGGATCGGAACCGGAAC
DUSP6 gRNA 3 OTS3	TTGACGATCTGAGACGAAAC

Generation of gRNA constructs

The DUSP4 and DUSP6 gRNAs were inserted into a PU6 vector which contained a gRNA scaffold site and puromycin and ampicillin resistant cassettes (Addgene, #60955) (**Fig. 2.1, left vector**). To sequentially digest the plasmid, 5 µg pU6 was incubated with 1 µl BstXI (Thermo Fisher Scientific) for 30 minutes at 55°C, then overnight at 37°C. Following this, the BstXI enzyme was heat inactivated by incubation at 80°C for 20 minutes, spin purified using the QIAquick PCR Purification Kit (Quigen) and eluted in 30 µl MQ. The purified DNA was digested by 1 µl Blpl (Thermo Fisher Scientific) using the same method to generate the pU6 double digest. Primers were designed for the gRNA oligonucleotide (**Table 2.5**) and reconstituted to 100 µM in MQ, and annealed using Taq polymerase buffer (Invitrogen) with the following cycle: 95°C for 5 minutes then -5°C per minute to 25°C. To ligate the gRNA, 1 µl annealed oligo, 7 µl double digest and 0.6 µl T4 DNA ligase (Promega) were incubated overnight at room temperature. 40 µl competent DH5α bugs were transformed with 7 µl of the ligated product. Alternatively, the DUSP1, DUSP3, DUSP10, DUSP12 and DUSP26 gRNAs were pre-made in a mammalian CRISPR vector that also contained the Cas9 gene under a CBh promoter (synthesised by Vectorbuilder, USA) (**Fig. 2.1, right vector**). These vectors were ordered in competent E.coli.

Figure 2.1 – Plasmids used to introduce gRNA's. GRNA's were inserted manually into the PU6 plasmid (left) in between the BstX1 and BlpI restriction sites or pre-made in the vectorbuilder plasmid (right).

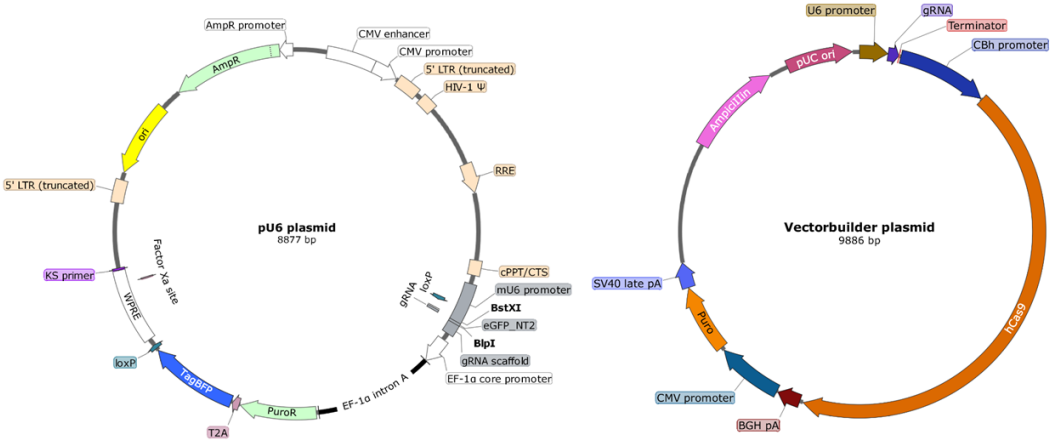

Table 2.5 – Primers used to introduce gRNA sequence into the PU6 plasmid. DUSP4 and DUSP6 gRNA sequences are in red and the BstXI and Blpl restriction enzyme sites are in blue and black respectively. FWD, Forward; REV, Reverse.

Gene	Primer
DUSP4 – FWD	TTGAGCGCACGTTGACCGAACCTGTTTAAGAGC
DUSP4 – REV	TTAGCTCTTAAACAGGTTCGGTCAACGTGCGCTCAACAAG
DUSP6 - FWD	TTGCATCGAGTCGGCCATCAACGGTTTAAGAGC
DUSP6 - REV	TTAGCTCTTAAACCGTTGATGGCCGACTCGATGCAACAAG

Plasmid propagation

The PU6 and vectorbuilder plasmids containing the DUSP gRNAs were inoculated and amplified. Briefly, 40 µl E.coli were streaked on agar plates (Invitrogen) containing 0.1% Ampicillin. The following day, colonies were picked into 3 ml 2.5% (w/v) Luria Broth Base (LB) (Invitrogen) and left shaking overnight at 37°C. 1.5 ml of bacteria was purified using the QIAprep Spin Miniprep Kit (Quigen) and the presence of the gRNA plasmid was confirmed on an agarose gel. Subsequently, the remaining 1.5 ml LB broth

was added to 100 ml LB broth containing 0.1% Ampicillin, left shaking overnight at 37°C and purified using the HiSpeed Plasmid Maxi Kit (Quigen). The gRNA plasmid was eluted in 1ml MQ and the concentration was quantified by absorbance at 260 nm on a NanoDrop ND-1000 spectrophotometer.

2.2.2. Genomic DNA extraction

To perform the T7 endonuclease 1 (T7E1) assay or prepare samples for sequencing, DNA was extracted from cells and the gRNA region was amplified via Polymerase chain reaction (PCR). Cells were trypsinized as described previously and re-suspended in fresh media. The cell suspension was centrifuged at 300 xg for 5 minutes and the pellet re-suspended in 50µl QuickExtract™ DNA Extraction Solution (Cambio). Cells were vortexed for 15 seconds, incubated at 65°C for 15 minutes and vortexed again for 15 seconds. Following this, samples were incubated at 100°C for 2 minutes and stored at -20°C or used immediately for PCR.

2.2.3. Determination of indels within a population

Polymerase chain reaction (PCR)

Indels present within a cell population were analysed directly via Sanger sequencing or indirectly via the T7E1 assay (**Fig. 2.2A**). The initial step for conducting both these analyses is the amplification of the corresponding gRNA target region. For each gene, primers (Sigma-Aldrich) were designed approximately 200 - 600 bp either side of the gRNA site (**Table 2.6**). Primers were also designed for the three off-target sites of DUSP6 gRNA 3 (**Table 2.6, last three rows**). Primers were reconstituted to 100 µM in Milli-Q water (MQ). The DUSP6 gRNA regions and off-target regions were amplified using the Phusion High-Fidelity DNA Polymerase (Thermo Fisher Scientific). In each 25 µl PCR reaction, 1.5 µl extracted DNA was added to a mastermix containing 0.5 U Phusion DNA polymerase, 0.5 µM forward and reverse primer, 0.2 mM of each dNTP and 1X Phusion HF Buffer. The PCR reaction was run as follows: 98°C for 30 seconds; 40 cycles of 98°C

for 10 seconds, 68°C for 30 seconds, 72°C for 1 minute; 72°C for 10 minutes; store at 4°C. For all other DUSP genes, DNA was amplified using Taq polymerase (Invitrogen). In each 50 µl PCR reaction, 1.5 µl extracted DNA was added to a mastermix containing 1.25 U Taq DNA polymerase, 1.5 mM Magnesium Chloride, 0.25 µM forward and reverse primer, 0.2 mM of each dNTP and 1X PCR Buffer. The PCR reaction was run as follows: 94°C for 3 minutes; 40 cycles of 94°C for 45 seconds, 60°C for 30 seconds, 72°C for 1 minute; 72°C for 5 minutes; store at 4°C. DNA product was confirmed on an agarose gel and then spin purified using the QIAquick PCR Purification Kit (Quigen).

Table 2.6 – Primers designed to amplify a gRNA target region. Primers were designed 200 - 600 bp either side of the gRNA site or an off-target site (OTS).

Target	Forward (5' - 3')	Reverse (5' - 3')
DUSP1	CTCAAAGGTACGCCCTCGG	GGAGCTGATGTCTGCCTTGT
DUSP3	CATGTCGGGCTCGTTCGAGCTC	CAGGGTTCCAGTTCCTTGGCC
DUSP4	GACTGCTATGTGACCGCGA	GAGGACTTGAACCTCGCACT
DUSP6	TGAGACGCTCGCTGTTTGTA	CTGAGCGGAGCAGAGGTATT
DUSP10	CGACAGGGTAGTAGTGGCAC	GACAGTGATCTTGCCCTGCT
DUSP12	ACTCGATGGTAGGGCAGGAA	AATCGGGGTGGGTGTCTAGC
DUSP26	TGGTAACTGGCTTTGGGCTT	GCTGCCTTTTCCCAGAGACA
DUSP6 gRNA3 OTS1	CGTGTGCTGCCAGTGTAAGA	ACCAGGGAAAGGAGGCAAGT
DUSP6 gRNA3 OTS2	ATAGTCTGCGAGTGGTTGCC	ACAGGCATATCAGAAGCTGGG
DUSP6 gRNA3 OTS3	GGAGGCTATTGGGGTCTTGA	CCTGGGGAGATTTGCTGAAGT

T7 Endonuclease 1 assay

T7E1 identifies and cleaves any mismatches in double-stranded DNA, therefore the proportion of cleaved product compared to full length product correlates with the amount of editing within the population (Sentmanat et al., 2018). 1x T7 Reaction buffer (New England Biolabs) was added to the purified DNA and samples were re-hybridised in a thermocycler by a denaturation step at 95°C for 5 minutes followed by slow cooling of -0.1°C per second to 25°C (**Fig. 2.2A**). 1 µl T7E1 (New England Biolabs) was added and samples were incubated at 37°C for 15 minutes to allow enzyme cleavage. Samples were electrophoresed on a 1.5% (w/v) agarose gel. The density of each band was quantified using the Image Studio Lite software (Licor). Following quantification, the formula displayed in **Figure 2.2B** was used to determine the percentage of edited cells.

Sanger Sequencing

Alternatively, samples were prepared for sequencing to determine the indels present in a subclone or percentage of indels within a mixed population (**Fig. 2.2A**). After PCR purification, the concentration of DNA was quantified by absorbance at 260 nm on a NanoDrop ND-1000 spectrophotometer. 10 ng/µl extracted DNA was sent for sanger sequencing along with 3.2 pmol/µl of the upstream or downstream primer (Source Bioscience). All sub-clone sequences were analysed with the ICE v2 CRISPR Analysis Tool (Synthego). This tool provides details on the frequency of each indel within each population.

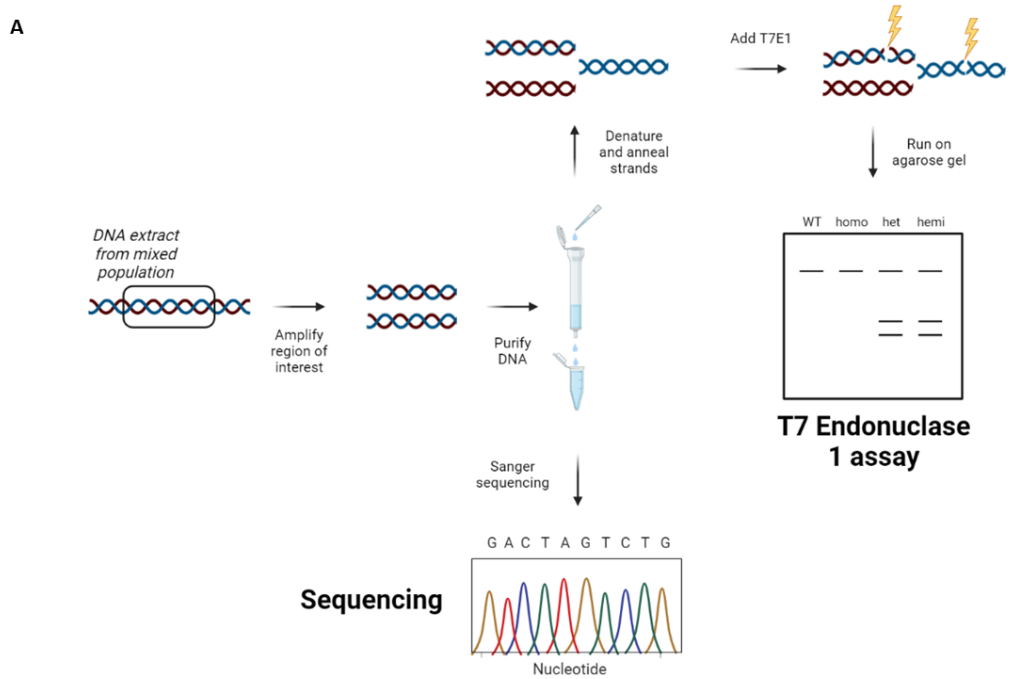

B

$$\%\text{NHEJ events} = 100 \times [1 - (1 - \text{fractioncleaved})^{(1/2)}],$$

where the fraction cleaved is defined as $\frac{(\text{density of digested products})}{(\text{density of digested products} + \text{undigested parental band})}$.

Figure 2.2 – Methods used to determine CRISPR/Cas9 efficiency. (A) Sample process workflow for Sanger sequencing and T7 endonuclease (T7E1) assay. A PCR was performed on DNA from a mixed population to amplify the region surrounding the gRNA site and then the amplified product was purified (Qiagen). Either the sample was sent directly for sanger sequencing or the T7E1 assay was performed. To this end, the DNA strands were denatured and re-annealed in a thermocycler and the T7E1 was added to cleave mismatched DNA. Lastly, samples were electrophoresed to identify the proportion of edited DNA. (B) The formula used to determine the proportion of indels within a sample. WT, wild-type; homo, homozygous; het, heterozygous; hemi, hemizygous; NHEJ, non-homologous end joining.

2.3. RNA-based assays

2.3.1. RNA extraction

To extract RNA from cells, cells were lysed using the mini RNeasy kit (Quigen). All RNA extractions were performed directly on monolayer cells in 12-well plates. Briefly, cells were washed twice in DPBS and then lysed

in 350 µl buffer RLT for 5 minutes. Cells were treated with an equal volume of 70 % ethanol and then transferred to the binding column. The samples were treated with an in-column DNAse 1 digestion kit (Qiagen). For the DNAse 1 digestion of each sample, 30 kunitz units of DNAse was mixed with 70 µl buffer RDD and after being applied to the column, was incubated for 15 minutes at room temperature. Following this, the column was washed with 700µl RWT buffer, and twice with 500 µl RPE buffer, and was eluted in 30 µl RNase/DNase free water. The concentration of RNA was quantified by absorbance at 260 nm on a NanoDrop ND-1000 spectrophotometer.

2.3.2. cDNA synthesis

RNA was immediately reverse-transcribed to cDNA using the Transcriptor High Fidelity cDNA Synthesis Kit (Roche). For each 20 µl reaction, 11 µl of RNA sample was mixed with 1.2 nmol random hexamer primer and incubated for 5 minutes at 65°C. Following this, 1x Transcriptor Reverse Transcriptase Reaction Buffer, 20 U Protector RNase inhibitor, a deoxynucleotide mix (1 mM each) and 10 U Transcriptor Reverse Transcriptase were added to the reaction. Samples were placed in the thermocycler for the following reaction: 25°C for 10 minutes, 55°C for 60 minutes, 85°C for 5 minutes. Samples were then stored at -20°C.

2.3.3. Quantitative real-time PCR

Primers for quantitative real-time PCR (qPCR) were ordered against each member for the DUSP family using the Harvard PrimerBank (https://pga.mgh.harvard.edu/primerbank/). For primers that did not amplify cDNA efficiently, new primers were designed using the Primer Blast online tool (https://www.ncbi.nlm.nih.gov/tools/primer-blast/). The design process contained the following parameters:

- Amplicon length between 80 – 200 bp
- Primer length between 18 – 22 bp
- Primer melting temperature ≤ 60°C

- Primer GC content < 65
- Primer Tm difference < 3°C

Following this, the OligoAnalyzer™ Tool (Integrated DNA Technologies) was used to determine whether primers could form hairpin structures, self-dimers or heterodimers. Primers used for qPCR reactions are presented in **Table 2.7**.

Table 2.7 – Primers deigned for qPCR of the DUSP family.

Target	Forward (5' - 3')	Reverse (5' - 3')
DUSP1	TGTGGAGGACAACCACAAGG	CTCGTCCAGCTTGACTCGAT
DUSP2	CTTGCCCTACCTGTTCCTGG	GTAGCGGAAAAGGCCCTCAA
DUSP3	AAGGACTCCGGCATCACATAC	AAGCCTGGTCAATGAAGTCGG
DUSP4	AGCATCATCTCGCCCAACTT	AGACCGGAAAGCTGAAGACG
DUSP5	CCTGCTGAATGTCTCCCGAC	GCCTCCCTTTTCCCTGACAC
DUSP6	TAGATACGCTCAGACCCGTG	TGTGCGACGACTCGTATAGC
DUSP7	CATCCGCTCCATCATCCCC	CCTCGTCGTAGAGCAGCAC
DUSP8	TCCCGAGGAAGGTGATGGAT	AGCTTGGAGCAGCAGATGTT
DUSP9	GGCATCCGCTACATCCTCAA	ACTCAATGGCCTCCGGAAAG
DUSP10	TGAAGCACACTCGGATGACC	CCTCGAACTCTAGCAACTGCC
DUSP11	ATAGGTGCCGGGGACATTG	TGGTTGCATGAGATGTGCTGA
DUSP12	AGCCAGGATTGTATTTCGGTG	CCGAGTCCACTGTTAGCACG
DUSP16	CTGCTGGAAAGTGGAACGGA	CCTGTTGCAACCTTCGCTTC
DUSP18	GCTGACTCCCCTAACTCACG	CCGGCATGACTTGGTCCAC
DUSP22	GGCAGTGGCTGAAGGAAGAA	GAGCCAGTGCCGGAAAACT
DUSP26	TCAATGTCTTCGAGTTGGAGC	TCCTGGTCTCCGAGATAGAGG
GAPDH	ATGACATCAAGAAGGTGGTG	CATACCAGGAAATGAGCTTG

Prior to each qPCR experiment, a PCR was run for each set of primers to confirm only one product is amplified and that the product matches the intended amplicon size. The melt curve analysis of the qPCR software also confirmed a single product was amplified. For each set of primers a primer efficiency test was also performed. This experiment contained a standard curve of cDNA using a 3-fold serial dilution starting with undiluted cDNA.

Subsequently, the average Ct was plotted against the Log(Sample quantity) and the gradient of the linear regression was converted into primer efficiency using the equation:

$$Efficiency\ (\%) = \left(10^{\frac{-1}{Slope}} - 1\right) \times 100$$

Primers were only used in the project if their efficiency was within 70 – 130%. To perform the qPCR, cDNA was initially diluted 1:10 in MQ water. For each 20 µl reaction, in a 96-well PCR plate (Bio-Rad) 2 µl diluted cDNA was mixed with 10 µl iTaq sybermix (Bio-Rad), 10 µM of the forward and reverse primer and MQ water. The plate was sealed with a Microseal 'B' Sealing Film (Bio-Rad) and placed in a CFX Connect PCR machine (Bio-Rad). The qPCR reaction was run as follows: 95°C for 2 minutes; 39 cycles of 95°C for 5 seconds, 60°C for 30 seconds; 95°C for 5 seconds then a melt curve with 0.5°C 5 second increments from 65°C to 95°C. Image analysis was performed on CFX Manager (Bio-Rad). Relative gene expression was determined using the threshold cycle (C_t) method (Schmittgen and Livak, 2008) where GAPDH was the internal control gene. In this method, the C_t value corresponds to the qPCR cycle at which the SYBR green signal crosses a threshold. Delta C_t (ΔC_t) is calculated by subtracting the C_t of the target gene from the C_t of GAPDH. Following this, delta delta C_t ($\Delta\Delta C_t$) is then calculated by subtracting the ΔC_t of the treated sample by the ΔC_t of the control sample. Lastly, the relative gene expression is then calculated using the formula: Fold change = $2^{-\Delta\Delta Ct}$.

2.4. Protein assays

2.4.1. Protein extraction

For Western blots

For western blotting experiments, protein extracts were obtained using a lysis buffer containing 50 mM Tris-base, 150 mM Sodium Chloride, 1% Triton X-100 and 0.02% Sodium Azide. Immediately before lysing cells, 1

mM protease inhibitor cocktail (Roche), 1 mM sodium orthovanadate and 1 mM sodium fluoride were added to the lysis buffer. Cell were rinsed with DPBS and cells were then incubated in 100 - 200 µl lysis buffer on ice. After 30 minutes, lysates were centrifuged at 13,000 rpm for 15 minutes at 4°C and the supernatants removed and stored at -20°C.

For Phosphoproteomics

For the phosphoproteomics experiments, protein extracts were obtained using a lysis buffer containing 8M urea and 20mM HEPES, pH 8.0. Immediately before lysing cells, 1 mM sodium orthovanadate, 1 mM sodium fluoride, 1 mM β-glycerol phosphate and 2.5 mM disodium pyrophosphate were added to the lysis buffer. Cells were rinsed twice in DPBS containing 1 mM sodium orthovanadate and 1 mM sodium fluoride and then incubated in 300 µl lysis buffer on ice. Cells were scraped into an Eppendorf tube and sonicated at 50% intensity for 15 seconds and rested for 10 seconds, repeating three times. Lastly, cells were centrifuged at 13,000 rpm for 15 minutes at 4°C and the supernatant was snap-frozen on dry-ice.

2.4.2. Bradford Assay

The protein concentration was determined using the Bradford assay. 3.5 µl lysate was diluted in 350 µl of 25 % (v/v) Coomassie brilliant blue G-250 dye (Bio-Rad, diluted in a ratio of 1:5 in distilled water). Following this, 150 µl sample was aliquoted into two wells of a 96-well plate and the absorbance was read at 595nm on a FLUOstar OPTIMA (BMG Labtech) microplate reader. To determine protein concentration from absorbance, a standard curve was also run using a 2-fold serial dilution series of bovine serum albumin starting at 2 mg/ml (Bio-Rad).

2.4.3. Western blotting

After protein had been extracted and the concentration determined in accordance with the methods described above, samples were prepared for SDS polyacrylamide gel electrophoresis. 15 - 30 µg of protein was added to

the loading buffer (125 mM Tris-base (pH 6.8); 10% (v/v) glycerol; 2% (w/v) SDS; 0.025% (w/v) bromophenol blue; 2.5% (v/v) β-mercaptoethanol), heated for 5 minutes at 100°C and directly loaded into a gel.

To make 1 mm polyacrylamide gel sandwiches, a 10% resolving gel solution (375 mM Tris-base (pH 8.8), 10% Acrylamide/bis; 0.1% (w/v) SDS; 0.075% (v/v) APS; 0.12% (v/v) TEMED) was prepared and loaded. After a 30-minute polymerisation, a 5% stacking gel (125 mM Tris-base (pH 6.8); 4% Acrylamide/bis; 0.1% (w/v) SDS; 0.1% (v/v) APS; 0.12% (v/v) TEMED) was prepared and loaded. Gel sandwiches were then placed in a vertical electrophoresis cell (Bio-Rad) and samples were loaded, alongside 7 µl Precision Plus Protein Standards (Bio-Rad). The tank was filled with running buffer (25 mM Tris-base; 192 mM Glycine; 0.1% (w/v) SDS) and the electrophoresis ran at 100 V (constant voltage) for 1 hour 45 minutes. Protein was transferred from the gel to an Immobilon-P PVDF membrane (Millipore) in a Mini Trans-Blot® Electrophoretic Transfer Cell (Bio-Rad). Filter paper was soaked in transfer buffer (25 mM Tris-base; 192 mM Glycine; 20% (v/v) methanol) and PVDF filters in 100% methanol for 5 minutes. In the cell cassette, the gel and PVDF membrane were sandwiched between six filter sheets and enclosed in the fiber pads whilst submerged in transfer buffer. An ice block was added to the cell and the transfer was run at 100 V (constant voltage) for 1 hour.

Membranes were then soaked in 100% methanol for 1 minute and washed 2 x 5min in Tris-buffered saline (15.4 mM Trizma-HCL; 4.62 mM Tris-base, 150 mM Sodium Chloride; pH 7.6 using 2 M HCL (TBS)) with 1% (v/v) Tween (TBST). Membranes were blocked in 10% (w/v) dried skimmed milk (Sigma-Aldrich) in TBS for 1 hour and probed in primary antibody overnight at 4°C (**Table 2.8**). Primary antibody was diluted in 5% (w/v) dried skimmed milk with 0.02% (w/v) Sodium Azide. Membranes were washed 3 x 5 minutes in TBST, followed by incubation in 0.2 µg/ml secondary antibody conjugated to HRP dissolved in 5% (w/v) dried skimmed milk for 1 hour. Washing steps were repeated and membranes were incubated in TBS until detection. To detect the bound antibodies, 1.5 ml of Amersham ECL Prime Western Blotting Detection Reagent (GE Lifesciences) was added dropwise

to the membrane and incubated in the dark for 5 minutes. Membranes were wrapped in cling film and exposed to Amersham Hyperfilm ECL (GE Lifesciences) in an x-ray cassette (FUJI), followed by development in a Xograph Compact X4 processor.

To strip off antibodies, membranes were washed 2 x 5 minutes in distilled water, incubated in 200 mM (w/v) sodium hydroxide at 37°C for 30 minutes, shaken at room temperature for 30 minutes, then washed 2 x 5min in TBST. Membranes were re-probed multiple times; however, membranes were not re-probed for proteins of similar molecular mass directly after each other. Antibodies were re-used up to three times. Western blots were imaged on a Densitometer (Bio-Rad GS-800) and bands were quantified on the Image Studio Lite software (Licor). During quantification, each band was initially normalised to the loading control; either GAPDH, Actin or total protein. Samples were subsequently normalised to either the control lane or the blot average intensity.

Table 2.8 – Antibodies used for western blotting. Antibodies were re-used up to three times to detect protein.

Antibody	Species	Dilution	Details
phospho-ALK (Y1604)	rabbit	1 : 1,000	Cell Signalling Technology (#3341S)
ALK	mouse	1 : 1,000	Cell Signalling Technology (#3791S)
phospho-ERK (T202/Y204)	mouse	1 : 2,000	Cell Signalling Technology (#9106S)
ERK	rabbit	1 : 2,000	Cell Signalling Technology (#9102S)
phospho-AKT (S473)	rabbit	1 : 2,000	Cell Signalling Technology (#4060S)
AKT	rabbit	1 : 2,000	Cell Signalling Technology (#9272S)
phospho-JNK (T183/Y185)	rabbit	1 : 2,000	Cell Signalling Technology (#4668S)
JNK	rabbit	1 : 2,000	Cell Signalling Technology (#9252S)

phospho-p38 (T180/Y182)	rabbit	1 : 2,000	Cell Signalling Technology (#9211S)
p38	rabbit	1 : 2,000	Cell Signalling Technology (#9212)
DUSP6	rabbit	1 : 1,000	Abcam (ab76310)
cPARP	rabbit	1 : 2,000	Cell Signalling Technology (#5625S)
GAPDH	rabbit	1 : 5,000	Cell Signalling Technology (#2118S)
Cas9	rabbit	1 : 5,000	Abcam (ab189380)
FLAG-M2	mouse	1:10,000	Sigma-Aldrich (F3165)

2.4.4. Phosphoproteomics

Two phosphoproteomic experiments were analysed in this project. The first investigated the role of BCI in NB cells and was previously performed by Dr. Vruti Patel (unpublished; **Chapter 4**). Dr. Vruti Patel seeded IMR-32 and KELLY cells in 100 mm petri dishes (Fisher Scientific). After 48 hours, cells were treated with 2 µM BCI for 2 hours followed by cell lysis. The second phosphoproteomic experiment, done by myself, investigated the role of DUSP6 in NB cells (**Chapter 6**). Briefly, 2E2 and 2E2g4 were treated with 1 µg/ml dox in T75 flasks and incubated for 7 days (Fisher Scientific). This promoted CRISPR/Cas9 expression and editing of the DUSP6 gene. Dox is known to influence the ERK and AKT signalling pathways (Chang et al., 2014, Chen et al., 2009a). Hence, cells were split into 100 mm petri dishes and incubated for 7-9 days in the absence of dox. During this incubation, cells were passaged into multiple 100 mm petri dishes so that biological replicates could be performed. Cells were treated with 30 nM lorlatinib for 1 hour and lysed. In both phosphoproteomic experiments, four biological replicates of the drug treatments were performed each at a different time.

Following this, samples were analysed using mass spectrometry (MS) as reported in Hijazi et al. (2020) and Casado et al. (2013) in collaboration with Dr. Vinothini Rajeeve and Prof. Pedro Cutillas at the Barts Cancer Institute.

In brief, the proteins in the protein lysates were digested into peptides using trypsin as previously described (Alcolea et al., 2012, Montoya et al., 2011). Phosphopeptides were enriched from total peptides by TiO_2 chromatography essentially as reported previously (Larsen et al., 2005). Dried phosphopeptides were dissolved in 0.1% Trifluoroacetic acid and analysed by nanoflow ultimate 3000 RSL nano instrument coupled on-line to a Q Exactive plus mass spectrometer (Thermo Fisher Scientific). Gradient elution was from 3% to 28% solvent B in 90 min at a flow rate 250 nL/min with solvent A being used to balance the mobile phase (buffer A was 0.1% formic acid in water and B was 0.1% formic acid in acetonitrile). The spray voltage was 1.95 kV and the capillary temperature was set to 255°C. The Q-Exactive plus was operated in data dependent mode with one survey MS scan followed by 15 MS/MS scans. The full scans were acquired in the mass analyser at 375 - 1500 m/z with the resolution of 70 000, and the MS/MS scans were obtained with a resolution of 17 500.

MS raw files were converted into Mascot Generic Format using Mascot Distiller (version 2.6.1) and searched against the SwissProt database (release Sep 2018) restricted to human entries using the Mascot search daemon (version 2.6.0). Allowed mass windows were 10 ppm and 25 mmu for parent and fragment mass to charge values, respectively. Variable modifications included in searches were oxidation of methionine, pyro-glu (N-term) and phosphorylation of serine, threonine and tyrosine. The data from these analyses were then given back to us for further study. An example of the data output is presented in **Table A2**.

2.4.5. Immunofluorescence

The abundance of cleaved Caspase 3 (cCas3), a measure of apoptotic signalling, was detected using immunofluorescence. Briefly, 5 mm acid-treated glass coverslips were coated with 0.5 mg/ml poly-L-lysine (MB Biomedicals UK, 2.5 mg/ml stock diluted in distilled water) in a 12-well plate and left to air dry for 1 hour. Coverslips were washed in media and cells were seeded. After chemical treatment, coverslips were washed in DPBS

three times and fixed in 4% PFA for 30 minutes at room temperature. Following this, the surface was blocked in PBS containing 1% bovine serum albumin (BSA) (w/v) and 0.05% (v/v) TritonX-100 for 1 hour and washed in PBS containing 0.1% (w/v) BSA and 0.05% (v/v) TritonX-100 3 x 5 minutes. Coverslips were incubated in a cCas3 antibody (Cell Signalling Technology, #9661; 1:250 dilution) or rabbit IgG control (Thermo Fisher Scientific, matched concentration to cCas3) for 1 hour. After repeating the washing steps, coverslips were incubated in goat anti-rabbit Alexa Fluor488-conjugated secondary antibody (Thermo Fisher Scientific; 1:300) containing 1 µg/ml DAPI (Severn Biotech Ltd.) for 1 hour. Primary and secondary antibodies were diluted in PBS containing 3% BSA (w/v) and 0.05% (v/v) TritonX-100. After repeating the washing steps, coverslips were mounted using ProLong Gold (Thermo Fisher Scientific) and left in the dark overnight.

Five low-resolution images were taken per sample and data analysis was performed in ImageJ (Schneider et al., 2012) and Fiji (Schindelin et al., 2012). For each image, cells stained with DAPI were counted using the 'Find maxima' function (**Fig. 2.3A**). The size threshold was kept constant within each experiment. If there were few cells with an increases of Cas3 cleavage, they were counted manually (**Fig. 2.3B**). However, if there was a high proportion of cells with an increase in Cas3 cleavage they were counted by subtracting Cas3-negative cells from total cells.

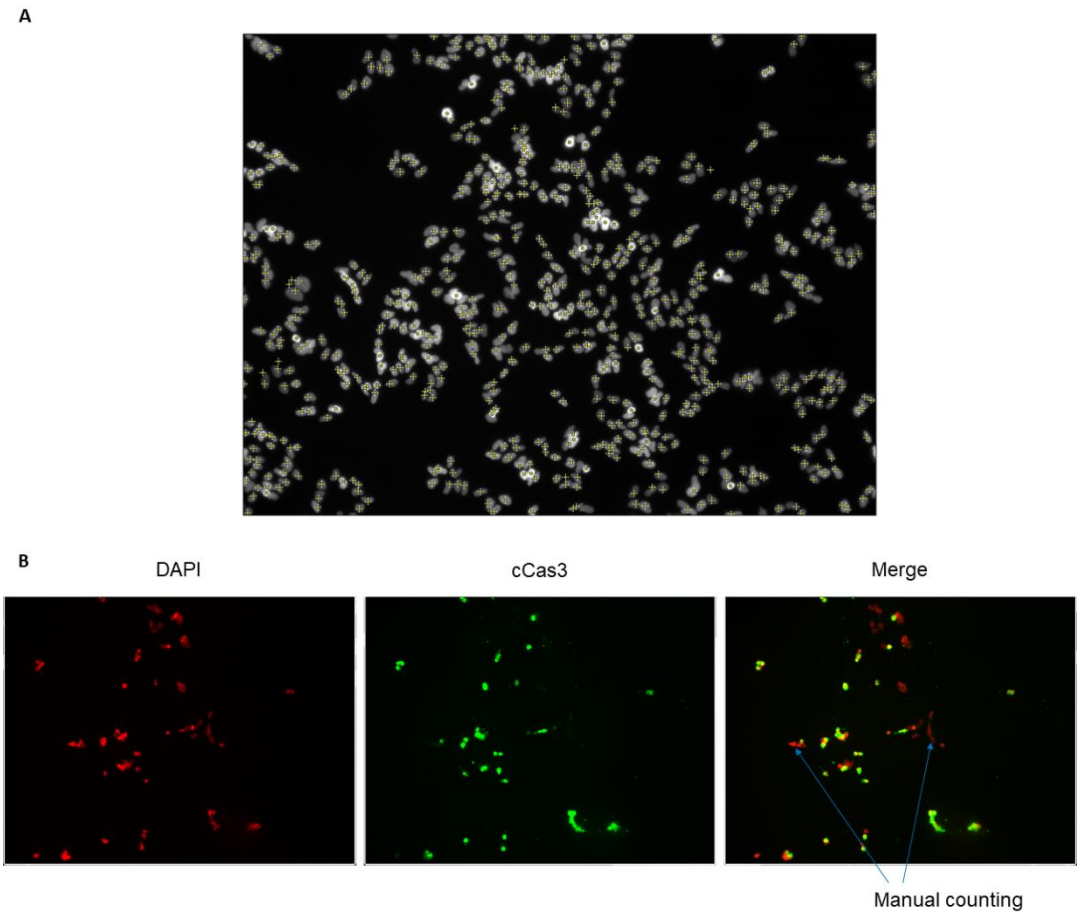

Figure 2.3 – Counting cells with high cCas3 using ImageJ. (A) The 'find maxima' tool was used to determine the number of cells present. The size threshold remained constant throughout each experiment. (B) In cases where there was a very high proportion of cells with high cCas3, the number of cCas3 cells was determined by subtracting the DAPI cells not overlaid with cCas3 (marked by arrows) from the total number of cells present.

2.5. Cell-based assays

2.5.1. Transient cell transfection with plasmid DNA

Plasmid transfections were carried out in either 6-well or 12-well plates using the Lipofectamine 2000 Reagent (Invitrogen). The lipofectamine 2000 reagent and DNA plasmid were diluted in OPTI-MEM (Gibco) and incubated separately for 5 minutes at room temperature. These were then mixed and incubated for 5 minutes before adding dropwise to cells. In a 12-well plates, lipofectamine was used at a 1:3 ratio with 200 µl total DNA-lipofectamine

mix per well whereas in 6-well plates, lipofectamine was used at a 1:2 ratio with 500 µl total DNA-lipofectamine mix per well.

2.5.2. Transient cell transfection with siRNA

NB transfection with siRNA was performed using lipofectamine RNAiMAX Reagent (Invitrogen). The lipofectamine RNAiMAX Reagent (Invitrogen) and siRNA's were diluted in OPTI-MEM (Gibco) and incubated for 5 minutes at room temperature. The RNAiMAX and siRNA's were then incubated together for 5 minutes before adding dropwise to cells. A range of Dharmacon ON-TARGETplus siRNA reagents were used as tools to decrease gene expression in both cell viability and biochemical assays (**Table A1**). Each siRNA reagent is a pool of 4 individual siRNAs that each target a different region of the gene. In cases where siRNA pools have been deconvoluted, a subset of individual siRNAs with the highest on-target effect (judged by qPCR; see below) were pooled and used for further assays. When used in cell viability assays, 5 nM siRNAs were added in triplicate to 96 well plates and cell viability was measured after 6 days. For assays where two siRNAs were added to the same well, 2.5 nM of each individual siRNA was added, ensuring total siRNA per well remained at 5 nM for all experiments. For biochemical analysis, siRNAs were added at 5 nM to 12 well plates and after 24 hours, cells were lysed and protein extracted. SiRNA targeting Kif11 (Invitrogen), a motor protein essential to mitotic division, was used as a positive control (induces efficient cell death) and non-targeting siRNA (SCR) as a negative control.

The large-scale siRNA screen in KELLY cells and DUSP-null subclones was performed on semi-automated robots in a reverse-transfection format. These assays were kindly assisted by Dr. Denise Barrios De Pilger and Dr. Robin Kettler (UCL). Briefly, 2.5 nM siRNA was aliquoted into a 384-well plate (Thermo Fisher Scientific) using an Echo Liquid Handler (Labcyte). Following this, 75 nl lipofectamine RNAiMAX Reagent was diluted in 10 µl OPTI-MEM (Gibco) and added to each well using a Tecan Fluent Robot (TECAN). The lipofectamine-siRNA mix was incubated for 30 minutes then

1000 cells were added in 40 µl media using a 96 well microplate dispenser. Cells were left to incubate for 7 days before cell viability was measured. Various optimisation assays were performed to minimise the time difference for lipofectamine-siRNA mix incubation between wells. Unfortunately, there remained some systematic variation. However, as the plate positions of each siRNA was deliberately varied for each experiment, we believe this variation did not skew the overall results.

2.5.3. Generation of inducible CRISPR/Cas9 system

CRISPR/Cas9 is a ubiquitous technique used to engineer biological systems (Ran et al., 2013). Prior to this project, a previous post doc in our lab (Dr. Vruti Patel) had already established an inducible CRISPR system where Cas9 expression was under the control of a tetracycline promoter in a lentiviral vector (Horizon; #VCAS11227). Briefly, IMR-32 and KELLY cells were seeded in 6-well plates. The following day, media was replaced with fresh media containing the lentiviral vector using a multiplicity of infection of 0.4. After 24 hours, cells were treated with 4 µg/ml blasticidin and underwent selection for 5 days, resulting in inducible cell populations termed iKELLY and iIMR-32. Subsequent treatment with doxycycline (dox) resulted in a dose-dependent increase in Cas9 protein (Dr. Vruti Patel, manuscript in preparation). Single cell cloning of the iKELLY and iIMR-32 cells was performed to identify subclones with highly inducible Cas9 expression, termed 2E2 and 2E11, respectively.

2.5.4. Generation of DUSP-null cells

Experiments using the DUSP6 gRNA vector were performed in the inducible cells (2E2 and 2E11 cells) so that all cells would contain the Cas9 machinery. Cells were transfected in 6-well plates with 2 µg DUSP6 gRNA vector. The following day, cells were treated with 0.5 µg/ml puromycin and underwent selection over 3 – 4 weeks. This resulted in cells with inducible Cas9 expression and the DUSP6 gRNA plasmid. For DUSP6 gRNA 1, gRNA 3 and gRNA 4, 2E2 derivatives were called 2E2g1, 2E2g3 and 2E2g4

respectively (similar terminology used for the 2E11 population). Subsequent treatment of with 1 µg/ml dox, a concentration that led to a robust Cas9 expression, then resulted in editing in the *DUSP6* gene, confirmed by a western blot (**Fig. 3.12A**).

As the CRISPR-Cas9 system was very efficient in targeting the *DUSP6* gene, later experiments were not performed in the inducible cells. Instead, the DUSP3, DUSP10, DUSP12 and DUSP26 gRNA vectors contained Cas9 (**Fig. 2.1, right vector**) and KELLY and IMR-32 cells were co-transfected with 600 ng gRNA vector and 100 ng GFP vector (pEGFP-N2GFP, Invitrogen). As the DUSP4 vector did not contain Cas9, in this case KELLY and IMR-32 cells were co-transfected with 300 ng gRNA vector, 300 ng Cas9 vector (Addgene, #62988) and 100 ng GFP vector. The following day, cells were imaged to monitor GFP expression and thus the rate of transfection and 1 µg/ml puromycin was added. Cells were maintained in puromycin for 10 days to select for cells containing the vector.

The DUSP1 gRNA was transfected into the 2E2g4 cells and DUSP6-null subclones. As the 2E2g4 cells and DUSP6-null subclones were already resistant to puromycin, these cells did not undergo selection. Instead, 3 days after transfection genomic DNA was extracted and the DUSP1 gRNA region was sent for sequencing. Editing within the mixed population was monitored using the ICE v2 CRISPR Analysis Tool (Synthego).

The DUSP3, DUSP4, DUSP6, DUSP10, DUSP12 and DUSP26 mixed populations underwent single cell clonal expansion to generate DUSP-null subclones. Cells were serial diluted to 1 cell in 200ul media per well and aliquoted into 96 well plates. Cells were monitored for 2 - 4 weeks as subclones expanded at varying rates. After 2 weeks incubation, 50 µl fresh media was added to each well. Gradually, subclones were expanded into 12-well plates at which point DNA was extracted. The gRNA region was amplified and sequenced. Subclones that contained editing were expanded to $T75^2$ flasks and frozen (described in **Chapter 2.1)**. Insertions and deletions (indels) present were analysed directly via Sanger sequencing

(described in **Chapter 2.2**). Loss of DUSP6 protein was also analysed by western blot (**Fig. 3.12**).

2.5.5. DUSP6 overexpression

Exogenous DUSP6 protein was re-introduced into KELLY cells and DUSP6-null subclones. To this end, a GenEZ™ ORF Cloning vector (GenScript) was purchased which contained the full DUSP6 protein coding sequence under the control of a CMV promoter (**Fig. 6.14**). Furthermore, rather than ending in a stop codon, the DUSP6 sequence is followed by a C-terminal FLAG tag. Importantly, GenScript sequence the vector before dispatch to verify 100% accuracy in sequence. Cells were transfected with 600 ng of the DUSP6-FLAG vector or an empty vector (pCI-Neo, Promega) as a negative control. After 24 hours, cells were incubated with 400 µg/ml G418 for 1 week and then 100 µg/ml G418 for 3 weeks to select for resistant cells. Overexpression of DUSP6 was verified via western blot (**Fig. 6.15**).

2.5.6. Resazurin assay

Cell growth and cell viability was quantified in 96-well plates by incubating cells with resazurin sodium salt (Sigma-Aldrich). Resazurin is a fluorogenic oxidation-reduction indicator which will be converted from a non-fluorescent blue to a highly fluorescent pink when reduced. This reaction of resazurin to resorufin correlates with the abundance of aerobic respiration and is therefore an indirect measurement of viable cells present (Czekanska, 2011).

To perform a resazurin assay, stock solution of 0.015% (w/v) resazurin was dissolved in DPBS and this was added to cells at a final concentration of 10%. Cells were left for 4 - 24 hours in the incubator and then the fluorescence intensity was measured on a FLUOstar OPTIMA (BMG Labtech) microplate reader at an excitation and emission wavelength of 540 nm and 590 nm respectively. A background reading of media alone was subtracted from each sample reading and then samples were normalised to the negative control. When there was high variability between experiments,

samples were normalised to the plate average. For cell growth assays, the resazurin assay was either performed on day 1 and day 7 or performed each day over 5 days (day 3 to day 7). For cell viability assays, the resazurin assay was performed 6 days after treatment.

2.5.7. MCB assay

Production of Reactive Oxygen Species (ROS) was quantified using monochlorobimane (MCB). MCB is a cell-permeable dye that becomes fluorescent upon reaction with reduced glutathione (GSH) (Cook et al., 1989). Cells were seeded into black-walled 96 well plates (Corning® Costar® cell culture plate, Fisher Scientific) and chemical treatments applied after 24 hours. Cells are incubated for 5 days and then all media was removed and 50 µM MCB added, diluted in DPBS. The fluorescence intensity was measured every 5 minutes for 75 minutes on a FLUOstar OPTIMA (BMG Labtech) microplate reader at an excitation and emission wavelength of 380 nm and 460 nm respectively. The change in fluorescence was defined as the difference in intensity between the 0- and 75-minute time points. As ROS are produced, GSH becomes oxidised to glutathione disulfide and exits the cell, resulting in a decrease in MCB reaction in the cells themselves. Considering the number of cells would also alter cellular GSH levels, cell viability was measured simultaneously and used to normalise MCB values.

2.5.8. Colony forming assays

To study the colony forming ability of NB cells, 400 cells were seeded in a 6-well plate and incubated for 15 - 20 days. To quantify the number of clones, each well was washed gently in DPBS, 1 ml 4% para-formaldehyde (PFA) was added and plates were incubated for 30 minutes. Following this, each well was washed twice in DPBS, then 1 ml crystal violet stain (0.05% (w/v) Crystal Violet (Sigma-Aldrich), 30% Ethanol, 0.15 M Sodium Chloride) was added and cells were rocked gently for 90 minutes. Subsequently, wells were washed twice with distilled water and air dried overnight.

Images were taken of each well using a digital camera and quantified using the ImageJ software (Schneider et al., 2012) and Fiji (Schindelin et al., 2012). In ImageJ, the 'thresholding' function was applied to convert the image into binary where darker areas are white (**Fig. 2.4**). White areas were counted and their area measured in pixels^2 using the 'Analyse Particles' tool.

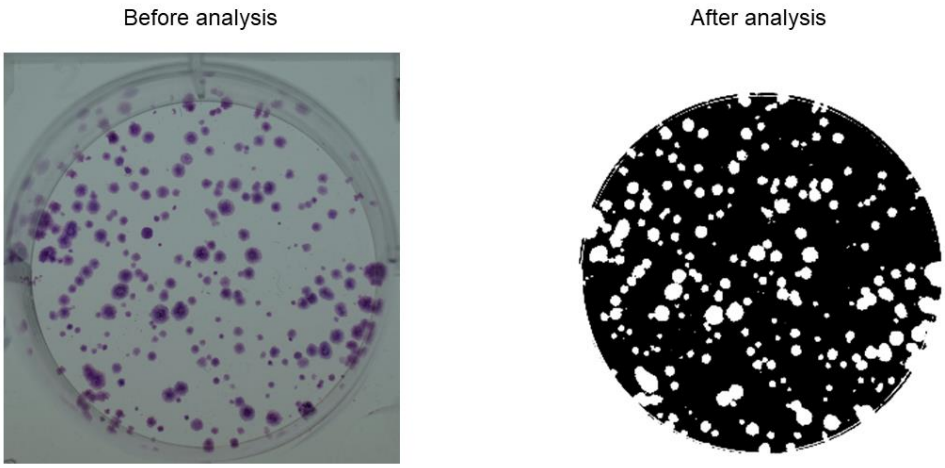

Figure 2.4 – ImageJ analysis of crystal violet staining. The thresholding function was used to convert the image into binary where darker areas are white. White areas were then counted and their area measured.

2.5.9. Microscopy

All phase contrast and immunofluorescence images were taken using a Hamamatsu Orca R2 monochrome camera on an IX71 inverted microscope (Olympus). Image analysis was subsequently performed using the ImageJ software (Schneider et al., 2012) and Fiji (Schindelin et al., 2012).

2.6. Bioinformatic analysis

2.6.1. Cox regression analysis

The clinical relevance of DUSP genes in NB progression was assessed using univariate and multivariate cox regression analysis (Cox, 1972). Two publicly available NB gene expression datasets were downloaded from the

R2: Genomics Analysis and Visualization Platform (http://r2.amc.nl), namely the ‘SEQC - 498 - RPM - seqcnb1’ dataset and the ‘Ora - 283 - rma_sketch - huex10t’ dataset. Raw gene expression values and survival data were imported into R (version 1.3.959) and a survival object was created using the ‘surv’ function. Following this, a univariate cox regression was fitted using the ‘coxph’ function for each covariate included in the analysis. For each covariate assessed, the Proportional Hazards Assumption was tested using the ‘cox.zph’ function to confirm that each covariate does not interact with time. In cases where the Proportional Hazards Assumption is violated, log(gene expression) was also assessed. Cases that still violated the Proportional Hazards Assumption were omitted from the analysis. Covariates that were statistically significant in the univariate analysis (where $p < 0.05$) were assessed in a multivariate analysis model using the same functions as the univariate analysis.

2.6.2. Phosphoproteomic data analysis

For the phosphoproteomic experiments performed in this project, there were three data analysis software’s used. Each of which are described below.

Biological pathway analysis

A biological pathway enrichment was performed on the BCI dataset using the FUNRICH Software (v3.1.4) (**Chapter 4.2.4**). FUNRICH is a stand-alone tool that incorporates biological information from a wide range of publicly available databases (Pathan et al., 2015). Thresholds for phosphoproteins to be included in the analysis were set at Log2-Fold Change > 2 and p-value < 0.1. FUNCRICH then identified biological pathways that were enrichment by these significantly altered phosphopeptides.

KSEA analysis

A kinase substrate enrichment analysis (KSEA) was performed by Dr. Vinothini Rajeeve and Prof. Pedro Cutillas (Barts Cancer Institute) on both phosphoproteomic datasets as described before (Casado et al., 2013). In this analysis, a z-score was calculated between the distribution of changes

in phosphorylation of substrates for given kinases relative to the distribution of all fold changes. The kinases that appeared statistically significant in one of the comparisons were included for further analysis. Statistical significance was determined using a z-test (Casado et al., 2013). Phosphosites were deemed functionally important if they were identified multiple times in the phosphositeplus online database (Hornbeck et al., 2015). Phosphoproteins that were visualised as a network were taken from the KSEA network and from published literature. These networks were visualised in Cytoscape (Shannon et al., 2003) using the StringApp (Doncheva et al., 2018) and Omics Visualiser plug-ins (Legeay et al., 2020).

IPA analysis

The Ingenuity Pathway analysis (IPA) (QIAGEN, Inc., https://targetexplorer.ingenuity.com/) was used to analyse the effect of DUSP6 in NB cells and its biochemical interaction with the ALK oncoprotein (**Chapter 6.2.4**). In this software, Qiagen have created a large database of molecular interactions which is manually curated by PhD scientists, termed the Qiagen knowledge base. The database has been used to generate a list of canonical signalling pathways. Changes in phosphorylation present in the phosphoproteomic dataset are mapped onto these pathways to show which have been perturbed. For each phosphoproteomic comparison, only phosphopeptides that met the criteria $p < 0.1$ were included. For each comparison this included between 400 – 1100 phosphorylation events. The software calculates a p-value and a z-score relating to the activation or inactivation of each canonical pathway. The p-value is determined by performing a right-tailed Fisher's Exact test with Benjamini-Hochberg correction. The z-score is a comparison between our dataset and the Qiagen knowledge base. The software states a z-score > 2 is deemed activation and < -2 is deemed inactivation. Only pathways that passed this z-score threshold in one or more comparisons are displayed. The pathways identified in the analysis were used to generate new hypotheses about the signalling pathways affected by DUSP6 in NB cells.

2.7. Statistical analysis

Where it was deemed appropriate, a range of statistical tests were performed. For comparisons made within a group, a one-way ANOVA was performed and the Dunnett post-Hoc test was applied. In cases where direct comparisons were made between two sets of data points (for example, when comparing two populations at one time point in a dose-response curve), an independent-samples t-test was performed. Significant changes are denoted throughout the thesis using '*' or '†' and significance levels are referenced in the figure legends. All statistical tests were performed in SPSS (IBM SPSS Statistics v27). Statistics was not performed on experiments that contained less than three biological replicates.

Chapter 3. Identifying growth-promoting DUSP genes in NB

3.1. Introduction

As described in **Chapter 1.4**, phosphotyrosine signalling is an integral part of NB progression (Huang and Weiss, 2013, Trigg and Turner, 2018, Palacios-Moreno et al., 2015). This is exemplified by the role of ALK, a global regulators of intracellular signalling that is heavily implicated in NB pathogenesis. As signalling is generally driven by kinase function, historically, phosphatases have been deemed as tumour-suppressive. However, it is now believed the situation is far more complex, with potential growth-promoting and -suppressing roles of PTPs identified in NB progression (Aurtenetxe et al., 2018, Nunes-Xavier et al., 2019a, Zhang et al., 2017). Indeed, as mentioned in the general introduction, treatment of NB cells with pan-PTP inhibitors is extremely cytotoxic, emphasizing the importance of these enzymes to NB function (Clark et al., 2015).

There are a range of DUSPs, especially MKPs, that are implicated in neuronal differentiation and NB cell survival, reviewed recently by Nunes-Xavier et al. (2019b). The MKPs demonstrate high specificity to the MAPKs whereas the aDUSPs have a broader range of substrates that can include the MAPKs. Treatment with RA results in a broad spectrum of changes to MKP and aDUSP mRNA expression in three NB cell lines (Nunes-Xavier et al., 2019b) (**Fig. 3.1**). Interestingly, after RA treatment mRNA expression not only varied between DUSPs but also between different cell lines. This hints that the intracellular signalling networks in NB cell lines are quite heterogenous. These findings also suggests that DUSPs are part of a complex regulatory network in NB differentiation with a high degree of transcriptional regulation. Indeed, Caunt et al. (2008a) demonstrated in HeLa cells that stimulation or inhibition of ERK signalling will alter the transcriptional response of a wide range of DUSPs. Considering both the stimuli and duration altered the response, this suggests a fine-tuned and orchestrated response to ERK activation. There is a large body of evidence demonstrating DUSPs may be involved in NB cell survival or neuronal differentiation, in particular via the MKPs, summarised below.

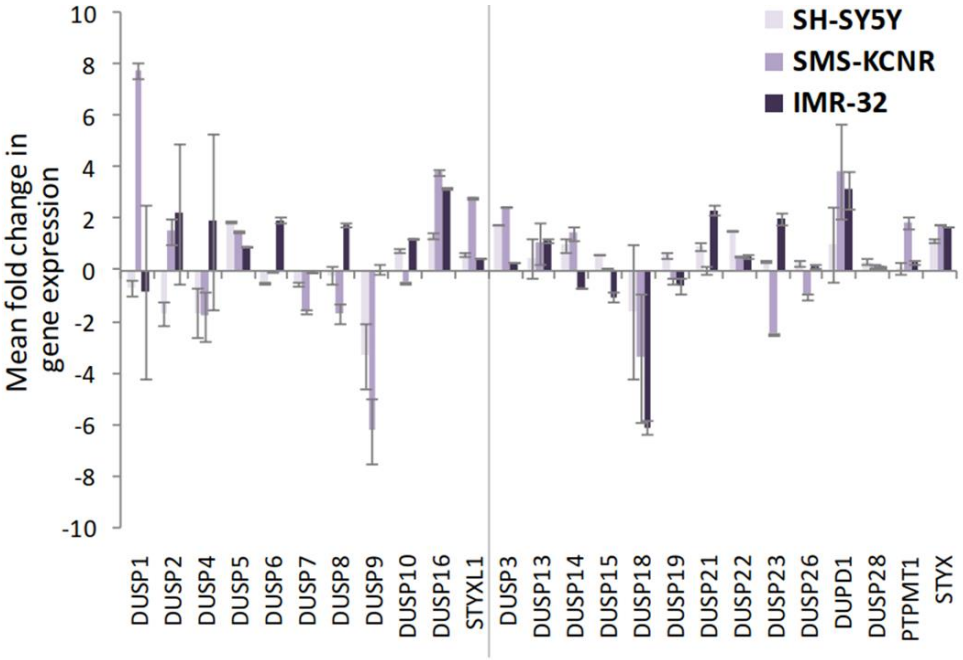

Figure 3.1 – Change in DUSP mRNA expression in response to RA treatment in NB cells. SH-SY5Y, SMS-KCNR and IMR-32 cells were treated with or without 10uM RA for 10 days and the then the fold change in mRNA expression of all atypical DUSPs and MKPs were assessed by qPCR. The transcriptional response to RA treatment is clearly fine-tuned and orchestrated as the response is dramatically different in each cell line. Taken from Nunes-Xavier et al. (2019b).

A myriad of studies demonstrate both growth-promoting and -suppressing roles of the MKPs in NB. Various reports implicate DUSP1 in neuronal cell differentiation and apoptosis. Initial studies demonstrated that during RA-induced differentiation in P19 cells, upregulation of p-ERK was accompanied by an increase in nuclear DUSP1 and cytoplasmic DUSP6, suggesting they intricately modulate ERK activity (Reffas and Schlegel, 2000). However, when differentiation is induced with silver nanoparticles, unlike RA, pERK signalling was upregulated but DUSP1 downregulated. Therefore, depending on the extracellular stimuli, cellular differentiation can be achieved via different mechanisms which can have contrasting effects on DUSP1 expression. Via modulation of the ERK pathway, *DUSP1* can promote apoptotic cell death. In SH-SY5Y cells treated with H_2O_2, knockdown of *DUSP1* increased ERK phosphorylation and suppressed H_2O_2-induced apoptosis (Kim et al., 2005). By promoting apoptosis, DUSP1 can also augment chemotherapeutic efficiency. A broad range of

chemotherapeutics are less toxic in the CD133+ sub-population of NB cells which correlated with reduced apoptotic cell death and DUSP1 expression and high p38 and ERK phosphorylation levels (Vangipuram et al., 2010). Overall, this suggests an anti-tumorigenic role of DUSP1 in NB cells by promoting apoptosis. However, anti-apoptotic roles have also been identified via regulation of JNK. In N1E115 cells and rat cortex neurons, hypoxia-reoxygenation led to an upregulation of DUSP1 and JNK phosphorylation (Koga et al., 2012). Following this, knockdown of *DUSP1* augmented JNK phosphorylation and increased neuronal death whereas DUSP1 overexpression had the opposite effect. More work using *in vivo* NB models are required to determine the particular context that DUSP1 promotes or suppresses apoptosis.

In a study analysing 48 primary tumour samples, *DUSP5* expression was associated to MYCN status, metastasis and poor prognosis (Aurtenetxe et al., 2018). *In vitro*, the researchers demonstrated that ERK-mediated cell proliferation was accompanied by increased *DUSP5* mRNA, whereas DUSP5 knockdown reduced cell proliferation. The authors suggested *DUSP5* expression could be used as a marker for poor NB prognosis. Interestingly, DUSP5 is also a putative target of the tumour suppressor p53 (Ueda et al., 2003). In rat PC12 cells, NGF treatment induced neuronal differentiation and led to an upregulation of p53-mediated *DUSP5* transcription, most likely as a negative feedback for ERK signalling (Brynczka et al., 2007).

Similarly, DUSP6 is also heavily implicated in neuronal cell differentiation. In NGF-treated PC12 cells, RA-treated mouse P19 cells and Forskolin-treated Schwann cells, cellular differentiation was accompanied by an upregulation of DUSP6 (Camps et al., 1998, Reffas and Schlegel, 2000, Bermingham Jr et al., 2001). In P19 cells, RA also upregulated ERK signalling and ERK activation was requisite for subsequent upregulation of DUSP6. In BE(2)-C and SH-SY5Y NB cells and the TH-MYCN transgenic mouse, treatment with RA led to significant upregulation of DUSP6 and RGS16, a GTPase-activating protein (Liu et al., 2005). Concurrent knockdown of DUSP6 and RGS16 was required to increase ERK signalling

and prevent the anti-proliferative effect of RA in SH-SY5Y cells. Furthermore, DUSP6 is also regulated by MYCN, a global regulator of transcription in NB. In SK-N-BE(2) and LAN-1 cells, MYCN can form a complex with SIRT1 which transcriptionally represses *DUSP6*, leading to an increase in NB cell proliferation (Marshall et al., 2011). Suppression of *DUSP6* was required for ERK activation which can phosphorylate and stabilise MYCN and promote cell proliferation.

Albeit sparser than the MKPs, there is also evidence that a minority of aDUSPs are implicated in NB. Both *DUSP23* and *DUSP26* mRNA are upregulated significantly during RA-induced neurogenesis in J1 mouse embryonic stem cells (Kim et al., 2016). DUSP23 was requisite for neuronal differentiation as treatment with *DUSP23* shRNA significantly reduced neurite outgrowth and the expression of neuronal-specific genes. Interestingly, knockdown of *DUSP23* led to a reduction of pJNK and pERK but an upregulation of pp38, suggesting a widespread role of DUSP23 on MAPK signalling. An anti-tumorigenic role of DUSP23 is also supported by evidence of *DUSP23* silencing in NB cell lines and tumours (Carén et al., 2011). CpG hypermethylation of *DUSP23* was highly associated to both MNA tumours and poor patient survival. In humans, *DUSP26* displays a preferential expression in neuroendocrine cells suggesting a potentially important physiological role in neuronal cells (Wang et al., 2006). Similar to RA treatment in mouse embryonic stem cells, NGF-induced neuronal differentiation of PC12 cells was followed by an upregulation of *DUSP26* mRNA (Kim et al., 2016). DUSP26 appears to modulate cell differentiation as DUSP26 overexpression suppressed NGF-induced neuronal differentiation in PC12 cells (Wang et al., 2006). DUSP26 expression is also highly associated to worse prognosis in NB (Shang et al., 2010). Knockdown of *DUSP26* decreased NB cell viability in SH-SY5Y and IMR-32 cells and results were validated *in vivo* (Shi et al., 2015). The researchers identified the p53 pathway as responsible as DUSP26 was able to dephosphorylate p53 directly and indirectly via p38. Lastly, a genome-wide association study identified single nucleotide polymorphisms (SNPs) in the *DUSP12* gene that correlated malignant progression of low-risk NB (Nguyễn

et al., 2011). Although the SNPs in the DUSP12 loci appear to have low penetrance, along with other genetic variations, they have a cumulative effect on malignant progression (Capasso et al., 2013).

The data presented above demonstrates that DUSPs may display growth-promoting or -suppressive characteristics in certain NB cells, but this depends on the cellular context. Relatedly, as described in **Chapter 1.3.2**, there is great heterogeneity in the dependence of a range of different tumour cell types on DUSP enzymes. Accordingly, our group hypothesised that the manipulation of function of DUSPs could offer a favourable outcome in NB. This would first need investigating in a wider range of NB cell lines to capture some of the heterogenous nature of NB (Ngan, 2015). Indeed a previous PTP-wide shRNA screen in our laboratory identified a handful of DUSPs that were potentially growth-promoting in IMR-32 cells (Dr. Ann Cichon, unpublished data). My initial aim therefore was to extend these findings, by performing a narrower and more focussed screen across the whole DUSP family, using small interfering RNA (siRNA) technology. This was performed in four cell lines, all of which are MYCN-amplified, representing the most aggressive form of the disease (**Table 2.2**). We believed this would identify DUSPs that are key to the regulation of NB cell growth. One of the enzymes identified in the previous shRNA screen had been DUSP6. This siRNA screen again identified DUSP6 as a candidate growth-promoter in NB cell lines and the later part of this chapter will focus in on a detailed analysis of its role.

3.2. Results

3.2.1. Identification of growth-promoting DUSPs

The primary aim of this work was to determine which DUSPs regulate NB cell growth. As mentioned, there is evidence that a wide range of DUSPs can function in a growth-promoting fashion in cancer (Low and Zhang, 2016, Gao et al., 2021). Furthermore, a previous PTP-wide shRNA screen identified a handful of DUSPs that were potentially growth promoting in IMR-32 cells (Dr. Ann Cichon, unpublished data). To investigate this further, a broad siRNA screen on both the MKP and aDUSP families was performed in 4 NB cell lines. The siRNAs used here are a pool of four pre-designed targeting siRNAs (**Table A1**). Pooling individual siRNAs is one strategy employed to improve gene knockdown and reduce off-target effects (Hannus et al., 2014, Kittler et al., 2007). In the data presented below, treatments were normalised to the plate average as there was large variability between replicates (**Fig. 3.2A-D**). Subsequently, in **Figure 3.2E**, the data was normalised to the non-targeting siRNA (SCR) and the error bars and statistical differences removed to allow clear visual comparison between cell lines. GAPDH is also included as an alternative negative control and Kif11 is included here and in subsequent siRNA treatments as a positive control. It is evident the majority of siRNAs demonstrated cell-specific effects where the largest responses were in the KELLY and LAN-1 cells. This could be partly due to transfection efficiency as Kif11 had a far greater effect on cell viability in LAN-1 and KELLY. There were surprisingly few growth-suppressing effects of DUSPs as only DUSP11 demonstrated a significant increase in cell growth in IMR-32 cells. Out of all the DUSPs, DUSP3 appeared the most potent, demonstrating a statistically significant decrease in cell viability in all cell lines with a particularly striking effect in KELLY cells. KELLY and LAN-1 cells both contain the F1174L ALK mutation which activates the ALK oncogene, whereas IMR-32 and SK-N-BE(2) cells contain WT ALK (**Table 2.2**). Interestingly, a range of DUSPs displayed a correlation with the ALK mutation status (**Fig. 3.2E**). For example,

knockdown of DUSP6 was significantly more effective in the KELLY and LAN-1 cell lines than IMR-32 and SK-N-BE(2) cells which suggests a potential role of DUSP6 in ALK-mutated NB cells. Furthermore, DUSP4 and DUSP13 appeared growth-promoting only in LAN-1 or KELLY cells respectively, but not in other cell lines (**Fig. 3.2E**). However, as mentioned previously, this could be due to the transfection efficiency as the transfectable cell lines happen to be ALK-mutant.

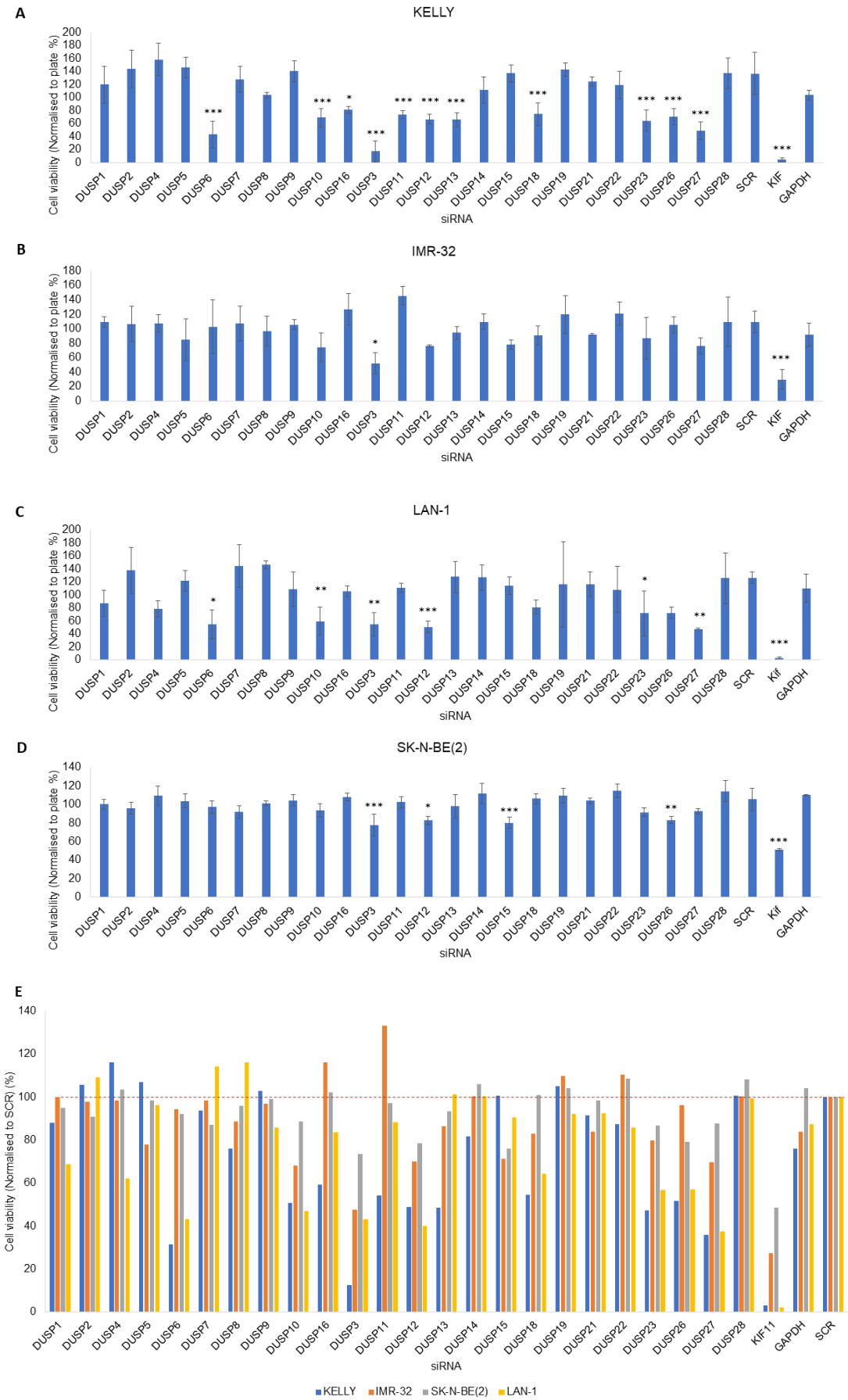
A
KELLY
Cell viability (Normalised to plate %)
siRNA
B
IMR-32
Cell viability (Normalised to plate %)
siRNA
C
LAN-1
Cell viability (Normalised to plate %)
siRNA
D
SK-N-BE(2)
Cell viability (Normalised to plate %)
siRNA
E
Cell viability (Normalised to SCR) (%)
siRNA
KELLY
IMR-32
SK-N-BE(2)
LAN-1

Figure 3.2 – Identifying growth-promoting or -suppressing DUSPs in NB cells. (A) KELLY, (B) IMR-32, (C) LAN-1 and (D) SK-N-BE(2) cells were transfected with 5 nM siRNAs targeting each DUSP gene and cell viability was assessed via a resazurin assay after 6 days ($n \geq 3$). Data is presented with MKPs on the left hand side and aDUSPs on the right. Non-targeting siRNA (SCR) and GAPDH included as negative controls and Kif11 (Kif) as a positive control. Data was normalised internally to the plate average and then expressed as a mean ± SD. One-way ANOVA compared to SCR; *$p \leq 0.05$; **$p \leq 0.005$; ***$p \leq 0.0005$. (E) To compare treatments between cell lines, data is also presented normalised to SCR.

To validate the on-target specificity of the pooled siRNAs, qPCR experiments were performed in KELLY cells for each DUSP siRNA. There were a handful of DUSP genes that were not included as primers could not be designed to their gene or their gene expression was too low. Oddly, this was the case for DUSP27. Transcriptomic profiling of NB cell lines revealed DUSP27 mRNA was undetectable in the majority (30 out of 39 cell lines analysed) and extremely low in the rest (**Fig. A1**) (Harenza et al., 2017). This was surprising and concerning considering the DUSP27 siRNAs caused significant loss of viability in KELLY and LAN-1 cells (**Fig. 3.2A** and **Fig. 3.2C**) and hinted at potential off-target effects of those siRNAs. As mentioned in the **Chapter 1.3**, most of the documented growth-promoting properties of DUSPs involve the MKP family. It was therefore important that all MKP family members were included in the on-target validation. There was significant suppression (≥50%) in DUSP gene expression for all bar the DUSP1 and DUSP2 siRNA pools (**Fig. 3.3**). The efficiency of DUSP1 siRNAs ranges between 0 – 33% demonstrating weak knockdown of this target. However, in most cases the DUSP gene was knocked down effectively. It was not possible to measure transfection efficiency using the Kif11 siRNA as gene knockdown was assessed after 24 hours and loss of cell viability occurred after 48 hours. Although there was therefore not a positive control, each individual qPCR experiment contained an siRNA pool that demonstrated <70% knockdown of target suggesting high transfection in each experiment. These results demonstrate a wide range of DUSPs may drive NB cell growth and in many cases these effects appear cell specific.

Furthermore, a handful of these DUSPs, in particular DUSP6, are potentially dependant on ALK signalling.

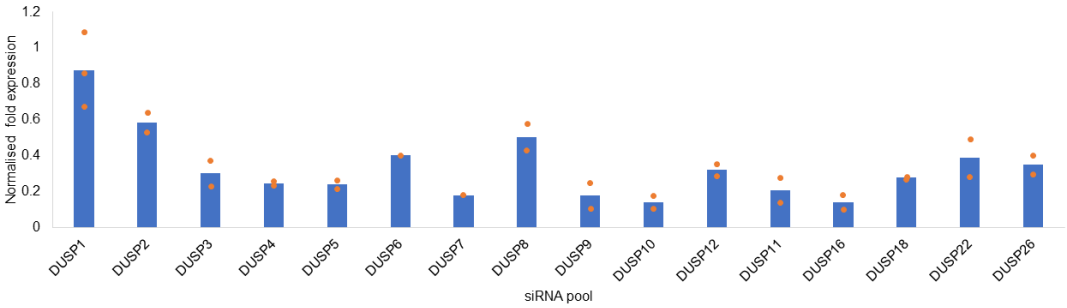

Figure 3.3 – Efficiency of DUSP siRNA pools. QPCR was performed on all DUSP genes in KELLY cells where primers could be designed, and the target gene was expressed (n ≥ 1). For each gene data was normalised to SCR and expressed as a mean with individual replicates overlaid as dot plots.

3.2.2. Survival analysis with DUSP gene expression

For genes that are able to drive disease, their expression could correlate with disease outcome. As a result, genetic biomarkers are useful in predicting the prognosis of a patient and what treatment they may require (Kamel and Al-Amodi, 2017). The cox regression analysis is a useful statistical method to determine whether the expression of one or more genes is related independently to patient survival (Cox, 1972). The output is displayed as a hazard ratio (HR) with a 95% confidence interval which is the probability that an event will occur as a function of time. Alongside each HR is a p value of statistical significance. There are a myriad of publicly available NB datasets which can be used to investigate gene expression in NB patients (Kocak et al., 2013, Rajbhandari et al., 2018, Wang et al., 2014a). I aimed to identify the DUSP genes that are associated with patient survival in the publicly available SEQC and NRC datasets which contained 498 and 283 patient samples, respectively (Wang et al., 2014a, Rajbhandari et al., 2018). These datasets were chosen as they contain patients across all INSS stages and display a wide range of clinical and pathological features. A univariate cox regression analysis was performed for all of the DUSP genes that were present in each database (**Table 3.1** and **Table 3.2**)

As a hallmark for NB malignancy, MYCN expression displayed a clear association to patient survival. Interestingly, a large proportion of DUSPs were also associated to patient survival in one or both of these datasets. This is most obvious for *DUSP4* and *DUSP26* which were statistically significant in both datasets.

Table 3.1 – Univariate cox regression of DUSP family genes and clinical variables in SEQC database. Hazard ratio (HR) and confidence interval (CI) is displayed for each gene. Transformation of gene expression put in brackets after gene name. INSS stage also put in brackets after INSS variable. Genes in bold displayed a p value < 0.05.

Variable	HR	95% CI	p value
DUSP1 (log)	0.22	0.13 ~ 0.38	4.7E-08
DUSP3 (log)	0.12	0.06 ~ 0.24	2.6E-10
DUSP4 (/1000)	1.27	1.19 ~ 1.36	2.2E-11
DUSP5 (log)	0.46	0.28 ~ 0.75	2.2E-03
DUSP6 (/1000)	0.95	0.9 ~ 1	4.8E-02
DUSP7 (/100)	0.50	0.33 ~ 0.77	1.7E-03
DUSP8 (/1000)	0.92	0.87 ~ 0.96	2.2E-04
DUSP9 (log)	0.36	0.16 ~ 0.81	1.3E-02
DUSP10 (/100)	0.96	0.92 ~ 1.01	9.5E-02
DUSP11 (/1000)	0.70	0.5 ~ 0.98	4.0E-02
DUSP12 (/1000)	1.00	0.98 ~ 1.03	8.4E-01
DUSP13 (log)	0.57	0.38 ~ 0.86	7.5E-03
DUSP14 (/1000)	0.65	0.5 ~ 0.84	1.2E-03
DUSP15 (/1000)	1.29	0.99 ~ 1.67	5.8E-02
DUSP16 (/1000)	0.84	0.79 ~ 0.91	2.5E-06

DUSP18 (/1000)	0.64	0.48 ~ 0.85	2.2E-03
DUSP19 (/100)	0.91	0.85 ~ 0.97	5.4E-03
DUSP21	0.99	0.96 ~ 1.03	7.9E-01
DUSP22 (log)	0.12	0.07 ~ 0.21	1.2E-13
DUSP23 (/1000)	0.99	0.97 ~ 1.01	1.5E-01
DUSP26 (log)	0.15	0.09 ~ 0.27	1.1E-10
DUSP27 (/10)	0.93	0.88 ~ 0.99	3.1E-02
EPM2A (log)	0.36	0.22 ~ 0.6	9.5E-05
PTPMT1 (/1000)	1.12	1.07 ~ 1.16	5.6E-08
RNGTT (/1000)	0.84	0.7 ~ 1	5.1E-02
STYX (/100)	1.04	0.86 ~ 1.25	6.8E-01
STYXL1 (/100)	1.00	0.97 ~ 1.03	8.4E-01
DUPD1	0.00	0 ~ 5.29	8.7E-02
MYCN	4.09	2.94 ~ 5.69	<2E-16
AGE	1.13	1.1 ~ 1.17	2.4E-15
INSS (1)	1 (reference)	-	-
INSS (2)	6.39	0.71 ~ 57.16	9.7E-02
INSS (3)	30.17	3.97 ~ 229.46	1.0E-03
INSS (4)	79.31	11.03 ~ 570.12	1.4E-05
INSS (4s)	9.46	1.06 ~ 84.64	4.4E-02

Table 3.2 – Univariate cox regression of DUSP family genes and clinical variables in NRC database. Hazard ratio (HR) and confidence interval (CI) is displayed for each gene. Transformation of gene expression put in brackets after gene name. Genes in bold displayed a p value < 0.05.

Variable	HR	95% CI	p value
DUSP1 (/1000)	0.93	0.88 ~ 0.99	1.8E-02
DUSP4 (/1000)	1.07	1.05 ~ 1.1	2.3E-08
DUSP5 (/100)	1.03	0.99 ~ 1.07	1.3E-01
DUSP6 (/1000)	0.99	0.95 ~ 1.03	4.9E-01
DUSP7 (/100)	1.18	0.97 ~ 1.43	9.5E-02
DUSP9 (/100)	1.14	1.02 ~ 1.27	2.3E-02
DUSP10 (/100)	0.97	0.71 ~ 1.32	8.3E-01
DUSP11 (/1000)	0.76	0.61 ~ 0.94	1.3E-02
DUSP12 (/1000)	2.05	1.4 ~ 3	2.1E-04
DUSP13 (/100)	1.32	0.9 ~ 1.95	1.6E-01
DUSP14 (/1000)	1.00	0.83 ~ 1.2	9.7E-01
DUSP15 (/1000)	1.02	0.89 ~ 1.17	7.8E-01
DUSP16 (/1000)	0.60	0.44 ~ 0.82	1.2E-03
DUSP18 (/1000)	0.24	0.05 ~ 1.1	6.7E-02
DUSP19 (/100)	0.85	0.75 ~ 0.97	1.5E-02
DUSP2	1.08	0.98 ~ 1.2	1.2E-01
DUSP21	1.06	0.88 ~ 1.28	5.5E-01
DUSP22 (/1000)	0.17	0.08 ~ 0.4	3.0E-05
DUSP23 (/1000)	0.59	0.34 ~ 1.03	6.4E-02
DUSP26 (/10000)	0.57	0.46 ~ 0.71	1.0E-06

EPM2A (/100)	0.63	0.5 ~ 0.78	3.8E-05
RNGTT (/1000)	1.00	0.99 ~ 1	3.5E-01
DUPD1	1.40	0.98 ~ 2.02	6.7E-02
MYCN	5.88	3.69 ~ 9.36	8.5E-14
AGE	1.13	1.07 ~ 1.19	4.7E-06

A benefit of the cox regression analysis is that you are able to combine multiple genetic and clinicopathological features into the same model. This allows the identification of genes that are independently associated to patient survival. To this end, a multivariate regression model was performed on all the variables that were statistically significant in the univariate regression model. (**Table 3.3** and **Table 3.4**). For the SEQC and NRC datasets, this combined 19 and 9 DUSP genes respectively with the other clinicopathological features. In the multivariate model, the majority of DUSP genes were no longer significant suggesting that the majority of these genes could not be classed as independent predictors of survival. The only DUSP gene that remained significant in the SEQC dataset was *PTPMT1*, a mitochondrial phosphatase that dephosphorylates lipids. A handful of DUSPs were also close to significance ($p < 0.1$) including *DUSP4*, *DUSP6* and *DUSP26*. It is worth nothing that high *DUSP6* expression associated with good prognosis (**Fig. 3.4A**). As DUSP6 was previously identified as a growth-promoting phosphatase in the siRNA screen (**Fig. 3.2**), its role is potentially more complex than based on its gene expression alone. *DUSP4* and *DUSP26* also remained significant in the NRC dataset along with *DUSP9*. These data were indicative of a role of DUSP4 and DUSP26 in NB progression. To confirm their relationship with patient survival, Kaplan-Meier plots were also generated using the same datasets for *DUSP4* and *DUSP26* gene expression (**Fig.3.4B-C**). DUSP4 appeared to play a tumour-promoting role in NB as high gene expression leads to very poor overall survival. Conversely, high *DUSP26* expression correlated with patient survival suggesting a tumour-suppressive role of DUSP26 in NB.

On the basis of the siRNA screen and cox regression analysis above, a selected subgroup of DUSPs remained of interest for further study: DUSP3, DUSP4, DUSP6, DUSP10, DUSP12, DUSP26. The majority of these DUSPs are investigated in **Chapter 5**. Taken together, the siRNA screen and cox regression analysis suggests DUSP6 displays a complex role in NB. Considering there is significant literature implicating DUSP6 in tumorigenesis (Ahmad et al., 2018), this chapter will now focus solely on the potential role of DUSP6 in NB progression.

Table 3.3 – Multivariate cox regression of DUSP family genes and clinical variables in SEQC database. Hazard ratio (HR) and confidence interval (CI) is displayed for each gene. Genes selected were significant in univariate analysis. Transformation of gene expression put in brackets after gene name. INSS stage put in brackets after INSS. Genes in bold displayed a p value < 0.05.

Variable	HR	95% CI	p value
DUSP1 (log)	0.56	1.46 ~ 0.21	2.3E-01
DUSP3 (log)	1.84	5.86 ~ 0.58	3.0E-01
DUSP4 (/1000)	1.11	1.24 ~ 1	5.5E-02
DUSP5 (log)	1.21	2.62 ~ 0.56	6.4E-01
DUSP6 (/1000)	1.05	1.11 ~ 1	7.1E-02
DUSP7 (/100)	0.64	1.37 ~ 0.3	2.5E-01
DUSP8 (/1000)	0.97	1.04 ~ 0.91	3.9E-01
DUSP9 (log)	1.79	4.54 ~ 0.71	2.2E-01
DUSP11 (/1000)	1.00	1.66 ~ 0.6	9.8E-01
DUSP13 (log)	0.98	1.85 ~ 0.52	9.6E-01
DUSP14 (/1000)	0.78	1.11 ~ 0.55	1.7E-01
DUSP16 (/1000)	0.92	1.01 ~ 0.83	9.4E-02
DUSP18 (/1000)	1.24	1.65 ~ 0.93	1.5E-01

DUSP19 (/100)	0.98	1.07 ~ 0.91	7.0E-01
DUSP22 (log)	0.56	1.69 ~ 0.19	3.0E-01
DUSP26 (log)	0.34	1.05 ~ 0.11	6.0E-02
DUSP27 (/10)	1.00	1.04 ~ 0.96	8.7E-01
EPM2A (log)	1.03	2.83 ~ 0.37	9.5E-01
PTPMT1 (/1000)	1.14	1.22 ~ 1.07	7.5E-05
MYCN	1.12	1.18 ~ 1.06	1.9E-05
AGE	1.08	1.14 ~ 1.03	2.6E-03
INSS (1)	1 (reference)	-	-
INSS (2)	6.24	56.64 ~ 0.69	1.0E-01
INSS (3)	13.51	107.44 ~ 1.7	1.4E-02
INSS (4)	28.17	212.13 ~ 3.74	1.2E-03
INSS (4s)	11.43	105 ~ 1.24	3.1E-02

Table 3.4 – Multivariate cox regression of DUSP family genes and clinical variables in NRC database. Hazard ratio (HR) and confidence interval (CI) is displayed for each gene. Genes selected were significant in univariate analysis. Transformation of gene expression put in brackets after gene name. Genes in bold displayed a p value < 0.05.

Variable	HR	95% CI	p value
DUSP1 (/1000)	0.96	0.9 ~ 1.03	2.5E-01
DUSP4 (/1000)	1.04	1.01 ~ 1.08	1.4E-02
DUSP9 (/100)	1.15	1.01 ~ 1.3	3.0E-02
DUSP11 (/1000)	1.05	0.8 ~ 1.37	7.4E-01
DUSP16 (/1000)	0.82	0.62 ~ 1.08	1.5E-01
DUSP19 (/100)	1.15	0.99 ~ 1.34	6.0E-02
DUSP22 (/1000)	0.62	0.27 ~ 1.45	2.7E-01
DUSP26 (/10000)	0.53	0.39 ~ 0.71	3.4E-05
EPM2A (/100)	0.90	0.68 ~ 1.19	4.6E-01
MYCN	4.43	2.44 ~ 8.07	1.1E-06
AGE	1.14	1.07 ~ 1.22	2.9E-05

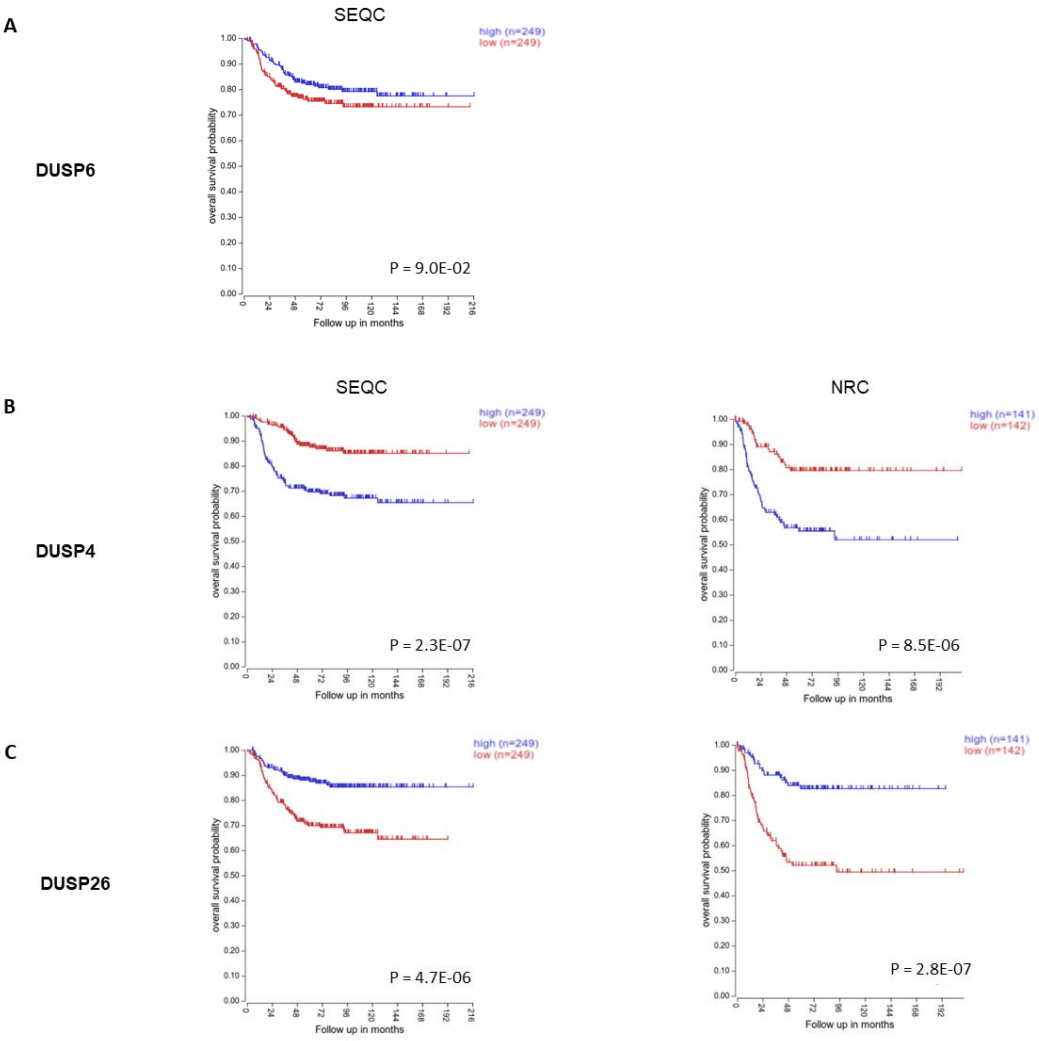

Figure 3.4 – Overall survival of NB patients dichotomised by *DUSP4*, *DUSP6* and *DUSP26* gene expression. Kaplan-Meier curves for (A) *DUSP6*, (B) *DUSP4* and (C) *DUSP26* genes in NRC and SEQC datasets where patients were split based on median gene expression. Statistical significance is determined by a logrank test followed by Bonferroni correction. Data generated using the R2: Genomics Analysis and Visualization Platform (http://r2.amc.nl).

3.2.3. Knockdown of DUSP6 suppresses KELLY cell viability

BCI, a dual DUSP1/6 chemical inhibitor, is currently being investigated for therapeutic efficacy in a wide range of cancers. I have investigated the effect of dual DUSP1 and DUSP6 inhibition using BCI in NB cells in **Chapter 4**. During this time, I also investigated whether concurrent knockdown of

DUSP1 and *DUSP6* would reduce cell viability to a greater extent than either siRNA alone (**Fig. 3.5**). At the time I was unaware that the DUSP1 siRNA pool was less effective than the DUSP6 pool, therefore this is taken into account when analysing these data. In accord with the siRNA screen in **Figure 3.2**, a significant reduction of cell growth was observed in KELLY cells after treatment with DUSP6 siRNA. However, in contrast to the siRNA screen the LAN-1 data was not validated, since loss of *DUSP6* did not have a significant effect on LAN-1 cell viability. In KELLY cells, and to a lesser extent in IMR-32 cells, the minor loss of DUSP1 mRNA appeared to have a slight growth enhancing effect, somewhat averaging out the effect observed by DUSP6 siRNA alone. As the concentration of total siRNA in each treatment was the same, this is not simply due to a reduction of DUSP6 siRNA in the DUSP1+6 treatment and may be due to contrasting roles of DUSP1 and DUSP6 in KELLY and IMR-32 cells. Notwithstanding the poor efficiency of the DUSP1 siRNA, these data do not support evidence that co-depletion of *DUSP1* and *DUSP6* can cause additive growth suppression.

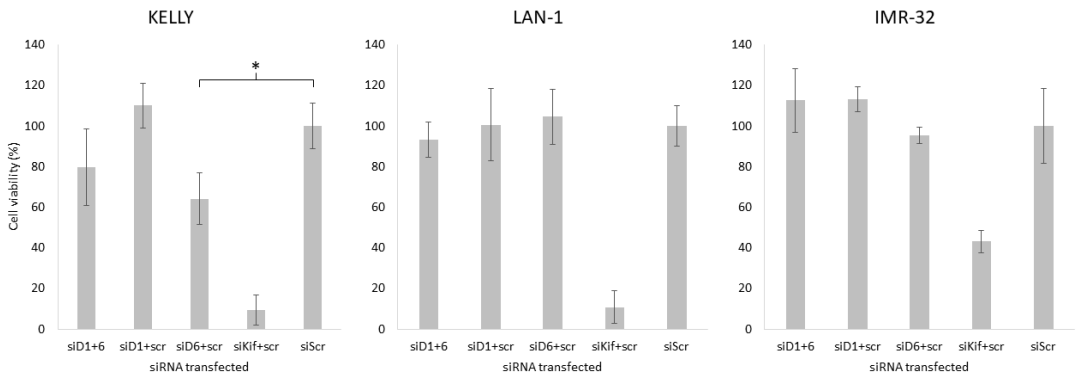

Figure 3.5 – Knockdown of *DUSP6* suppresses KELLY cell viability. KELLY, LAN-1 and IMR-32 cells were treated with 2.5 nM siRNA pools against DUSP1 and DUSP6 (total of 5 nM siRNA per well) for 6 days and cell viability was measured using the resazurin assay ($n \geq 4$). DUSP6 siRNA caused a statistically significant reduction of cell viability in KELLY cells. Data are expressed as a mean ± SD. One-way ANOVA compared to SCR; $*p \leq 0.05$.

As well as investigating their role in cell growth and survival, a key goal of this study was to determine which phosphatases regulate MAPK signalling pathways in NB cells. Hence, the biochemical effect of knocking down

DUSP1 and *DUSP6* alone and in combination was investigated by performing an immunoblot on the MAPK and AKT signalling pathways in KELLY cells (**Fig. 3.6**). As it is possible for DUSP enzymes to function as part of a negative feedback loop if their substrates are activated (Caunt and Keyse, 2013), the experiment was performed under basal conditions and in the presence of EGF, a growth factor known to stimulate the ERK pathway (Wee and Wang, 2017). As mentioned previously, the knockdown of DUSP1 via siRNA was incomplete, therefore it is unclear whether acute loss of DUSP1 protein affects MAPK signalling. Treatment with EGF for 30 minutes caused a significant increase in pERK, although suprisigingly, this was unaffected by knockdown of *DUSP6* or by the minor loss of DUSP1. Furthermore, although there was an effect on cell viablity, concurrent suppression of *DUSP6* and partial suppression of *DUSP1* did not alter ERK signalling under basal or stimulated conditions. There was a reproducible increase in pAKT signalling after treatment with EGF for 30 minutes, however this was also not influenced by loss of *DUSP6* or minor loss of *DUSP1*. There was also a visible increase in pJNK signalling after treatment with EGF for 30 minutes in cells depleted in *DUSP1*, *DUSP6* or both. Unfortunately, the pJNK antibody has a high degree of background, therefore it could not be quantified accurately. These results hint at the possibility of other phosphatases controlling MAPK and AKT signalling in KELLY cells.

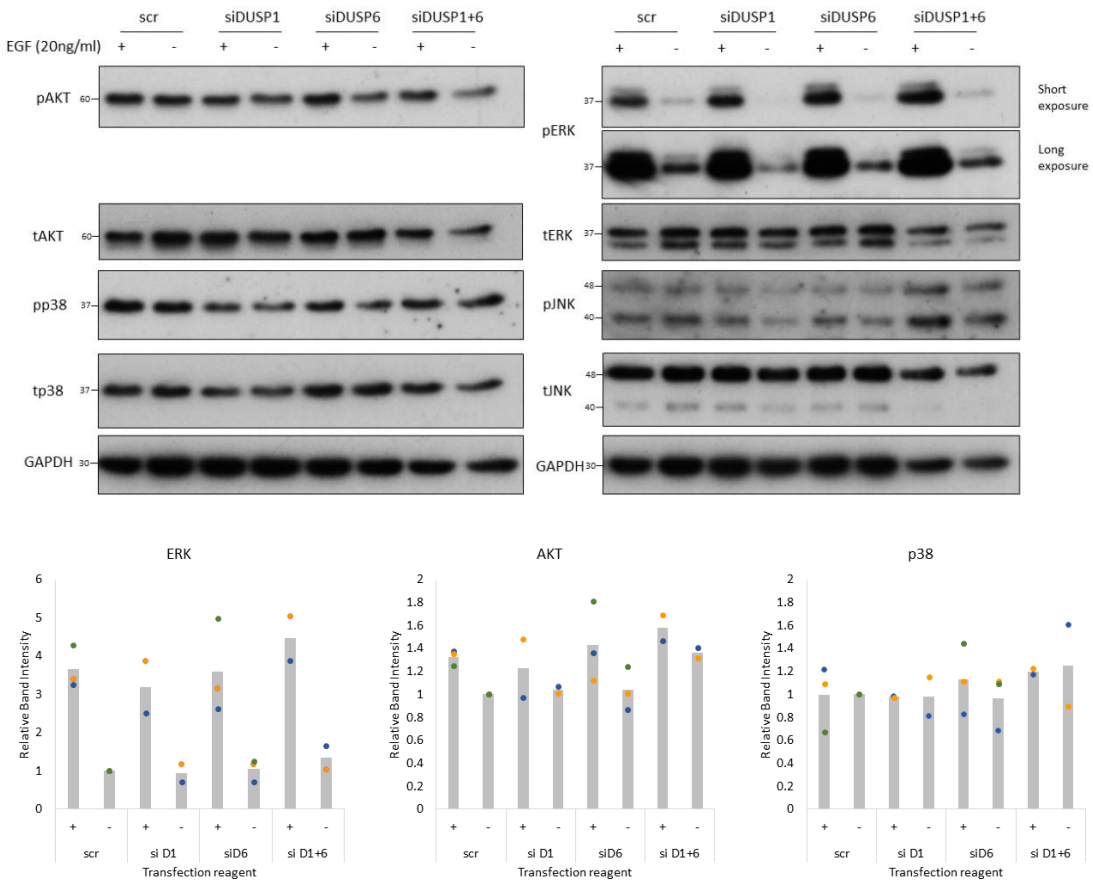

Figure 3.6 – MAPK signalling appears unaffected in KELLY cells after knockdown of *DUSP6* and a minor suppression of *DUSP1*. KELLY cells were treated with 2.5nM siRNA pools against DUSP1 and DUSP6 (total of 5 nM siRNA per well) for 24 hours. 30 minutes before cells were lysed, cells were stimulated with 20 ng/ul EGF (n ≥ 2). For quantification, each phospho-protein was normalised to total protein followed by a second normalisation to SCR siRNA. High background signal in the JNK blots prevented accurate quantification. No significance was observed in a one-way ANOVA when comparing siRNA treatment to SCR.

3.2.4. DUSP6 siRNAs display potent off-target effects in KELLY cells

The previous experiment suggested that loss of *DUSP6* does not affect MAPK signalling under basal conditions or after treatment with EGF for 30 minutes. Considering literature suggests DUSP6 is primarily an ERK-phosphatase, we were sceptical that the decrease in cell viability observed with DUSP6 siRNAs is not due to the loss of *DUSP6* (Ahmad et al. 2018). As mentioned previously, the siRNAs used in this study were equimolar pools of 4 individual siRNAs, designed to increase both potency and specificity. In an effort to confirm whether the loss of viability of the siRNA is due to loss of *DUSP6* protein, the DUSP6 siRNA pool was deconvoluted to determine if the individual capacity of each siRNAs to deplete DUSP6 protein correlated with their ability to suppress NB cell growth. DUSP6 expression was analysed in KELLY cells by both qPCR and Western blotting analysis after treatment with the individual and pooled DUSP6 siRNAs (**Fig. 3.7A-B,** Western blot jointly performed with Dr. Andrew Stoker). In both the qPCR and Western blot, individual siRNAs 6.1 and 6.2 caused the largest reduction in DUSP6 expression, comparable to the siRNA pool. Conversely, 6.3 and 6.4 reduced DUSP6 expression significantly less. In parallel, the effect of DUSP6 individual siRNAs on KELLY cell viability was also investigated. (**Fig. 3.7C,** performed by Dr. Andrew Stoker). As expected, the DUSP6 pooled siRNA caused a significant loss of the DUSP6 protein and cell viability. However, it appears that the cell growth effect was primarily through the 6.3 siRNA and this only reduced DUSP6 protein by ~40%. More strikingly, both the 6.1 and 6.2 siRNAs did not affect cell growth. While these data demonstrate the effective knockdown of DUSP6 protein by siRNAs, they suggest that unfortunately the DUSP6 pooled siRNA has significant off-target effects which is causing loss of NB cell viability. These data also demonstrate that the cell growth effect of an siRNA pool can be due to predominantly one of the individual siRNAs. In light of the survival data in response to 6.1 and 6.2 siRNA, whether DUSP6 has a prominent role in KELLY cell growth remains

elusive. To investigate this further, we sought to abolish DUSP6 expression from these cells by using CRISPR/Cas9.

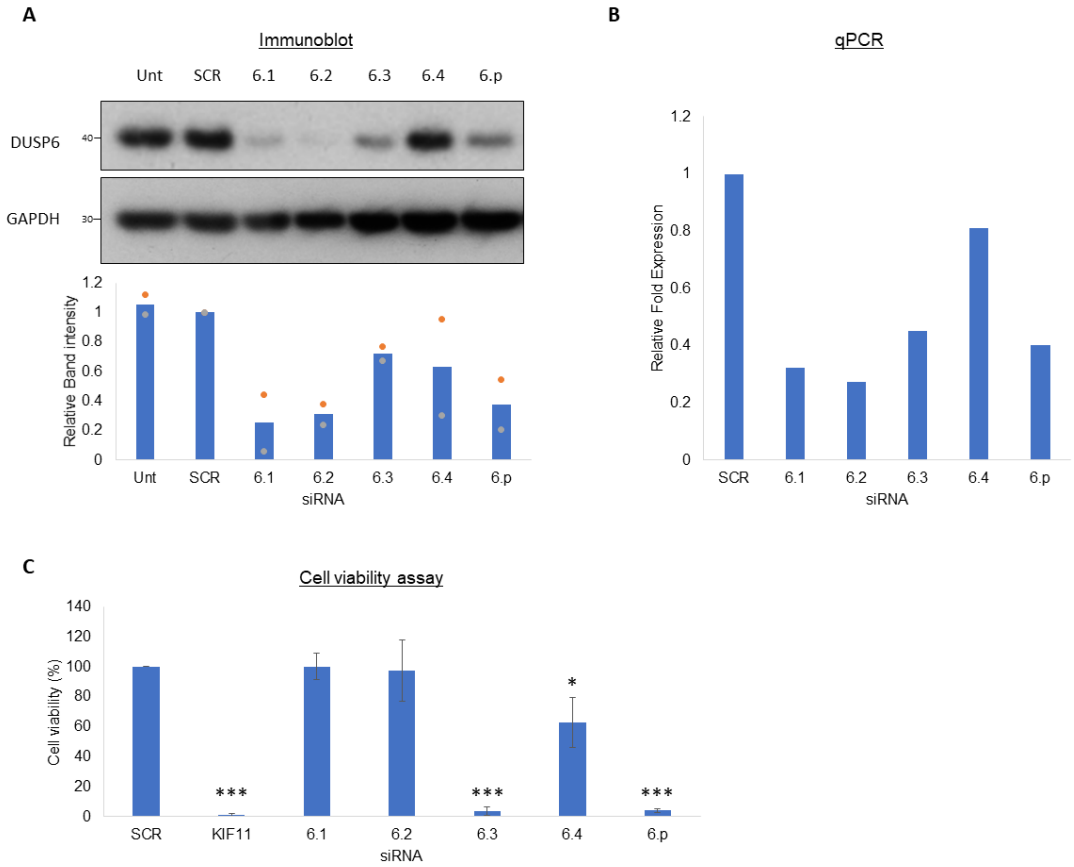

Figure 3.7 – Deconvolution of DUSP6 siRNAs. KELLY cells were treated with 5 nM total of the individual and pooled DUSP6 siRNAs for 24 hours followed by a (A) Western blot for DUSP6 (n = 2) and a (B) qPCR for *DUSP6* gene expression (n = 1). For Western blot quantification, DUSP6 was normalised to GAPDH followed by a second normalisation to SCR siRNA. (C) In parallel, KELLY cells were treated with 5 nM individual and pooled DUSP6 siRNA for 7 days and cell viability was measure using the resazurin assay (n = 4). One-way ANOVA compared to SCR; *$p \leq 0.05$; ***$p \leq 0.0005$. Cell viability assay and Western blot were performed by Dr. Andrew Stoker.

3.2.5. Generation of DUSP6-null KELLY and IMR-32 cells

The previous data demonstrates that the DUSP6 siRNA pool, although effective at depleting DUSP6 protein, causes significant off-target toxicities. To circumvent these issues, we decided to use CRISPR-Cas9 to completely remove DUSP6 protein from NB cells. This approach is well established and our group have previously generated dox-inducible NB cell line derivatives for efficient CRISPR/Cas9 activation of gRNAs (Dr. Vruti Patel, see **Chapter 2.5.3**). A gRNA generated by Dr. Patel, gRNA 3, is presented in **Fig. 3.8A**. Although this gRNA targeted a region upstream of the DUSP6 start codon, Dr. Patel demonstrated a reduction in DUSP6 protein in IMR-32 cells. After 12 days treatment with dox, Cas9 is induced and DUSP6 expression is significantly reduced in the iIMR-32-gRNA 3 mixed population, termed 2E11g3, compared to the non-gRNA control (**Fig. 3.8B**, Dr. Vruti Patel). It is worth noting there are a range of mixed populations and subclones that derive from NB cell lines generated here and in subsequent chapters. For clarity, the nomenclature used for each population is described in **Appendix 4**.

The data presented in **Chapter 3.2.3** highlights the importance of identifying off-target toxicities. Hence, I investigated whether CRISPR-Cas9 editing results in point mutations in unintended regions of the genome. The top three regions likely to exhibit off-target effects were identified in the Benchling software (Doench et al., 2016). The editing in these regions was compared to editing in the gRNA 3 site of the *DUSP6* gene (**Fig. 3.8C**). There does not appear to be any major editing in the off-target sites in the mixed populations within the detection limit of the Sanger sequencing. Promisingly, there remained significant editing in the *DUSP6* gene, demonstrated by the mismatching of sequencing after the gRNA site, suggesting the CRISPR-Cas9 is functioning solely on this region (**Fig. 3.8C**).

To investigate whether DUSP6 is important to NB cell growth, it is important to completely remove DUSP6 protein. In an effort to achieve this, the 2E11g3 mixed population was single cell cloned, as described in **Chapter 2.5.4**, to identify DUSP6-null subclones. Out of 15 subclones sequenced, only 1 appeared WT, with 14 clones demonstrating either homozygous or compound hemizygous deletions (**Table 3.5**). This demonstrates that the CRISPR machinery was very effective at introducing indels into the *DUSP6* gene. However, it is unlikely the smaller indels reduce DUSP6 protein as they do not alter the DUSP6 coding region. Surprisingly, no heterozygous clones were identified. Clones 1D7 and 2F8 had larger indels in both alleles. This suggests that either CRISPR can introduce the same deletion in both alleles, or once an indel is introduced into one allele, this could be used as the template during non homologous end joining. For clones with very large indels (> 100bp), namely 2F8 and 3E9, a Western blot was performed to assess DUSP6 expression. There was a ~50% depletion of DUSP6 in 3E9 (**Fig. 3.8D**). Sequence alignment of subclones demonstrated that the 380bp deletion in one allele of 3E9 removes a significant proportion of the DUSP6 N-terminal domain. Although the second allele of 3E9 has a 2bp insertion upstream of the start codon (**Fig. 3.8E**), DUSP6 protein expression decreased by ~50%, as expected. The 146bp deletion in both alleles of 2F8 removes the DUSP6 start codon (**Fig. 3.8E**) which paradoxically increased DUSP6 protein expression. On further investigation, this is likely due to the presence of an alternative start codon further downstream, as documented by Dowd et al. (1998).

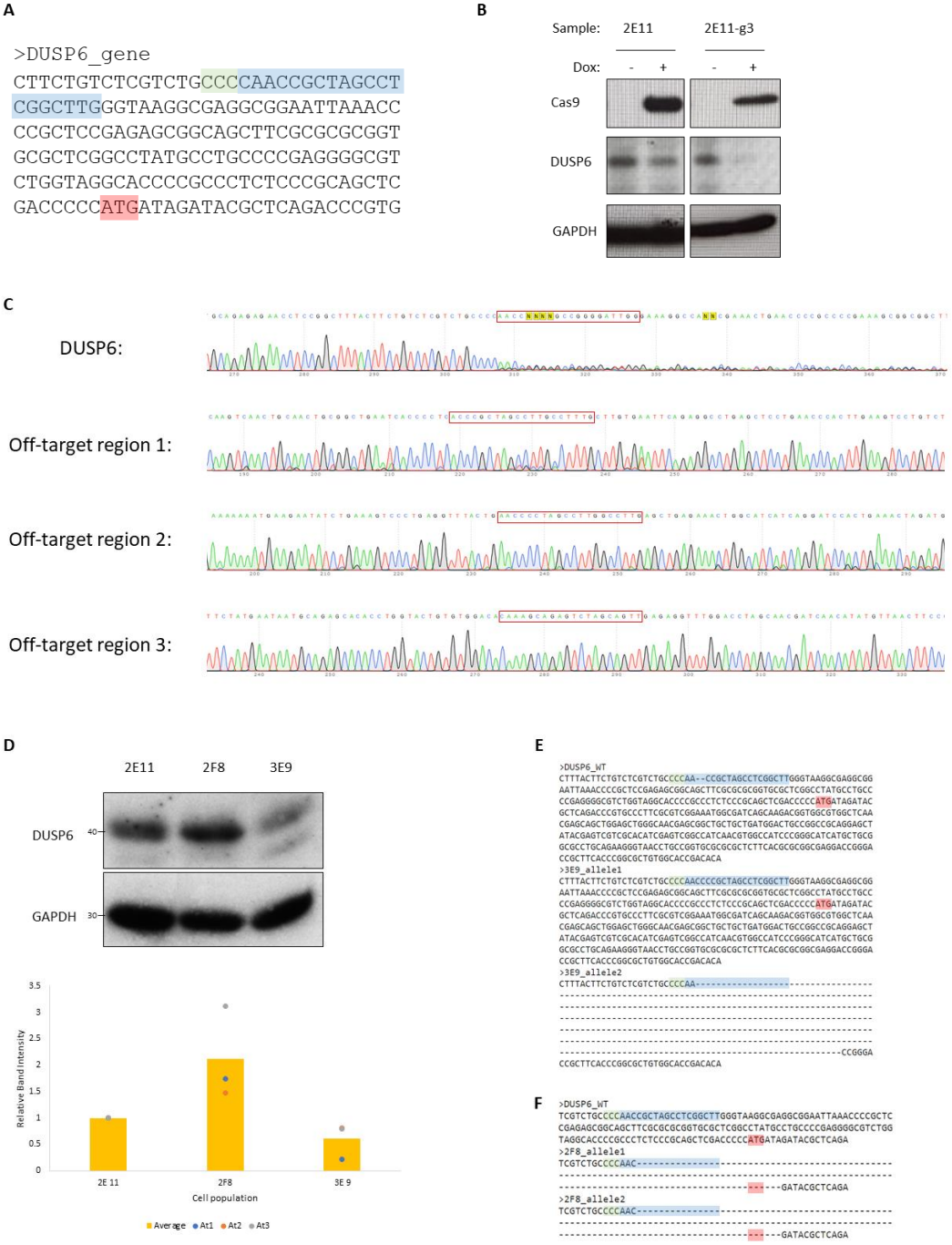

Figure 3.8 – Loss of DUSP6 using gRNA 3. (A) DNA sequence of the region upstream and downstream of the DUSP6 start codon. The gRNA 3, PAM site and DUSP6 start codon are highlighted in blue, green and red respectively. (B) The iIMR-32-gRNA 3 (2E11g3) and iIMR-32 non-transfected control (2E11) were treated with 1 µg/ml dox for 12 days and a Western blot was performed for DUSP6 (Performed by Dr. Vruti Patel). (C) Sequence traces of genomic regions containing the gRNA 3 site in the DUSP6 gene and the top three off-target sites identified in the Benching software (highlighted in the red boxes). 2E11g3 cells were treated for 6 days with 1 µg/ml dox and genomic DNA was sequenced. (D) Basal

DUSP6 expression in the 2E11g3 subclones compared to the non-transfected control (2E11) (n = 3). For quantification, DUSP6 was normalised to GAPDH followed by a second normalisation to 2E11. One-way ANOVA compared to 2E11 but no significance was found. Sequence alignment of a region of the WT DUSP6 sequence alongside both alleles of subclones 3E9 (D) and 2F8 (E). In all DNA sequences, highlighted in green, blue and red are the PAM sequence, gRNA 3 and DUSP6 start codon respectively.

Table 3.5 – DUSP6-null subclones generated from the 2E11g3 mixed population. 15 single cell clones derived from the 2E11g3 mixed population were sequenced and the majority displayed homozygous or compound hemizygous deletions.

Sample	Zygosity	Indel
3B10	WT	
1B5	Compound hemizygous	6bp and 13bp deletion
1C11		1bp insertion and 8bp deletion
3E9		2bp insertion and 380bp deletion
2C3		2bp and 13bp deletion
2B3		19bp deletion and 23bp deletion
2E11		5bp deletion and unknown 2nd allele
2D8		1bp and 2bp deletion
1G6		42bp and 86bp deletion
2D9	Homozygous	1bp insertion
1E2		1bp insertion
3E6		3bp insertion
1D7		19bp deletion
2F8		146bp deletion
3F5		1bp deletion

To investigate whether partial depletion of DUSP6 (clone 3E9) or translation from a second codon (clone 2F8) hampers cell growth, clones were plated at the same density and the number of cells were quantified after 7 days. The growth of the 2F8 population was marginally slower than the control 2E11g3 population but this was not statistically significant. This suggests that using the internal DUSP6 start codon does alter IMR-32 cell growth. Alternatively, during the cloning process, cells may have been selected for that can tolerate loss of DUSP6 or have intracellular changes that compensate for loss of DUSP6. However, clone 3E9 grew significantly slower than 2E11g3 (**Fig. 3.9A**). Interestingly, the growth rate of 3E9 varied greatly in each individual replicate, demonstrated by the larger error bars. This was a surprising finding as the DUSP6 siRNA did not reduce IMR-32 cell viability (**Fig. 3.2E** and **Fig. 3.5**). Although the DUSP6 siRNA pool has off-target toxicities, it does effectively reduce DUSP6 expression. Hence, I treated each cell population with the DUSP6 siRNA pool to see whether additional depletion of DUSP6 protein could further reduce 3E9 cell growth (**Fig. 3.9B**). Treatment with the DUSP6 siRNA pool decreased cell growth of 3E9 by ~15%. Considering this the same as in 2E11g3 and 2F8, this suggests the DUSP siRNA pool is causing a minor off-target toxicity in all cell populations as opposed to a DUSP6-specific effect.

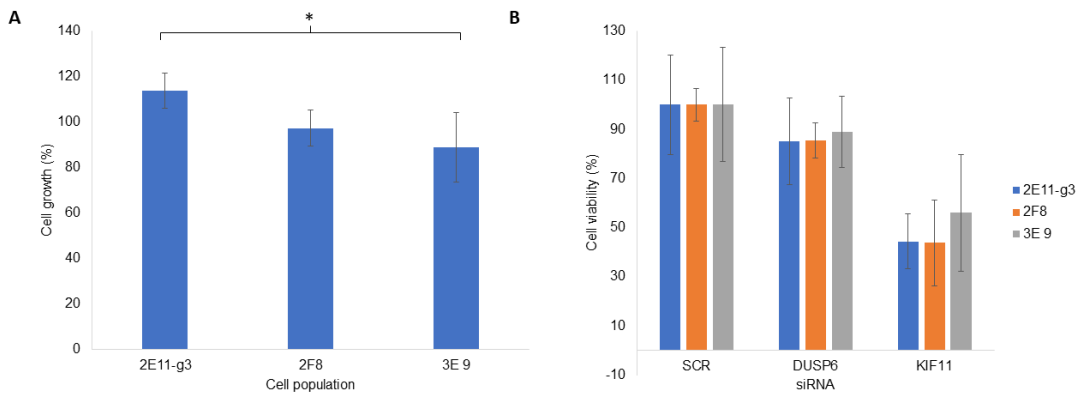

Figure 3.9 – Partial loss of *DUSP6* does not affect cell growth or response to DUSP6 siRNA. (A) Cell growth of subclones 2F8 and 3E9 and the 2E11g3 were measured using the resazurin assay over 6 days (n = 5). (B) The 2E11g3 population and subclones 2F8 and 3E9 were treated with 5 nM siRNA and cell viability was measured using a resazurin assay after 6 days (n = 3). Data are expressed as a mean ± SD. One-way ANOVA compared to 2E11g3; *$p \leq 0.05$.

My principal aim was to remove DUSP6 protein from the KELLY and IMR-32 populations to see the effect of DUSP6 on NB cell growth and intracellular signalling. As editing with the gRNA 3 generated a wide range of deletions but did not appear to abolish DUSP6 expression, alternative gRNAs were required which completely remove DUSP6 protein. With this in mind, I generated two further gRNAs (gRNA 1 and 4). The CRISPR-Cas9 machinery is clearly very efficient at introducing indels into the target gene, therefore it appears critical that the gRNA targets the right location. Hence, the gRNAs were carefully designed to maximise indel effectiveness. The catalytic CTD contains the HCX_5R region and general acid loop involved in catalysis, therefore any out-of-frame mutations upstream of this region should remove protein catalytic activity (**Fig. 3.10A**). The design of gRNA 1 and 4 are described in **Chapter 2.2.1**. Both gRNAs target a region in the N-terminal domain of the *DUSP6* gene, proximal to the start codon (**Fig. 3.10**). Unfortunately, the aforementioned start codon at position Met14 was not known about during the design of the gRNA 1, which targets a region directly after the *bona fide* start codon. Hence, only larger mutations that remove the second start codon are likely to prevent protein translation. Consequently, a third gRNA termed gRNA 4 was designed further downstream (**Fig. 3.10A**). The SNAP2 software also allowed us to design the gRNAs in regions that were also important for protein function (**Fig. 3.10B**). The software predicts the effect of each amino acid substitution on protein function. Although CRISPR will mainly introduce indels as opposed to substitutions, this helped us predict the effect of an in-frame indel. Each editing event will take place approximately 3-4 base pairs (1-2 amino acids) downstream of the PAM site (**Fig. 3.10B**). Considering there are red regions proximal to the gRNA 4 PAM site, I expected in-frame mutations to also be detrimental to protein function.

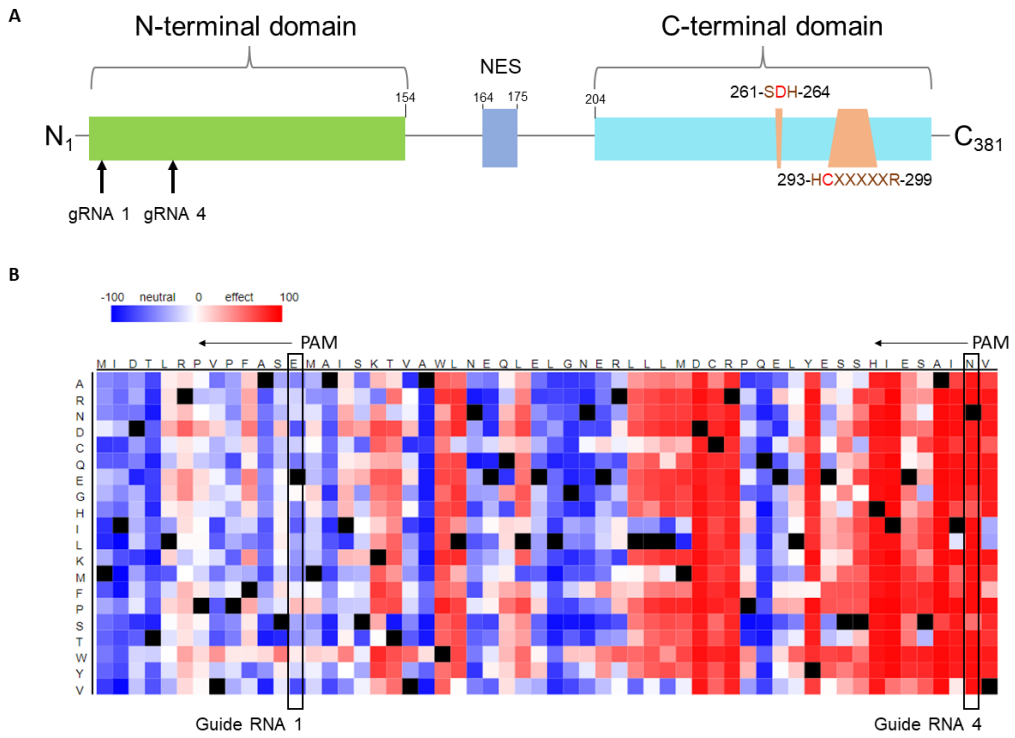

Figure 3.10 – Designing gRNA 1 and gRNA 4. (A) Schematic of the DUSP6 protein domain structure depicting N- and C-terminal domains separated by a nuclear export signal (NES). The C-terminal domain contains the HCX_5R and SDH motifs required for catalysis and gRNA 1 and 4 were designed in the N-terminal region. (B) The functional effect of each sequence variant in the first 56 amino acids of the DUSP6 gene (SNAP2 online tool). Each column represents an amino acid in the DUSP6 sequence and each row represents an alternative amino acid. The heatmap depicts the predicted effect on protein function for each amino acid substitution where blue and red are neutral and strong disruptive effect, respectively. The black boxes depicts the amino acid containing the PAM site. Indel events occur approximately 3-4 base pairs (1-2 amino acids) downstream of the PAM site, where the arrow depicts the direction of editing.

The iKELLY and iIMR-32 cell populations, termed 2E2 and 2E11 respectively, were transfected with gRNA 1 and selected by treatment with puromycin. After treatment with dox, a T7 assay was used to demonstrate the proportion of editing in the iKELLY- and iIMR-32-derivative mixed populations, 2E2g1 and 2E11g1 respectively. As DNA was taken from the cells when the cells were split, each cell population has a slightly different time series but cover a similar length of time. After 24 hours treatment with dox, there was no editing in either cell population, however editing in the 2E11g1 population after 48 hours demonstrated the CRISPR machinery is

functional in a short space of time (**Fig. 3.11A**). Editing efficiency was greatest after 5 days dox treatment where 33% of cells contained indels. Interestingly, the proportion of editing in the 2E11g1 population does not increase proportionally to dox treatment as one would expect. Editing in the 2E2g1 population only reached 16% after 2-3 weeks of dox treatment suggesting editing is not enhanced by prolonged treatment with dox (**Fig. 3.11A**). 2E11 and 2E2 cell populations not transfected with gRNA were also treated with dox and showed no editing in the *DUSP6* gene. Subsequently, a western blot was performed demonstrating significant reduction in DUSP6 expression in both the 2E11 and 2E2 populations (**Fig. 3.11B**). Surprisingly, expression of DUSP6 was greatly reduced to in 2E11g1 and 2E2g1 populations compared to uninduced cells, significantly lower than the editing demonstrated in the T7 assay. This suggests the T7 assay significantly underestimates the proportion of cells that have indels. Oddly, the expression of DUSP6 before dox treatment was higher in the 2E2 and 2E11 populations with gRNA 1 than without it. Following this, the 2E11g1 and 2E2g1 mixed populations were single cell cloned using the same protocol as with gRNA 3, to identify DUSP6 knock-out subclones. The KELLY cell line appeared more reluctant to grow into colonies from single cells than IMR-32 cells, hence, previous work with gRNA 3 was performed in IMR-32 cells only. Nonetheless, in both cell lines various clones were identified with a significant reduction in DUSP6 protein (**Fig. 3.11C**). Unfortunately, there appeared to be a faint residual DUSP6 band present in many subclones which when quantified represents ~10-20% of basal DUSP6 expression. This suggests that either this is a background band from the DUSP6 antibody binding onto the membrane or complete knock-out of DUSP6 has not been achieved due to the second start site at Met14.

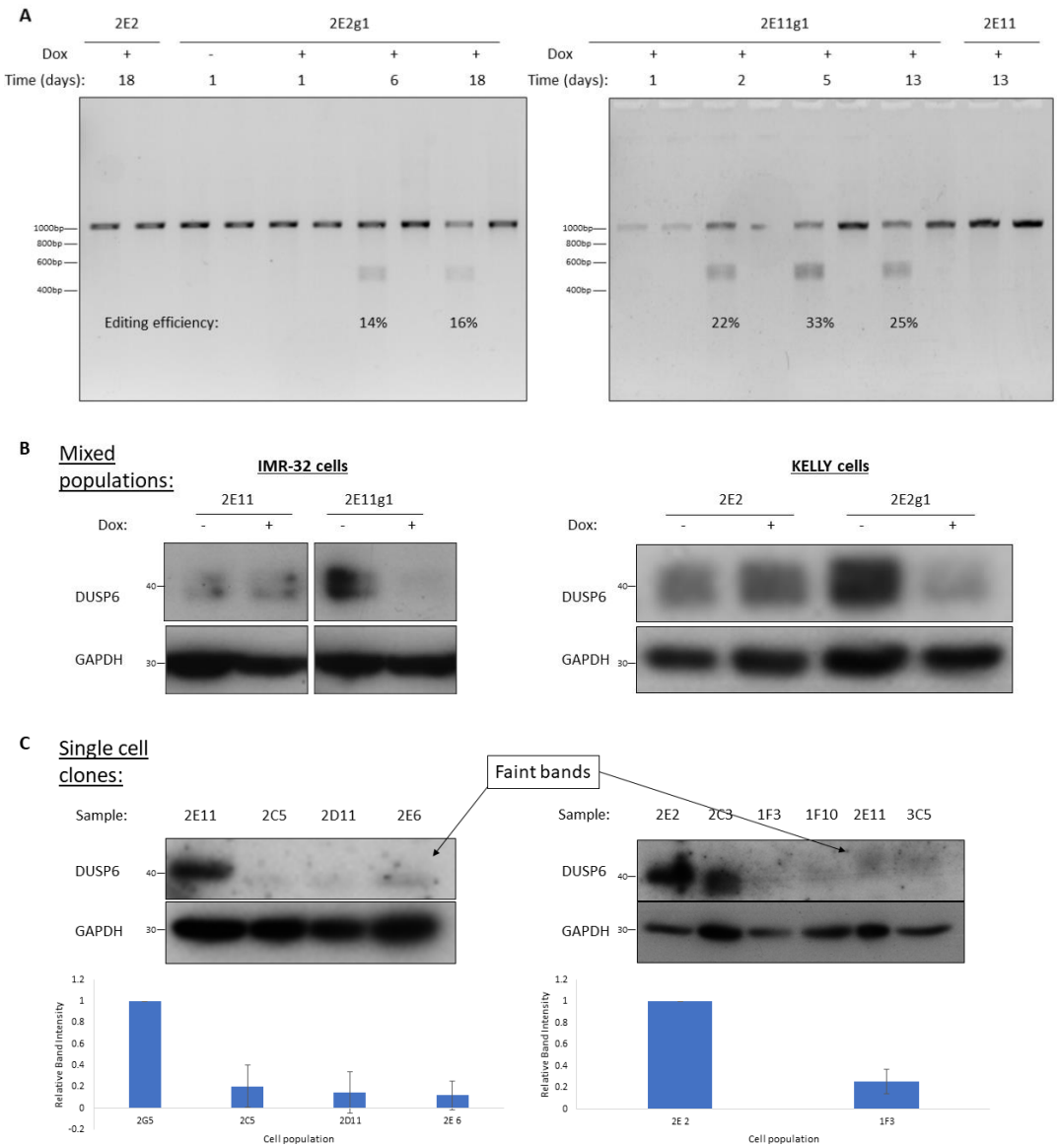

Figure 3.11 – Depletion of DUSP6 using gRNA 1. (A) T7 assays were performed on the iIMR-32 and iKELLY cells after treatment with 1ug/ml dox for an increasing number of days. The non-transfected IMR-32 (2E11) and KELLY (2E2) populations were used as controls. The proportion of cleaved product was used to determine the editing efficiency of the CRISPR/Cas9. (B) Each mixed population was treated with 1 ug/ml Dox for 4 days and a Western blot was performed for DUSP6 (n = 1). (C) Basal DUSP6 expression in the 2E11 and 2E2 subclones compared to the non-transfected controls (2E11 and 2E2) (n = 3). For quantification, DUSP6 was normalised to GAPDH followed by a second normalisation to the non-transfected control. Data are expressed as a mean ± SD.

As opposed to investigating what these residual bands may be, it appeared more time efficient to see whether gRNA 4 would generate complete knock out of DUSP6 protein. To this end, the gRNA 4 vector was transfected into

the 2E2 and 2E11 cell populations and selected for in a similar manner to gRNA 3 and gRNA 1 (**Fig. 3.12A**). Dox treatment of both the 2E11g4 and 2E2g4 mixed populations led to a significant reduction in DUSP6, where over-exposure of the DUSP6 membranes was required to demonstrate any remaining protein (**Fig. 3.12A**). This is higher editing than previously observed with gRNA 3 or gRNA 1. DUSP6 expression also appeared to be reduced slightly in the 2E2 population after dox treatment which reached statistical significance. This is likely a consequence of the dox treatment as dox is known to influence ERK signalling therefore could alter DUSP gene expression (Chen et al., 2009a). Considering the location of the gRNA 4 on the *DUSP6* gene, I hypothesised that any recombination induced by the CRISPR/Cas9 machinery led to a frame shift resulting in targeted degradation of a dysfunctional protein.

To assess the effect of complete loss of DUSP6, each population was single cell cloned as performed previously and a range of subclones were analysed for DUSP6 expression (**Fig. 3.12B-C**). Out of 21 2E11g4 subclones, 20-30% demonstrated DUSP6 expression to some extent, in accord with what is expected if all subclones underwent editing and 33% of mutations were in frame. Nevertheless, no subclone appeared to retain WT levels seen in 2E11g4, suggesting that all have recombined at some level. A range of subclones did not demonstrate any residual protein and most likely have no DUSP6 expression (**Fig. 3.12B**). Similarly, out of 8 2E2g4 subclones, 1E8, 2B3, 3C4 and 3C10 displayed no DUSP6 protein (**Fig. 3.12C**). A range of KELLY (2E2g4) and IMR-32 (2E11g4) subclones were selected and sent for sequencing to identify indel positions. Demonstrated in **Figure 3.13** are the IMR-32 subclone 1D5 and the KELLY subclones 1E8, 3C4 and 3C10 as they are used in subsequent experiments. Sanger sequencing demonstrated either homozygous or compound hemizygous mutations in each subclone confirming that they will not translate functional DUSP6 protein. For clarity, the IMR-32 subclone 1D5 will be termed IMRD6-1 and the KELLY subclones 1E8, 3C4 and 3C10 will be termed KELD6-1, KELD6-2 and KELD6-3 respectively (**Fig. 3.13A**). Although this is a very

small sample size, the same indels are present in different clones, suggesting the CRISPR machinery preferentially causes certain indels.

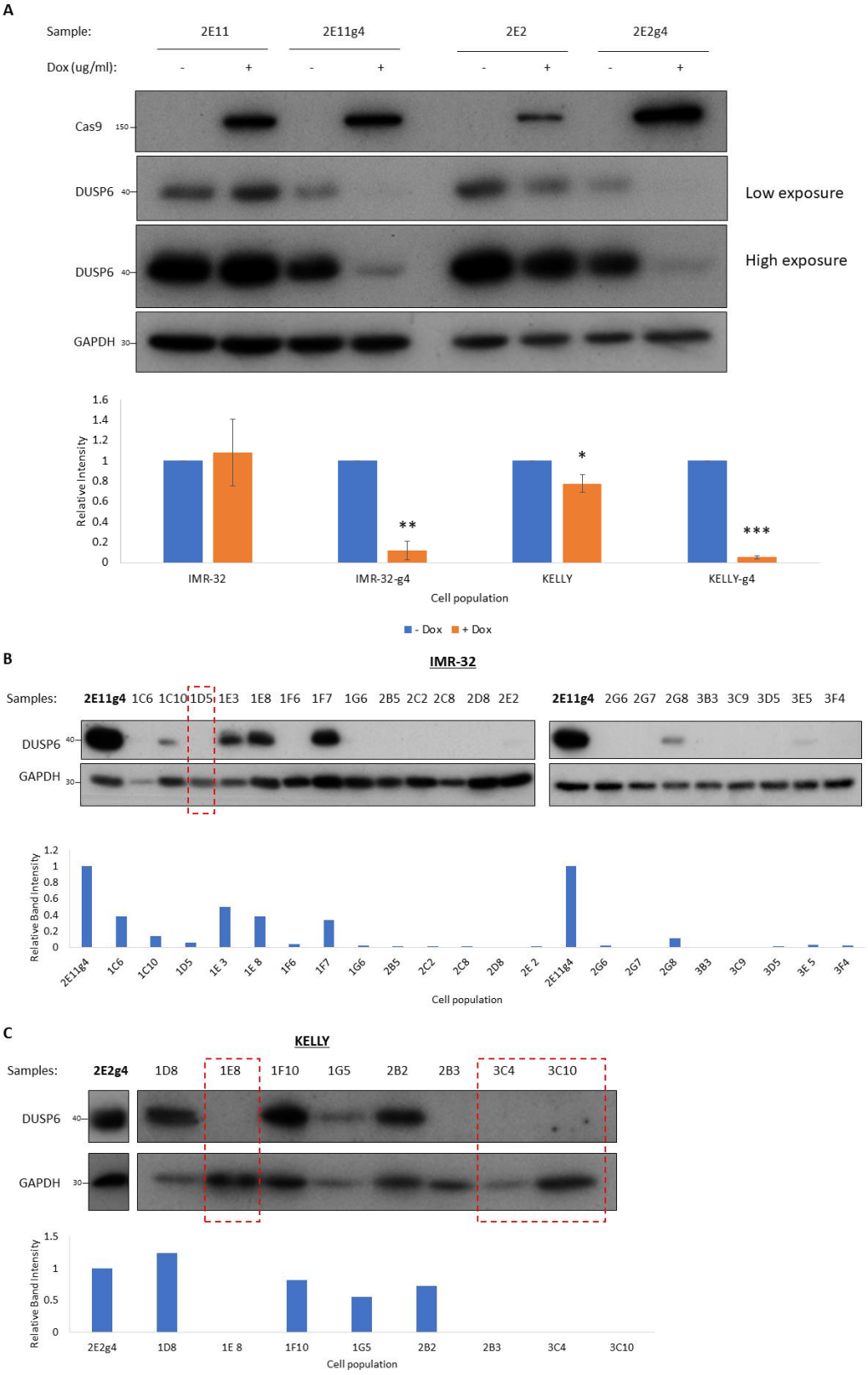

Figure 3.12 – Generating DUSP6-null subclones using gRNA 4. (A) The 2E11g4 and 2E2g4 mixed populations were treated with 1 µg/ml dox for 4 days and a Western blot was performed against DUSP6 (n = 3). Basal DUSP6 expression in the 2E11 (B) and 2E2 (C) subclones compared to untreated control cells (n = 1). Highlighted in red boxes are subclones that were sequenced and used in further studies. For quantification, DUSP6 was normalised to GAPDH followed by a second normalisation to the non-transfected control. Data are expressed as a mean ± SD. One-way t-test compared to 1; *p ≤ 0.05; **p ≤ 0.005; ***p ≤ 0.0005.

A

Cell line	Sub-clone	Identifier	Indel
IMR32	1D5	IMRD6-1	1bp deletion and 1bp insertion
KELLY	1E8	KELD6-1	1bp insertion and 13bp deletion
	3C4	KELD6-2	1bp deletion and 1bp insertion
	3C10	KELD6-3	1bp insertion and 13bp deletion

B

```
WT              AGGAGCTATACGAGTCGTCGCACATCGAGTCGGCCAT-CAACGTGGCCATCCCGGGCATC
1D5_allele2     AGGAGCTATACGAGTCGTCGCACATCGAGTCGGCCATCCAACGTGGCCATCCCGGGCATC
1D5_allele1     AGGAGCTATACGAGTCGTCGCACATCGAGTCGGCCAT--CACGTGGCCATCCCGGGCATC
                ************************************   ********************

WT              AGGAGCTATACGAGTCGTCGCACATCGAGTCGGCCATC-AACGTGGCCATCCCGGGCATC
1E8_allele2     AGGAGCTATACGAGTCGTCGCACATCGAGTCGGCCATCAAACGTGGCCATCCCGGGCATC
1E8_allele1     AGGAGCTATACGAGTCGTCGCACATCGA--------------GTGGCCATCCCGGGCATC
                ******************************              ******************

WT              AGGAGCTATACGAGTCGTCGCACATCGAGTCGGCCAT-CAACGTGGCCATCCCGGGCATC
3C4_allele2     AGGAGCTATACGAGTCGTCGCACATCGAGTCGGCCATCCAACGTGGCCATCCCGGGCATC
3C4_allele1     AGGAGCTATACGAGTCGTCGCACATCGAGTCGGCCAT--CACGTGGCCATCCCGGGCATC
                ************************************   ********************

WT              AGGAGCTATACGAGTCGTCGCACATCGAGTCGGCCATC-AACGTGGCCATCCCGGGCATC
3C10_allele2    AGGAGCTATACGAGTCGTCGCACATCGAGTCGGCCATCAAACGTGGCCATCCCGGGCATC
3C10_allele1    AGGAGCTATACGAGTCGTCGCACATCGA--------------GTGGCCATCCCGGGCATC
                ******************************              ******************
```

Figure 3.13 – Sequences of KELLY and IMR-32 DUSP6-null subclones. (A) Summary of the KELLY and IMR-32 subclones that were assessed in subsequent experiments. (B) Sequence alignment of a region of the WT DUSP6 sequence alongside both alleles of 2E11g4 subclone 1D5 and 2E2g4 subclones 1E8, 3C4 and 3C10. Highlighted in green and blue are the PAM sequence and gRNA 4 respectively.

3.2.6. Genetic deletion of DUSP6 reduces KELLY cell growth

The IMR-32 sub clones generated when targeting DUSP6 with gRNA 3 each displayed a significant difference in relative cell growth. This is most likely due to clonal variation in the population as opposed to an effect from loss of DUSP6. We hypothesised that assessing the cell growth across a mixed population would be a more reliable estimate on the overall effect on cell growth, especially considering editing with gRNA 4 results in an 80-90% reduction in DUSP6 protein in the mixed population. After treatment with dox for 4 days, there was no apparent effect of DUSP6 depletion on IMR-32 cell proliferation. This is similar to what was observed with the DUSP6 siRNA (**Fig. 3.5**). However, loss of DUSP6 in the KELLY cells resulted in a

marginal, yet statistically significant, reduction in cell growth (**Fig. 3.14A**). This ~10% drop is far less than the effect with DUSP6 siRNAs, but suggests that DUSP6 does promote NB cell growth in KELLY cells. It is worth noting that, without dox treatment, the 2E2g4 population grew quicker than the 2E2 population (data not shown). As the 2E2g4 population is already partially deficient in DUSP6 (**Fig. 3.12A**), this suggests that the expression of DUSP6 can have a differential effect on cell survival.

Considering there is a change in the KELLY mixed population, we investigated whether this is reproduced in the DUSP6-null subclones. (**Fig. 3.14B**) Interestingly, the KELD6-1 population grew significantly slower than 2E2g4 cells but KELD6-2 cells did not. Neither population expresses DUSP6, therefore the difference in growth could simply be due to the heterogenous nature of clonal derivatives. Alternatively, the cell growth effect of DUSP6 deletion may only occur in certain cases where cells cannot adapt or use a compensatory mechanism. With a clear difference in cell growth, subsequent biochemical signalling analysis was performed in KELD6-1. It is also worth noting that similar to the siRNA screen, the cell growth effect correlates with the cell line ALK-mutation status. This correlation is explored further in **Chapter 6** using a range of ALK-mutated cell lines.

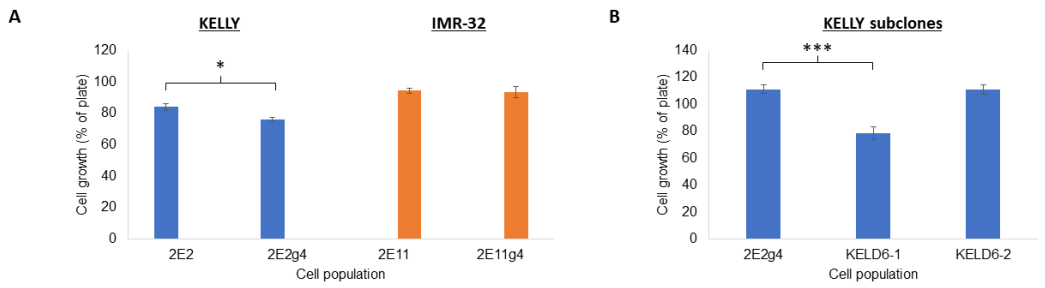

Figure 3.14 – Loss of DUSP6 reduces KELLY cell growth. (A) Cell growth of 2E2 and 2E11 cell populations with and without gRNA 4 was measured using the resazurin assay over 6 days (n = 3). Cells were treated with 1 µg/ml Dox and growth was normalised to untreated cells and then subsequently normalised to 2E11 cells. Data are expressed as a mean compared to plate average ± SD. (B) Cell growth of 2E2g4 and subclones was measured using the resazurin assay over 6 days (n = 3). Data are expressed as a mean compared to plate average ± SD. One-way ANOVA compared to control cells; *$p \leq 0.05$; ***$p \leq 0.0005$.

By completely removing an MKP from these cells, we would expect there to be an increase in intracellular signalling through at least one of the MAPK pathways. To address this, 2E2g4 and 2E11g4 cells (without dox stimulation therefore with wild type DUSP6 expression) were stimulated with EGF to upregulate the ERK pathway and a western blot was performed to assess the changes in intracellular signalling (**Fig. 3.15**). Similar to before, treatment with EGF in 2E2g4 cells induced a rapid accumulation of pERK which remained significantly higher than basal levels over 6 hours. Interestingly, there is a biphasic pattern of ERK phosphorylation levels, peaking at 10 minutes and 90 minutes, suggesting an initial feedback is in place to restrain pERK signalling. However, the loss of DUSP6 does not appear to have a significant effect on regulation of pERK in this context. Pairwise comparison of each time point demonstrates pERK is increased in the KELD6-1 population, but due to the large variation between replicates it is not statistically significant. Conversely, the effect of EGF on pAKT and pp38 is minor, and the loss of DUSP6 does not affect their phosphorylation. Compared to KELLY cells, the MAPK signalling pathways are less functional in the IMR-32 cells, hence it is harder to detect each phospho-protein. Furthermore, treatment with EGF did not upregulate the ERK pathway further suggesting these cells are less dependent on the ERK signalling pathway. Due to the weak bands present, it is unclear whether loss of DUSP6 affects MAPK signalling. There is a potential increase in pp38 signalling in response to EGF which was abolished by DUSP6 depletion, however this was not reproduced when the experiment was repeated. Overall, the results suggest that in response to EGF, DUSP6 does not significantly restrain either the MAPK or AKT signalling pathways. It is plausible that an alternative DUSP is compensating for the loss of DUSP6 in the DUSP6-null subclones or that different stimulants would result in a greater DUSP6 response to MAPK signalling.

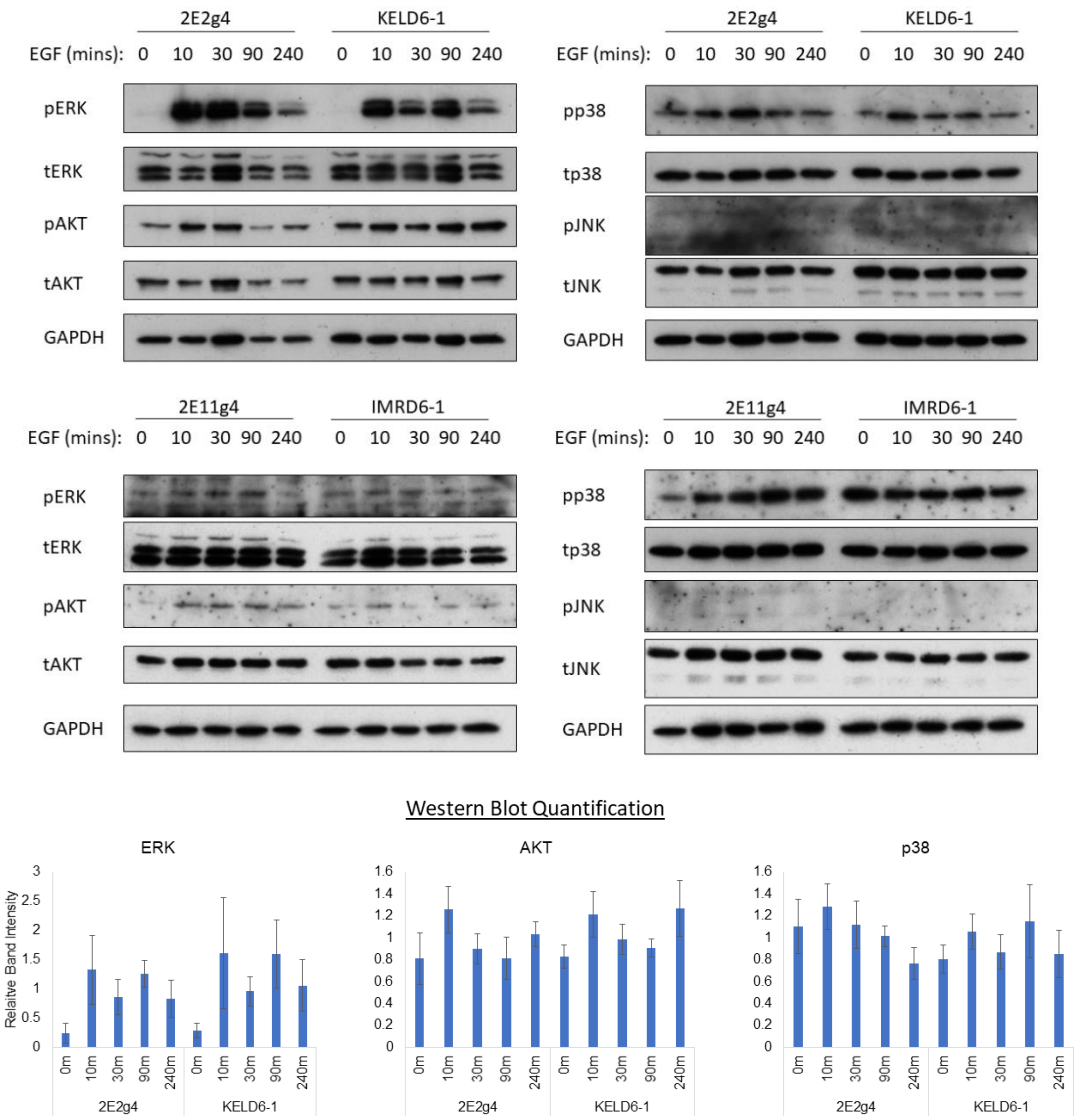

Figure 3.15 – Loss of DUSP6 has no apparent effect on the MAPK or AKT signalling pathways. KELLY and IMR-32 cells were treated with 30 ng/ml EFG for 10, 30, 90 and 240 minutes and a western blot was performed (n ≥ 3). For quantification, each phospho-protein was normalised to their respective total protein followed by a second normalisation to all bands within that experiment. High background signal in the JNK blots and low phosphoprotein abundance in the IMR-32 cells prevented accurate quantification. Data are expressed as a mean ± SD. One-way ANOVA performed for each phospho-protein demonstrates no significance when comparing the same time-points between 2E2g4 and KELD6-1 cells.

3.3. Discussion

The DUSPs are an important family of PTP enzymes that regulate a wide range of biological processes. There is mounting evidence that DUSP function is involved in tumour progression, predominantly via regulation of the MAPKs (Gao et al., 2021, Low and Zhang, 2016). Considering there is a wide range of signalling pathways, including the MAPK pathways, implicated in NB progression, we hypothesised that manipulation of DUSP function may be a novel way to inhibit NB cell growth. Hence, our aim was to identify the DUSPs that display a growth promoting role in NB and identify the pathways they may act upon. The work presented above identified a range of candidate DUSPs from both the MKP and aDUSP subfamilies that are potentially involved in NB cell survival. Six candidate DUSPs were selected to analyse further, including DUSP6; the others are investigated in **Chapter 5**. DUSP6 also appeared growth-promoting in a previous shRNA screen in our laboratory (Dr. Ann Cichon, unpublished data) and is heavily implicated in tumorigenesis elsewhere (Messina et al., 2011, Wittig-Blaich et al., 2017, Chan et al., 2008). Therefore in this chapter, loss of DUSP6 was investigated using two approaches: siRNA knockdown and CRISPR/Cas9-mediated gene deletion. CRISPR/Cas9 depleted DUSP6 protein which marginally reduced KELLY cell growth. However, loss of DUSP6 did not appear to alter the ERK signalling pathway in response to EGF treatment.

A previous shRNA screen had identified a wide range of PTP enzymes that could potentially promote IMR-32 cell growth (Dr. Ann Cichon, unpublished data). Complementing this study, I depleted every DUSP enzyme via pools of siRNAs in four NB cell lines and cell viability was measured. There was a surprisingly large number of DUSPs that appeared growth-promoting from this screen. Large-scale siRNA screens generally have a high rate of false positives due to off-target effects (Echeverri et al., 2006). We believed this would be mitigated by using pools of 4 siRNAs, each at a lower concentration, which the manufactures, Dharmacon, claim dilutes any off-target effect and reduces the number of false positives. These On-

TARGETplus Dharmacon siRNAs are also chemically modified in order to further minimise off-target issues (Jackson and Linsley, 2010). Unfortunately, deconvolution of the individual DUSP6 siRNAs still demonstrated that these siRNAs do have significant off-target effects. We were therefore sceptical that other siRNAs also reduce cell growth via off-target toxicities (investigated further in **Chapter 5**). The importance of identifying off-target effects is demonstrated in large-scale drug discovery, where *in vitro* pharmacological profiling has become an essential part of drug development process (Bowes et al., 2012). This remains true for RNAi-based therapeutics where the understanding of off-target effects has significantly improved the safety profile of siRNA candidate drugs (Bartoszewski and Sikorski, 2019). Alternative methods of pooling siRNAs have been identified which should be investigated further (Kittler et al., 2007, Hannus et al., 2014). Nonetheless, these data highlight the importance of validating siRNAs not just by looking at their on-target effect but also by looking at their off-target effect.

Interestingly, although many DUSPs appeared growth-promoting, there were no clear 'tumour-suppressor-like' DUSPs identified in the screen. As the general dogma is that ERK signalling drives tumorigenesis, we would expect ERK inhibition via DUSPs to lead to cell death. It is therefore striking that in these cell lines there are no obvious DUSPs restraining cell growth via ERK inhibition. This cannot be attributed to lack of on-target effect as DUSP knockdown efficiency was consistently high. This is potentially because these NB cells are already proliferating at their fastest rate *in vitro*, however further experiments are required to elucidate whether this is the case. It is more likely that DUSPs can compensate for each other to restrain ERK signalling. Nunes-Xavier et al. (2019b) demonstrated RA treatment in NB cells causes a large and varied DUSP transcriptional response, therefore there are likely multiple DUSPs available which can function on ERK signalling.

Advances in genomic technologies has allowed the identification of gene expression signatures which are linked to cancer progression and patient survival. These gene signatures can serve as biomarkers, helping predict

response to treatment options and deciding treatment regimens (Kamel and Al-Amodi, 2017). Gene expression is often dichotomised into ‘high’ and ‘low’ based on the median expression, mean expression or alternative methods for identifying an optimal breakpoint. However, a recent study demonstrated the cox regression analysis is more accurate when dealing with continuous variables such as gene expression (Raman et al., 2019). The cox regression analysis determines the effect of one or more variables on the time of an event (Cox, 1972). In this instance, the association of DUSP gene expression and patient survival was assessed. This approach also allows the combination of clinical and pathological features into the same analysis to demonstrate whether one variate can maintain significance independently of others. *DUSP4* and *DUSP26* both appeared to be independent predictors of patient survival in the NRC dataset and were close to significance in the Ora dataset. Kaplan-Meier survival plots demonstrated high *DUSP4* expression correlated with poor patient prognosis whereas the converse was true for *DUSP26*. In a recent study of 48 NB samples, DUSP5 expression also correlated tumour stage, MYCN expression and metastasis (Aurtenetxe et al., 2018). One would predict DUSP5 to therefore have a growth-promoting role in NB. However the authors attributed high DUSP5 expression to ERK negative feedback. Indeed, knockdown of *DUSP5* increased NB cell growth (Aurtenetxe et al., 2018). Considering DUSP4 and DUSP26 are also both ERK phosphatases, this suggests their association with patient prognosis may be more complex than simply growth-promoting or -suppressing. Furthermore, there is also the possibility that changes in gene expression are simply a passenger effect which is driven by progression of the tumour. Whether these candidate genes truly influence NB cell growth is investigated further in **Chapter 5**.

Following these larger analyses, DUSP6 looked an interesting candidate to investigate further. As mentioned previously, DUSP6 has been implicated in the progression of a wide range of cancers (Messina et al., 2011, Wittig-Blaich et al., 2017, Chan et al., 2008). Hence, a key goal of this study was to characterise the growth-promoting aspect of DUSP6 in NB. To address

this, a LOF phenotype was generated using three methods: chemical inhibition, siRNA-mediated gene knockdown and molecular genetic disruption (**Fig. 3.16**). As demonstrated in **Figure 3.16** work relating to chemical inhibition of DUSP6 is investigated in **Chapter 4**. In this chapter, significant off-target effects were identified when using the DUSP6 siRNA pool, therefore CRISPR-Cas9 was employed to introduce indels in the *DUSP6* gene. A range of gRNAs were designed and gRNA 4 successfully abolished DUSP6 expression in the mixed population and its subclone derivatives. Design of gRNA's targeting DUSP6 also identified an alternative start codon at Met14. Using the transcription initiation site predictor tool, Met14 has a preferential Kozak sequence to Met1 suggesting translation could occur from this site (Gleason et al., 2021). Although immunoblotting for DUSP6 generally gives a single band, other studies have demonstrated doublet bands due to this alternative start codon (Ekerot et al., 2008). The inducible system allows you to assess the effect of acute loss of protein within a heterogenous population. This is particularly useful as there is a high degree of heterogeneity between individual clones, visible from the effect of DUSP6 depletion on cell growth. This heterogeneity results from the significant genetic, epigenetic and phenotypic bottleneck as you decrease the mixed population to a single clone. On top of this, growing a clonal cell population from a single cell causes stress on the cells which is morphologically visible. It is likely this stress will alter the intracellular signalling of each clone. Also, during this period of 4-6 weeks the cells go through multiple rounds of cell division in which time the cells will adapt to their extracellular environment. Together these effects may cause each subclonal population to be somewhat distinct at an epigenetic level. In light of this, future experiments will use at least two subclones to assess the effect of a gene knockout.

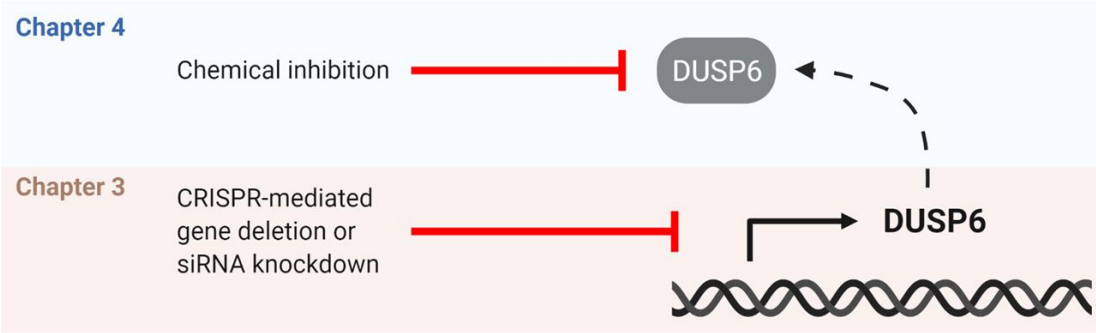

Figure 3.16 – Generating DUSP6 loss-of-function phenotypes. In **Chapter 3**, loss of DUSP6 was investigated using CRISPR/Cas9-mediated gene deletion or knockdown via siRNA. Following this, the therapeutic potential of a dual DUSP1/6 inhibitor, BCI, will be investigated in **Chapter 4**.

Loss of DUSP6 appeared to marginally reduce KELLY cell growth in the mixed population but did not affect IMR-32 cells. Differences between NB cell lines is unsurprising considering cellular heterogeneity is a hallmark of NB (Ngan, 2015). We have also shown these cells respond differently to EGF-mediated ERK signalling demonstrating ERK regulation is distinct between these cell lines. A growth-promoting role of DUSP6 is counter-intuitive as ERK signalling is known to drive NB cell growth (Lopez-Delisle et al., 2018, Eleveld et al., 2015, Xie et al., 2019). Nonetheless, a growth-promoting role of DUSP6 have been observed in various cancers (Messina et al., 2011, Wittig-Blaich et al., 2017, Chan et al., 2008). In glioblastoma multiforme, *DUSP6* is overexpressed in primary cell cultures and is upregulated in long term cultures (Messina et al., 2011). It appears DUSP6 suppressed ERK signalling in this setting but how this translates into tumour progression remains unclear. Paradoxically, it appears that ERK-driven tumorigenesis may become addicted to the negative feedback control of ERK. Shojaee et al. (2015) demonstrates that negative feedback of ERK is essential for pre-B acute lymphoblastic leukaemia (ALL) transformation. Initial assays demonstrated that activation of $NRAS^{G12D}$ or the tyrosine kinase BCR-ABL1 in pre-B ALL cells led to significant cell death. The minority of cells that survived displayed significant expression of ERK feedback regulators DUSP6, ETV5 and SPRY2, and eventually led to a robust oncogenic transformation. To investigate this further, pre-B ALL cells

from the bone marrow of WT and DUSP6$^{-/-}$ mice were transformed with NRAS^{G12D} or BCR-ABL1. Strikingly, loss of DUSP6 prevented oncogenic transformation in both cases. The authors suggested these ERK negative regulators may represent an additional class of therapeutic targets in pre-B ALL. As well as driving cell growth, ERK can also induce apoptosis (Sugiura et al., 2021). Hence, we hypothesise that altering the DUSP6-ERK feedback mechanism can promote ERK-mediated apoptosis. Indeed, in NIH-3T3 cells knockdown of *DUSP6* induced apoptosis in cells with overexpression of HER2 but not in cells without (Kanda et al., 2021). As cell death was driven by ERK activation, it appears the magnitude of ERK signalling, partly dictated by DUSP6 regulation, could pass an apoptotic threshold. This does not appear to be the case for DUSP6 alone. In another study, knockdown of SPRY2, another negative regulator of ERK, inhibited glioblastoma cell proliferation and induced apoptosis but did not affect normal astrocytes (Park et al., 2018). Similar to DUSP6, cell death caused by *SPRY2* knockdown required ERK activation. This could be a mechanism predominantly at play when cancer cell growth is driven by ERK activity. In melanoma cells *DUSP6* knockdown reduced cell viability only in cell lines with the BRAF V600E mutation (Wittig-Blaich et al., 2017). Although the authors demonstrate cell death was driven by activation of apoptosis, they did not investigate whether this was mediated by increased ERK signalling. This is in accord with the data demonstrated here in NB cells. KELLY cells have higher basal ERK signalling than IMR-32 (**Fig. 3.15**), presumably due to their mutated ALK receptor, and they are susceptible to DUSP6 depletion (**Fig. 3.14**). Using the data described above from other cancers, a model proposing the role of DUSP6 in KELLY cells is presented in **Figure 3.17**. Here, ERK signalling is high to maintain cell growth and results in a strong negative feedback by DUSP6. However, as DUSP6 is removed, ERK signalling becomes deregulated and results in increased apoptotic signalling and NB cell death. To explore this further, experiments measuring apoptotic signalling in KELLY cells after DUSP6 depletion would be beneficial.

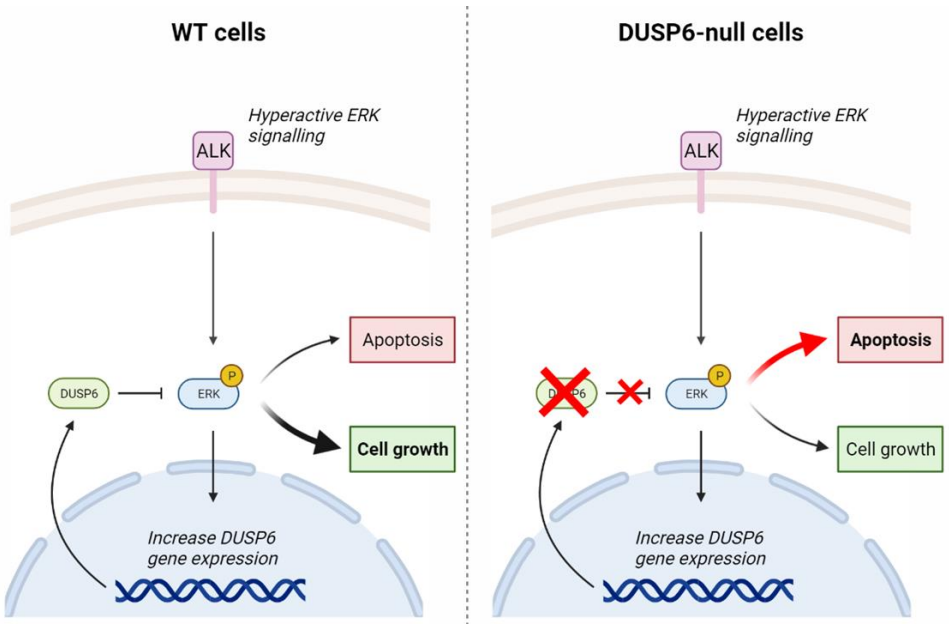

Figure 3.17 – Loss of ERK negative feedback regulation triggers apoptotic signalling. In this model, oncogenic signalling via ERK drives KELLY cell growth. ERK signalling also upregulates DUSP6 transcriptionally and DUSP6 negative feedback of ERK maintains optimal ERK stimulation to drive cell growth. However, if DUSP6 is removed from these cells, loss of the DUSP6 feedback loop alters ERK phosphorylation levels which in turn passes an apoptotic threshold and drives apoptotic signalling.

However, this model complicated by the fact that loss of DUSP6 doesn't affect ERK signalling in the NB cells under basal conditions or after EGF stimulation (**Fig. 3.15**). This basic model of excessive ERK activation may therefore not apply straightforwardly in NB cells. There are various possibilities explaining this. DUSP6 has a dual function where it is able to both dephosphorylate ERK and anchor ERK in the cytoplasm (Karlsson et al., 2004). Hence, DUSP6 may prevent ERK entry into the nucleus restraining ERK signalling as opposed to dephosphorylating it. This could be assessed by investigating ERK localisation either by immunofluorescence or nuclear fractionation followed by an immunoblot. Alternatively, DUSP6 may be compensated for by other ERK-specific DUSPs. A previous study in thyroid cancer cell lines containing the BRAF^{V600E} mutation demonstrated knockdown of *DUSP5* significantly

altered DUSP6 protein expression and vice versa (Buffet et al., 2017). Interestingly, these responses varied depending on the cell line and time point. This indicates that there could be a compensatory mechanism between DUSP5 and DUSP6. Furthermore, Caunt et al. (2008a) demonstrated EGF or PDBu stimulation in HeLa cells altered transcription of multiple DUSPs at the same time, further suggesting DUSPs may function in a cooperative nature. This possibility is investigated further in **Chapter 5**. Lastly, there are some indications DUSP6 can dephosphorylate other targets. Initial studies suggested DUSP6 is an ERK-specific phosphatase principally due to the specific contacts required between the DUSP6 kinase interacting motif (KIM) and the ERK KIM docking site to activate DUSP6 phosphatase activity (Nichols et al., 2000, Liu et al., 2006). However, there are various studies demonstrating DUSP6 dephosphorylates other MAPKs (Ndong et al., 2014, Zhang et al., 2011, Hu et al., 2019, Lee et al., 2021). Furthermore, a recent study by Ma et al. (2020) identified DRP1 as a non-MAPK substrate of DUSP6. One potential explanation for this discrepancy is that DUSP6 may be activated by ERK to target other proteins. Zhang et al. (2011) demonstrated DUSP6 could form a tertiary complex with ERK and p38. ERK bound the non-catalytic domain of DUSP6 which allowed dephosphorylation of p38. If ERK can truly act as a scaffold to promote DUSP6-mediated dephosphorylation of other targets, there is likely a myriad of other DUSP6 targets yet to be identified. What these DUSP6 targets could be is investigated in **Chapter 6**.

Overall, the data presented above identified a wide range of DUSPs that may be involved in regulating NB cell growth. Moreover, the expression of *DUSP4* and *DUSP26* appeared to be associated with NB prognosis. Many of these DUSP candidates will be explored further in **Chapter 5**. Characterisation of the DUSP6 individual siRNAs highlighted the importance of validating the on- and off-target effects of each approach. These data also suggest the siRNA screen may contain other false positives. Following this, CRISPR-Cas9 was effectively employed to abolish DUSP6 protein in KELLY and IMR-32 cells. The role of DUSP6 appears cell specific as loss of DUSP6 decreases KELLY cell growth but not IMR-32.

We suggested a speculative model as to how DUSP6 promotes KELLY cell growth were loss of DUSP6 triggers ERK-mediated apoptosis (**Fig. 3.17**). However, EGF-mediated ERK signalling was unaffected in the DUSP6-null clones. Furthermore, little change was seen in the JNK, p38 and AKT pathways. This raises the question of whether DUSP6 has an alternative target in NB cells that may also drive cell growth. Considering there are other DUSP6 substrates in the literature, both MAPK and non-MAPK related, this is something which merits further exploration.

Chapter 4. Investigating the therapeutic potential of BCI and BCI-215

4.1. Introduction

Despite being implicated in numerous diseases, therapeutically targeting PTPs has had limited success with no PTP inhibitor entering the pharmaceutical market to date. As previously mentioned, the difficulty in generating a clinical inhibitor primarily stems from *in vivo* target specificity and cell permeability (Tautz et al., 2006, Barr, 2010). Fortunately, since the growing realisation that aberrant PTP function significantly contributes to disease, extensive research has been geared towards identifying more selective and cell permeable inhibitors (Zhang, 2017, Stanford and Bottini, 2017). With mounting evidence of its role in disease (Ahmad et al., 2018), much effort has been put into the generation of a specific DUSP6 inhibitor. To date, five chemical inhibitors have been identified which are somewhat specific towards DUSP6 (**Fig. 4.1**). Phosphatase inhibition of Adociaquinone B, NSC 95397 and NSC 357756 were initially demonstrated through screening the National Cancer Institute diversity set *in vitro*, however issues surrounding selectivity remains a recurrent theme (Lazo et al., 2002, Cao et al., 2009). Adociaquinone B displayed higher inhibitory activity towards the cell cycle regulator CDC25B, a different dual-specific phosphatase (Cao et al., 2009). The chemical NSC 357756 appeared promising with *in vitro* and *in vivo* DUSP6 inhibition, but when used to generate NSC 357756 congeners, they were highly selective towards DUSP1 (Lazo et al., 2006, Vogt et al., 2003). NSC 95397 also demonstrated DUSP1 and DUSP6 inhibition in a chemical complementation assay but has reported interactions to a myriad of other proteins such as the CDC25 phosphatases, AKT, CtBP and S100A4 (Vogt et al., 2008, Dulyaninova et al., 2011, Yang et al., 2014, Blevins et al., 2015).

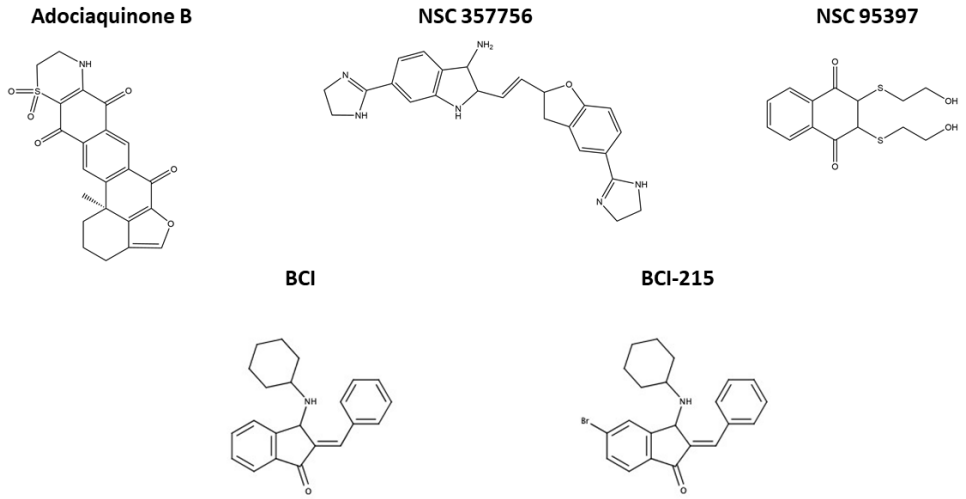

Figure 4.1 – Chemical inhibitors of DUSP6. Chemical structures were drawn using the Chemdraw software.

Significant progress though has been made in the development of allosteric inhibitors. These inhibitors avoid the highly conserved catalytic cleft which normally causes selectivity issues (Krishnan et al., 2018, Marsh-Armstrong et al., 2018). A breakthrough study by Molina et al. (2009) identified BCI as a potent DUSP1 and 6 inhibitor in an *in vivo* zebrafish chemical screen (**Fig. 4.1**). Previous competitive inhibitors of DUSP6 were also able to inhibit DUSP1 suggesting these DUSPs have analogous structural properties (Vogt et al., 2008, Cao et al., 2009). Molecular docking experiments revealed BCI to function allosterically, binding a region proximal to that of the DUSP6 catalytic active site (Korotchenko et al., 2014). The effect of concurrent inhibition of DUSP1 and DUSP6 is broad as they reside in the nuclear and cytoplasmic compartments respectively and dephosphorylate a range of MAPKs (**Fig. 4.2**). BCI appears selective for DUSP1/6 as it did not block CDC25B, PTP1B or DUSP3 activity *in vitro* (Molina et al., 2009), however a larger screen against alternative PTP and non-PTP targets has not been performed. Structure-activity relationship studies using BCI analogs identified an improved inhibitor termed BCI-215 (**Fig. 4.1**) that displayed comparable DUSP6 inhibition in an *in vitro* phosphatase assay but decreased cellular toxicity in transgenic zebrafish embryos (Korotchenko et al., 2014). Promisingly, in a phosphokinase profile screen in breast cancer cells, BCI-215 selectively upregulated the MAPKs and their

downstream kinases but not any other signal transduction pathway (Kaltenmeier et al., 2017).

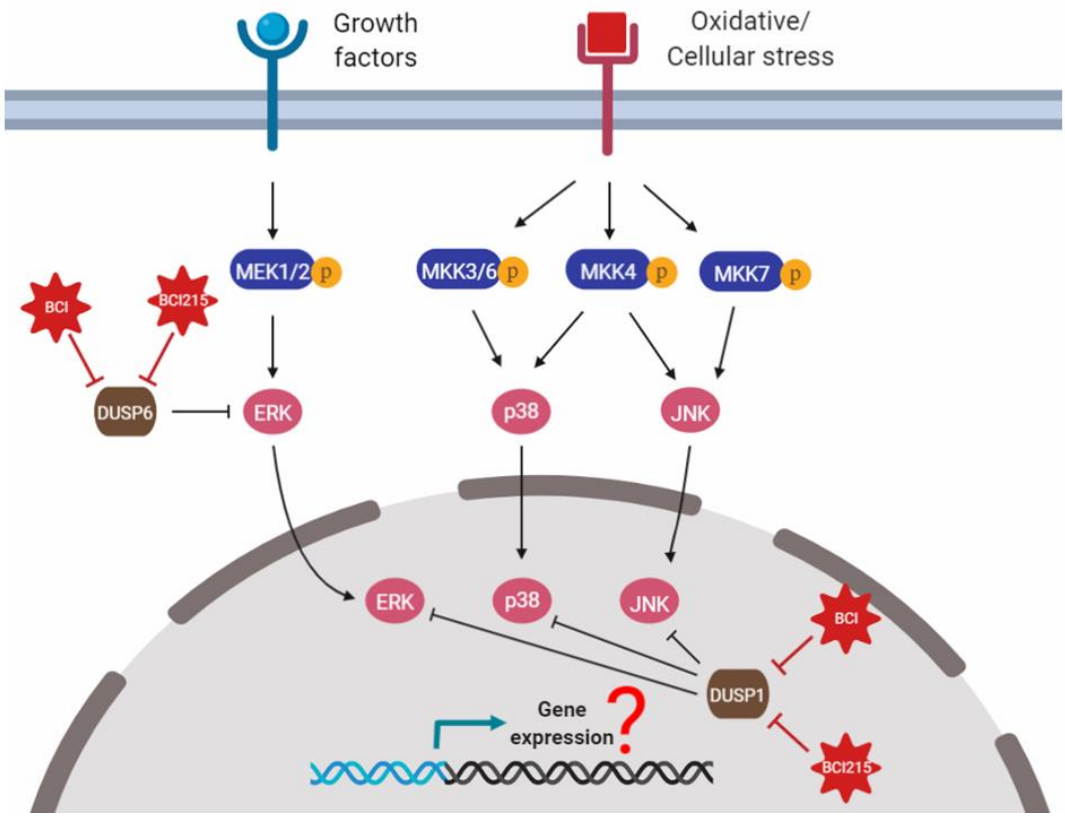

Figure 4.2 – Effect of dual DUSP1/6 inhibition by BCI and BCI-215. As DUSP6 dephosphorylates ERK and DUSP1 dephosphorylates ERK, p38 and JNK, the intracellular effect of inhibiting all three MAPKs will be diverse.

As a potential therapeutic, BCI has demonstrated cytotoxicity in a wide range of cancer models, both *in vitro* and *in vivo* (Wu et al., 2018, Kaltenmeier et al., 2017, Shojaee et al., 2015, Ramkissoon et al., 2019, Shin et al., 2018). BCI overcame tyrosine kinase inhibitor (TKI) resistance in pre-B ALL cells and cisplatin resistance in gastric cancer cells by activating the DNA-damage response pathway leading to accumulation of ROS (Wu et al., 2018, Shojaee et al., 2015). Treatment of pre-B ALL cells with BCI increased pERK, pJNK and pp38 and induced p53-mediated cell death (Shojaee et al., 2015). Paradoxically, in gastric cancer cells, BCI increased pERK but downregulated the ERK response genes (Wu et al., 2018). In breast cancer cells, treatment with BCI and BCI-215 also upregulated pERK, pp38 and pJNK, and induced apoptosis (Kaltenmeier et al., 2017).

Interestingly, chemical inhibition of pp38 partially desensitised cells to BCI-215 toxicity, but this was not the case for ERK or JNK inhibition hinting at potential off-target effects of BCI-215. In SH-SY5Y cells, treatment with BCI appeared to cause dose-dependent cytotoxicity suggesting BCI could be used to target NB cells therapeutically (Mendell and MacLusky, 2019). In this setting, BCI increased the phosphorylation levels of ERK however the researchers did not investigate the effect on other MAPKs.

In summary, the potential therapeutic value of BCI is clear as it displays significant cytotoxicity in various cancer models, however it remains possible that these inhibitors have additional intracellular targets. I aimed to investigate whether specific inhibition of DUSP1 and DUSP6 via BCI and BCI-215 causes cytotoxicity in a range of NB cells. Furthermore, I propose that these inhibitors could be useful tools for elucidating the intracellular role of DUSP1 and DUSP6 in a NB setting.

4.2. Results

4.2.1. BCI and BCI-215 are cytotoxic in NB cell lines

Previous data in **Chapter 3** demonstrate DUSP6 may be growth-promoting in KELLY cells (**Fig. 3.14**). This supports a hypothesis that chemical inhibition of DUSP6 may be therapeutically viable for NB treatment. BCI and BCI-215 demonstrated cytotoxicity in a range of cancer contexts (Wu et al., 2018, Kaltenmeier et al., 2017, Shojaee et al., 2015, Ramkissoon et al., 2019, Shin et al., 2018). To investigate the cytotoxicity of BCI in NB cells, dose-response assays were performed in 4 NB cell lines and HEK293T cells as a non-NB control line (**Fig. 4.3A**). Treatment with 4 μM of either BCI or BCI-215 abolished cell viability in all cell lines. There was a broad spectrum of potency of BCI and BCI-215 where all cell lines, except SK-N-AS cells, were more sensitive than the HEK293Ts, suggesting a potential, selective sensitivity of NB cells to specific DUSP1/6 inhibition. The SK-N-AS cells were the least sensitive to BCI and BCI-215. IMR-32 was most sensitive to both chemicals, with the lowest EC50 value compared to all other cell lines.

In all cases, BCI-215 was more potent than BCI, especially in KELLYs where the EC50 was more than 2-fold lower (**Fig. 4.3B**). Whereas the literature suggests BCI-215 displays reduced off-target toxicities compared to BCI, this increased potency is also indicative of a higher effectiveness of BCI-215 on the target (Korotchenko et al., 2014).

To understand how quickly BCI and BCI-215 reduce cell viability, KELLY cells were treated with 2 µM BCI and BCI-215 and imaged after 24 hours. Both BCI and BCI-215 appear to induce acute cytotoxicity since 24 hours treatment of either chemical induced significant cell death (**Fig. 4.3C**). This is especially true for BCI-215 where only a few viable cells remain visible after 24 hours, reflecting its increased potency compared to BCI. Nonetheless, it is likely these chemicals also reduce the proliferative capacity of NB cells. In subsequent western blots, cells were treated with 2 µM BCI and BCI-215 as this causes significant cytotoxicity and anti-proliferative effects after 24 hours. It is worth mentioning that the chemical treatments in **Figure 4.3C** were on far higher cell densities than the cell viability assays of **Figure 4.3A**, therefore one would expect cells to be somewhat less sensitive to BCI and BCI-215. Following this, all cell lines were treated with 2 µM and 4 µM BCI over 72 hours to determine whether reduced proliferation and greater cytotoxicity would be achieved over a longer treatment. Treatment with 2 µM BCI did not appear to induce greater cytotoxicity in KELLY cells over 3 days suggesting an acute effect of BCI during the initial 24 hours (**Fig. 4.3D**). Nonetheless, increasing the BCI concentration to 4 µM demonstrated significant cytotoxicity in all cell lines where only a minority of cells remained viable (**Fig. 4.3D, dead or dying cells indicated by white arrows**).

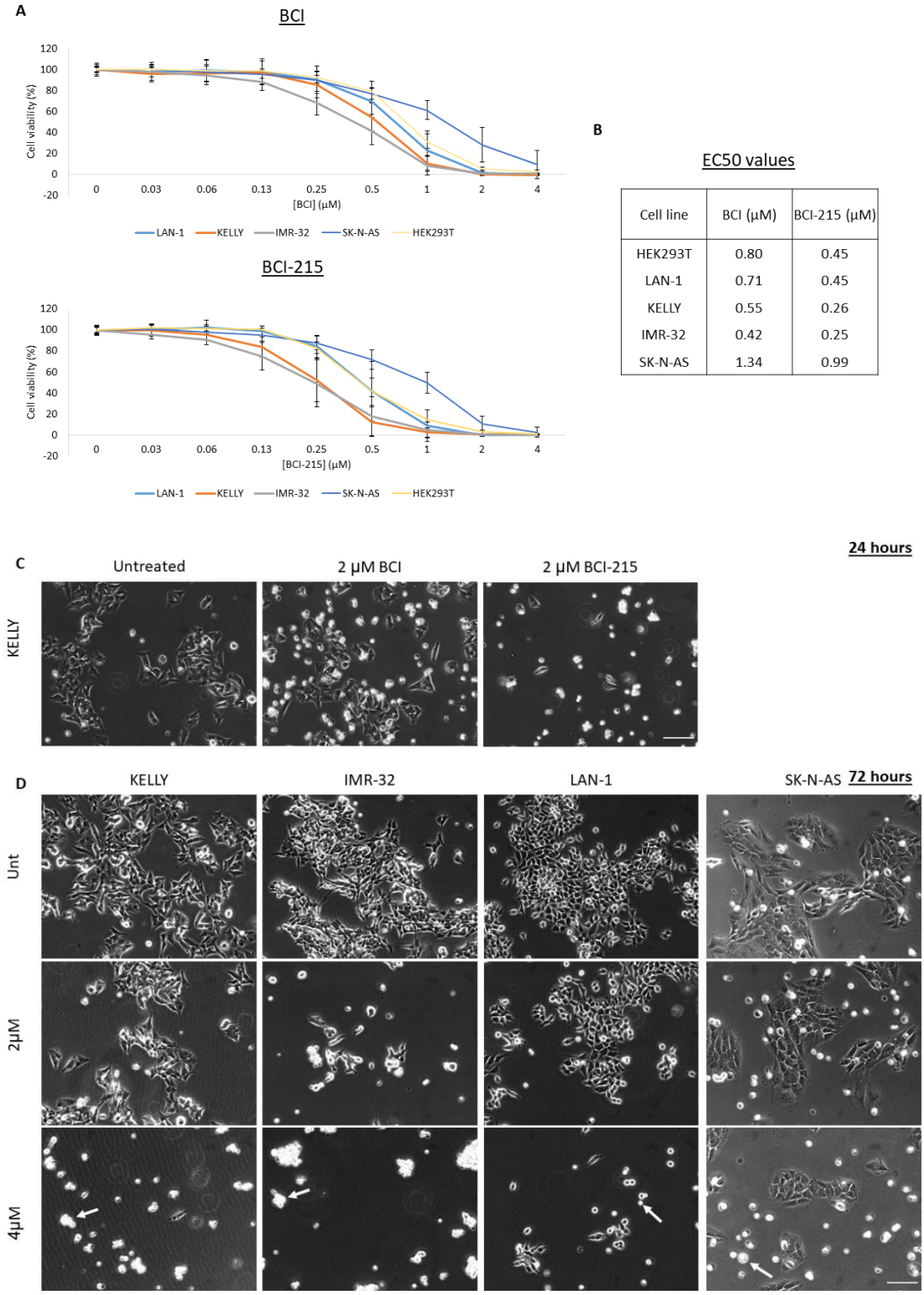

Cell line	BCI (µM)	BCI-215 (µM)
HEK293T	0.80	0.45
LAN-1	0.71	0.45
KELLY	0.55	0.26
IMR-32	0.42	0.25
SK-N-AS	1.34	0.99

Figure 4.3 – Cytotoxicity of BCI and BCI-215 in NB cell lines. (A) HEK293T and NB cell lines cells were treated with increasing doses of BCI and BCI-215. Cell survival was measured after 6 days using a resazurin assay. Data were normalised to cells treated with 0 µM dose (DMSO only) and then expressed as a mean ± SD (n ≥ 3). (B) EC50 values for

dose-response curves displayed in Figure 4.2.1A. EC50 values are estimates between two known values. (C) KELLY cells were treated with 2 µM BCI and BCI-215 and images were taken after 24 hours (n = 1). (D) KELLY, IMR-32, LAN-1 and SK-N-AS cells were treated with 2 µM and 4 µM BCI and images were taken after 72 hours (n = 1). Untreated cells contain DMSO only. White arrows indicate examples of dead or dying cells. Scale bar = 100 µm.

The intracellular effects of BCI and BCI-215 could be very diverse as between DUSP1 and DUSP6, the ERK, p38 and JNK pathways are all likely to be regulated. Furthermore, as various reports demonstrate DUSP6 is able to regulate AKT signalling and the PI3K/AKT/mTOR pathway has significant crosstalk with the RAS/MEK/ERK pathway (Bermudez et al., 2008, Carracedo et al., 2008), it is likely that AKT signalling is also affected by treatment of BCI and BCI-215. To test whether these chemicals influence the MAPK or AKT pathways, KELLY cells were treated with 2 µM BCI and BCI-215 over 24 hours and an immunoblot was performed (**Fig. 4.4)**. As the assumed, major substrate of DUSP6, we would expect the greatest changes in ERK phosphorylation (Kidger and Keyse, 2016). Surprisingly, although there was uneven loading, pERK correlated with tERK suggesting loss of DUSP6 does not alter ERK phosphorylation. As total ERK varied significantly, pERK was also normalised against GAPDH and similar results were observed (data not shown). However, both BCI and BCI-215 increased JNK, AKT and p38 phosphorylation. Similar to their cytotoxicity, the effects on JNK, AKT and p38 phosphorylation were more potent with BCI-215 although the results were more variable. The protein quantification required normalisation to untreated samples which removes the variation between untreated sample and decreases the statistical power of the ANOVA. Nonetheless, the increase in pp38 at 2 and 4 hours treatment with BCI was statistically significant but not with BCI-215. Interestingly, the duration of response differed between BCI and BCI-215 as pAKT, p38 and pJNK peaked at 2 hours for BCI and at 4 hours for BCI-215. Unexpectedly, these results suggest that DUSP1 and DUSP6 are unlikely to be regulating the ERK signalling pathway in KELLY cells (similar to what was observed in **Chapter 3**) but may restrain signalling via the stress response MAPKs or

AKT. Considering DUSP1 is known to dephosphorylate JNK, and to a lesser extent p38 (Liu et al., 1995), these data suggest BCI may be directly inhibiting DUSP1 leading to an increase in the stress-inducible JNK and p38 MAPKs.

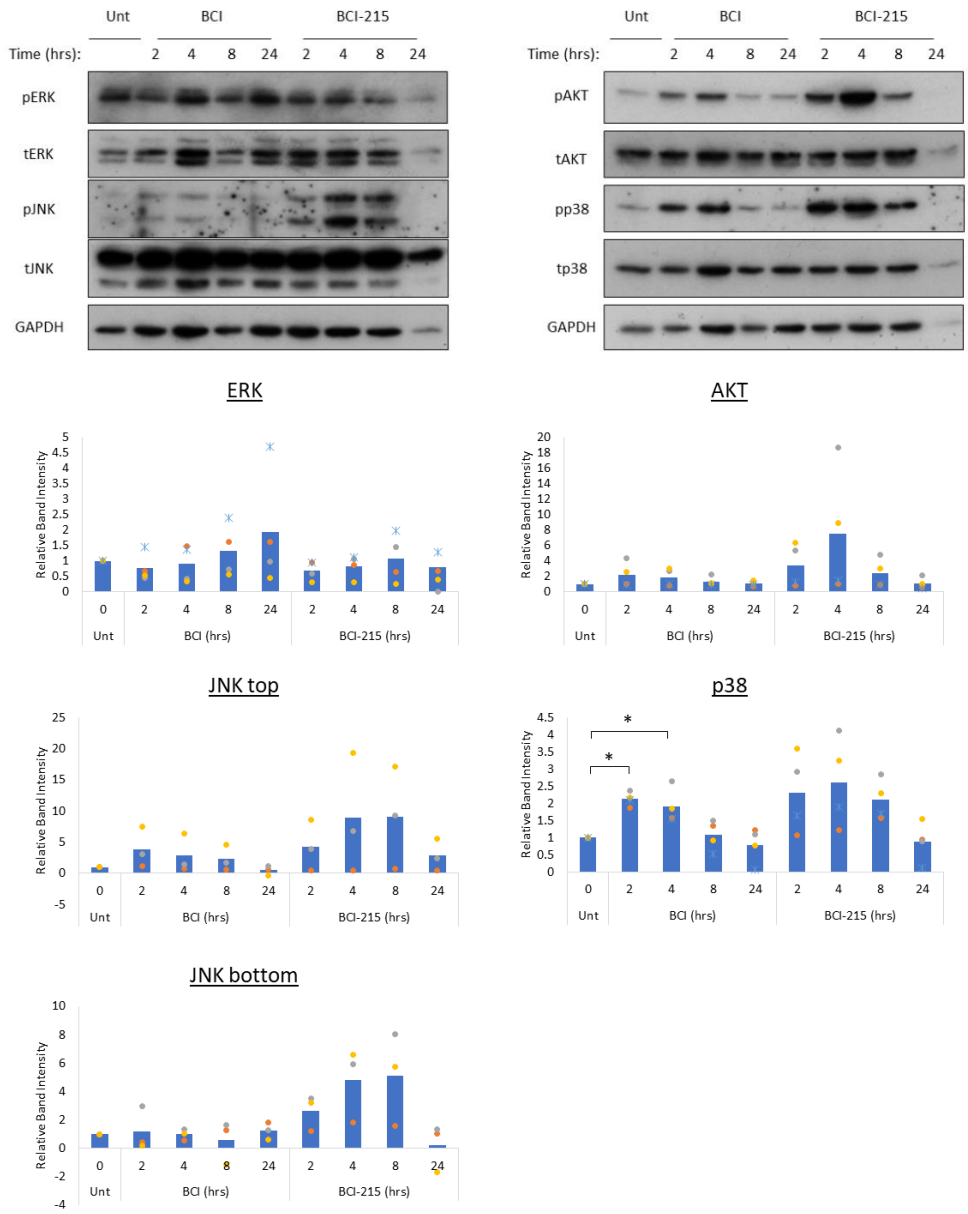

Figure 4.4 – Effect of BCI and BCI-215 on MAPK and AKT signalling pathways. KELLY cells were treated with 2 µM BCI or BCI-215 for 2, 4, 8 and 24 hours and then assessed via a Western blot for phosphorylated MAPK and AKT levels (n ≥ 3). For quantification, each phosphoprotein was normalised to their respective total protein followed by a second normalisation to the untreated sample. Data are expressed as a mean with individual experiments as overlaid dot plots. One-way ANOVA compared to untreated cells; *p ≤ 0.05.

4.2.2. MAPK or AKT inhibition does not antagonise BCI cytotoxicity

Based on the intracellular response to treatment with BCI, it remains unclear what mechanism is driving BCI and BCI-215 cellular cytotoxicity. We hypothesised that BCI-mediated cytotoxicity is via inhibition of DUSP1 or DUSP6 which leads to an upregulation of the JNK and p38 pathways thus resulting in NB cell death. However, we were also suspicious that BCI and BCI-215 may function on an unidentified pathway. Targeting disparate substrates concurrently can generate valuable information about the substrates and the mechanism of cell death depending on whether synergy or antagonism occurs. For example, if BCI-mediated cytotoxicity is via the JNK pathway, we would expect to see an antagonistic effect between BCI and the JNK inhibitor. To investigate this, KELLY cells were treated concurrently with MAPK or AKT inhibitors alongside BCI. For these assays, the MEK inhibitor U0126 was used as an indirect inhibitor of ERK signalling. Prior to the synergy assays, the MAPK and AKT inhibitors were validated by immunoblot to demonstrate inhibition of their respective kinase target (data not shown). Each inhibitor displayed a dose-dependent inhibition of their target where the highest concentration of each inhibitor completely abolished kinase phosphorylation. It is worth noting the p38 inhibitor, SB200190, although preventing kinase function, does not prevent p38 phosphorylation as the inhibitor binding site is distal to the catalytic T180/Y182 residues (Gardner et al., 2015, Hildesheim et al., 2004, Wilson et al., 1997). Hence, there remained a large signal of pp38 on the immunoblot after SB200190 treatment.

Following this, a dose-response matrix of BCI with each MAPK or AKT inhibitor was performed and the SynergyFinder online tool was used to determine a synergy score (Ianevski et al., 2020). As demonstrated in the dose-response matrices, concurrent treatment of BCI with another inhibitor results in a lower cell viability at lower concentrations of each individual drug (**Fig. 4.5A**). Various models have been developed to understand the effect of different drug combinations, each with their own merits and limitations

(Yadav et al., 2015, Foucquier and Guedj, 2015). Synergy maps were generated using the Bliss, zero interaction potency (ZIP) and Loewe model (**Fig. 4.5B and Fig. A2**). The Bliss and ZIP models were very consistent for each drug combination and although the Loewe model gave more extreme results the overall pattern was similar. The only exception was the combination of BCI and the AKT inhibitor MK-2206 which caused extreme synergy in the Loewe model but not for the Bliss or ZIP model. As the Loewe model requires an accurate dose-response curve, this could potentially result from poor fitting of the MK-2206 dose-response curve. Nonetheless, as the ZIP model is described as a combination of the Bliss and Loewe models and provides a more accurate prediction of synergy (Yadav et al., 2015), this has been used from here on (**Fig. 4.5B**). The SynergyFinder software states that a synergy score >10 is likely to be synergistic and <-10 is likely to be antagonistic (Ianevski et al., 2020). The overall ZIP synergy scores for inhibition of ERK, JNK, AKT and p38 were 2.5, 2.7 and 3.3 and 5.1 respectively (**Fig. 4.5B**). Surprisingly, this suggests that these inhibitors act in an additive manner with BCI and do not antagonise BCI-mediated cell death. Especially at low concentrations, where the inhibitors are deemed to be most specific, either additive or mild synergy with BCI is observed. Considering the JNK and p38 inhibitors were fairly cytotoxic themselves, it is unsurprising they do not protect NB cell from BCI-mediated cell death. Overall, this data suggests that BCI triggers cell death cells via alternative pathways unrelated to the MAPKs or AKT.

A

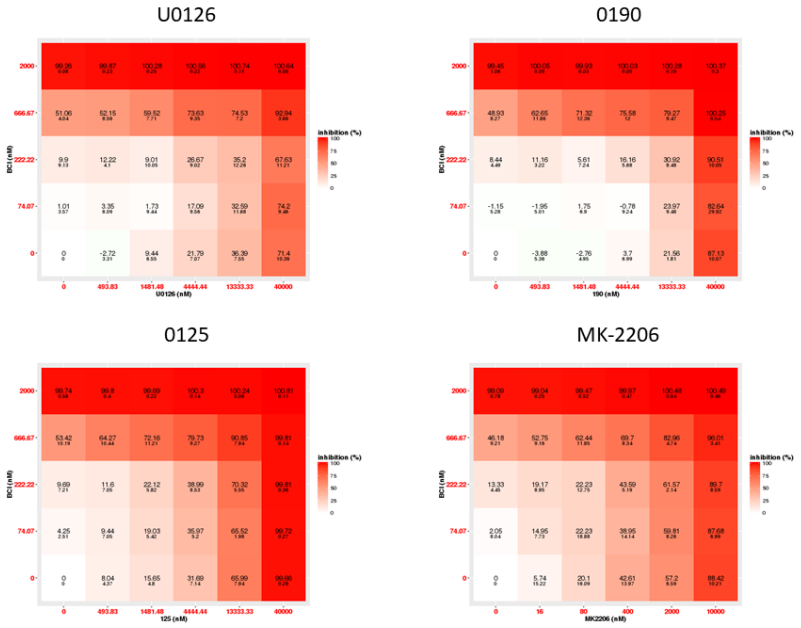
U0126
0190
0125
MK-2206
BCI (nM)
inhibition (%)
U0126 (nM)
190 (nM)
125 (nM)
MK2206 (nM)

B

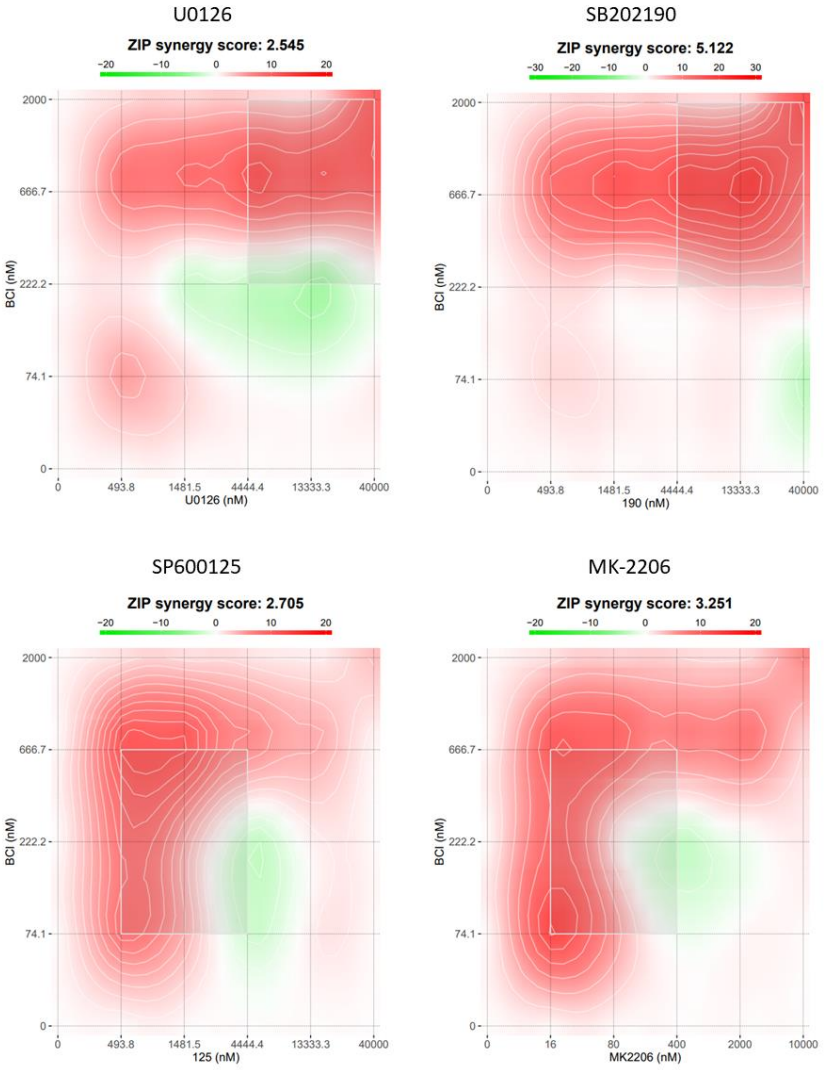
U0126
ZIP synergy score: 2.545
SB202190
ZIP synergy score: 5.122
SP600125
ZIP synergy score: 2.705
MK-2206
ZIP synergy score: 3.251
BCI (nM)
U0126 (nM)
190 (nM)
125 (nM)
MK2206 (nM)

Figure 4.5 – Identifying synergy and antagonism between BCI and MAPK or AKT inhibitors in KELLY cells. (A) A dose-response matrix of loss of cell viability, termed 'inhibition (%)', after treatment of BCI and a MAPK or AKT inhibitor. KELLY cells were treated with increasing concentrations of BCI concurrently with an ERK (U0126), AKT (MK-2206), JNK (SP600125) p38 (SB202190) inhibitor and cell survival was measured after 6 days using a resazurin assay. Data were normalised to cells treated with DMSO and then expressed as a mean ± SD (n = 3). (B) A 2D synergy map was generated using the ZIP reference model. Red regions depict synergy and green regions depict antagonism. A synergy score of >10 and <-10 is deemed synergistic and antagonistic respectively. Data generated using the SynergyFinder 2.0 tool (Ianevski et al., 2020).

Following this analysis of the cellular response to BCI, we sought to determine whether inhibition of the MAPK or AKT pathways would influence the biochemical response to BCI. As there are some areas of mild synergy, for example at low concentrations of MK-2206, one would expect inhibition of that pathway to influence the function of BCI. KELLY cells were treated with BCI alone or in combination with the MAPK or AKT inhibitors and an immunoblot was performed (**Fig. 4.6**). It is worth noting this experiment was only performed once which must be considered when analysing the results. Similar to what has been observed before, treatment with BCI did not alter ERK signalling. Furthermore, BCI led to an upregulation of p38, JNK and AKT signalling, but with a far more consistent duration of the response. There is no significant effect of inhibiting the MAPKs on ERK signalling in response to BCI as pERK remained unaffected by each treatment. Inhibition of ERK signalling resulted in a striking increase in pAKT signalling after 4 hours in response to BCI treatment, however this could be due to underloading of that sample. Interestingly, it appears that inhibiting the p38 pathway elongated the duration of the JNK response to BCI treatment as pJNK remained visible after 24 hours. Conversely, inhibiting JNK has no effect on p38 signalling. Cells were not treated with MAPK and AKT inhibitors alone therefore it is unclear whether this is related to BCI function. The increased duration in JNK signalling could simply result from additional stress induced by inhibition of the p38 pathway. Indeed, previous reports demonstrate JNK activation in response to SB202190 treatment (Muniyappa and Das, 2008). Unfortunately, the pJNK antibody produced a

weak signal therefore the blot could not be quantified accurately. These data suggest that the addition of a MAPK or AKT inhibitor does not appear to alter the biochemical response of KELLY cells to BCI treatment.

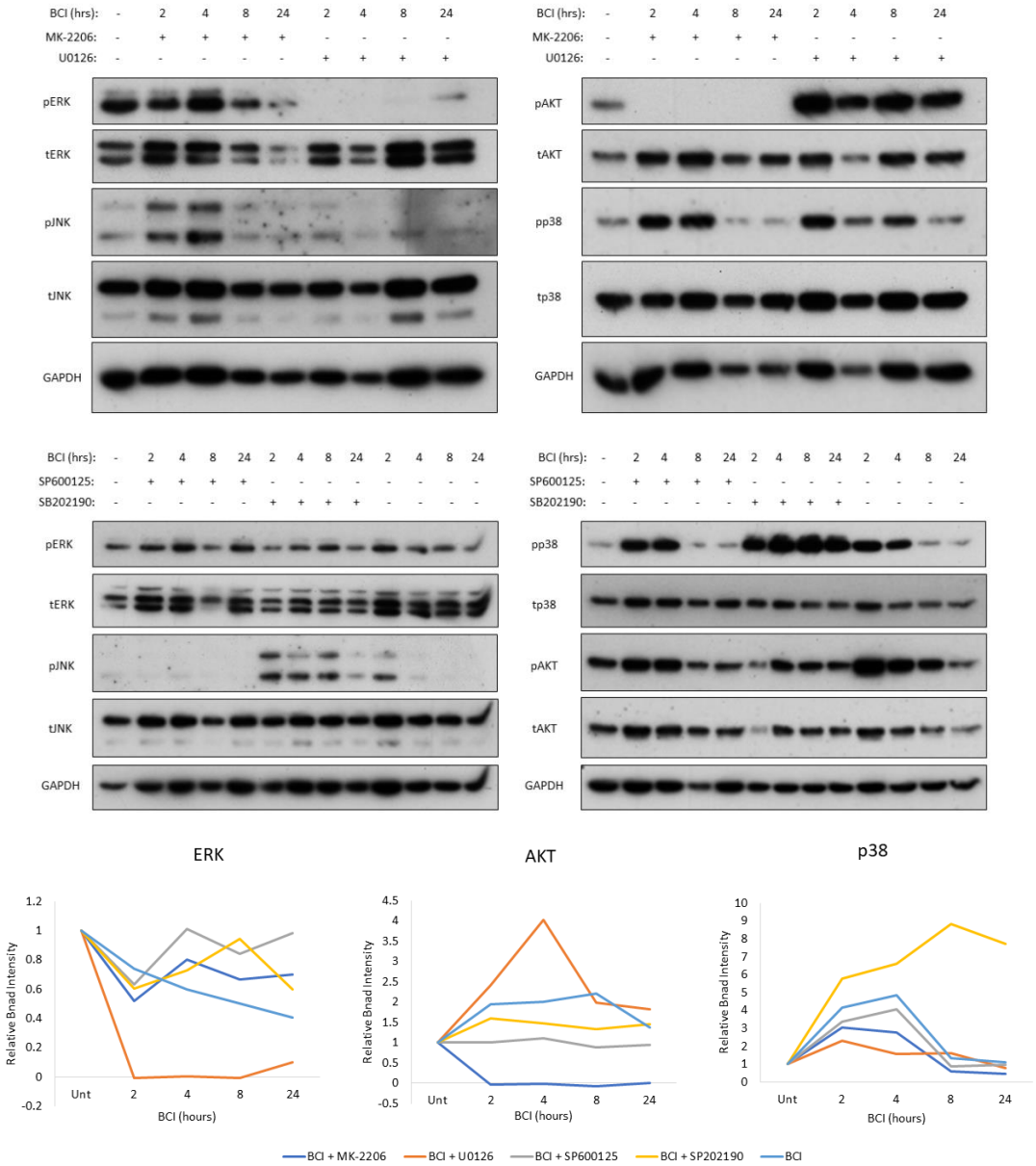

Figure 4.6 – Intracellular effect of combining MAPK and AKT inhibitors with BCI in KELLY cells. Cells were treated with 10 µM of U0126, SP600125, SB202190 or 1 µM MK-2206 alone or in combination with 2uM BCI for 2, 4, 8 and 24 hours (n = 1). Cells were lysed and assessed via a Western blot for phosphorylated MAPK and AKT levels. For quantification, each phosphoprotein was normalised to their respective total protein followed by a second normalisation to untreated.

4.2.3. BCI and BCI-215 do not induce ROS but trigger cleavage of PARP and caspase 3

We sought to determine the mechanism by which BCI induces cellular cytotoxicity. Given that the stress-activated MAPKs JNK and p38 are both activated upon treatment with BCI and BCI-215 in KELLY cells, it is plausible this leads to the generation of ROS. There are various reports that demonstrate treatment with BCI leads to significant ROS production accompanied by an increase in apoptosis (Wu et al., 2018, Shojaee et al., 2015, Shin et al., 2018). To investigate this, cells were treated with increasing concentrations of BCI and BCI-215 and reduced glutathione (GSH) was measured using Monochlorobimane (MCB) after 24 hours (**Fig. 4.7A-B**). MCB is a cell-permeable dye that becomes fluorescent upon binding reduced GSH. If BCI causes ROS production, GSH becomes oxidised and leaves the cell, hence the intracellular pool of reduced GSH and fluorescent signal will decrease. Loss of cell viability induced by BCI and BCI-215 would also affect the MCB intensity independently of ROS production therefore in parallel, cell viability was also measured (**Fig. 4.7A**). A ratio of MCB:cell viability is presented in **Figure 4.7B**. At concentrations where BCI and BCI-215 do not affect cell viability no ROS was produced, indicated by the high fluorescence intensity of MCB. For higher concentrations of BCI and BCI-215 that decrease cell viability, the reduction of MCB fluorescence was equivalent to the reduction of cell viability. Surprisingly, these data suggests that in NB cells BCI and BCI-215 do not cause ROS production.

Apoptosis is a principal mechanism employed by chemotherapeutic drugs to target cancer cells. As BCI demonstrates anti-tumour activity in other cancer models via activation of apoptosis we sought to determine whether the same is true in NB. A major component of apoptosis is the upregulation of the caspase signalling pathway which results in cleavage and activation of effector caspases such as caspase-3 and -7 (Shi, 2002). This is followed by cleavage of a range of substrates including PARP-1, another hallmark of apoptosis (Kaufmann et al., 1993). Accordingly, the cleavage of both PARP-

1 (cPARP) and caspase-3 (cCas3) were determined in cells after treatment with BCI and BCI-215. Surprisingly, there was no change in cPARP after treatment with 2 µM BCI over 24 hours (**Fig. 4.8**). However, treatment with 2 µM BCI-215 resulted in a steep increased in cPARP from 4 – 24 hours, suggesting this inhibitor could induce apoptotic cell death. Following this, the presence of cleaved caspase-3 (cCas3) was investigated by immunofluorescence. Untreated wells contained very few cells which stained positive for cleaved caspase-3 (**Fig. 4.9**). In accord with the cPARP immunoblot, cCas3 was unaltered by 2 µM BCI after 24 hours. Treatment with 4 µM BCI increased the proportion of cells with high cCas3 to 2.3%. Interestingly, this is similar to the quantity of cCas3 after treatment with 2 µM BCI-215, further indicating that the BCI-215 is broadly twice as potent as BCI. Considering treatment with 2 µM BCI caused a reduction in cell viability in **Figure 4.3**, at this concentration BCI may be cytostatic as cleavage of caspase-3 remains low. Treatment with 4 µM BCI-215 results in a significant increase in cleavage of caspase-3 suggesting an induction of apoptotic signalling. Morphological features of apoptosis including nuclear fragmentation and cell shrinkage are also visible after 24 hours (**Fig. 4.9B, white arrows**). Considering 4 µM BCI-215 is more cytotoxic than 4 µM BCI, one would expect a far greater induction of apoptosis after treatment with 8 µM BCI. Overall, these data could suggest BCI, and to a greater extent BCI-215, induce cytotoxicity in KELLY cells at least partly via the activation of apoptosis.

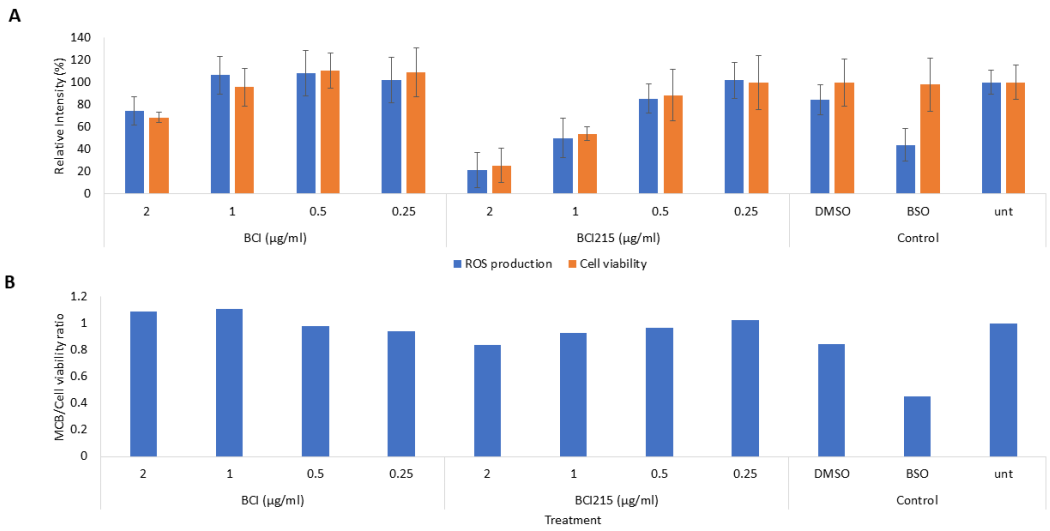

Figure 4.7 – BCI and BCI-215 do not activate ROS in KELLY cells. (A) KELLY cells were treated with increasing doses of BCI and BCI-215 and assessed after 24 hours for cell viability using a resazurin assay and ROS production using MCB. (B) MCB values were normalised to cell viability. High fluorescence intensity indicated high levels of reduced glutathione (GSH) and therefore low ROS production. Data are normalised to the plate and expressed as a mean ± SD (n = 2). Buthionine sulfoximine (BSO, a GSH synthesis blocker) included as positive control.

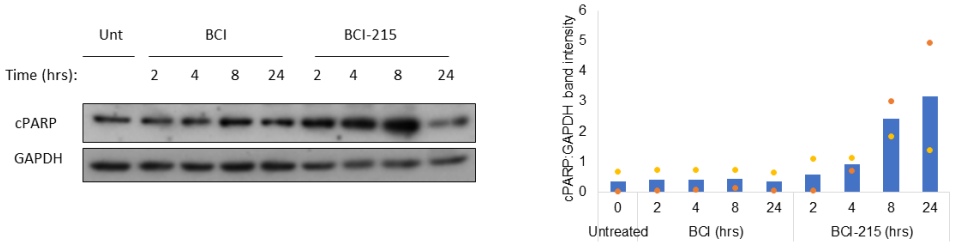

Figure 4.8 – BCI-215 increases cleavage of PARP in KELLY cells. KELLY cells were treated with 2 µM BCI or BCI-215 for 2, 4, 8 and 24 hours and then assessed via a Western blot for cleaved PARP (cPARP) (n = 2). For quantification, cPARP was normalised to GAPDH followed by a second normalisation to total mean. Data are expressed as a mean with individual experiments as overlaid dot plots.

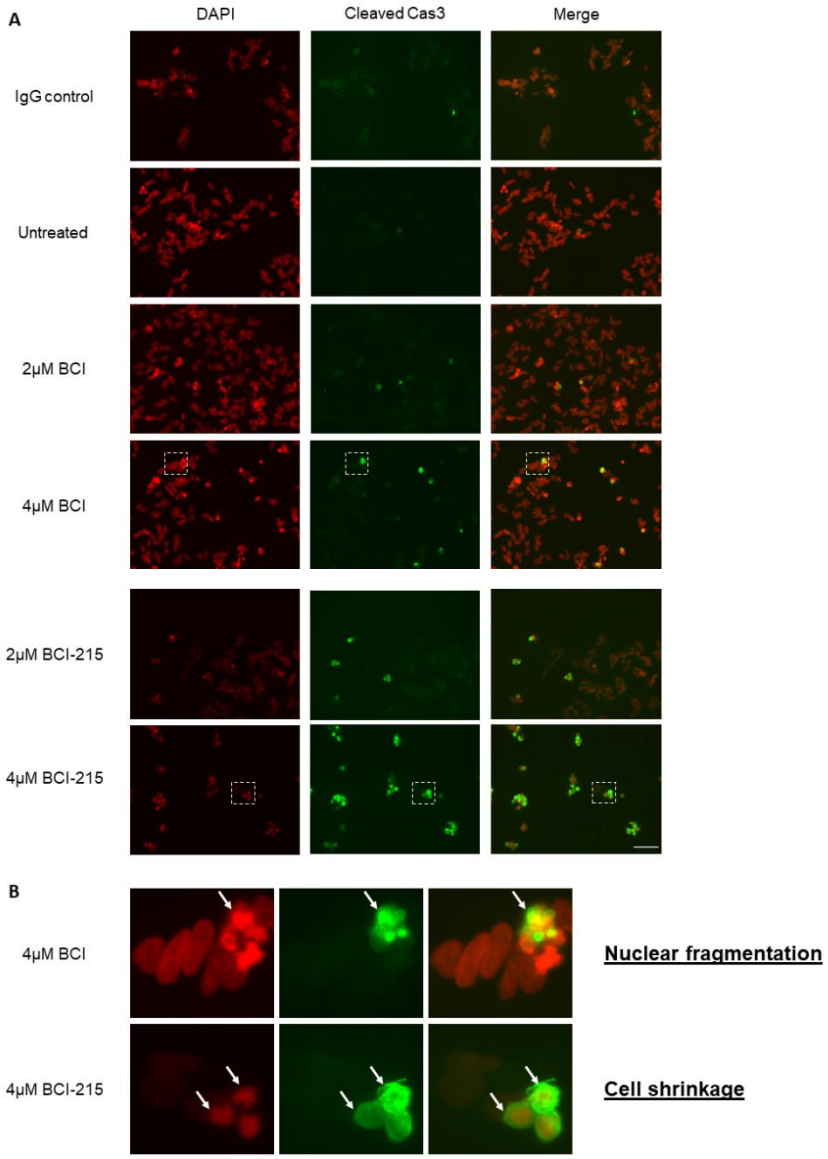

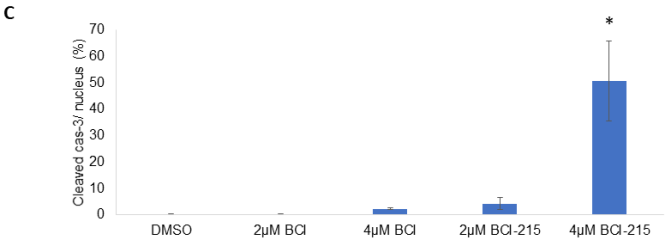

Treatment	Cleaved cas-3/ nucleus (% ± SEM)
DMSO	0.40 ± 0.09
2μM BCI	0.40 ± 0.06
4μM BCI	2.31 ± 0.27
2μM BCI-215	4.28 ± 2.35
4μM BCI-215	50.66 ± 15.22

Figure 4.9 – BCI and BCI-215 increase cleavage of Cas3. (A) Cells were treated with 2 μM or 4 μM BCI or BCI-215 for 24 hours followed by immunofluorescence for DAPI (red) and cleaved Cas3 (green). Scale bar = 100 μm. (B) White dashed boxes from Fig. 4.9A are enlarged to demonstrate nuclear fragmentation and cell shrinkage (depicted by white arrows). (C) Quantification of cCas3. Data are expressed as a mean ± SEM (n = 3). One-way ANOVA compared to untreated cells; *$p \leq 0.05$.

4.2.4. BCI perturbs the JNK and mTOR signalling pathways

Treatment with BCI did not appear to influence ERK but upregulated JNK, p38 and AKT signalling. However, inhibition of these pathways did not antagonise BCI cytotoxicity suggesting alternative pathways are driving cell death. We hypothesised that there were alternative pathways activated by BCI independently of DUSP1/6. To investigate this, a phosphoproteomic screen was performed to determine the global effect of BCI on the NB phosphoproteome. This experiment was performed by a previous post doc in our group, Dr. Vruti Patel, in collaboration with Dr. Pedro Cutillas' group at the Barts Cancer Institute. KELLY and IMR-32 cells were treated with 2 µM BCI for 2 hours, lysed and sent for MS-based phosphoproteomic analysis (**Fig. 4.10A**). In both cell lines there were more significantly upregulated phosphoproteins than downregulated (**Fig. 4.10B-D**). Furthermore, there were far more significantly differentially phosphorylated sites identified in KELLY cells than IMR-32 cells. This was especially true for the downregulated phosphoproteins as only 39 were identified in IMR-32 proteins (**Fig. 4.10D**). Promisingly, there was a large overlap in upregulated phosphopeptides suggesting there may be a conserved pathway activated by BCI in KELLY and IMR-32 cells. We also checked the phosphosites that correspond to ERK1/2 catalytic activity. In both ERK isoforms there was a downward trend in KELLY cells but they do not reach significance due to the large variation between replicates (**Fig. 4.10E**). This is opposite to what is expected if DUSP6 is targeted ERK and so once again suggests ERK is not regulated by DUSP1 or DUSP6.

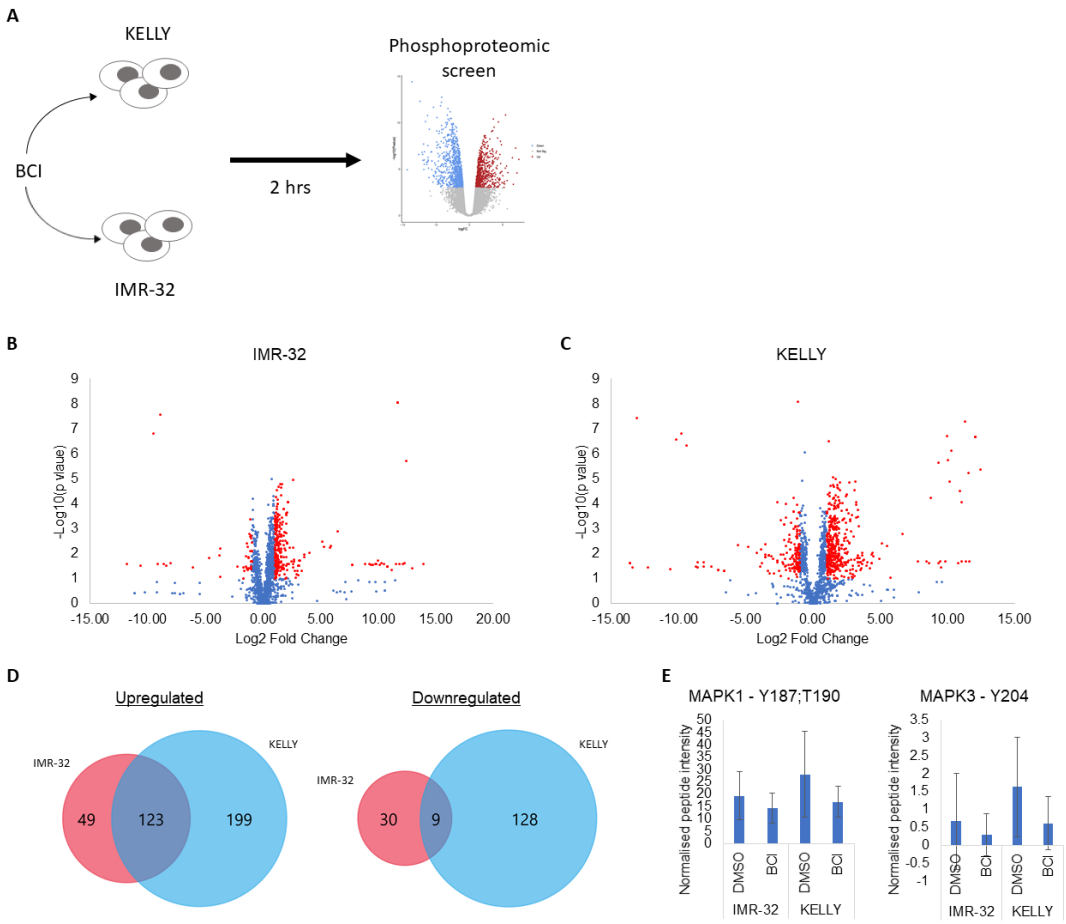

Figure 4.10 – Phosphoproteomic analysis of BCI treatment in KELLY and IMR-32 cells. (A) IMR-32 and KELLY cells were treated with 2 µM BCI and sent for phosphoproteomic analysis (performed by Dr. Vruti Patel). Phosphoproteomic changes of BCI treatment in (B) IMR-32 and (C) KELLY cells are displayed as volcano plots (n = 4). Thresholds for significant phosphopeptides were set as Log2-Fold Change > 1 and p value < 0.1 (red data points). P-values were generated by an independent samples t-test. (D) Venn diagrams of the significantly upregulated and downregulated phosphoproteins shared between IMR-32 and KELLY cells. (E) Normalised peptide values for phosphorylation sites of ERK1 (MAPK3 - Y204) and ERK2 (MAPK1 – Y187;T190). Data are expressed as a mean ± SD.

Following this, we sought to identify the pathways that were regulated by BCI. A common method used to understand how intracellular signalling pathways are perturbed is to compare a set of genes or proteins to publicly available molecular signatures. With this in mind, a biological pathway enrichment was performed on the phosphoproteins that were significantly upregulated or downregulated (**Fig. 4.11**). As there were less proteins

altered in the IMR-32 cells, far less significant pathways were identified. The only pathways of interest significantly altered in IMR-32 cells were the aurora kinases (**Fig. 4.11A, red arrows**). Activation of aurora kinase signalling is known to promote NB progression (Shang et al., 2009, Morozova et al., 2010), therefore an increase in this signalling pathway could promote NB cell growth. However, it is also possible overactivation of the aurora kinases could result in excessive oncogenic signalling and be detrimental to NB cell survival. Interestingly, in KELLY cells there is a significant downregulation of both mTORC1 and its downstream target S6K1 demonstrating a clear suppression of this pathway (**Fig. 4.11B, red arrows**). There were a wide range of pathways upregulated in KELLY cells that do not appear to relate to DUSP1/6 function. This could be indicative of off-target toxicities induced by BCI as opposed to the inhibition of a single molecular target.

The enrichment analysis performed above is limited by the fact that each protein can contain multiple phosphosites. Furthermore, each phosphosite can have a different consequence on protein function. Hence, the molecular changes caused by different phosphosites on the same protein will not be captured in the analysis. An alternative approach that incorporates phosphosite-specific data into the analysis is the KSEA (Casado et al., 2013). This method determines the activity of kinase pathways based on the number of kinase substrates identified in the dataset. A KSEA analysis was performed in both cell lines to identify the kinases significantly altered by BCI (**Fig. 4.12**). The majority of kinases display a similar response in IMR-32 and KELLY cells, further suggesting BCI has a conserved mechanism of action. In line with the pathway enrichment analysis, there is a significant downregulation of mTOR and RPS6KB1 in both cell lines (**Fig. 4.12A**). This again suggests that BCI treatment causes a suppression of mTOR signalling. In support of this, BCI downregulated phospho-RPS6 in pre-B ALL cells suggesting mTOR/RPS6 inhibition is a conserved response to BCI treatment (Shojaee et al., 2015). As expected, the JNK signalling pathway (denoted MAPK9) appeared upregulated in both cell lines and significantly so in IMR-32 cells (**Fig. 4.12A**). The phosphoproteins related to

the JNK and mTOR signalling pathways identified in the literature and the KSEA are displayed in **Figure 4.12B-C**. There is a visible downregulation and upregulation and of mTOR-related and JNK-related phosphoproteins, respectively. In IMR-32 cells, the PLK3 kinase also appeared significantly upregulated. However, on further inspection this was due to AFT2 and JUN phosphorylation, two substrates of JNK, present in the JNK signalling network plot.

Overall, these data demonstrates BCI has a broad effect on the NB cell phosphoproteome. Furthermore, these data identified a number of proteins related to JNK and mTOR signalling that were differentially phosphorylated. Considering the JNK signalling pathway did not appear responsible for BCI-mediated cell death, other kinases identified in the KSEA such as mTOR merit further exploration.

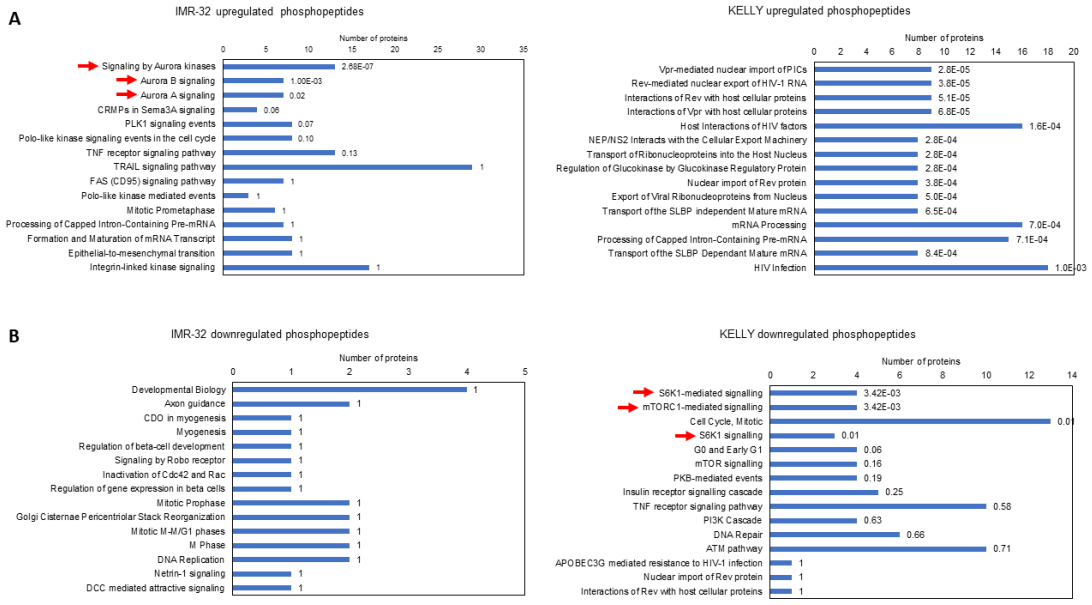

Figure 4.11 – Biological pathway enrichment of the phosphoproteomic dataset. Biological pathway enrichment was performed on the significantly differentially phosphosites using the FUNRICH software (v3.1.4) (Pathan et al., 2015). The top 15 differentially (A) upregulated and (B) downregulated pathways are presented with the Bonferroni-adjusted p values adjacent to each bar. Red arrows indicate statistically significant pathways of interest.

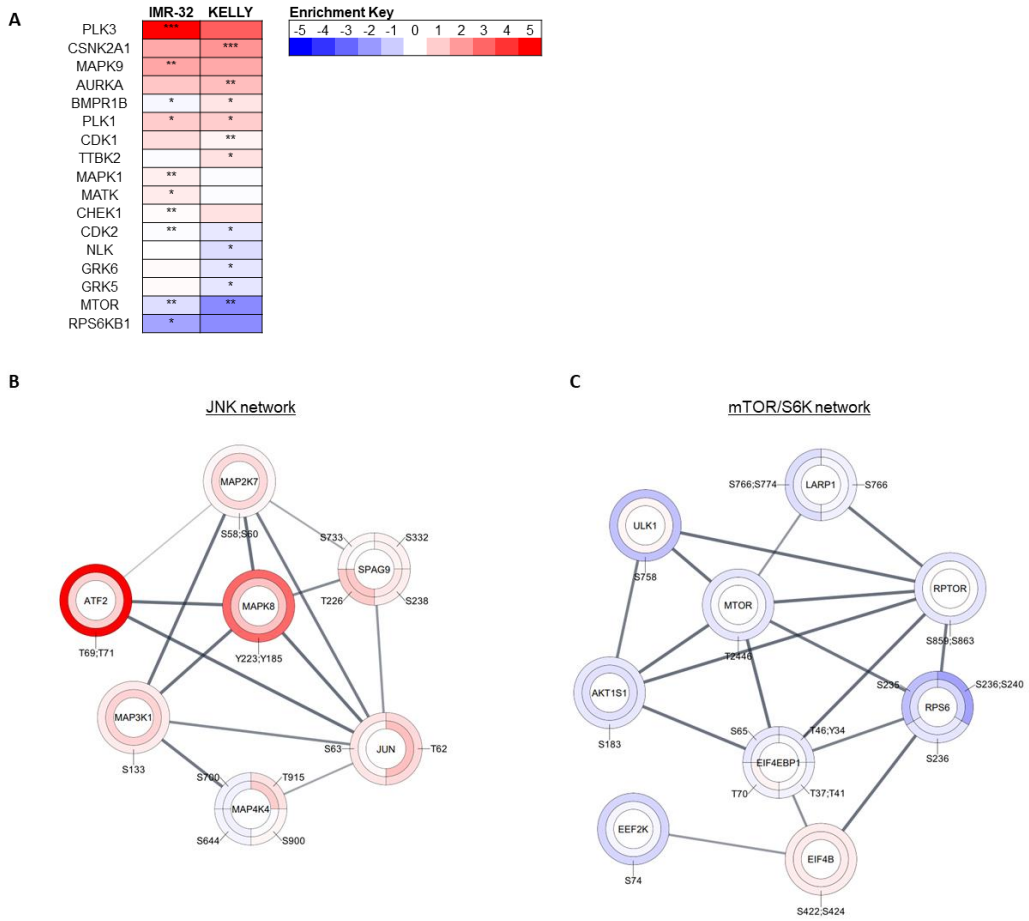

Figure 4.12 – KSEA reveals JNK and mTOR pathway enrichment. (A) A KSEA of the phosphoproteomic dataset. The enrichment key is based on the z-score value, a normalized score for each kinase. PLK3 z-score is greater than 5. Only statistically significant kinase substrates in one or both columns are displayed. The p-value represents a statistical assessment of the z-score (previously described in Casado et al. (2013)). A network of proteins related to (B) JNK or (C) mTOR signalling based on STRING and visualised in Cytoscape. Inner and outer ring represents Log2-Fold Change in KELLY and IMR-32 respectively. Red and blue colours indicates increase and decrease in Log2-Fold Change respectively.

4.2.5. Complete loss of DUSP6 and partial loss of DUSP1 do not affect BCI cytotoxicity

We have shown that BCI causes a clear upregulation of the stress-inducible MAPKs, indicative of a role of DUSP1 in BCI function. However, the phosphoproteomic data demonstrates BCI also alters a wide range of other pathways such as mTOR/RS6K, but does not affect ERK signalling. As it is difficult to see how these changes are all due to inhibition of DUSP1 or DUSP6, we wanted to investigate the on-target effect of BCI and BCI-215 on DUSP1 and DUSP6. The optimal way to validate the on-target effect of a drug is to de-sensitise cells by removing their target. In **Chapter 3**, CRISPR-Cas9 was used to generate KELLY and IMR-32 derivates which lack DUSP6 expression. Dose-response curves were therefore performed using BCI and BCI-215 in DUSP6-null cells compared to WT cells (**Fig. 4.13A**). There was no change in response to BCI or BCI-215, where cell viability overlapped for all inhibitor concentrations, suggesting BCI cytotoxicity does not operate through DUSP6 inhibition under these circumstances. Although cytotoxicity is not a result of DUSP6 inhibition, it is likely these chemicals are still inhibiting DUSP6 phosphatase function.

To investigate the role of DUSP1 in BCI-mediated cell death, KELLY WT and DUSP6 KO cells were treated with a vector containing Cas9 and DUSP1-gRNA. Samples were co-transfected with a vector containing GFP to monitor the transfection efficiency in each cell population. Following this, cells were treated with BCI and cell viability was measured over 6 days. Sequencing of genomic DNA prior to the cell viability assay revealed the proportion cells that contained out-of-frame indels in the *DUSP1* gene (**Fig. 4.13B**). As the efficiency of transfection was very variable, the frequency of indels therefore varied between each experiment. Nonetheless, the presence of indels in the DUSP1 gene did not alter the cytotoxicity of BCI in KELLY WT cells and DUSP6 KO cells (**Fig. 4.13C**). Even in instances where indel frequency was greater than 80% there was no attenuation of BCI toxicity. Together, this challenging result suggests that these inhibitors reduce NB cell viability via major off-target toxicities.

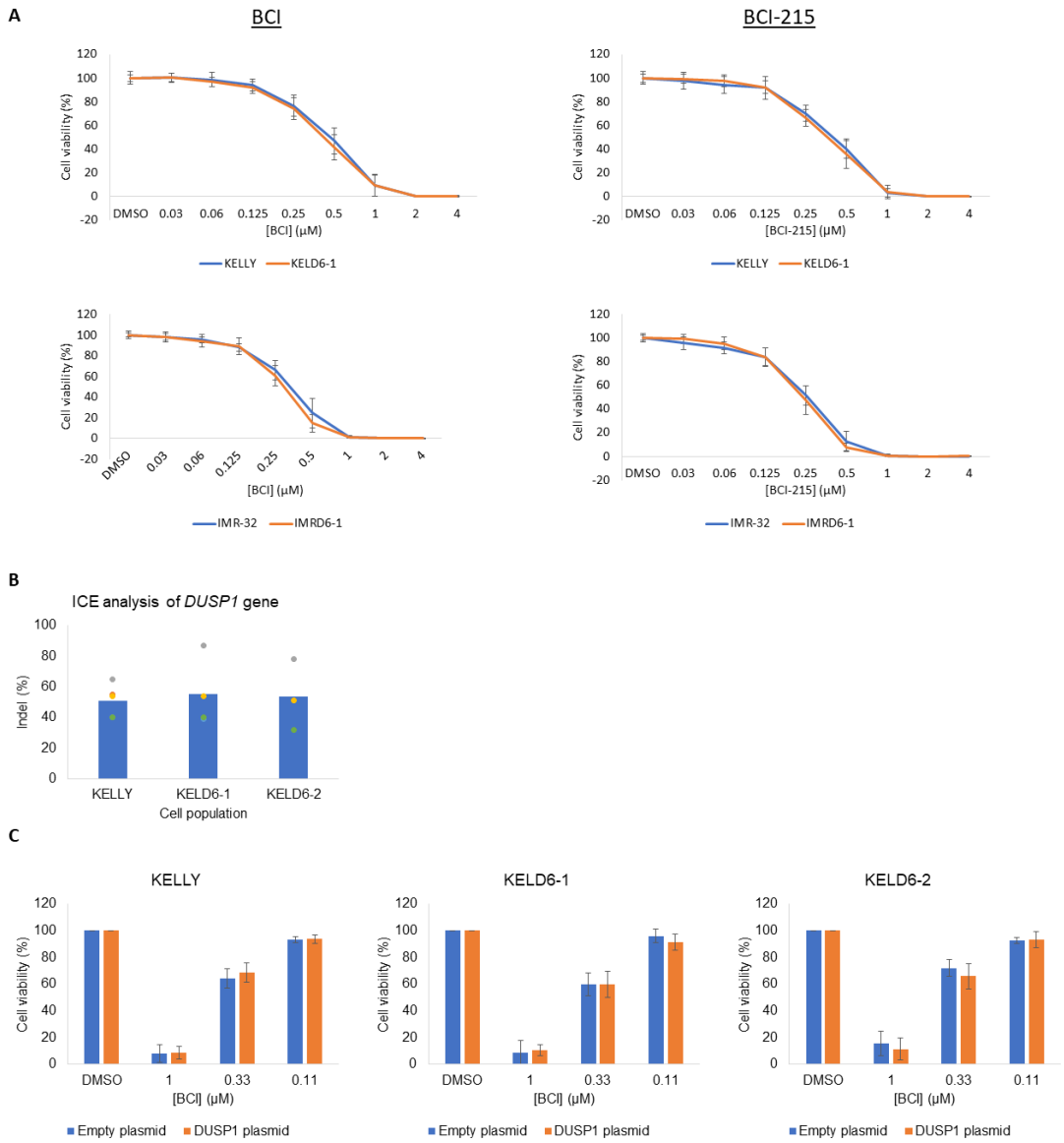

Figure 4.13 – Cytotoxicity of BCI and BCI-215 after DUSP1 and DUSP6 depletion. (A) KELLY and IMR-32 WT and DUSP6-null cells were treated with increasing concentrations of BCI and BCI-215 and after 6 days, cell survival was measured via a resazurin assay. Data were normalised to cells treated with DMSO and then expressed as a mean ± SD (n = 3). An independent samples t-test was performed at ~EC50 values (0.5 μM and 0.25 μM for KELLY and IMR-32 cells respectively) and was not significant. (B) KELLY WT and DUSP6-null cells were transfected with the DUSP1 gRNA or an empty plasmid. After 3 – 5 days, genomic DNA was extracted and sent for sanger sequencing. The ICE online tool (Synthego) was then used to determine the frequency of indels in the DUSP1 gene. Data was expressed as a mean with individual experiments overlaid as a dot plot (n ≥ 3). (C) In parallel, cells were treated with 1 μM, 0.33 μM and 0.11 μM BCI and incubated for 6 days and cell survival was measured using a resazurin assay. Data was expressed as a mean ± SD (n ≥ 3). A one-way ANOVA was performed and comparisons between equivalent BCI treatments were not significant.

4.3. Discussion

The aim of this study was to see whether BCI and the 2nd generation analog BCI-215 could be used as potential therapeutics to target NB cells. BCI has been identified as a potential therapy in many cancer models as it displays potent cytotoxicity. Furthermore, in SH-SY5Y cells BCI causes dose-dependent cell death indicating that this may also be the case in NB (Mendell and MacLusky, 2019). As well as this, there are potential growth-promoting roles of DUSP1 and DUSP6 in NB. Overexpression of DUSP1 in N1E115 cells suppressed JNK signalling and apoptosis whereas knockdown of DUSP1 had the opposite effect suggesting a potential anti-apoptotic role of DUSP1 in NB (Koga et al., 2012). A previous shRNA screen performed in our lab on the PTP family of genes suggested loss of DUSP6 is also detrimental to NB cell growth (performed by Dr. Ann Cichon, unpublished data). Together, this data provided a rationale to investigate whether BCI could be used therapeutically to target NB cells. Considering the discovery of PTP inhibitors has had limited success, especially for DUSP inhibition, BCI also provided an alternative route to understand the role and importance of DUSP1 and DUSP6 to NB cell growth.

Initial results demonstrated that BCI is cytotoxic in NB. This was unsurprising as this had previously been observed in SH-SY5Y cells (Mendell and MacLusky, 2019). There appeared to be some specificity to NB cells as BCI was less cytotoxic in HEK293T cells, suggesting DUSP1 or DUSP6 could be helping to drive cell growth in NB cells. Similar effects have been observed by Wu et al. (2018) where BCI was more toxic in gastric cancer cells as opposed to gastric epithelial cells. Colony forming assays have also been performed by a previous post doc (Dr. Vruti Patel) demonstrating BCI also reduced the potential of NB cells to form colonies (unpublished data). The morphology of NB cells 3 days after treatment demonstrate both BCI and BCI-215 trigger NB cell death. During drug development, drug agents can either have a cytotoxic effect and induce cell death or a cytostatic effect and inhibit cell proliferation (Kummar et al., 2006, Anttila et al., 2019). This study demonstrates that in NB cells BCI an BCI-

215 functions in a cytotoxic fashion over a period of days. Although this might result in a reduced tumour burden, cytotoxic agents are generally more non-specific than cytostatic agents (Anttila et al., 2019) and this appears to be the case for BCI.

Considering growth-promoting roles of DUSP6 in other cancers (Chan et al., 2008, Messina et al., 2011), we hypothesised BCI would function primarily via DUSP6 inhibition. Hence, we expected an upregulation in ERK signalling in response to BCI. It was surprising that BCI did not activate ERK signalling in an immunoblot or in the phosphoproteomic analysis. Instead, immunoblotting revealed short-term activation of the p38, JNK and AKT pathways. Furthermore, the phosphoproteomic data revealed a number of differentially phosphorylated pathways including JNK and mTOR signalling. Previous reports have demonstrated BCI upregulated different MAPK signalling pathways depending on the cancer model. Wu et al. (2018) demonstrate an increase in pERK in response to BCI. Phosphorylation of the other MAPKs were not assessed. Pre-treatment with the MEK inhibitor U0126 prevented BCI causing further cell death suggesting, in gastric cancer, ERK is involved in the BCI mode of action. Conversely, Kaltenmeier et al. (2017) demonstrated in breast cancer cells that BCI and BCI-215 triggered an upregulation of ERK, JNK and p38 signalling. Cell death by BCI-215 could be partially rescued by p38 inhibition indicating p38 could be involved in BCI-mediated cell death. We sought to investigate whether BCI mediated its function via a MAPK by performing synergy assays of BCI with MAPK and AKT inhibitors. If these pathways were involved, you would expect their inhibition to antagonise the function of BCI. Unfortunately, none of the inhibitors attenuated the cytotoxicity of BCI. Conversely, there were many areas in the synergy plots where these inhibitors displayed mild synergy with BCI. Considering both the JNK and p38 inhibitors themselves reduced cell viability, clearly a fine balance of these pathways is required to maintain cell growth.

In line with this, we hypothesised that inhibition of a pathway which is responsible for BCI-mediated cell death would alter the biochemical response after treatment with BCI. Interestingly, concurrent treatment of BCI

with a p38 inhibitor resulted in a greater JNK response than BCI alone. It is likely that this effect is independent of BCI. A previous study in myoblasts demonstrated p38 could restrain JNK signalling (Perdiguero et al., 2007). As p38 drives DUSP1 transcription, loss of p38 reduced DUSP1 expression which resulted in increased JNK activity. Alternatively, considering JNK and p38 share multiple upstream regulators this could simply be due to compensation of the JNK pathway (Wagner and Nebreda, 2009). Indeed, previous studies demonstrate that the p38 inhibitor SB202190 can induce a robust JNK response in lung and breast cancer cells (Muniyappa and Das, 2008). A clear caveat is that the pJNK antibody produces a weak signal in an immunoblot. As the weak signal is not in the linear range of detection, subtler shifts could be misinterpreted as changes in protein signal. Interestingly, activation of the stress-inducible MAPKs by BCI-215 preceded apoptosis. However, activation of JNK and p38 by 2 μM BCI was insufficient to activate apoptosis. This suggests BCI-215 triggers apoptosis via non-MAPK related pathways. If repeated, it would be useful to probe cPARP after treatment with 4 μM BCI as this induced significantly higher cellular toxicity than 2 μM BCI.

At least in KELLY cells, apoptosis did not appear to be driven by the production of ROS. ROS are reactive oxygen-containing molecules which, when produced to physiologically high concentrations, can result in cellular stress and cell death (Ghosh et al., 2018). ROS can cause cell death via multiple pathways, including apoptosis (Redza-Dutordoir and Averill-Bates, 2016). Indeed, in SH-SY5Y cells ROS production appeared to be a requirement for 4-hydroxytamoxifen-induced apoptosis demonstrating a key role of ROS in NB cell death (Espada et al., 2012). However, in breast cancer cells BCI and BCI-215 cause cytotoxicity without activation of oxidative stress suggesting these compounds can trigger apoptosis independently of ROS (Kaltenmeier et al., 2017). Similarly, in our assay neither BCI nor BCI-215 appeared to activate ROS. It is surprising that loss of cell viability is not accompanied by increasing ROS considering the cells are under significant stress. It is worth noting MCB is an indirect measure of ROS production. Alternative assays which directly measure ROS such as

using the carboxy-H2DCFDA dye (Wu and Yotnda, 2011) could be more accurate and would be beneficial to perform in future. Furthermore, ROS production itself does have an inhibitory effect on tyrosine phosphatase function due to oxidation of the catalytic cysteine (Salmeen et al., 2003). Hence, it is important not to conflate the molecular inhibition of phosphatases by BCI with oxidative inhibition mediated by ROS production after BCI treatment.

Considering JNK and p38 are both inhibited by DUSP1, we hypothesised BCI may function via DUSP1 inhibition (Liu et al., 2006, Groom et al., 1996). However, in the phosphoproteomic analysis BCI induced significant changes to the intracellular phosphoproteome indicative of a broader role than inhibition of a molecular target. Hence, we became sceptical that, as opposed to specifically inhibiting DUSP1 or DUSP6, BCI was inducing significant off-target toxicities. Sadly, removal of DUSP1, DUSP6 or both did not appear to influence BCI-mediated cytotoxicity. In this study, depletion of DUSP1 was only partial as there will be cells that were not transfected and indels that would be in-frame. It would therefore be beneficial to repeat these studies in complete DUSP1 knock out cells to confirm BCI cytotoxicity is independent of DUSP1. Nonetheless, even when greater than 80% of genomic DNA contained indels, there was no attenuation of BCI cytotoxicity. This does not mean BCI does not inhibit DUSP1/6 although it does show, at least in NB cells, that cytotoxicity caused by BCI is fraught with off-target toxicities.

A speculative model for how BCI and BCI-215 function in NB cells is depicted in **Figure 4.14**. Here, treatment with BCI results in significant changes to a wide range of intracellular pathways, such as JNK, mTOR and aurora kinase. Together these changes are responsible for the cytotoxicity of BCI and result in apoptosis. BCI is still likely inhibiting DUSP1 and DUSP6 which could also be influencing the JNK and p38 pathways. However, no effect on the ERK signalling pathway is observed.

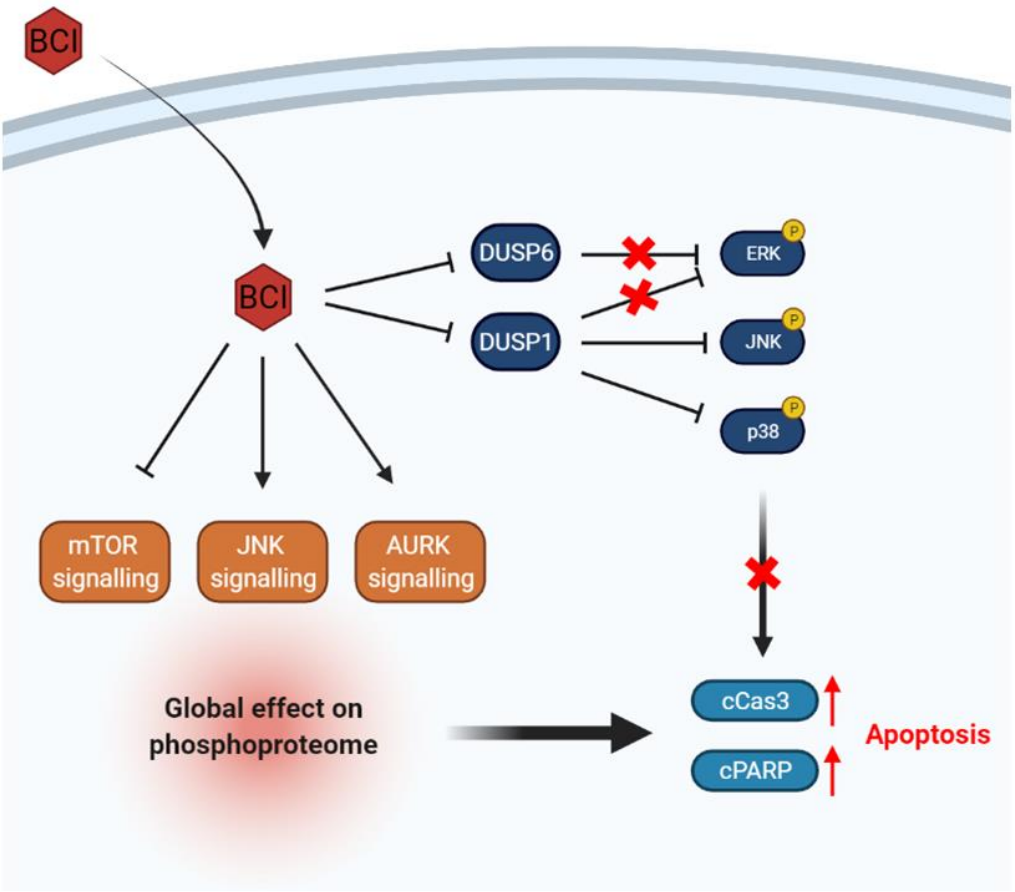

Figure 4.14 – Speculated mechanism of BCI-induced cell death in NB cells. Treatment with BCI has a global effect on the phosphoproteome which includes changes to mTOR, JNK and Aurora kinase (AURK) signalling. This broad effect on the phosphoproteome has a cytotoxic effect in NB cells resulting in apoptosis. BCI also inhibits DUSP1 and DUSP6 which likely activates the stress-inducible MAPKs, however this does not affect BCI cytotoxicity, indicated by red cross above arrow. Importantly, we also do not observe any changes in ERK signalling indicated by the red crosses above these arrows.

To date no study has investigated BCI cytotoxicity or effects on intracellular signalling in DUSP1/6-null cells. A screen against 43 human kinases screen in breast cancer cells demonstrated BCI-215 selectively upregulated the MAPKs (Kaltenmeier et al., 2017). Conversely, a recent study in macrophage cells demonstrated BCI suppressed NF-κB and STAT3 signalling independently of the MAPKs (Cai et al., 2021). Furthermore, BCI treatment in pre-B ALL cells resulted in a huge net loss of tyrosine phosphorylation (Shojaee et al., 2015). This suggests BCI inhibits global kinase activity as opposed to a specific molecular target. BCI specificity has

only been compared to three other phosphatases *in vitro*, Cdc25b, PTP1b and DUSP3, and none were inhibited (Molina et al., 2009). Considering the BCI-mechanism of action is allosteric and MD simulations demonstrate tight binding into a site proximal to the active site, it is unlikely there are other PTP enzymes that BCI is inhibiting (Korotchenko et al., 2014). Nonetheless, it would be beneficial to measure the binding affinity of BCI to a range of other PTPs.

The apparent off-target effects of BCI are indicative of the difficulties posed when therapeutically targeting PTPs. As mentioned in the general introduction, specific inhibition of a PTP is extremely difficult. There has been some success in the field, most obviously with the development of novel SHP2 inhibitors (Stanford and Bottini, 2017, Chen et al., 2016c, Garcia Fortanet et al., 2016). There are currently four SHP2 inhibitors in Phase 1 or 2 clinical trials, predominantly to curtail RAS-driven tumour growth (Yuan et al., 2020). Unfortunately, it has recently been demonstrated that a range of active-site targeting SHP2 inhibitors also display off-target effects (Tsutsumi et al., 2018). In Swiss 3T3 cells, the widely used SHP2 inhibitor NSC-87877 was unable to suppress PDGF-mediated ERK signalling. Tsutsumi et al. (2018) also showed a range of other SHP2 inhibitors could dephosphorylate PDGFRβ in mouse embryonic fibroblasts lacking SHP2 protein. This is not only the case for PTP inhibition. Recent studies have highlighted the degree of off-target toxicities displayed by cancer drugs that were once thought to be specific (Niessen et al., 2017, Lin et al., 2019a). Lin et al. (2019a) performed a CRISPR-wide screen to validate the on-target effect of a panel of drugs in clinical or pre-clinical trials. Surprisingly, all of the cancer drugs that lacked a resistance mutation displayed cytotoxicity in cells depleted of their molecular target. Another study investigated the proteome-wide effect of three 3rd generation EGFR inhibitors (Niessen et al., 2017). Each inhibitor bound to a wide range of other proteins as well as their intended target EGFR. When viewed together, these data highlight the importance of using cells where the target has been knocked out in order to validate the specificity of a molecular inhibitor. Furthermore, when combined with the data from **Chapter 3**, suppression of

DUSP1 or DUSP6 via siRNA or BCI result in clear off-target toxicities. Hence, the use of CRISPR appears the most reliable tool to investigate LOF.

In this chapter, I aimed at evaluating the potential of using BCI and BCI-215 as therapeutic options in NB. Furthermore, I sought to use BCI as a tool to determine the role of DUSP1 and DUSP6 in NB cells. Both chemicals clearly displayed cytotoxicity in all cell lines tested. However, this remains true in KELLY and IMR-32 cells depleted of DUSP1 and DUSP6 protein, unambiguously demonstrating cytotoxicity is directed via off-target mechanisms. Although these compounds are unsuitable as therapeutics in NB, this does not mean they cannot be used in other cancer contexts. For example, in targeting gastric cancer growth BCI decreases tumour growth and overcomes cisplatin resistance *in vivo* (Wu et al., 2018). In such settings, further experiments are required to confirm that these effects are mediated by specific inhibition of DUSP1 or DUSP6. As a tool to investigate the function of DUSP1 and DUSP6 in NB cells, it is highly likely BCI is still inhibiting these proteins. In this regard, the immunoblots performed after BCI treatment suggest DUSP1 and DUSP6 may regulate JNK, p38 and AKT signalling in NB cells. However, ERK does not appear to be affected, in agreement with conclusions from **Chapter 3**. This is further demonstrated in the phosphoproteomic screen performed where BCI did not activate ERK signalling in KELLY or IMR-32 cells. Considering ERK drives NB cell growth in KELLY cells downstream of the ALK oncogene, one would expect tight regulation of this pathway (Lopez-Delisle et al., 2018, Xie et al., 2019). DUSP1 and DUSP6 do not appear to restrain ERK signalling hence there may be other PTP enzymes controlling this important pathway

Chapter 5. Broadening the search for growth-promoting DUSPs in NB

5.1. Introduction

Although the previous work in **Chapter 3** and **Chapter 4** focused on whether DUSP6 is involved in NB cell growth and survival, there are a myriad of other MKPs and aDUSPs that are implicated in tumorigenesis and could therefore also play a role in NB (Nunes-Xavier et al., 2019b, Low and Zhang, 2016, Keyse, 2008, Cain and Beeser, 2013). The majority of this published research focuses on the MKPs since their intracellular roles and substrates are better understood. RTK signalling, partly via ERK, is an integral driver of NB (Rozen and Shohet, 2021), which implies that DUSPs would also be functionally important. Indeed, DUSPs have been implicated in neuronal differentiation and are transcriptionally regulated by a wide range of the neuronal mediators (Pérez-Sen et al., 2019). Supporting this, the siRNA screen performed in **Chapter 3** identified a range of candidates that could promote NB cell growth (**Fig. 3.2**). Loss of DUSP6 caused a minor, albeit statistically significant, growth reduction in KELLY cells. The broad siRNA screen identified various other DUSPs, namely DUSP3, DUSP4, DUSP10, DUSP12 and DUSP26, that could be growth-promoting in NB. Each of these DUSPs share a catalytically active DUSP domain which allows them to dephosphorylate their substrate(s). Nonetheless, current knowledge of their molecular function, substrates, and roles in cancer, is extremely varied (**Table 1.1**). Summarised below is a brief description of each DUSP and their potential involvement in NB tumorigenesis.

DUSP4

DUSP4 was one of the first MKPs to be characterised and displays high sequence similarity with DUSP1 (Misra-Press et al., 1995). Similar to DUSP1, DUSP4 is a nuclear DUSP able to dephosphorylate p38, JNK and to a lesser extent ERK (Seternes et al., 2019). DUSP4 is upregulated in response to a wide range of growth factors suggesting it can regulate RTK activity. Generation of DUSP4-KO mice has demonstrated DUSP4 plays a prominent role in the immune system (Al-Mutairi et al., 2010). Importantly, this study demonstrated DUSP4 is not a functionally redundant DUSP and

functioned independently of DUSP1. DUSP4 is also linked to a wide range of cancers. *DUSP4* gene expression was associated to tumorigenesis in breast, lung, liver and glioblastoma (Chitale et al., 2009, Yokoyama et al., 1997, Wang et al., 2003, Waha et al., 2010). Accordingly, *DUSP4* gene expression was associated with a worse NB prognosis in my cox regression analysis and associated Kaplan Meier data (**Fig. 3.4B**). Furthermore, in NB DUSP4 appears to be an important node of signalling downstream of RTKs as its expression is associated with KIT, TrkA and ALK gene expression (Van den Eynden et al., 2018, Lebedev et al., 2019). However, these correlations with gene expression and clinical outcome do not demonstrate directly what its mechanistic involvement in tumour growth may be. Some insight can be gleaned from a study in diffuse large B cell lymphoma (DLBCL) where *DUSP4* was hypermethylated across multiple DLBCL cell lines and tumour samples (Schmid et al., 2015). Ectopic expression of WT DUSP4, but not that of catalytically inactive DUSP4, induced apoptosis via JNK inhibition suggesting a tumour-suppressive role of DUSP4. Nonetheless, a recent report highlights a pro-survival role of DUSP4 in clear cell Renal cell carcinoma where *DUSP4* silencing promoted JNK, ERK and p38 signalling and induced autophagic cell death (Zeng et al., 2021). Clearly the role of DUSP4 is context dependent and further work is required to determine whether DUSP4 can directly influence NB pathogenesis.

DUSP10

DUSP10 was initially deemed a JNK- and p38-selective phosphatase that localises in both the cytoplasm and nucleus (Tanoue et al., 1999). However, since then studies have shown DUSP10 can regulate ERK activity (Liu et al., 2021). Furthermore, DUSP10 has non-MAPK targets as it can dephosphorylate IRF3 and regulate YAP1 activity (James et al., 2015, Jiménez-Martínez et al., 2019a). It is also worth noting that DUSP10 has a large N-terminal extension with currently unknown function (Tanoue et al., 1999). Alongside its multiple intracellular substrates, there are numerous stimuli that alter *DUSP10* gene expression (Jiménez-Martínez et al., 2019b). Consequently, DUSP10 has been linked to a plethora of

physiological and pathological conditions (**Fig. 5.1**). Various studies have implicated DUSP10 in tumorigenesis, predominantly as a tumour promoter (Reviewed in Jiménez-Martínez et al. (2019b)). Thus far this is most evident in colorectal cancer (CRC). *DUSP10* expression is significantly elevated in CRC tumour samples and various polymorphisms have been identified in the *DUSP10* gene associated to increased risk of CRC (Nomura et al., 2012, Jiménez-Martínez et al., 2019a). Manipulation of *DUSP10* expression demonstrated DUSP10 regulated CRC proliferation *in vitro* and *in vivo* by altering YAP1 activity (Jiménez-Martínez et al., 2019a). However, similar to the other stress-inducible MAPKs DUSP8 and DUSP16, there is little documented evidence of DUSP10 in NB pathogenesis. This could potentially be due to the fact JNK and p38 signalling has been investigated less than ERK signalling in NB. Although principally drivers of apoptosis, anti-apoptotic roles of JNK and p38 have been identified in NB cells (Marengo et al., 2013, Chen et al., 2016a). Whether DUSP10 could influence these mechanisms has not yet been elucidated.

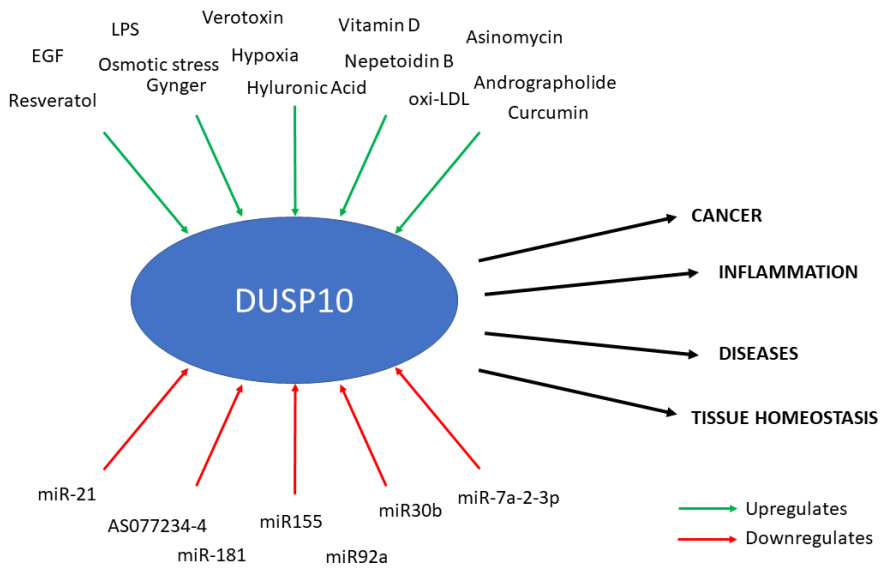

Figure 5.1 – DUSP10 is transcriptionally regulated by a wide range of stimuli. There are a broad range of intracellular stimuli that alter DUSP10 gene expression. This in turn can influence various pathological and physiological conditions including cancer, disease, inflammation, and tissue homeostasis. Modified from Jiménez-Martínez et al. (2019b).

DUSP3

DUSP3 is the best characterised aDUSP with a plethora of substrates identified to date (**Fig. 1.10**). Similar to the MKPs, DUSP3 is able to dephosphorylate ERK and JNK (Alonso et al., 2001, Rahmouni et al., 2006). Whereas many MKPs are transcriptionally regulated by the MAPKs and are activated or upregulated by binding their MAPK target, DUSP3 on the other hand is not transcriptionally regulated by the MAPKs and its catalytic activity is increased by a range of non-MAPK targets, namely VRK3, Zap70 and Tyk2 (Kang and Kim, 2006, Alonso et al., 2003, Hoyt et al., 2007). In accord with its broad range of substrates, the function of DUSP3 appears to differ depending on the cell type and stimulus (Pavic et al., 2015). As mentioned in **Chapter 1.3.2**, DUSP3 is involved in a range of cellular processes implicated in tumorigenesis including cell cycle control, proliferation and senescence (Monteiro et al., 2018) (**Fig. 1.10**). However, there is little literature surrounding the role of DUSP3 in NB. DUSP3 could potentially play a role in neuronal differentiation as RA treatment in SH-SY5Y and SMS-KCNR cells let to an upregulation of *DUSP3* mRNA (**Fig. 3.1**, (Nunes-Xavier et al., 2019b)). Conversely, treatment of SH-SY5Y cells with silver nanoparticles downregulated *DUSP3* mRNA and also caused neuronal differentiation, highlighting the stimulus-specific regulation of DUSP3 (Dayem et al., 2014). DUSP3 can also regulate multiple RTK signalling pathways including STAT/JAK, EGFR and FAK signalling (Chen et al., 2017, Hoyt et al., 2007, Kim et al., 2020, Wang et al., 2011). Interestingly, high *DUSP3* expression is also associated with good patient prognosis in two large NB datasets (**Fig. 5.2**), although as demonstrated in **Chapter 3**, *DUSP3* was not an independent predictor of patient survival in the cox regression analysis.

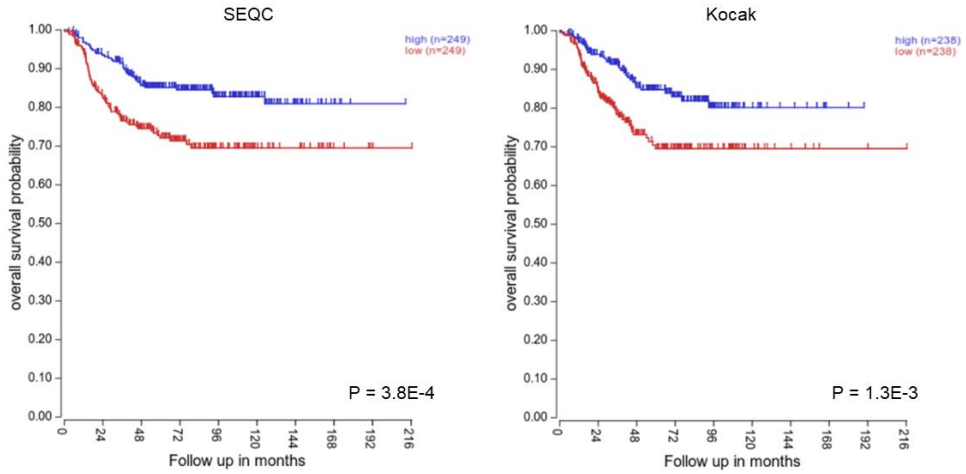

Figure 5.2 – *DUSP3* gene expression is associated to overall survival of NB patients. Patients were split based on median expression of gene. Data was taken from the SEQC and Kocak datasets in the R2: Genomics Analysis and Visualization Platform (http://r2.amc.nl). Statistical significance is determined by a logrank test followed by Bonferroni correction.

DUSP26

As mentioned in **Chapter 1**, DUSP26 was originally deemed an MKP due to dephosphorylation of ERK and p38 (Vasudevan et al., 2005, Hu and Mivechi, 2006). However, subsequent experiments identified a wide range of proteins which are DUSP26 targets (**Table 1.1**). In many instances, DUSP26-mediated dephosphorylation has required a binding partner that can increase DUSP26 catalytic activity (reviewed in Thompson and Stoker (2021)). DUSP26 is highly expressed in neuroendocrine cells and can suppress neuronal cell differentiation (Wang et al., 2006). Analogous to DUSP3, DUSP26 influences neuronal differentiation via multiple RTK signalling pathways. In PC12 cells, DUSP26 directly interacted with and dephosphorylated TrkA and FGFR1 in response to NGF (Yang et al., 2017). Furthermore, an alternative study demonstrated DUSP26 also downregulated EGFR which consequently prevented neuronal differentiation (Wang et al., 2008). Considering these pathways are integral to neuronal differentiation, this highlights the importance of fine-tuned DUSP26 activity in these cells (Csanaky et al., 2019, Chang et al., 2003).

Interestingly, a Chip-Sec analysis demonstrated *DUSP26* is a MYCN transcriptional target in NB cell lines (Zeineldin et al., 2020). MYCN is a global regulator of transcription therefore further studies are required to determine whether there is a functional role of DUSP26 downstream of MYCN.

DUSP12

Initial identification of DUSP12 in humans revealed a C-terminal Zinc-binding domain that was required for protein activity *in vivo* (Muda et al., 1999). Interestingly, the Zinc-binding domain prevents oxidation of the catalytic cysteine (Bonham and Vacratsis, 2009). As a result, DUSP12 can function during oxidative stress and protect HeLa cells from H_2O_2-induced cell death. DUSP12 has also been shown to regulate a range of other cellular processes such as cell cycle progression and stress granule disassembly (Kozarova et al., 2011, Geng et al., 2017). The DUSP12 phosphatase activity was dispensable to the cell cycle changes suggesting DUSP12 has additional functions as well as its enzymatic role. There is little literature surrounding the role of DUSP12 in neuronal cells but there are some associations with NB tumour progression. A genome-wide association study identified *DUSP12* as a susceptibility gene in low-risk NB (Nguyễn et al., 2011). Although the SNPs in the *DUSP12* loci appear to have low penetrance, along with other genetic variations, they have a cumulative effect on malignant progression (Capasso et al., 2013).

Many of these candidate DUSPs discussed above have potential roles in NB pathogenesis and associations to NB patient survival. However, studies on whether they directly influence NB cell growth is lacking. In this chapter, my primary aim was to elucidate further whether these DUSPs are growth-promoting in IMR-32 and KELLY cells and what their molecular function may be. The data generated using the DUSP6 siRNAs in **Chapter 3** suggests the siRNAs used in the screen may cause non-specific toxicity (**Fig. 3.7**). On the other hand, the CRISPR-Cas9 system demonstrated depletion of DUSP6 protein with minimal off-target effects. I therefore generated DUSP-

null single cell clones using this system and analysed whether they indeed influence NB cell growth using cell growth and colony forming assays. Furthermore, it would be beneficial to understand the function of DUSPs in these NB cell lines. Hence at the end of this chapter a broader biochemical analysis is performed to see which DUSPs regulate MAPK signalling in NB cells.

5.2. Results

5.2.1. Deconvolution of candidate DUSP siRNA pools

The DUSP siRNA screen performed in **Chapter 3** identified a range of DUSPs that appeared growth-promoting. The DUSPs chosen that will be characterised further were DUSP3, DUSP4, DUSP6, DUSP10, DUSP12 and DUSP26. An inherent limitation of large siRNA screens is the presence of false positives (Echeverri et al., 2006). Indeed, with the DUSP6 siRNA pool the potent phenotypic effect of the individual siRNAs did not correlate well with *DUSP6* knockdown (**Fig. 3.7**), even though the pool effects appears cell type specific (**Fig. 3.5**). To characterise the other DUSP candidates, their siRNA pools were deconvoluted to determine whether gene knockdown correlates with loss of viability (Cell viability assays were performed conjointly with Ali Sahin) (**Fig. 5.3**). The DUSP4 siRNA pool was not deconvoluted as it did not decrease cell viability in the DUSP screen. For the DUSPs included, knockdown of the DUSP gene with the siRNA pool was greater than 50% and comparable to that seen previously in **Figure 3.3** (**Fig. 5.3A**). Furthermore, the DUSP10, DUSP12 and DUSP26 siRNA pools remained extremely potent at reducing cell viability (**Fig. 5.3B**). The DUSP3 siRNA pool was less potent here than previously observed, although the DUSP3 siRNAs displayed high variability between assays. Cell viability assays were also performed in LAN-1 cells to see whether the effect of the individual siRNAs were cell-specific. This does not appear to be the case as the overall pattern between each siRNA was similar in both cell lines.

In all cases, gene knockdown with the siRNA pool is equal or greater than the individual siRNAs. Similarly, in most cases, effect of the siRNA pool is comparable to the most potent individual siRNA. There is a general correlation between gene knockdown and effect on cell viability but there are also cases where the trend is not followed. The DUSP3 siRNAs do follow this trend. 3.1 suppresses *DUSP3* expression the most and decreases cell viability the most. However, the extent of this is far greater than the degree of gene knockdown. DUSP10 and DUSP12 are relatively similar. In both cases individual siRNA 2 and 3 knockdown the gene the greatest (70 – 80%). However, 10.1, 10.2 and 10.3 have similar effect on cell viability but 10.1 does not suppress the *DUSP10* gene to the same extent. Hence 10.1 likely displays some off-target toxicity. Likewise, 12.3 reduces cell viability significantly more than 12.2 suggesting 12.3 displays a degree of off-target toxicity. Lastly, the DUSP26 siRNAs correlate well as 26.1 and 26.3 suppress the *DUSP26* gene the least and cause the smallest reduction in cell viability. Nonetheless, 26.2 has a significantly greater effect on cell viability, but is only marginally better at suppressing gene expression suggesting it displays off-target effects. Overall, unlike the DUSP6 siRNAs, there appears to be a pattern for each DUSP between gene knockdown and effect on cell viability. However, there are some discrepancies which suggests some of the siRNAs display off-target toxicities as might be expected. This is especially true in cases where an individual siRNA decreases cell viability by > 80% but shows comparable gene knockdown to a different siRNA. With this in mind, it appeared sensible to knockout each of the DUSP genes using CRISPR/Cas9 to assess whether an alternative LOF approach would reproduce these findings.

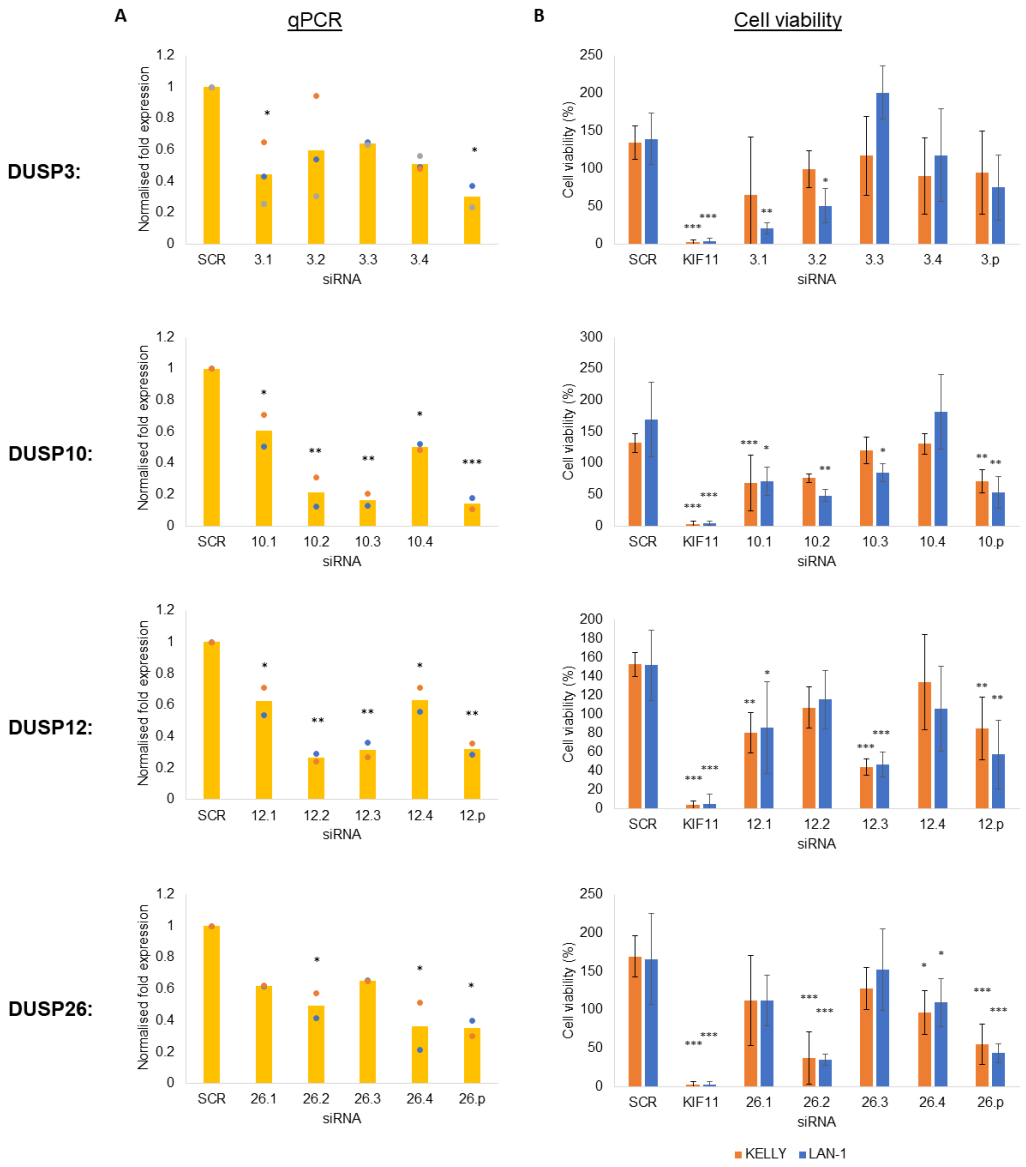

Figure 5.3 – Deconvolution of siRNA pools for candidate DUSPs. (A) The knockdown of individual and pooled siRNAs was determined after 24 hours treatment via qPCR (n ≥ 2). Data presented as a mean with individual experiments overlaid as dot plots. (B) The effect on cell viability of individual and pooled siRNAs was determined using the resazurin assay over 6 days (n ≥ 4) (Performed conjointly with Ali Sahin). Data are normalised to the plate average and then expressed as a mean ± SD. In both assays, cells were treated with 5 nM siRNA. One-way ANOVA compared to SCR; *p ≤ 0.05; **p ≤ 0.005; ***p ≤ 0.0005.

5.2.2. Generation and characterisation of DUSP-null NB cells

Knockdown of each DUSP gene using RNAi appears to be hampered by off-target toxicities exaggerating the growth-promoting properties of the target. The CRISPR/Cas9 system employed in **Chapter 3** to knockout the *DUSP6* gene did not appear to have any off-target toxicities (**Fig. 3.8C**). We therefore decided to generate DUSP-null subclones for the other DUSP candidates. To this end, gRNA's were generated to target N-terminal regions for each DUSP protein (**Fig. 5.4A**). Previous experiments with DUSP6 gRNA 1, 3 and 4 demonstrated that the gRNA position may be important for efficient depletion of protein. The position of the catalytic HCX_5R 'PTP motif' responsible for dephosphorylation varies greatly for each DUSP. We designed the DUSP gRNAs in regions upstream of the HCX_5R motif so that out-of-frame mutations will prevent phosphatase function. It is important to note that the aforementioned DUSP12 Zinc-binding domain is near the C-terminal end of the protein and is deemed important to DUSP12 function (Kozarova et al., 2011). The DUSP12 gRNA would also disrupt this region preventing phosphatase-independent functions. As demonstrated in **Figure 5.4B**, the gRNAs generated had minimal off-target regions with mismatches of 3 or greater in all cases. Furthermore, similar to **Chapter 3.2.5**, the SNAP2 software was also used to design gRNAs in regions that were also important for protein function (**Fig. 5.4C**). This software was used to predict the effect of an in-frame mutation. Each editing event will take place approximately 3-4 base pairs (1-2 amino acids) downstream of the PAM site (**Fig. 5.4C, PAM site in black box**). Based on the red regions proximal to the PAM site for each DUSP sequence, we expect these gRNAs to also reduce functional protein from in-frame mutations.

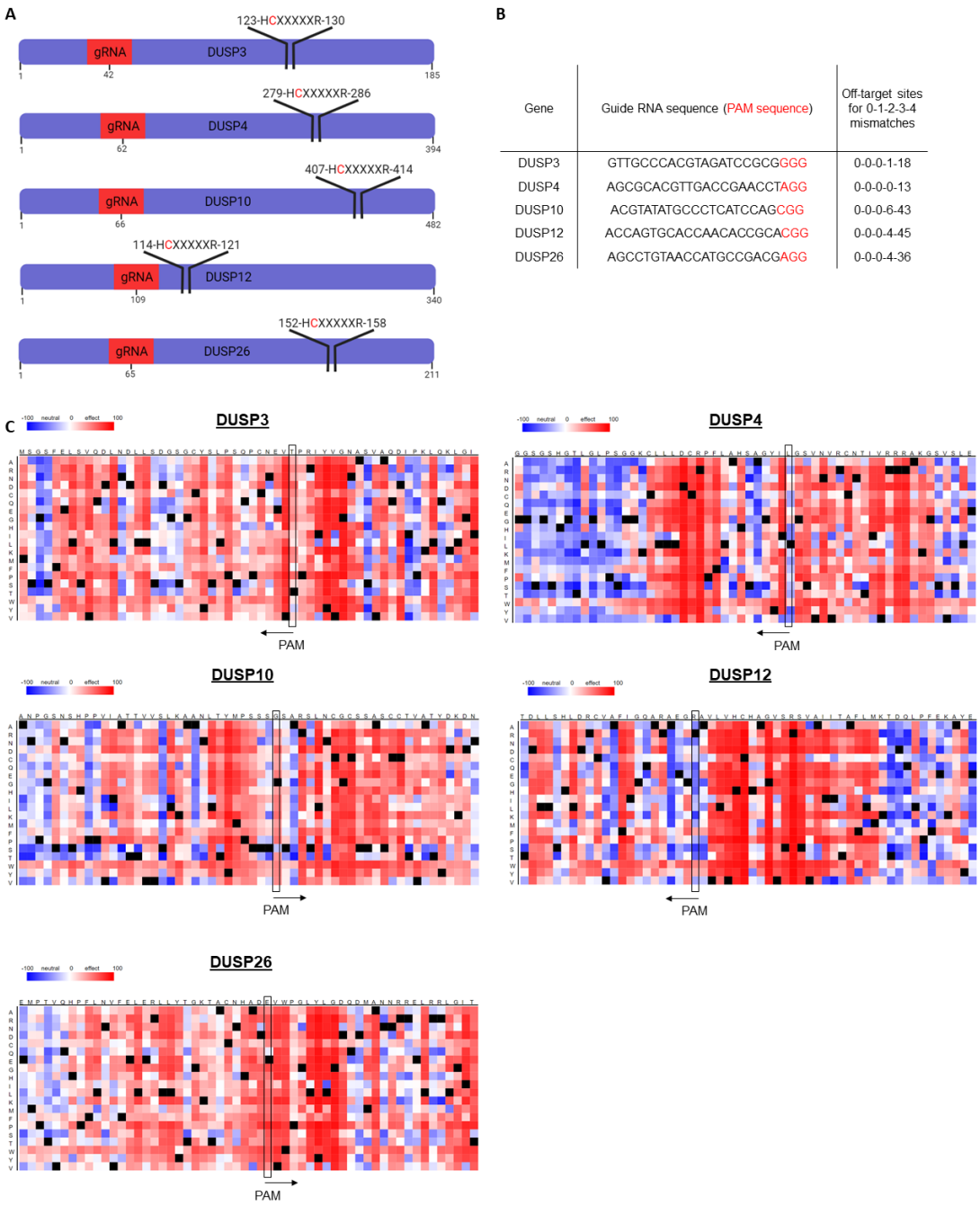

Gene	Guide RNA sequence (PAM sequence)	Off-target sites for 0-1-2-3-4 mismatches
DUSP3	GTTGCCCACGTAGATCCGCGGGG	0-0-0-1-18
DUSP4	AGCGCACGTTGACCGAACCTAGG	0-0-0-0-13
DUSP10	ACGTATATGCCCTCATCCAGCGG	0-0-0-6-43
DUSP12	ACCAGTGCACCAACACCGCACGG	0-0-0-4-45
DUSP26	AGCCTGTAACCATGCCGACGAGG	0-0-0-4-36

Figure 5.4 – Design of candidate DUSP gRNA sequences. (A) Schematic of DUSP protein sequence including the position of the gRNA (displayed in red box) and the HCX_5R PTP motif. (B) Table containing the sequence of each gRNA with the PAM site in red and the number of off-target mis-match sites in the genome for 0 – 4 mismatches. (C) The functional effect of each sequence variant in the first ~50 amino acids of each DUSP candidate (SNAP2 online tool). Each column represents an amino acid in the DUSP sequence and each row represents an alternative amino acid. The heatmap depicts the predicted effect on protein function for each amino acid substitution where blue and red are neutral and strong disruptive effect, respectively. The black boxes depicts the amino acid

containing the PAM site. Indel events occur approximately 3-4 base pairs (1-2 amino acids) downstream of the PAM site, where the arrow depicts the direction of editing.

A different CRISPR/Cas9 system was employed to that used with the DUSP6 gRNA. Considering the Cas9 protein is very efficient at introducing indels, transient transfection of a plasmid containing the Cas9 protein and gRNA appeared more efficient than using the inducible system. Each CRISPR/Cas9 system is described in **Chapter 2.5.3** and **Chapter 2.5.4**. To this end, a vector containing both the Cas9 open reading frame under a CBh promoter and each DUSP gRNA under the U6 Promoter was purchased (**Fig. 2.1, right vector**). Following transient transfection and puromycin selection, the mixed populations were single cell cloned to generate DUSP-null sub-clones. After 7 days incubation with the vector, a significant population of cells contained indels in the gene of interest (**Fig. 5.5A**). If loss of DUSP protein suppressed NB cell growth, it is possible this population would be outcompeted over time by the WT population. To check whether this was the case, the DUSP10 IMR-32 and KELLY mixed populations were incubated a further two weeks and sequenced again. The DUSP10 population was chosen as this had intermediate levels of indels and we would therefore notice if the indel frequency increased or decreased. Surprisingly, the indel frequency marginally increases in both cell populations after two weeks (**Fig. 5.5B**). This could imply the *DUSP10* gene deletion offers a growth-advantage in these NB cells. This is unlikely as DUSP10 predominantly display growth-promoting properties in various cancer models (Jiménez-Martínez et al., 2019b), however its role in NB is not well understood. Alternatively, this result could simply be within the variability of the sanger sequencing or the ICE analysis software. The indel pattern introduced into the *DUSP10* gene did not change over this time period (**Fig. 5.5C-D**). This demonstrates that the sequencing results are reproducible and stable and so it is reassuring to know the mixed populations do indeed have a high percentage of stable indels. There is also a striking preference for certain indel sizes. Recent studies demonstrate indel generation occurs in a predictable manner where 1bp indels are by far the most common indel introduced (van Overbeek et al., 2016, Chakrabarti

et al., 2019). This remains true in KELLY and IMR-32 cells where 1bp indels are the most abundant. Surprisingly, there is also a preference for 19bp deletions in the IMR-32 population (**Fig. 5.5D**).

Mixed populations were then single-cell cloned. A range of subclones were sequenced and two distinct subclones containing out-of-frame indels in both alleles were selected for further analysis (**Table 5.1,** indel locations in **Fig. A3**). Out of the subclones chosen, 6 contained homozygous mutations and 4 contained compound hemizygous mutations. It is worth noting the KELD4-2 clone displayed a homozygous 3bp deletion and 1bp insertion. I am not aware of any previous study that demonstrates this type of indel. Although immunoblots were not performed against each DUSP protein, these indels will completely abolish the catalytic domain and thus the function of each phosphatase. Hence, we hypothesise that these dysfunctional DUSP proteins would be targeted for proteasomal degradation.

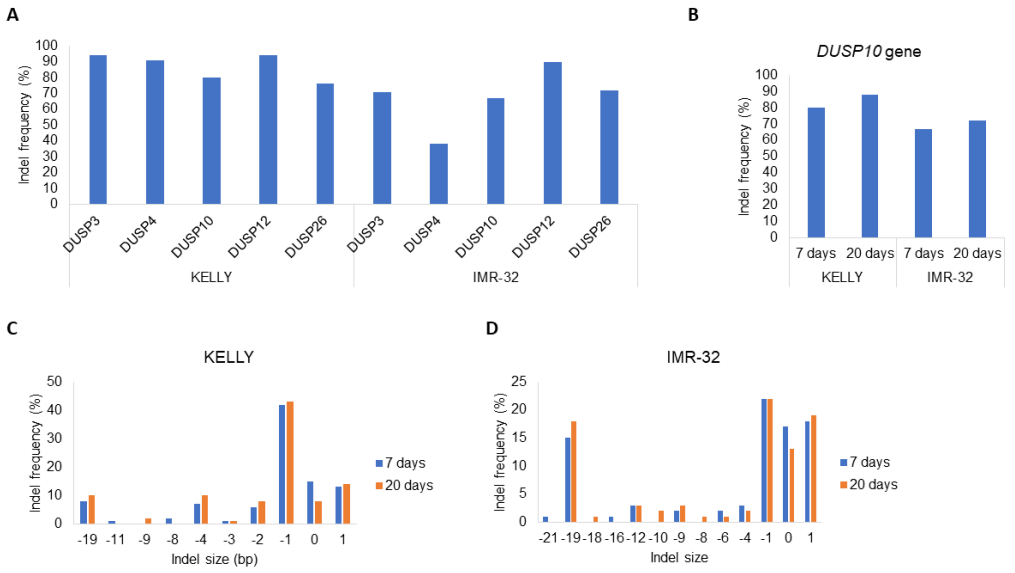

Figure 5.5 – Characterisation of indels in mixed populations. (A) Sequencing of KELLY and IMR-32 mixed populations demonstrated high indel frequency with the majority of gRNAs. Cells were incubated for 7 days after transfection before sequencing was performed. The DUSP10 mixed populations were incubated for a further 2 weeks. The (B) indel frequency and (C-D) indel sizes of the KELLY and IMR-32 DUSP10 mixed populations after incubation for 7 and 20 days.

Table 5.1 – Single cell clones generated from the DUSP mixed population. Various clones were sent for sequencing for each DUSP gene. Two sub-clones were selected that contained out-of-frame indels in both alleles to be characterised further.

DUSP-null subclone	Zygosity	Indel
KELD3-1	Homozygous	1bp insertion
KELD3-2	Compound hemizygous	1bp insertion and 1bp deletion
KELD4-1	Homozygous	3bp deletion and 1bp insertion
KELD4-2	Homozygous	4bp deletion
KELD10-1	Homozygous	1bp deletion
KELD10-2	Homozygous	1bp insertion
KELD12-1	Compound hemizygous	4bp deletion and 5bp deletion
KELD12-2	Compound hemizygous	1bp insertion and 1bp deletion
KELD26-1	Compound hemizygous	7bp deletion and 2bp insertion
KELD26-2	Homozygous	2bp deletion

The previous siRNA screen demonstrated these DUSP genes may have growth-promoting roles in NB cells (**Fig. 3.2**). This was especially true in KELLY and LAN-1 cells where loss of cell viability was more pronounced. The deconvolution of siRNAs identified a range of potential off-target effects (**Fig. 5.3**), but we still expected the reduction of cell viability to be primarily from loss of the DUSP target. We hypothesised loss of the DUSP target genes in KELLY cells would reduce their growth rate. To this end, cell growth assays were performed on each DUSP-null subclone compared to KELLY cells transfected with a vector not containing a gRNA (KELLY_E) (**Fig. 5.6**). Cells were seeded on day 0 and cell abundance was measured daily from day 3 to day 7 using a resazurin assay. Surprisingly, in the majority of cases the cells grew at a similar rate regardless of whether the

DUSP gene was present or not. The only statistically significant difference observed was a decrease in cell growth in the KELD3-1 population. The difference in growth between KELD3-1 and KELD3-2 once again highlights the heterogeneity observed between different clonal populations. It is possible that over a greater time-period there would be a more pronounced difference. For example, the DUSP12 and DUSP26 subclones grow marginally faster than wild type KELLY cells after 4 days (**Fig. 5.6**). Compared to the acute effect of DUSP knockdown with siRNAs, these DUSP-null subclones represent a long-term response to loss of DUSP protein. Therefore, some differences are expected between this method and siRNA treatment. As mentioned previously, during the long-term selection process, it is possible that subclones have evolved to tolerate loss of the targeted DUSP or have new compensatory changes. Nonetheless, none of these DUSPs appeared to consistently display growth-promoting roles in KELLY cells.

An alternative measure of cell survival is the ability of a cell population to form a colony (Franken et al., 2006). Hence, colony forming assays were performed over 2 – 3 weeks for each cell population (**Fig. 5.7A-E**). Both the size and number of colonies were measured. Unfortunately, in one assay the KELLY_E population formed very few colonies which, as all other cell populations are normalised to this, distorted that experiment (**Fig. 5.7A, grey dots**). Hence, the data is also presented not including this set (**Fig. 5.7B**). Although some of the DUSP clones formed a different number and size of colonies compared to KELLY_E cells, none of these differences reached statistical significance, partly due to the large variation between replicates (**Fig. 5.7B-C**). It is worth mentioning that the automated method used for counting colony size and number will also introduce a degree of error which probably contributes to this variability (**Chapter 2.5.8**). Clonogenic capacity is also used to investigate the cancer stem-cell nature of each population (Fedr et al., 2013). Depending on the cell population, between 10 – 50% of cells were able to form colonies (**Fig. 5.7D**). Only the DUSP3 subclones formed fewer colonies than the control across all replicates. The differences between KELLY_E cells and DUSP3-null cells is

highlighted in **Figure 5.7E** where there is a clear reduction in both colony size and number. Considering the KELD3.1 subclone also grew slower than KELLY_E cells over 4 days (**Fig. 5.6**), the role of DUSP3 in KELLY cells is worth exploring further.

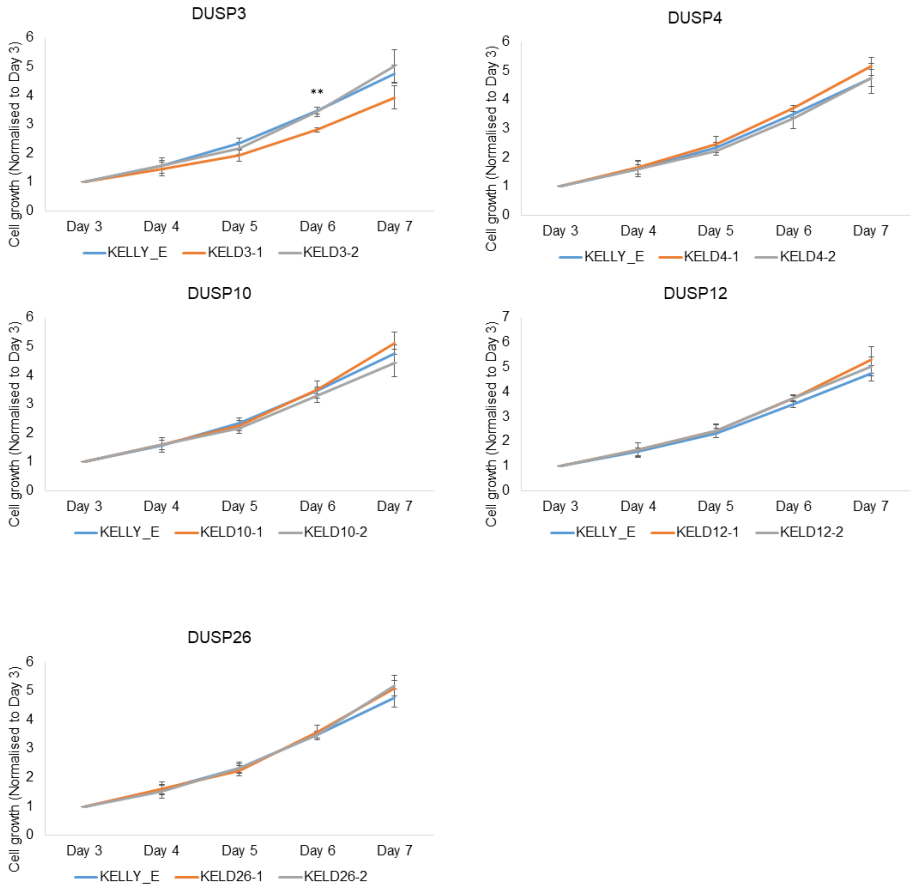

Figure 5.6 – DUSP candidates do not promote KELLY cell growth. Cell growth assay of each DUSP-null clone compared to KELLY cells transfected with a vector not containing a gRNA (KELLY_E). Cells were seeded on day 0 and cell growth was measured everyday from day 3 to day 7 using a resazurin assay (n = 3). Independent samples t-test performed at each timepoint compared to the KELLY_E cells, **$p \leq 0.005$.

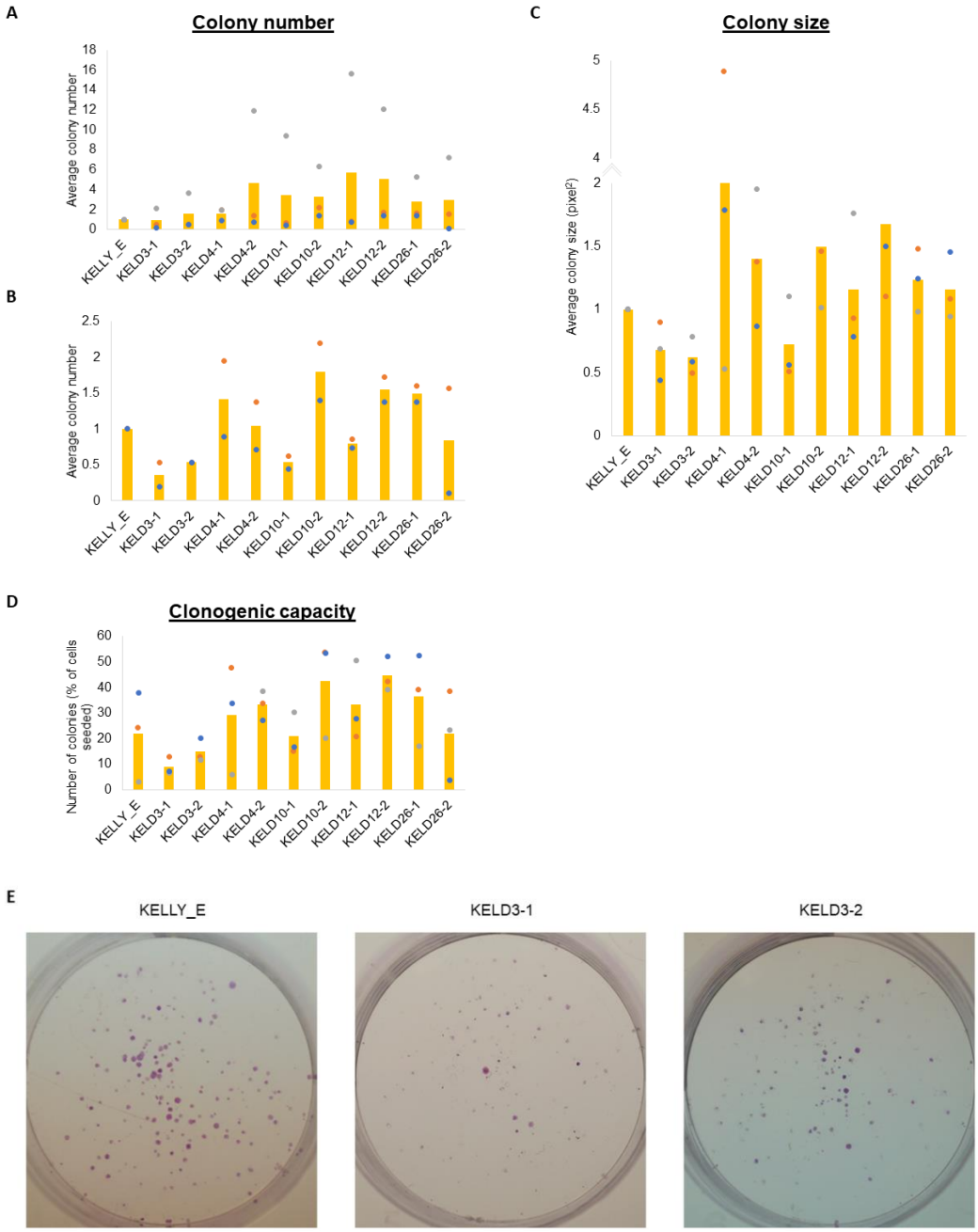

Figure 5.7 – Loss of DUSP3 suppresses KELLY clonogenicity. The (A-B) colony number, (C) colony size and (D) clonogenic capacity of DUSP-null clone compared to KELLY_E cells in a clonogenic assay (n = 3). Cells were incubated for 15 – 19 days before fixing and staining with crystal violet. In figures A - C each cell populations was normalised to KELLY_E population whereas in Figure D colonies were a percentage of total cells seeded (400 cells per well). Colony number is displayed (A) with and (B) without the third biological replicate. One-way ANOVA performed on Figure 5.7A-D but, compared to KELLY_E cells, none of the subclones reached statistical significance. (E) Representative images from clonogenic assay for DUSP3-null clones and KELLY_E cells.

The potential off-target effects from using siRNAs is exemplified by the DUSP6 siRNA pool where the effect on cell viability was unrelated to gene knockdown (**Fig. 3.7**). Considering the apparent difference in cell growth and survival patterns between the DUSP siRNA study and the CRISPR-mediated gene deletion study, we were still concerned that loss of cell viability caused by the DUSP siRNAs was not a result of gene knockdown. The DUSP-null subclones should be the optimal tool to assess the proportion of siRNA-mediated reduction of cell viability that is actually driven by loss of DUSP protein. To this end, the DUSP-null sub-clones were treated with their respective DUSP-targeting siRNA pools (**Fig. 5.8**). As expected, the effect of each DUSP siRNA pool in KELLY_E cells was comparable to that observed in the original siRNA screen. Strikingly, in the majority of cases, removal of the siRNA target does not affect the degree of siRNA-mediated reduction of cell viability. The KELD10-2 population is marginally resistant to the DUSP10 siRNA pool as there is an increase in cell viability of 13%. However, the converse is true for the DUSP3-null subclones as they are more sensitive to DUSP3 siRNA. This is a challenging result and suggests that this group of diverse siRNAs are decreasing NB cell viability aberrantly via pathways unrelated to DUSP function.

Together, these results demonstrate that gene deletion of a single DUSP gene is unlikely to have a significant effect on NB cell growth. There is a potential reduction in NB cell survival by depletion of DUSP3 protein as demonstrated in the clonogenicity assays. However, the growth assays are currently inconclusive as the two DUSP3-null subclones displayed distinct results. Hence, further experiments, with a greater number of subclones or a mixed population would be useful to elucidate whether DUSP3 indeed has a role in NB cell growth.

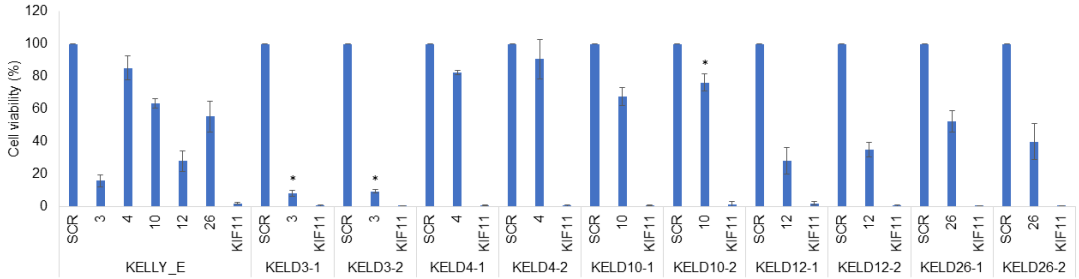

Figure 5.8 – DUSP siRNA pools cause significant off-target toxicities. KELLY_E and DUSP-null cells were treated with 5 nM DUSP siRNAs and cell viability was measured over 7 days (n = 3). Each cell populations was normalised to their respective SCR and data is presented as a mean ± SD. Independent samples t-test performed for each DUSP siRNA compared to the same treatment in KELLY_E cells, *$p \leq 0.05$.

5.2.3. DUSP5 promotes IMR-32 cell growth in a DUSP6-dependent mechanism

There is a lot of redundancy between the DUSP substrates, especially between the MKPs. Furthermore, transcriptomic profiling of the DUSP genes after various stimuli demonstrates they are regulated in a concerted manner (Caunt et al., 2008a, Nunes-Xavier et al., 2019b). This raises the question as to whether DUSPs may be able to compensate for one another or even be dependent upon each other. Up to this point, I have only investigated NB cell growth after depletion of a single DUSP. We hypothesised that removing multiple DUSPs would prevent potential compensatory mechanisms in NB cells. A recent study demonstrated melanoma cells with *BRAF* or *NRAS* mutation have a synergistic dependency on DUSP4 and DUSP6 (Ito et al., 2021). KELLY cells also have hyperactive ERK signalling due to an ALK F1174L mutation. Hence, a large siRNA screen was performed in DUSP4 and DUSP6-null subclones to see whether there are any co-dependencies between these DUSPs and others (**Fig. 5.9**). This was carried out in 384-well format using a semi-automated robotics platform in collaboration with Prof. Robin Ketteler at UCL. To adjust for the scale of the assay, siRNA treatments were reverse-transfected into each cell population. Due to the variability within and between each assay,

quintuplicate technical replicates were included per assay (For full method see **Chapter 2.5.2**).

The siRNA pools that were deconvoluted in **Figure 5.3** demonstrated the same loss of viability in KELLY and LAN-1 cells suggesting these off-target toxicities are not cell-specific, although cell-specific effects were identified with the DUSP6 pooled siRNA (**Fig. 3.5**). Logically, by comparing the potency of DUSP siRNAs in WT and DUSP-null cells, this experimental design should control for the off-target toxicities shown by siRNA pools. In this system, we hypothesise that we would see an additional decrease in cell viability in the DUSP-null cells resulting from loss of some other DUSP proteins. Furthermore, for the DUSPs that have been deconvoluted, I selected sub-pools of individual siRNAs that were not deemed to have the least off-target toxicities (**Fig. 3.7 and Fig. 5.3**). For example, the 6.1 and 6.2 individual siRNAs were combined to form a new DUSP6 pool which clearly depletes DUSP6 protein but does not show any off-target toxicities (**Fig. 3.7**). As the different DUSP-null cells included have different control lines, it is also worth mentioning that wild type KELLY cells were used as the control cell group.

Only a small proportion of siRNAs displayed different effects on cell viability in the DUSP4 and DUSP6 subclones compared to WT KELLY cells (**Fig. 5.9**). Furthermore, none of the siRNAs displayed a statistically significant difference between DUSP knockout and WT KELLY cells. However, there were two interesting changes, namely, DUSP5 and DUSP22 siRNA treatments, within the DUSP6 dataset and to a lesser extent in the DUSP4 dataset. In WT KELLY cells, one of the DUSP5 and DUSP22 replicates appeared to completely abolish cell viability (purple data point in **Fig. 5.9A**, blue data point in **Fig. 5.9B**) which we deemed an anomaly, skewing the data. Without this data point, in WT KELLY cells knockdown of either DUSP5 or DUSP22 do not significantly affect cell viability. However, treatment with either the DUSP5 or DUSP22 siRNAs appear to reduce cell viability less in the DUSP6 knockout cell populations, apparently trending towards growth-suppressive function (**Fig. 5.9B**). Nonetheless, due to the large variation between replicates this is not statistically significant. These

data could suggest DUSP6 blocks a growth-suppressive action of DUSP5 or DUSP22, although further experiments are required to validate this. In support of this, knockdown of DUSP6 in breast cancer cells results in an increase in DUSP5 mRNA, therefore it is possible that DUSP6 suppresses *DUSP5* or *DUSP22* gene expression. Alternatively, DUSP6 may be influencing the function of DUSP5 or DUSP22. DUSP5 is an ERK-specific phosphatase whereas DUSP22 has a plethora of intracellular targets (**Table 1.1**) (Patterson et al., 2009). It is possible DUSP6 is preventing DUSP5- or DUSP22-mediated regulation of a target, such as ERK, either by directly competing for the same target or by an indirect mechanism. In this setting, DUSP6 must be removed to allow the suppressive function of DUSP5 or DUSP22 on NB cell growth.

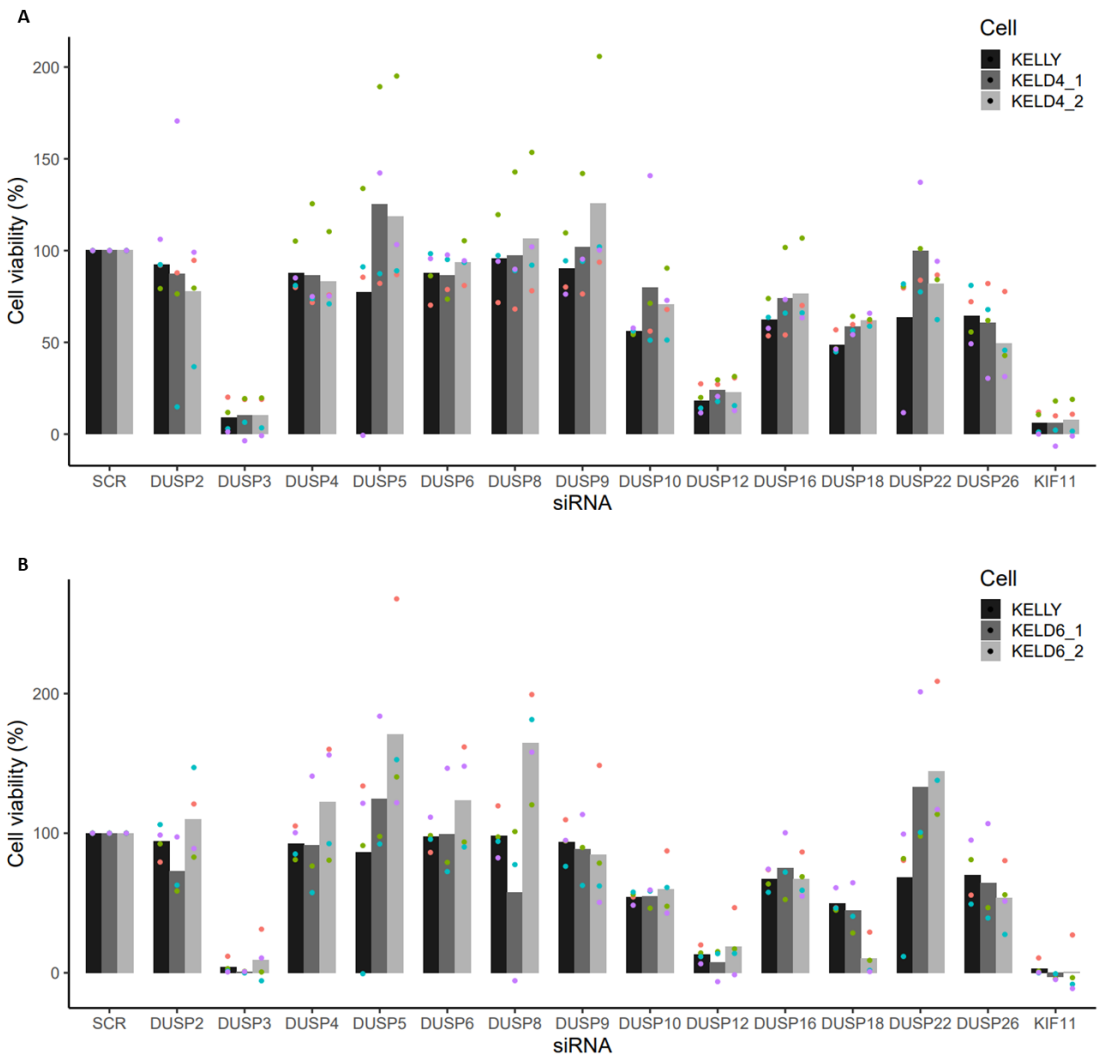

Figure 5.9 – Investigating compensatory mechanisms between DUSP proteins. Cell viability of (A) DUSP4 and (B) DUSP6 subclones compared to WT KELLY cells after treatment with 5 nM DUSP siRNA (n ≥ 3). Cell viability was assessed via a resazurin assay after 6 days. Data normalised to SCR and expressed as a mean with the individual experiments overlaid. One-way ANOVA performed for each siRNA comparing DUSP4- and DUSP6-null subclones with WT KELLY cells. No statistically significant differences were found.

The compensatory screen shown above was performed in 384-well plates using semi-automated robots. Although careful pilot experiments were performed to optimise this set-up, there was still high variance between technical and biological replicates. Furthermore, the optimal control KELLY cell population was not used in this experiment. Therefore, to complement and validate this assay we sought to repeat this screen manually in 96-well plates with the DUSP6-null cells as this population displayed more differences to WT KELLY cells compared to DUSP4-null cells. As well as validating the compensatory links between DUSP6, DUSP5 and DUSP22, this assay would also be performed in IMR-32 cells to see whether these interactions could be replicated. As opposed to using WT KELLY cells as the control, the DUSP6-null subclones were compared to their parental cell populations, 2E2g4 and 2E11g4. To this end, KELLY and IMR-32 DUSP6-null cells were treated with a subset of DUSP siRNAs that are known to regulate ERK signalling or are implicated in NB cell growth (**Fig. 5.10A-B**). Surprisingly, the growth-suppressing effect of DUSP5 and DUSP22 displayed by KELLY DUSP6-null cells was no longer present (**Fig. 5.10A**). This could possibly be due to the different control cell line being used (2E2g4 instead of WT KELLY cells) or due to the variability between replicates. However, in IMR-32 cells, a range of DUSP siRNAs appeared to reduce cell viability but were marginally less potent in DUSP6-null cells (**Fig. 5.10B**). Coincidentally, this includes DUSP5 and DUSP22, where the DUSP5 difference is statistically significant. A speculative model explaining how this could work mechanistically is depicted in **Figure 5.10C**. Here, DUSP5 promotes IMR-32 cell growth directly and indirectly via DUSP6 inhibition. However, there is no evidence in the literature that such a mechanism could exist, therefore further studies are required to determine

whether this is truly possible. Moreover, the data presented so far does not suggest DUSP6 can play a growth-suppressive role in NB cells.

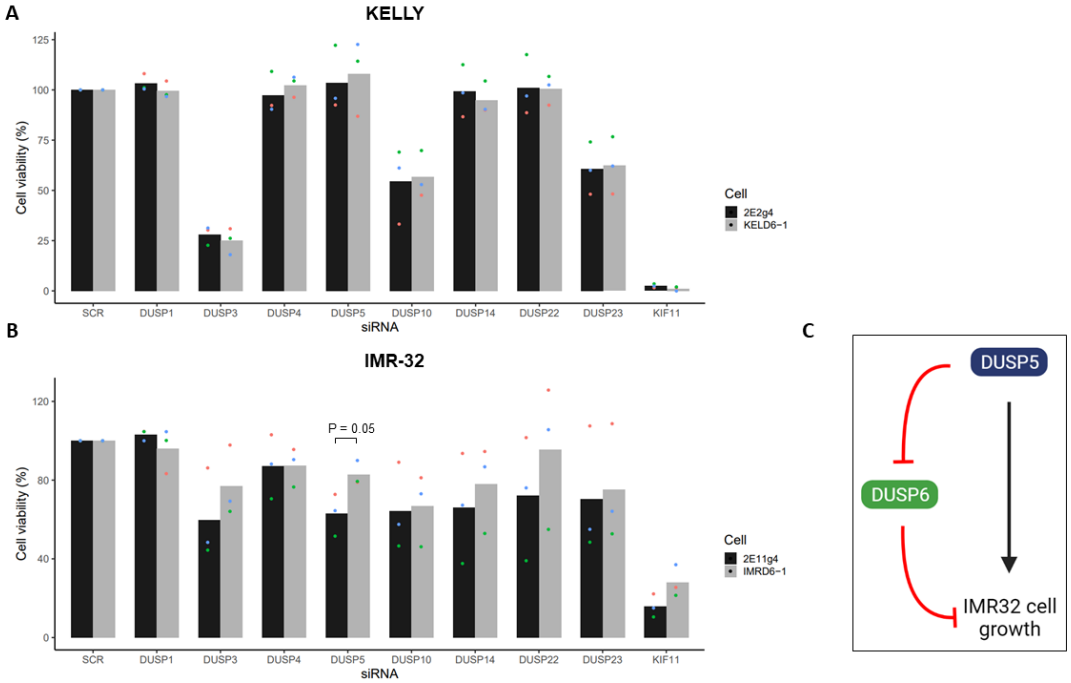

Figure 5.10 – DUSP5 promotes IMR-32 cell growth via DUSP6. (A) 2E2g4 and (B) 2E11g4 and DUSP6-null cells were treated with 5 nM siRNA targeting a wide range of DUSPs (n = 3). Cell viability was assessed via a resazurin assay after 6 days. Data normalised to SCR and expressed as a mean ± SD. Independent samples t-test between cells with and without DUSP6; p value stated in Figure. (C) Schematic of epistatic relationship between DUSP5 and DUSP6 in IMR-32 cells.

5.2.4. Acute loss of a single MAP kinase phosphatase is not sufficient to alter MAPK or AKT signalling

The data presented above suggests that DUSPs, when examined individually, do not have very significant effects in driving NB cell growth, at least in IMR-32 or KELLY cell lines. This is a surprising finding considering RTK signalling is an important regulator of NB cell growth. This is especially true for ERK signalling as NB cell growth can be driven by the ALK-ERK axis (Lopez-Delisle et al., 2018). Hence, one would expect alterations of MKP gene expression to influence NB cell growth. This raises a key

question of what is then regulating ERK signalling in these cells? We have previously demonstrated that loss of DUSP6 does not appear to alter ERK phosphorylation in response to EGF stimulation (**Fig. 3.15**). There are reports that other PTP enzymes could potentially restrain ERK signalling (Toledano-Katchalski et al., 2003, van Vliet et al., 2005). Nonetheless, we hypothesised some of these MKPs would function on ERK in NB cells. To investigate this, KELLY cells were treated with siRNAs targeting each MKP and an immunoblot was performed against the MAPKs and AKT (**Fig. 5.11**). The assay was performed in the presence and absence of FGF as ERK stimulation may be required to see the DUSP restrain MAPK activity. Although the phenotypic effect of these siRNAs is fraught with off-target toxicities, qPCR assays demonstrate they do still knockdown the target gene (**Fig. 3.3 and Fig. 5.3**). For that reason, we thought these siRNAs could still be used to probe the effect on intracellular signalling pathways. To further reduce off-target toxicities, for deconvoluted genes the same sub-pools of individual siRNAs were used to that in **Figure 5.9** and **Figure 5.10**.

As expected, treatment with FGF causes a significant upregulation of ERK signalling (**Fig. 5.11**). In cells with and without FGF stimulation, loss of an MKP does not have a statistically significant effect on ERK signalling. Paradoxically, there is a slight decrease in FGF-mediated ERK signalling after depletion of *DUSP1*, *DUSP2* or *DUSP4*. This would suggest ERK signalling is somewhat dependent on its negative feedback. However, as demonstrated in **Figure 3.6**, the DUSP1 siRNAs were very ineffective, therefore the role of DUSP1 on MAPK signalling is yet to be determined. In both unstimulated and stimulated cells, there is a slight increase in ERK signalling after loss of *DUSP8* potentially suggesting a mild role of DUSP8 in suppression of ERK. This could be direct as DUSP8 can dephosphorylate ERK (Liu et al., 2016). DUSP8 also shows broader phosphatase activity on the p38 and JNK kinases but neither are altered by *DUSP8* depletion. Nonetheless, there does not appear to be an MKP that significantly restrains ERK signalling. In FGF stimulated cells, p38 phosphorylation appears to be dependent on DUSP4 and AKT phosphorylation on DUSP9, however these effects are marginal and not significant. Overall, although there are some

minor changes, these results suggest that no single MKP can restrain MAPK or AKT signalling in KELLY cells.

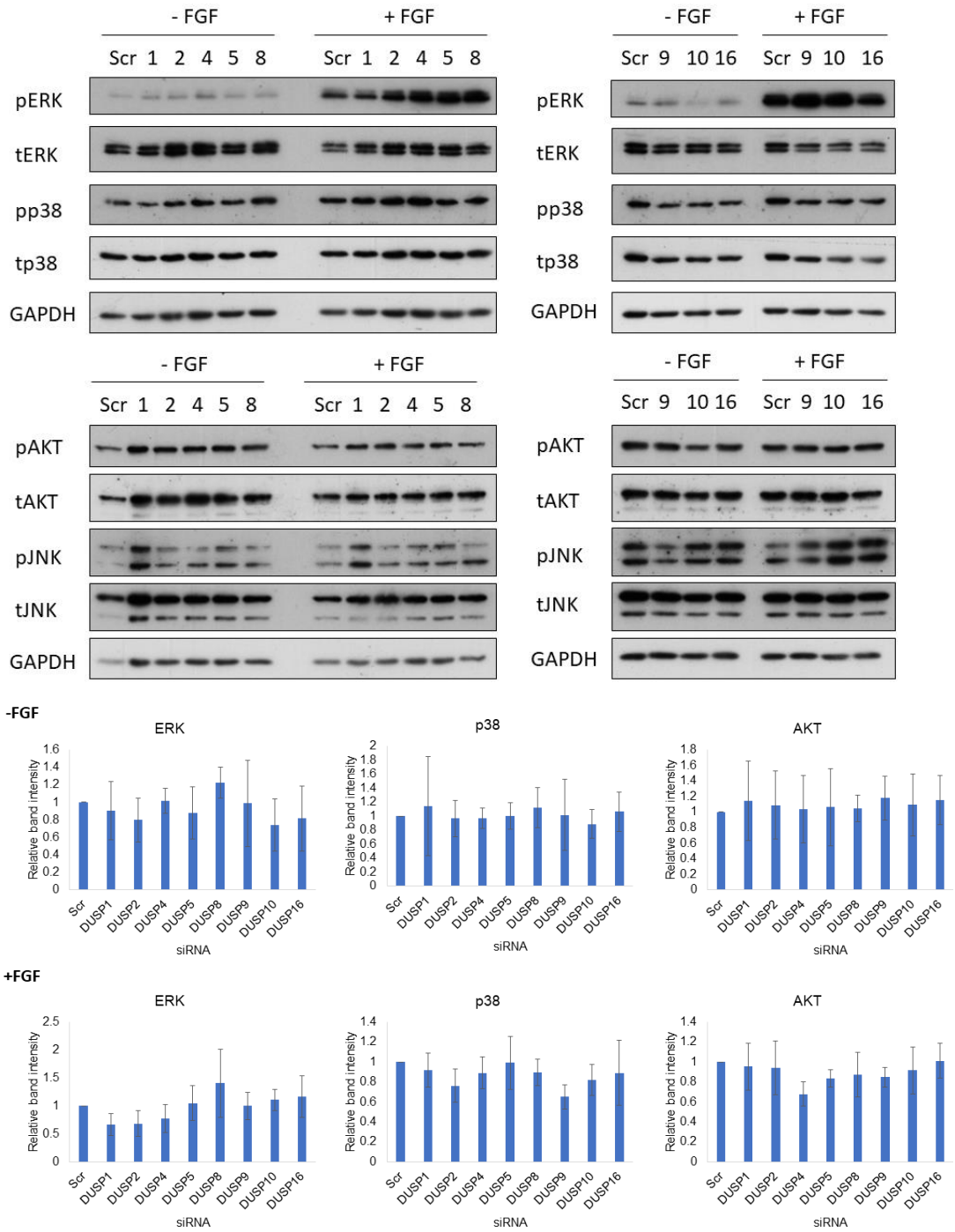

Figure 5.11 – Individual MKPs do not have tight control of MAPK or AKT signalling. KELLY cells were treated with 5 nM siRNA for 24 hours and an immunoblot was performed against the MAPKs and AKT. 1 hour prior to lysis, cells were incubated with or without 20 ng/µl FGF (n ≥ 3). For quantification, each phospho-protein was normalised to GAPDH followed by a second normalisation to SCR siRNA. One-way ANOVA compared to SCR was performed but no statistically significant differences were found.

5.3. Discussion

A wide range of MKPs and aDUSPs have been implicated in NB cell growth in various cell culture systems (Nunes-Xavier et al., 2019b). Considering loss of DUSP6 did not significantly affect MAPK or AKT signalling pathways (**Chapter 3**), the aim of this chapter was to broaden the search for other DUSPs that could regulate these pathways and potentially drive NB cell growth. Experiments focussed on the DUSP candidates that appeared growth-promoting in the siRNA screen (**Chapter 3**). For each DUSP enzyme, two NB cell subclones were identified after CRISPR/Cas9 targeting that contained out-of-frame indels. Only loss of DUSP3 appeared to reduce the growth rate and clonogenic potential of NB cells, but only in one subclone. Another consequence of generating these DUSP-deficient cells was that I could attempt to validate the actions of their respective siRNAs. This in fact revealed the significant and concerning off-target toxicities inherent in the siRNA pools. Potential compensatory and epistatic mechanisms between DUSPs was also explored where there appeared to be an antagonism between loss of DUSP6 and knockdown of *DUSP5* and *DUSP22*. Lastly, each member of the MKP family was knocked down using siRNAs to understand which DUSP enzyme regulates MAPK signalling. Surprisingly, only DUSP8 appeared as a potential candidate DUSP that could regulate ERK signalling, suggesting that the majority of DUSPs are not individually very influential in controlling MAPK signals in KELLY cells and may therefore act in redundant fashion or regulate unidentified pathways.

An advantage of CRISPR/Cas9-mediated gene deletion is that cells depleted of a target gene can be used to determine the specificity of alternative LOF approaches. The data presented above suggests the siRNAs used, although having potent on-target effects on mRNAs, also display significant off-target toxicities when measured in cell survival assays. We were very careful to deconvolute the siRNAs and found a good correlation between mRNA knockdown and cell viability data. Nonetheless, from the data presented in **Figure 5.8** it is hard to conceive how siRNA-

mediated reduction of cell viability could result from anything other than an off-target mechanism. Harrowingly, in cases such as DUSP3 and DUSP6, these toxicities can significantly suppress cell proliferation. Furthermore, although data from **Chapter 3** suggested the siRNA pool effects are cell specific (**Fig. 3.5**), siRNA pools used here displayed similar potency in KELLY and LAN-1 cells, more suggestive of non-specific toxicity. It is possible that a phenotype generated from siRNA-mediated gene depletion can result from specific silencing of an unintended gene. In HeLa cells, siRNA targeting the PICH checkpoint helicase (siPICH) reduces PICH protein levels but concurrently depleted MAD2 protein (Hübner et al., 2010). The authors demonstrated that MAD2, as opposed to PICH, was responsible for the alterations to spindle checkpoint signalling caused by siPICH. However, the data presented above identified off-target toxicity for *all* of the DUSP siRNA pools which suggests a direct off-target effect on one alternative gene is very unlikely.

Since the discovery that LOF using siRNAs can produce high-rates of false positives, a wide range of methods have been employed to circumvent these off-target effects (**Table 5.2**) (Jackson and Linsley, 2010). As mentioned in **Chapter 3**, one such method is the pooling of individual siRNAs (Kittler et al., 2007, Hannus et al., 2014). Hannus et al. (2014) have developed an alternative pooling method where up to sixty individual siRNAs are combined. Indeed, the siRNA pools affected the global transcriptome less than individual siRNAs suggesting fewer off-target effects. A different approach, termed endoribonuclease-prepared short interfering RNAs uses the enzymatic digestion of double-stranded RNA by an RNase III to generate a large pool of siRNAs (Kittler et al., 2007). However, there is a dearth of studies that remove the target protein to characterise the off-target effects of these approaches. In one study where the target gene was removed to determine RNAi specificity, similar off-target toxicities were found (Huang et al., 2017). ShRNA-mediated knockdown of *MELK*, a serine/threonine kinase, significantly reduced breast cancer cell proliferation. However, the same results were observed in MELK-null cells confirming the off-target toxicity of the shRNA. The authors also employed

a novel CRISPR-mediated transcriptional repressor of MELK to demonstrate that acute depletion of MELK did not affect cell proliferation. Interestingly, a recent study has demonstrated how commercial non-targeting shRNA's are also able to induce potent off target effects demonstrating that controls should also be validated alongside on-target RNAi technologies (Czarnek et al., 2021). Overall, these data suggest a screen of RNAi-mediated knockdown in cells devoid of the target gene is an important strategy to validate siRNA specificity. Furthermore, the effect on cell viability of many DUSP siRNAs in the siRNA screen appears unrelated to the knockdown of the DUSP target.

Table 5.2 – Common siRNA off-target effects and the strategies employed to minimise them. Modified from Jackson and Linsley (2010).

Off-target effect	Strategies to mitigate off-target effect
microRNA-like — siRNAs down-regulate multiple transcripts with sequence complementarity to the siRNA seed region	siRNA redundancy Rescue Pooling multiple siRNAs Chemical modification of the seed region
Immune stimulation — siRNAs can activate TLRs	Elimination of pro-inflammatory sequences Chemical modification
Saturation of the RNAi machinery — exogenous siRNAs and shRNAs can saturate the endogenous RNAi machinery	None yet identified

Collectively, although the initial siRNA screen looked promising, the siRNA and CRISPR data have unfortunately demonstrated that there are in fact no single DUSPs that greatly affect NB cell line proliferation under our

conditions. In fact, the data demonstrate that siRNA pools simply do have high off-target effects. This is a surprising result considering many of these DUSPs are implicated in tumorigenesis and have been previously studied in NB. Loss of DUSP3 protein did affect the clonogenic potential of KELLY cells. However, the growth assay results were inconclusive as only one out of the two clones had a reduced growth rate. The reduced capacity to form colonies suggests DUSP3 is influencing the ability of these cells to continually proliferate. Clonogenic potential is also a measure of cancer stem cell nature (Fedr et al., 2013), therefore DUSP3 may be able to suppress this stem-cell phenotype in KELLY cells. It is well documented that DUSP3 can affect a wide range of physiological processes that result in reduced cell proliferation (Rahmouni et al., 2006, Russo et al., 2020, Torres et al., 2017). In HeLa cells, DUSP3 expression displayed a biphasic pattern during the cell cycle where it fine-tuned ERK and JNK activation (Rahmouni et al., 2006). Knockdown of DUSP3 resulted in cell cycle arrest and cellular senescence due to augmented upregulation of ERK and JNK signalling. In a different study, loss of *DUSP3* appeared to deregulate a wide range of cell cycle-associated proteins (Russo et al., 2020). These data suggest DUSP3 plays an integral role in cell cycle progression. DUSP3 can also influence DNA damage. Knockdown or pharmacological inhibition of DUSP3 radiosensitized tumour cells as DNA strand breaks were augmented and cell survival decreased in a clonogenic assay (Torres et al., 2017). Considering DUSP3 appeared to reduce NB cell proliferation at least in one form of assay, further experiments are warranted to validate this and to explore the molecular mechanisms behind it.

As mentioned in **Chapter 3**, the use of single cell clones is a very reductionist approach since genetic and phenotypic heterogeneity is completely removed. Furthermore, especially in NB, the importance of tumour heterogeneity in cancer progression and drug response has become increasingly important (Schmelz et al., 2021). This could be reflected in the variation between DUSP-null single cell clones in cell growth and clonogenic assays. It is worth mentioning that the DUSP-null single cell clones generated in this chapter derive from the WT KELLY population genetically

heterogenous population whereas in **Chapter 3**, a subclone with high Cas9 expression had been already selected prior to generation of DUSP6-null subclones. Hence, the WT KELLY cells used in **Chapter 5** may have some population heterogeneity, which may include both genetic and epigenetic variation. A recent study used barcoded sgRNA libraries to knockdown every protein in the genome and identify sub-clones sensitive to TRAIL-mediated apoptosis (Boettcher et al., 2019). An additional benefit of the screen was that clonal heterogeneity could be monitored over time. Interestingly, treatment with the TRAIL-R antibody resulted in a significant difference in the CRISPR screen output from different clonal populations derived from the same parental population demonstrating the heterogeneity between populations (Boettcher et al., 2019). With this in mind, the inducible CRISPR system used in **Chapter 3** appears more appropriate as loss of target protein can be analysed within a bulk population. Alternatively, pooling of single cell clones with similar proliferation rates into a pseudo bulk population could also decrease clonality effects (Henkel et al., 2020).

There are a range of DUSPs that are thought to be functional in NB cells. One line of thought is that DUSPs may function more as a network, rather than as independent entities. This notion stems primarily from the redundancy of MKPs on the MAPK substrates. Caunt et al. (2008a) demonstrated EGF or PDBu stimulation in HeLa cells altered transcription of multiple DUSPs. Interestingly, siRNA targeting of DUSP sub-families revealed the nuclear DUSPs (DUSP1 DUSP2, DUSP4 and DUSP5) were collectively important at restraining ERK signalling. A recent study demonstrated NRAS- or BRAF-mutant melanoma cells had a digenic dependency on DUSP4 and DUSP6 (DUSP4/6) (Ito et al., 2021). CRISPR-mediated depletion of DUSP4/6 decreased cell proliferation far greater than knock out of either gene alone and importantly, this was dependent on ERK signalling. Promisingly, melanoma cells which became resistant to ERK inhibition were sensitised to DUSP4/6 depletion demonstrating potential therapeutic benefit of dual DUSP4/6 inhibition. Alongside DUSP4/6, 685 other synergistic dependencies were identified that were not seen in the single-gene knock out analysis highlighting the importance of redundant and

compensatory proteins (Ito et al., 2021). Our group has previously investigated co-expression profiles between DUSP family members in publicly available NB patient datasets (Oscar Chatin, unpublished data). Interestingly, a wide range of DUSP enzymes display a strong correlation or inverse correlation in gene expression. This was particularly clear for DUSP1, DUSP5 and DUSP6 (**Fig. 5.12**) and demonstrates co-regulatory patterns are likely present in NB cells. We investigated whether loss of DUSP4 or DUSP6 could sensitise KELLY cells to loss of a different DUSP enzyme. In a large-scale analysis, DUSP6 appeared to restrain the suppressive function of DUSP5 and DUSP22 on KELLY cell growth. However, this could not be repeated in a smaller-scale experiment. Following this, in IMR-32 cells it appeared DUSP5 was growth-promoting. However, this effect was lost in DUSP6-null cells suggesting DUSP5 promoted cell growth via DUSP6. This suggests DUSP5 and DUSP6 may be part of the same regulatory network, in agreement with the strong correlation in gene expression (**Fig. 5.12**). As mentioned in **Chapter 3**, alteration in *DUSP5* gene expression may influence DUSP6 expression and vice versa (Buffet et al., 2017). Considering both are known regulators of ERK signalling, it would be beneficial to see whether ERK phosphorylation changes after combined *DUSP5/6* knockdown. Unfortunately, there were no other clear co-regulatory patterns identified I n the combinatorial DUSP depletion study. This is possibly due to the fact that the siRNAs only result in partial mRNA suppression, however one would still expect to see a growth effect when <50% gene expression is suppressed.

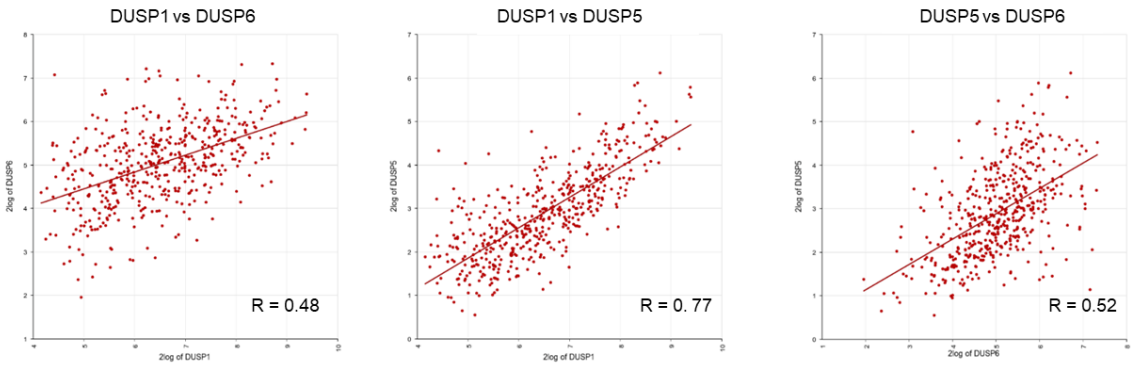

Figure 5.12 – Correlation of *DUSP1*, *DUSP5* and *DUSP6* gene expression in NB patients. There is a strong positive correlation between DUSP1, DUSP5 and DUSP6 gene expression. Data is presented from the SEQC dataset, extracted from the R2: Genomics Analysis and Visualization Platform (http://r2.amc.nl). The R values are displayed at bottom right of each chart (Oscar Chatin, unpublished data).

As RTK signalling pathways are important regulators of neuronal cell proliferation and differentiation (Annenkov, 2014), it is unsurprising they are important to NB pathogenesis. Indeed, a wide range of RTKs are associated to NB patient survival and can drive NB cell growth (Rozen and Shohet, 2021). Many of these pathway's signal through or interact with the RAS/MEK/ERK signalling pathway. Interestingly, there are a higher frequency of mutations in the ERK signalling pathway at relapse in NB suggesting this is a pathway used by cancer cells to evade current treatment regimens (Eleveld et al., 2015). The DUSP family are well characterised as negative feedback regulators of the MAPK signalling pathways (Discussed in **Chapter 1**). Furthermore, there are a range of neuronal mediators that regulate DUSPs transcriptionally suggesting an important role during neuronal cell function (Pérez-Sen et al., 2019). We expected that some DUSPs would be important at restraining ERK signalling, especially in cells with hyperactive ERK. It was therefore very surprising that knockdown of the MKPs individually did not significantly affect MAPK signalling after FGF stimulation. There is however a hint that DUSP8 may restrain ERK signalling. Although originally classified as a JNK/p38-specific phosphatase, DUSP8 is also able to dephosphorylate ERK. In rat cardiac myocytes and mouse embryonic fibroblasts, loss of DUSP8 upregulated ERK signalling

but not that of JNK or p38 (Liu et al., 2016). Exogenous DUSP8 immunoprecipitated with ERK and JNK in HEK293 cells suggesting dephosphorylation of ERK is direct. It is worth noting that the experiment performed here was only performed in KELLY cells which, due to the mutated ALK receptor, have hyperactive ERK signalling. Although we hypothesised this hyperactivation would increase sensitivity to DUSP function in these cells, it could possibly have desensitised the cell population to feedback of this pathway. Alternatively, similar to that observed with DUSP6 in **Chapter 3**, many DUSPs are able to anchor ERK in the cytoplasm as well as dephosphorylate ERK (Caunt et al., 2008b, Karlsson et al., 2004). In this regard it would be beneficial to analyse ERK localisation after DUSP knockdown.

Unfortunately, the data presented here collectively suggests that the majority of DUSPs are individually not essential to NB cell growth, at least in KELLY cells. There is a potential role for DUSP3 in promoting NB cell proliferation which we suspect could be via cell cycle regulation. Whether there are compensatory mechanisms in NB cells was also investigated phenotypically using the DUSP4 and DUSP6-null NB cells and it appears that DUSP5 promotes IMR-32 cell growth in a DUSP6-dependent mechanism. Although this suggests DUSP5 and DUSP6 could co-operate to regulate ERK, the findings in **Chapter 3** and **Chapter 4** suggested DUSP6 did not alter MAPK signalling. Therefore, the pathway that DUSP5 and DUSP6 co-regulate is unclear. However, the most surprising finding is that similar to DUSP6, individual knockdown of the majority of MKPs did not alter ERK signalling in KELLY cells. This leaves us with the question: what is the role of DUSPs in NB cells? We do expect at least some of them to regulate ERK, however ERK was unaffected under the conditions tested. It is possible DUSPs function in a very redundant manner, compensating for each other as a network. To address this, it would be beneficial to assess the effect of DUSP6 depletion on DUSP gene expression. Alternatively, DUSPs may have non-MAPK targets in NB cells that are not yet identified.

Another way to address this question is to consider that DUSPs may not be required until significant perturbation of their pathway. In this regard,

significant alteration of intracellular signalling may be required to reveal a DUSP function. With this in mind, the ALK receptor regulates a wide range of downstream pathways, including ERK, and is regarded as an oncogene in NB pathogenesis. Hence, inhibiting ALK signalling would disrupt a large cohort of signalling pathways (Trigg and Turner, 2018) and could reveal the role of these DUSPs. Whether DUSPs could be important downstream of ALK signalling is investigated in **Chapter 6** in the context of DUSP6

.

Chapter 6. Characterising the role of DUSP6 in ALK-mutated NB

6.1. Introduction

Phosphotyrosine signalling via RTK canonical pathways has a widespread role in neural crest (NC) cell development (Fantauzzo and Soriano, 2015). The expression of different RTK sub-groups is restricted both spatially and temporally allowing fine-tuned regulation of NC development into their derivatives. It is therefore unsurprising that signalling via these pathways is pivotal to NB pathogenesis (Discussed in **Chapter 1.4**). Indeed, as mentioned previously a wide range of RTKs are associated to NB patient prognosis (Rozen and Shohet, 2021). Nevertheless, the majority of NB treatment options remain relatively non-specific as researchers continually seek targetable molecular aberrations in NB. The RTKs represent one area where a range of specific molecular inhibitors have been developed and could therefore be deployed (Pottier et al., 2020). With respect to NB, the ALK receptor remains the best characterised RTK as it is mutated or amplified in ~8-10% and ~2-3% NB tumours respectively (Mossé et al., 2008, Janoueix-Lerosey et al., 2008, Carén et al., 2008). Moreover, therapeutic targeting of RTKs in NB is most promising in the context of ALK, where a wide range of inhibitors are currently in clinical trials (Brenner and Gunnes, 2021).

The ALK oncogene is a large multidomain protein and a member of the insulin receptor superfamily. The majority of work in NB focuses on the full length ALK receptor which sits within the cell's plasma membrane. In this setting ALK is activated in a ligand-dependent manner by the recently identified ALK activating ligands 1 and 2 (ALKAL1 and 2) (Guan et al., 2015). However, many mutations in the ALK receptor lead to a ligand-independent constitutively active form of ALK (**Fig. 6.1**). It is worth noting ALK also exists in a growing number of fusion proteins where ALK is activated via oligomerisation, however these have not been observed in NB (**Fig. 6.1A**) (Hallberg and Palmer, 2016). A large genomic analysis of 1596 NB tumour samples identified three ALK mutation hotspots and a range of other minor sites (Bresler et al., 2014). The mutations in the ALK-mutated cell lines used in this study were F1174L (KELLY and SH-SY5Y) and

R1275Q (LAN-5). Both of these mutations accelerate autophosphorylation of the tyrosine kinase domain leading to constitutive activation of ALK (**Fig. 6.1B**) (Bresler et al., 2014). As mentioned in **Chapter 1**, knockdown or chemical inhibition of ALK prevents NB cell growth, demonstrating its downstream pathways are important to NB cell proliferation (Janoueix-Lerosey et al., 2008). Furthermore, a large body of evidence demonstrates ALK and MYCN cooperate to drive an aggressive NB phenotype (Zhu et al., 2012, Schönherr et al., 2012, Berry et al., 2012). In NB, ALK can signal via three major signalling pathways; PI3K/AKT, MAPK/ERK and JAK/STAT, which are each implicated in MYCN function and NB progression (**Fig. 6.2**) (Trigg and Turner, 2018).

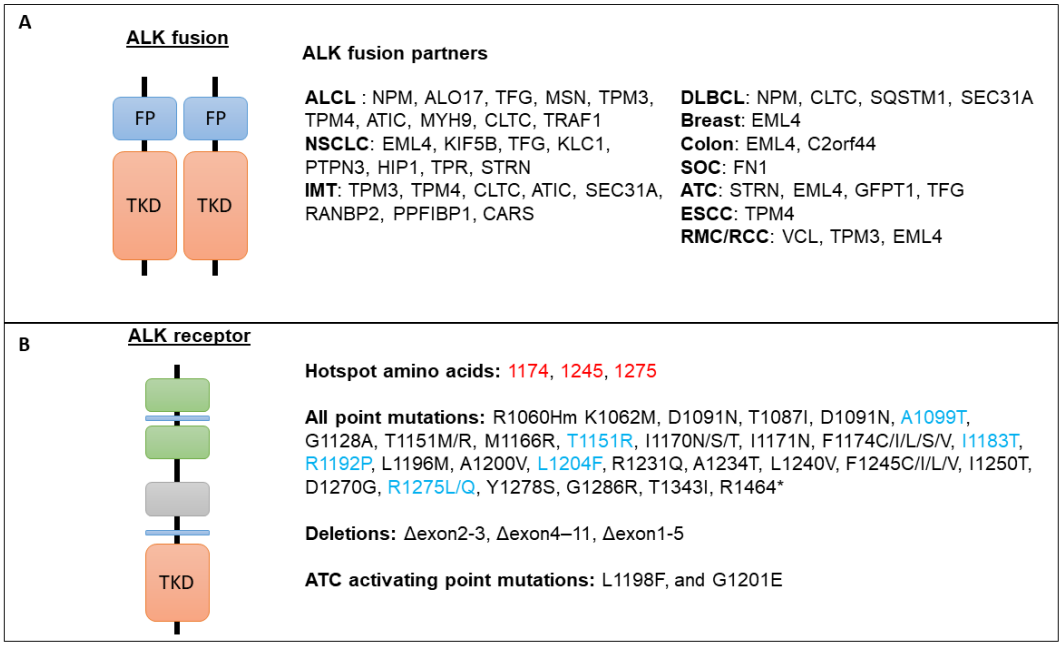

Figure 6.1 – Summary of the ALK aberrations in ALK-positive cancer. (A) Schematic of ALK fusion protein where the ALK tyrosine kinase domain (TKD) is fused to a fusion partner (FP). Each fusion has been described in numerous cancers, such as anaplastic large cell lymphoma (ALCL), non-small-cell lung cancer (NSCLC), inflammatory myofibroblastic tumour (IMT), diffuse large B-cell lymphomas (DLBCL), oesophageal squamous cell carcinoma (ESCC), renal medulla carcinoma (RMC), renal cell carcinoma (RCC), breast cancer, colon carcinoma, serous ovarian carcinoma (SOC) and anaplastic thyroid carcinoma (ATC). (B) Schematic of the ALK receptor. ALK mutations are predominantly found in NB, NSCLC and ATC. Germline mutations in NB are highlighted in blue; *truncation. Modified from Hallberg and Palmer (2016).

Initially, studies in the TH-MYCN transgenic mice demonstrated that PI3K inhibition reduced tumour growth suggesting PI3K/AKT signalling may alter NB progression via MYCN regulation (Chesler et al., 2006). *In vitro*, PI3K inhibition led to GSK3 activation which in turn phosphorylates and destabilises MYCN, resulting in apoptotic cell death. A subsequent study revealed the PI3K/AKT/mTOR pathway as an important driver in MNA NB (Vaughan et al., 2016). Concurrent inhibition of mTORC1 and 2 led to phosphorylation and rapid proteasomal degradation of MYCN. However, in contrast to the previous report, inhibition of the PI3K subunit α did not alter MYCN expression suggesting, in this case, MYCN was regulated in a PI3K-independent mechanism. Functional GSK3β was requisite for MYCN degradation, therefore, as mTOR can phosphorylate AKT (Sarbassov et al., 2005), it is plausible that mTOR-mediated stabilisation of MYCN is achieved indirectly via GSK3β inhibition. Recently, a third mechanism was identified whereby PI3K/AKT regulates MYCN via HMG-box transcription factor 1 (HBP1) (Claeys et al., 2019). In a range of NB cell lines, inhibition of both ALK and PI3K led to upregulation of HBP1 expression which was mediated by the FOXO3 transcription factor. Further analysis in IMR-5 cells demonstrated MYCN transcriptionally downregulated HBP1 and exogenous HBP1 expression resulted in a significant downregulation of MYCN target genes. Unsurprisingly, abrogating PI3K/AKT signalling alone or in combination with MYCN inhibition represents a potential therapeutic route in NB (Chesler et al., 2006, Segerström et al., 2011).

A range of studies demonstrated oncogenic ALK signalling activates STAT3 (Sattu et al., 2013, George et al., 2008, Chen et al., 2008). In one study, after identification of the ALK/STAT3 axis, knockdown of *STAT3* reduced ALK-mediated activation of MYCN and NB cell proliferation (Sattu et al., 2013). Although the specific interaction between STAT3 and ALK was not identified, the dependence of MYCN on STAT3 activation highlights the importance of this signalling pathway in NB cells.

It is well documented that mutations occurring in different components of the MAPK pathway, including ALK, lead to its hyper-activation in NB (Eleveld et al., 2015). Such mutations are more frequent in relapsed

samples, suggesting they are secondary mutations acquired due to the harsh conditions of multimodal chemotherapy. One study investigating constitutive ALK activation in the TH-MYCN transgenic mouse model identified RET, another RTK oncogene, as a downstream target of mutated ALK (Cazes et al., 2014). As mentioned in **Chapter 1**, RET expression is strongly associated to NB patient survival. Lopez-Delisle et al. (2018) demonstrated ALK-ERK-ETV5 signalling upregulates RET which cooperates with MYCN to drive NB cell growth. Promisingly, in MNA/ALK^{F1178L} nude mice, simultaneous inhibition of ALK and RET significantly reduced tumour growth. Furthermore, as ERK functions as a node for RTK signalling, the therapeutic efficacy of MEK inhibitors has been investigated (Tanaka et al., 2016, Eleveld et al., 2015, Hart et al., 2017). Although initially demonstrating positive results *in vitro*, trametinib monotherapy was unbeneficial in ALK-addicted NB due to pro-survival feedback mechanisms via AKT and ERK5 (Umapathy et al., 2017). Nonetheless, MEK inhibitors remain appealing in NB due to their success in other cancers driven by MAPK activation and have entered clinical trials in combination with ribociclib, a CDK4/6 inhibitor, in relapsed high-risk NB patients (NCT02780128).

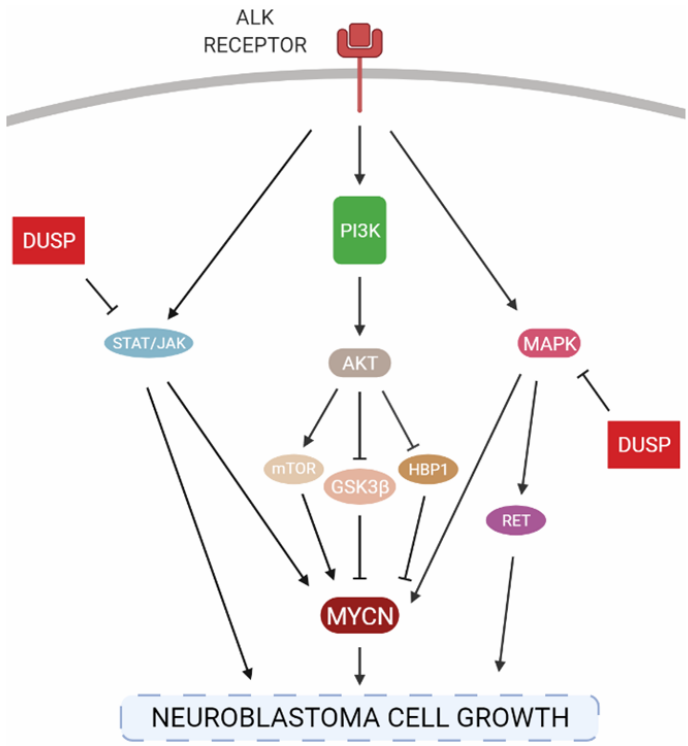

Figure 6.2 – ALK signalling pathways in NB. PI3K, STAT/JAK and MAPK represent three major signalling pathways activated by ALK in NB. Each pathway is implicated in NB cell growth and each have reported interactions with MYCN, either directly or indirectly. The term DUSP represents the MKPs and aDUSPs that can regulate the JAK/STAT or MAPK signalling. Hence, manipulating DUSP function could have major effects on ALK signalling in this setting.

The ALK mechanism of action requires ATP binding to promote kinase activity. Hence, a range of tyrosine kinase inhibitors (TKIs) have been developed that interact with the ATP-binding pocket (Hallberg and Palmer, 2016). Crizotinib was the first ALK-targeting TKI to be assessed in clinical trials, targeting the ALK-EML4 fusion protein in non-small cell lung cancer (NCT00585195; NCT00932451). Promising results in NSCLC inevitably led to the investigation of ALK inhibition in other ALK-driven cancers such as anaplastic large cell lymphoma (ALCL) and NB. As a 1st generation pan ALK/MET/ROS1 inhibitor, crizotinib has subsequently been approved by the FDA to treat ALK-positive NSCLC and ALCL and ROS1-positive NSCLC. However, it has become apparent that long-term treatment of crizotinib can lead to acquired resistant mutations in the ALK receptor, predominantly at F1174L (Choi et al., 2010, Bresler et al., 2014). Over the past decade a

range of 2nd and 3rd generation inhibitors have been generated. Many of these inhibitors demonstrate an improved potency over crizotinib and have entered clinical trials for NB treatment (Brenner and Gunnes, 2021). Importantly, these modified TKIs have far fewer resistance mutations compared to crizotinib (Hallberg and Palmer, 2016). Thus far only one mutation has been identified that results in resistance to lorlatinib (Shaw et al., 2016). Lorlatinib is a 3rd generation inhibitor of ALK/ROS1 that displayed higher potency than crizotinib in NB cell lines (Guan et al., 2016, Infarinato et al., 2016). Promisingly, lorlatinib demonstrated significant tumour regression in pre-clinical studies, including in the aggressive Th-ALK^{F1174L}/MYCN mouse model (Guan et al., 2016, Infarinato et al., 2016). Lorlatinib is currently in two phase 1 trials for NB which are currently recruiting (NCT03107988 and NCT04753658). In one of these trials the dose-escalation phase has been published and there is a clear anti-tumour response by lorlatinib (Goldsmith et al., 2020). Interestingly, resistance to lorlatinib does not appear to result from acquired mutations in ALK but rather due to activation of alternative or downstream pathways such as the PI3K/AKT/mTOR or RAS/ERK signalling pathways (Redaelli et al., 2018).

As discussed in **Chapter 3.1** and **Chapter 5.1**, DUSPs are able to regulate a wide range of signalling pathways. Many identified DUSP substrates, such as ERK and STAT3, function downstream of ALK therefore one would expect DUSPs to influence ALK signalling (**Fig. 6.2**). Indeed, it has become apparent that DUSPs are transcriptionally regulated downstream of ALK. Lambertz et al. (2015) identified a 77-gene signature for ALK activity in NB which included *DUSP4*, *DUSP5* and *DUSP6*. In CLB-GA cells, chemical inhibition of ALK significantly decreased the gene expression of *DUSP4*, *DUSP5* and *DUSP6* and in SK-N-AS cells, overexpression of constitutively active ALK upregulated these genes. In accord, two recent RNA-Sequencing studies demonstrated ALK can transcriptionally regulate multiple DUSPs (**Fig. 6.3**) (Van den Eynden et al., 2018, Borenäs et al., 2021). Treatment with crizotinib or lorlatinib significantly downregulated *DUSP2*, *DUSP4*, *DUSP5*, *DUSP6* and *DUSP22* in CLB-BAR cells (**Fig. 6.3A**) (Van den Eynden et al., 2018). Results for DUSP4 were validated

using an immunoblot where both DUSP4 and pERK were downregulated following ALK inhibition. A subsequent study by Borenäs et al. (2021) also demonstrated ALK inhibition causes many changes in DUSP expression in NB1 cells (**Fig. 6.3B**). Notably, there was a striking decrease in *DUSP6* expression. However, this cannot be as simple as negative feedback on ERK, since ALK stimulation by ALKAL2 also downregulated *DUSP6*. Furthermore, in both datasets ALK inhibition upregulated a handful of DUSPs suggesting other regulatory mechanisms are at play.

A

Van den Eyden et al. (2018)

	CLB-BAR$^{\Delta exon4\text{-}11}$		CLB-GE^{F1174V}		CLB-AS^{WT}	
Gene	CRIZ	LOR	CRIZ	LOR	CRIZ	LOR
DUSP1	-0.62	-0.58	-0.16	-0.22	-0.04	0.33
DUSP2	-1.11	-1.11	-0.68	-0.46	-0.34	1.22
DUSP3	-0.34	-0.25	-0.08	-0.09	0.00	-0.04
DUSP4	-2.04	-2.74	-0.13	-0.29	0.05	0.09
DUSP5	-0.87	-2.36	-1.09	-1.45	-0.21	-0.06
DUSP6	-2.87	-4.85	-0.54	-0.99	-0.03	-0.03
DUSP7	-0.51	-0.65	-0.16	-0.30	0.10	0.16
DUSP8	-0.57	-0.22	-0.31	-0.07	0.27	0.89
DUSP9	1.12	1.53			0.23	0.42
DUSP10	0.79	1.17	-0.20	-0.05	-0.05	0.10
DUSP11	-0.43	-0.41	0.28	0.46	-0.05	-0.26
DUSP12	0.51	0.52	-0.04	-0.11	0.17	0.10
DUSP13						
DUSP14						
DUSP15	-0.49	-0.66	0.02	-0.26		
DUSP16	-0.08	0.06	-0.04	0.10	-0.06	0.02
DUSP18	0.06	0.21	0.21	-0.05	0.21	0.06
DUSP19	0.58	0.73	0.40	0.36	-0.15	-0.28
DUSP22	-2.45	-1.11	0.08	0.12	-0.06	0.11
DUSP23						
DUSP26	0.28	0.37	0.25	0.24	0.42	0.00
DUSP27						
DUSP28	0.12	0.50	0.19	-0.01	0.03	0.19

B

Borenäs et al. (2021)

	NB1^{Amp}		IMR32^{WT}	
Gene	ALKAL2	LOR	ALKAL2	LOR
DUSP1	-0.30	-0.04	-0.08	0.09
DUSP2	-0.32	0.97	-0.02	-0.06
DUSP3	-0.01	-0.17	-0.05	-0.06
DUSP4	-0.33	-2.26	-0.20	-0.33
DUSP5	-0.87	-2.30	-0.08	-0.49
DUSP6	-2.92	-6.47	-0.06	-0.28
DUSP7	-0.51	-0.49	-0.18	-0.07
DUSP8	-0.31	-0.40	0.14	0.18
DUSP9	-0.26	-4.13	0.20	0.18
DUSP10	0.58	0.84	0.10	-0.19
DUSP11	-0.09	0.06	-0.11	0.06
DUSP12	0.05	-0.47	-0.01	-0.09
DUSP13	0.58	-2.66	-0.04	-0.05
DUSP14	0.02	-0.44	0.01	-0.21
DUSP15	1.56	1.12	-0.04	-0.19
DUSP16	0.01	-0.31	0.09	0.05
DUSP18	-0.56	0.29	-0.05	0.09
DUSP19	0.20	0.38	0.04	0.53
DUSP22	0.24	0.41	-0.04	0.11
DUSP23			-3.49	-1.19
DUSP26	0.32	0.70	-0.07	-0.05
DUSP27			-1.84	-0.89
DUSP28	0.16	0.59	-0.13	-0.19

Log2-fold change

-5 -4 -3 -2 -1 0 1 2 3 4 5

Figure 6.3 – Transcriptional regulation of the DUSP family by ALK. RNA sequencing data from (A) Van den Eynden et al. (2018) and (B) Borenäs et al. (2021) after treatment with 250 nM crizotinib (CRIZ), 30 nM lorlatinib (LOR) or 1 µg/ml ALK activating ligand ALKAL2 for 24 hours as indicated. The cell lines used are described in the top row with their ALK status in superscript. Log2-Fold Change values are displayed both in the table and as a heatmap overlaid. Red and blue indicate the treatment increased and decreased DUSP expression respectively. Grey indicates the DUSP was not present in the dataset and each cell is coloured red to blue for high to low fold change respectively.

The data in **Chapter 5** suggested that DUSPs are either very redundant, or they regulate pathways unrelated to MAPK signalling, or both. The data above suggests that a wide range of DUSPs are highly regulated by ALK signalling which implies that they are functionally important in NB cells. I hypothesised that major disruption to the ALK receptor may reveal pathways regulated by DUSPs. Furthermore, this could also show whether

the DUSPs are important to ALK-driven cell growth. If so, then I hypothesised that DUSP(s) could represent an alternative therapeutic target functioning downstream of ALK. To investigate this, I first confirmed that the DUSP family is indeed transcriptionally regulated by ALK in ALK-mutated NB cell lines. Using the DUSP6-null cells generated in **Chapter 3**, the ALK/DUSP6 axis was then characterised further. The two aims of this chapter were to understand i) how DUSP6 is regulated downstream of ALK and ii) what the DUSP6 substrate(s) are in NB cells. To pinpoint what DUSP6 may be targeting and what pathways it is influencing, at the end of the chapter a phosphoproteomic screen was performed in the DUSP6-null cells after treatment with the ALK inhibitor.

6.2. Results

6.2.1. DUSP6 is regulated by ALK independently of ERK

As demonstrated in **Figure 6.3**, many DUSPs are regulated transcriptionally by ALK signalling (Van den Eynden et al., 2018, Borenäs et al., 2021). Collectively, these data were performed in three cell lines with hyperactive ALK signalling: CLB-BAR, CLB-GE and NB-1. Initially, I wanted to confirm that the same was true in KELLY and LAN-5 cells which contain the F1174L and R1275G mutations in ALK, respectively. To this end, the gene expression of various DUSPs known to regulate ERK signalling were assessed after lorlatinib treatment in both these cell lines (**Fig. 6.4A**). In accord with previous studies, lorlatinib significantly downregulated *DUSP4*, *DUSP5* and *DUSP6* expression but suppression of the *DUSP6* gene was the greatest (>80% suppression of *DUSP6* compared to ~65 and ~50% suppression of *DUSP4* and *DUSP5* respectively). Interestingly, *DUSP2* expression is increased >2-fold in LAN-5 cells. As LAN-5 cells display neuronal characteristics, I hypothesised that *DUSP2* expression may be important to ALK function in ALK-mutated neuronal cells. Unfortunately, when repeating this assay in SH-SY5Y cells, another ALK-mutated NB cell

line with a neuronal phenotype, *DUSP2* expression was unaffected by ALK inhibition, making this hypothesis likely untenable (**Fig. 6.4B**). To further characterise the transcriptional control of ALK on *DUSP6* gene expression, a range of NB cell lines were treated with lorlatinib for 6 and 24 hours. There was a striking suppression of *DUSP6* gene expression specifically in NB cells with mutations in the ALK receptor, confirming the tight control of DUSP6 expression by ALK (**Fig. 6.4C**). This also suggests that under basal conditions the ALK pathway is fairly inactive in NB cells with WT ALK.

The RAS/ERK signalling cascade is a well characterised mediator of ALK signalling in NB cells (Van den Eynden et al., 2018, Lopez-Delisle et al., 2018). Previous data in **Chapter 3** and **Chapter 5** suggests that DUSP6 does not dephosphorylate ERK, however it is still possible that ERK regulates *DUSP6* expression. An immunoblot was performed to assess basal DUSP6 expression and pERK levels across different cell lines (**Fig. 6.4D**). Interestingly, there is a strong correlation of pERK levels and DUSP6 expression between the different cell lines indicating DUSP6 may be transcriptionally regulated by ERK. Following this, cells were treated with a MEK inhibitor to confirm that ALK suppressed DUSP6 expression via the ERK pathway (**Fig. 6.4E**). MEK inhibition significantly downregulated DUSP6 expression, however not to the same extent as ALK inhibition. Considering the MEK inhibitor was fully active here (demonstrated by the loss of ERK signalling in **Fig. 6.6**), this suggests there may be alternative pathways used by ALK to regulate *DUSP6*. As this was only at 6 hours, it is possible that MEK inhibition would induce similar suppression of the *DUSP6* gene at later time points. Overall, these data suggests that although ERK is not a DUSP6 substrate, DUSP6 is tightly regulated in a transcriptional manner by the ALK-ERK signalling pathway.

We also investigated whether DUSP6 could be upregulated if ALK were stimulated with an ALK agonist. Previous reports using ALK ligands demonstrate ALK stimulation in cells with a WT ALK receptor (Guan et al., 2015, Borenäs et al., 2021). If DUSP6 was regulated by ALK-ERK signalling, we hypothesised MEK inhibition could antagonise this. As the IMR-32 and SK-N-AS cells contain WT ALK, these cells were treated with

ALKAL1 and a MEK inhibitor for 24 hours and an immunoblot was performed for DUSP6 expression and pERK levels (**Fig. 6.5A**). Unfortunately, ALK did not appear stimulated by ALKAL1 in either cell line. Considering previous reports only show ALK stimulation after 1hr in IMR-32 cells it is possible the signal reduces over time (Guan et al., 2015). There appears a minor upregulation in DUSP6 expression in IMR-32 cells after treatment with ALKAL1 suggesting DUSP6 could be upregulated by ALK in this cell lines. However, this experiment was only performed once and there was not an increase in pERK signalling. To at least show that lorlatinib is targeting the ALK receptor, NB1 cells were treated with the ALK ligand, lorlatinib or both. NB1 cells were chosen as these cells were stimulated by ALKAL1 to the greatest extent in a previous studies (Borenäs et al., 2021). Treatment with ALKAL1 induced a significant upregulation of pALK and pERK (**Fig. 6.5B**). Both of which were inhibited by concurrent treatment with lorlatinib demonstrating lorlatinib is functioning on the ALK receptor. Interestingly, ALKAL1 treatment also suppressed DUSP6 expression, similar to that observed in Borenäs et al. (2021) (**Fig. 6.3B**), suggesting a complex regulation of DUSP6 in NB1 cells. Unfortunately, NB1 cells subsequently tested positive for mycoplasma and so they were not used for further experiments.

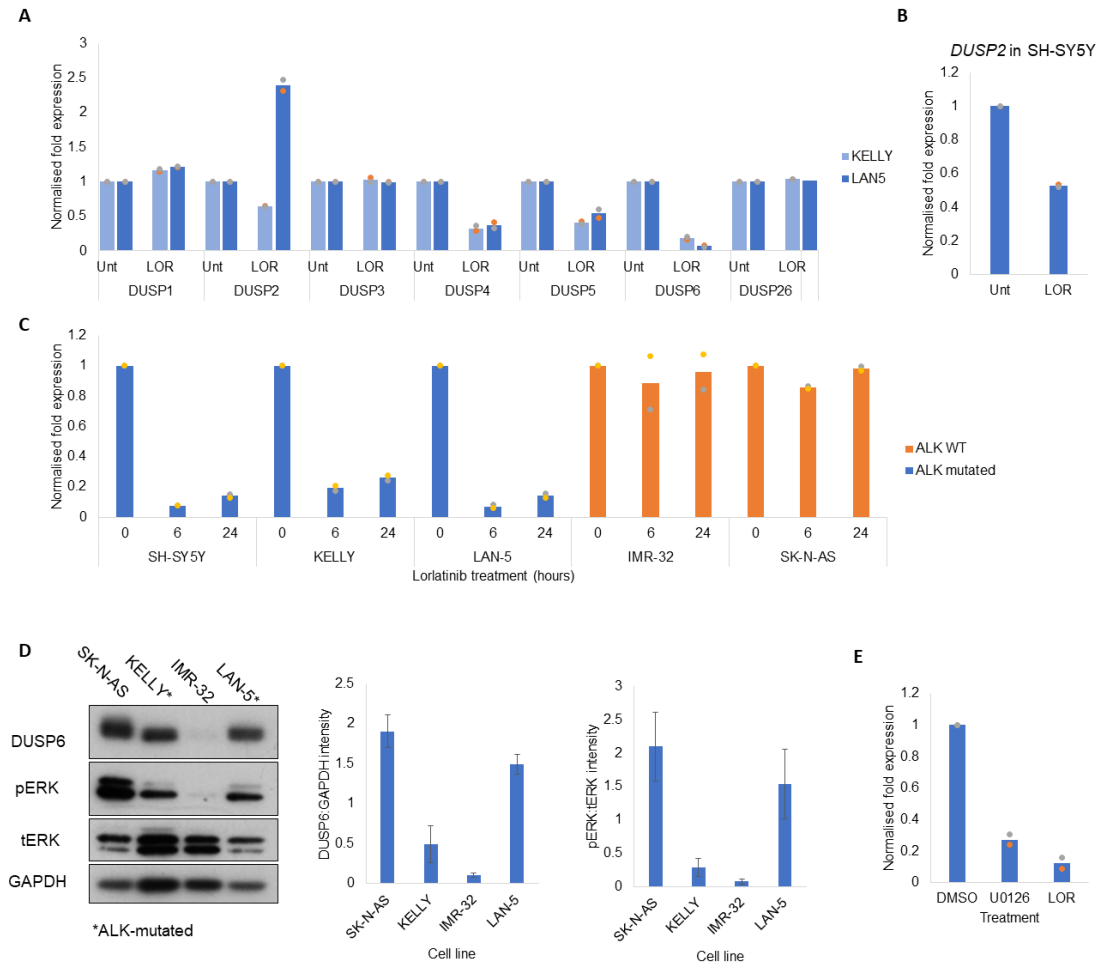

Figure 6.4 – ALK suppresses DUSP6 gene expression in ALK-mutated NB cells. QPCR of DUSP genes that regulate ERK signalling in (A) KELLY and LAN-5 and (B) SH-SY5Y cells after treatment with 30 nM lorlatinib (LOR) for 6 hours (n = 2). (C) qPCR of DUSP6 gene expression across NB cell lines after treatment with 30 nM LOR for 6 and 24 hours (n = 2). (D) Immunoblot of the basal DUSP6 and ERK phosphorylation level in NB cell lines (n = 3). For quantification, DUSP6 and pERK were normalised to GAPDH and tERK respectively, followed by a second normalisation to the immunoblot average (n = 3). (E) qPCR showing the gene expression of DUSP6 after treatment with 10 µM U0126 and 30 nM LOR for 6 hours (n = 2).

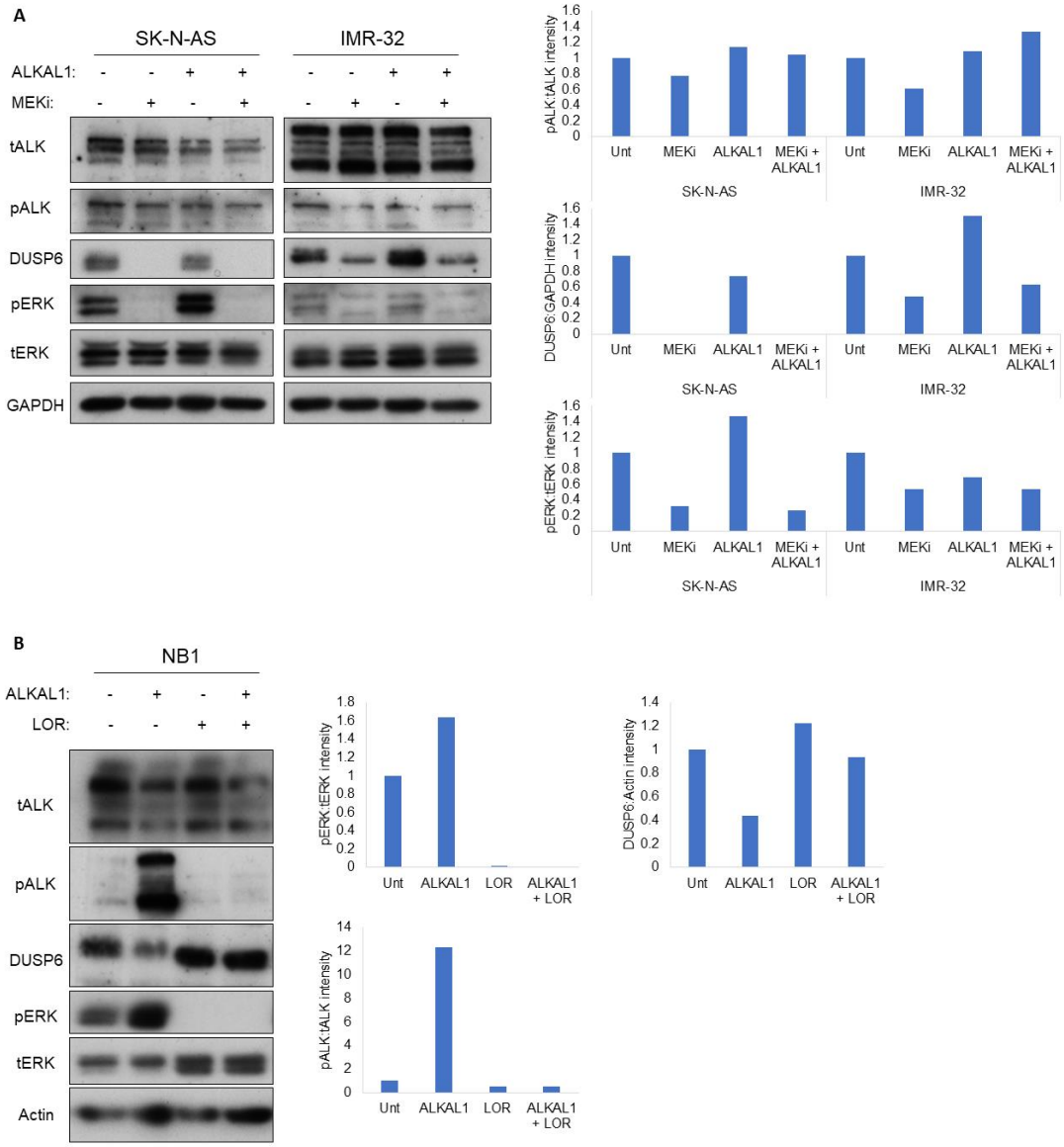

Figure 6.5 – Stimulating the ALK receptor in NB cell lines. (A) Immunoblot for DUSP6, ERK and ALK phosphorylation levels in IMR-32 and SK-N-AS cells after stimulation of 1 µg/ml ALKAL1 and 10 µM MEKi (U0126) for 24 hours (n = 1). (B) Immunoblot for DUSP6 expression and ERK and ALK phosphorylation levels in NB1 cells after stimulation of 1 µg/ml ALKAL1 and 10 µM LOR for 1 hour (n = 1). For quantification, DUSP6 was normalised to the loading control and pERK and pALK were normalised to their unphosphorylated form, followed by a second normalisation to untreated.

The data above indicated ALK may regulate DUSP6 in an ERK-dependent and -independent manner. To investigate this possibility, the effect of MEK inhibition and ALK inhibition on DUSP6 protein expression was assessed in a range of NB cell lines (**Fig. 6.6**). It is worth noting that depending on the cell line, the effect of ALK and MEK inhibition on ERK and DUSP6 varied greatly, highlighting the heterogenous nature of NB cells. A model of each scenario is presented in **Figure 6.7**. In IMR-32 and SK-N-AS cells, MEK inhibition significantly downregulated pERK and DUSP6 expression demonstrating that in these cells ERK tightly controls DUSP6 expression. In contrast, ALK inhibition had no effect on ERK phosphorylation levels suggesting that, consistent with the previous qPCR experiments, under basal conditions the ALK receptor is not active unless mutated. The only exception is that treatment with lorlatinib for 6 hours caused a transient increase in DUSP6 protein expression in IMR-32 cells. As ERK signalling is unaffected, this suggests that the ALK receptor may downregulate DUSP6 in this context.

In KELLY and LAN-5 cells, ALK inhibition caused significantly greater inhibition of DUSP6 expression than MEK inhibition. This is especially true after 24 hours where MEK and ALK inhibition decreased DUSP6 expression by ~40% and ~90% respectively. Considering pERK is suppressed to a similar extent by MEK and ALK inhibition, this strongly suggests that ALK can regulate DUSP6 expression independently of ERK (as depicted in **Figure 6.7**). Interestingly, in SH-SY5Y cells, MEK inhibition caused significantly less inhibition of pERK than lorlatinib. In this instance, suppression of DUSP6 by lorlatinib may be due to inhibition of various pathways, including MEK, that converge on ERK signalling. Indeed, various other kinases, such as the PI3K or PKC, are known to activate ERK independently of MEK (Grammer and Blenis, 1997, Aksamitiene et al., 2010). Nonetheless, these data suggest that in KELLY and LAN-5 cells, inhibition of ALK causes a significant downregulation of DUSP6 expression in an ERK-dependent and -independent manner.

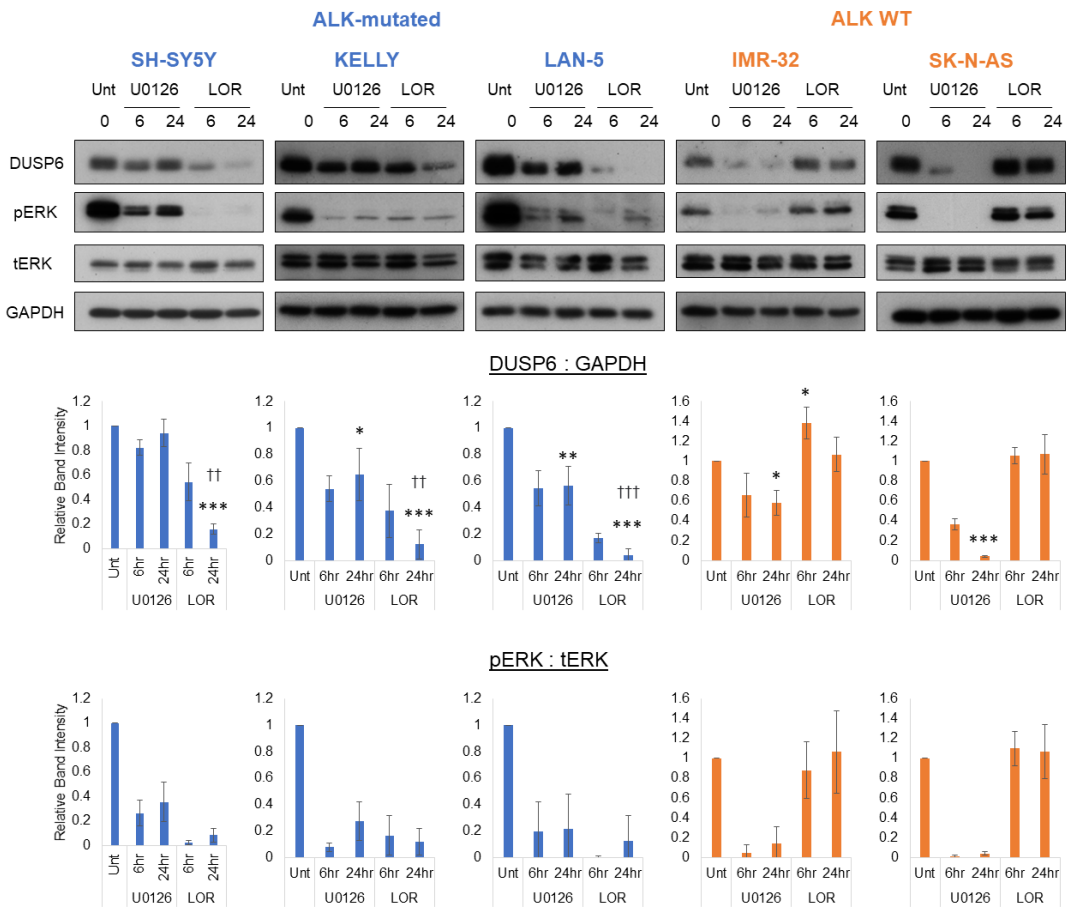

Figure 6.6 – ALK regulates DUSP6 independently of ERK in KELLY and LAN-5 cells. (A) Immunoblot for DUSP6 expression and ERK phosphorylation levels after treatment with 30 nM lorlatinib or 10 µM U0126 for 6 and 24 hours ($n \geq 3$). For quantification, DUSP6 and pERK were normalised to GAPDH and tERK followed by a second normalisation to DMSO. One-way ANOVA compared to DMSO; *$p \leq 0.05$; **$p \leq 0.005$; ***$p \leq 0.0005$. One-way ANOVA compared to 24hr U0126; ††$p \leq 0.005$; †††$p \leq 0.0005$.

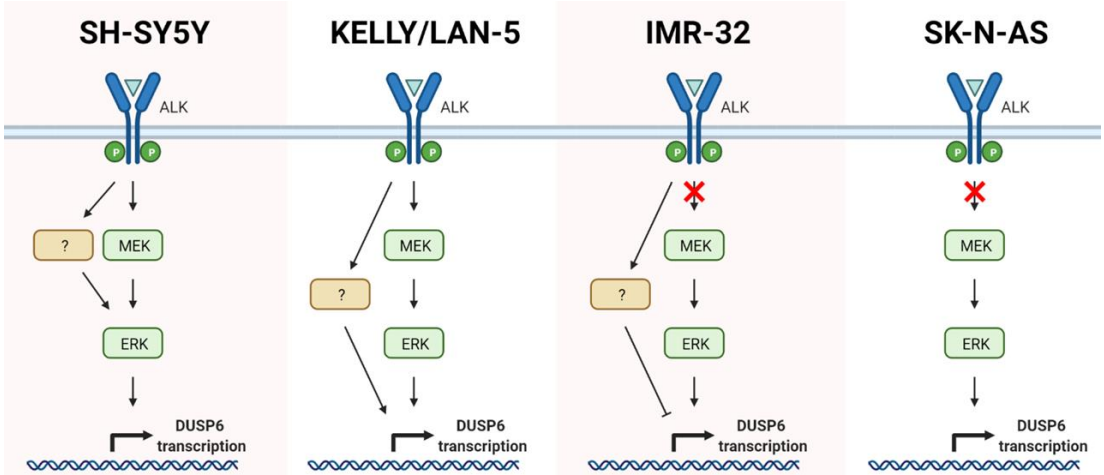

Figure 6.7 – Working model of DUSP6 transcriptional regulation by ALK in NB cell lines. In SH-SY5Y cells, DUSP6 is transcriptionally regulated by ALK-ERK signalling in a MEK-dependent and -independent manner. In KELLY and LAN-5 cells, DUSP6 is transcriptionally regulated by ALK in an ERK-dependent and -independent manner. In IMR-32 cells, DUSP6 is downregulated by ALK but not via MEK/ERK. In SK-N-AS cells, DUSP6 is not regulated by ALK. The yellow box represents an alternative unidentified pathway.

Although it has been known for many years that DUSP6 expression is tightly controlled by ERK transcriptionally, it has become apparent that DUSP6 is also regulated at the translational and post-translational level (Ahmad et al., 2018, Chen et al., 2019). Hence, ALK could also regulate DUSP6 via these alternative mechanisms. I sought to investigate how ALK regulates DUSP6 by using the protein synthesis inhibitor cycloheximide (CHX) and the proteasome inhibitor MG132. In these experiments, cells were treated with CHX or MG132 either in the presence or absence of lorlatinib. The length of lorlatinib treatment was kept constant for each experiment (4, 10 and 18 hours in **Figure 6.8A**, **Figure 6.8B** and **Figure 6.8C**, respectively) so the effect of protein synthesis or proteosome inhibition was monitored over time.

After treatment with CHX, the half-life of DUSP6 varies significantly between the NB cell lines (**Fig. 6.8A**). For example, in SK-N-AS cells the turnover of DUSP6 protein is ~1 - 2 hours whereas in KELLY cells treatment with CHX for 4 hours was not sufficient to significantly deplete DUSP6 protein. Consequently, experiments in KELLY cells were repeated over a longer time frame (**Fig. 6.8B**). As expected, treatment with lorlatinib abrogated ERK signalling after 1 hour in ALK-mutated cells and had no effect on ERK

phosphorylation levels or DUSP6 expression in ALK-WT cells (**Fig. 6.8A**). Interestingly, the loss of DUSP6 in SK-N-AS cells correlates with an increase in pERK (Similar results with MG132, comparison of pERK and DUSP6 quantification in **Figure A4**). So far, this is the only evidence to suggest that DUSP6 can downregulate ERK signalling in NB cells. Experiments using CHX were an attempt to gage whether ALK inhibition affects DUSP6 turnover. Interestingly, the rate of protein turnover decreases in LAN-5 cells after treatment with lorlatinib (**Fig. 6.8A**). However, this is difficult to interpret as ALK inhibition decreases DUSP6 expression itself. It is possible that ALK inhibition prevents DUSP6 degradation and therefore prevents DUSP6 turnover. But lorlatinib-mediated reduction of DUSP6 expression could itself affect the rate of degradation.

Following this, cells were treated with MG132 for 4 and 18 hours to assess whether the proteasomal degradation of DUSP6 was affected by ALK inhibition (**Fig. 6.8C**). Similar to treatment with CHX, the rate of DUSP6 accumulation varied between different cell lines. In SK-N-AS cells, DUSP6 expression appears to increase after 4 hours and then, counterintuitively, decrease over 18 hours, suggesting an alternative route of degradation other than the proteosome. In AS and IMR-32 cells, ALK inhibition did not alter DUSP6 expression in response to MG132. Furthermore, in KELLY cells, the rate of DUSP6 accumulation appears similar even though lorlatinib significantly suppressed DUSP6 expression. Conversely, in LAN-5 cells MG132 did not cause an accumulation of DUSP6, suggesting DUSP6 is not degraded by the proteosome under basal conditions (**Fig. 6.8C**, lower exposure demonstrates no change in DUSP6 expression after 18 hours). However, treatment with MG312 whilst ALK is inhibited, although DUSP6 RNA expression decreases, caused DUSP6 to accumulate very slightly over 18 hours, suggesting the protein is partially targeted for degradation. We are also cautious that the longer treatment of MG132 may be having off-target effects in these cells as 18 hours of MG132 abrogated lorlatinib-mediated inhibition of pERK. Overall, these data suggest ALK may inhibit DUSP6 degradation in LAN-5 cells, however, due to the potential off-target effects of MG132, further studies are required to confirm this.

Interestingly, immunoblotting for DUSP6 also produces a different size band depending on the cell line and the condition. This is most visible in SK-N-AS cells where DUSP6 forms a smear as opposed to a clean band (**Fig. 6.8A** and **Fig 6.8C**). Accumulation of DUSP6 protein after treatment with MG132 appears to increase the expression of a higher molecular weight form of DUSP6 in IMR-32, LAN-5 and potentially KELLY cells (**Fig. 6.8C**) As previously mentioned, DUSP6 has an alternative start codon at position Met14 and that this may be preferentially used to Met1 (Dowd et al., 1998). However, whether there is a functional or regulatory difference between each isoform is unclear. Alternatively, the increased molecular weight could represent a post-translational modification of DUSP6. A wide range of DUSP6 post-translational modifications have been identified including phosphorylation, ubiquitination and sumoylation (Chen et al., 2019, Ma et al., 2020, Marchetti et al., 2005).

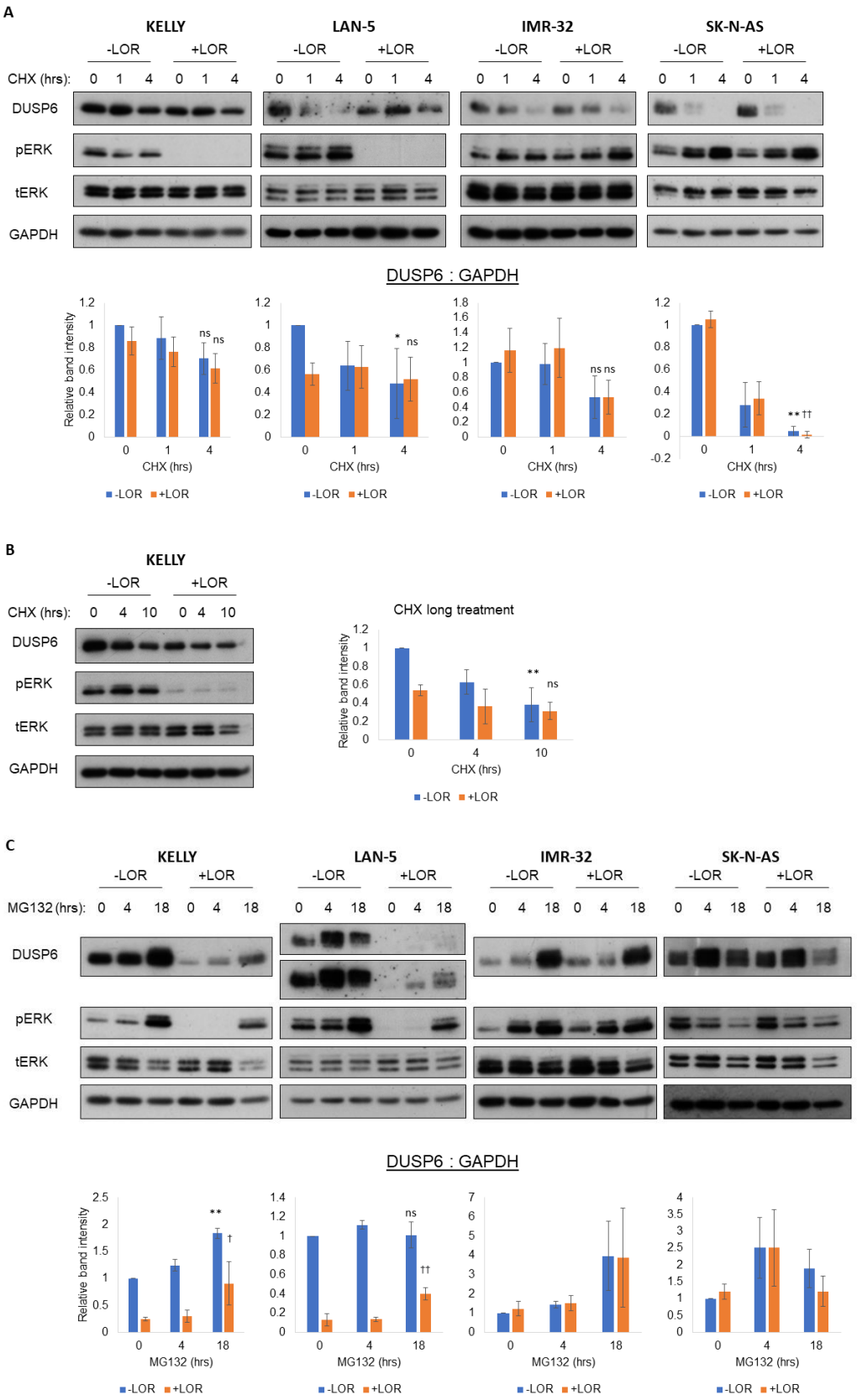

Figure 6.8 – ALK can regulate DUSP6 in a transcriptional and post-translational manner. NB cell lines we treated with 40 µg/ml CHX for (A) 1 and 4 hours or (B) in the presence or absence of 30 nM lorlatinib (LOR) followed by immunoblotting for DUSP6 and

pERK (n ≥ 2). Lorlatininb treatment was kept constant at (A) 4 hours and (B) 10 hours. (C) NB cell lines we treated with 10 mM MG132 for 4 and 18 hours in the presence or absence of 30 nM lorlatinib (LOR) followed by immunoblotting for DUSP6 and pERK (n ≥ 3). Lorlatininb treatment was kept constant at 18 hours. For quantification, DUSP6 and pERK were normalised to GAPDH and tERK followed by a second normalisation to DMSO. One-way ANOVA compared to DMSO; *$p \leq 0.05$; **$p \leq 0.005$. One-way ANOVA compared to 30 nM LOR treatment; †$p \leq 0.05$; ††$p \leq 0.005$.

6.2.2. Complete loss of DUSP6 sensitises KELLY cells to ALK inhibition

Overall, the previous studies demonstrate that in ALK-mutated NB cells, ALK signalling is essential to maintain high levels of DUSP6 expression in a mechanism that is partly ERK-independent. I hypothesised that for ALK to drive tumorigenicity high DUSP6 expression is therefore required. As mentioned in **Chapter 6.1**, crizotinib and lorlatinib are 1st and 3rd generation ALK inhibitors currently under investigation as treatment options for ALK-positive tumours (NCT03052608, NCT03107988). Using the DUSP6-null KELLY cells generated in **Chapter 3**, I sought to investigate whether loss of DUSP6 could improve the potency of these ALK-targeting drugs. It is worth mentioning, KELLY cells have the F1174L mutation which can confer crizotinib resistance (Choi et al., 2010, Bresler et al., 2014). Nonetheless, Bresler et al. (2011) demonstrate crizotinib can still effectively inhibit ALK signalling in NB cells, but a greater inhibitor concentration is required. Dose-response assays using crizotinib and lorlatinib were performed in IMR-32 and KELLY WT and DUSP6-null cells. As expected, lorlatinib did not reduce cell viability at any concentration in IMR-32 cells demonstrating no off-target toxicities (**Fig 6.9A**). Crizotinib decreased cell viability in IMR-32 cells at concentrations greater than 0.25 µM suggesting this inhibitor is toxic at concentrations higher than this. Promisingly, loss of DUSP6 appeared to sensitise KELLY cells to ALK inhibition to varying extents (**Fig 6.9B**). KELD6-1 and KELD6-2 demonstrated the greatest sensitivity, with a significant drop in EC50 values. Surprisingly, DMSO alone appeared to have a growth effect on KELD6-1 and KELD6-2 cells and varied between

cell population. With this in mind, assays on KELD6-3 were performed in a lower concentration of DMSO to remove this effect. Unfortunately, the sensitisation to ALK inhibition was not present with KELD6-3 which could be due to the fact that assays with KELD6-3 were performed at a different time to KELD6-1 and KELD6-2 or may reflect heterogeneity of the subclones.

Considering the variable sensitivity between each of the DUSP6-null subclones to the ALK inhibitors, I sought to determine whether acute loss of DUSP6 would cause a more consistent degree of sensitisation. To achieve this, dose-response assays were performed in the 2E2 and 2E2g4 populations generated in **Chapter 3** after treatment with dox for 1 week. **Figure 3.12A** demonstrates dox treatment causes significant depletion of DUSP6 protein after 7 days. Surprisingly, loss of DUSP6 in the mixed population did not induce the same sensitisation to lorlatinib or crizotinib as that seen in the single cell clones (**Fig. 6.10**). There is a marginal downwards shift in the 2E2g4 curves treated with ALK inhibitor, but this is not statistically significant. This could be due to residual DUSP6 protein present within the cell population, but considering the proportion of cells with complete loss of DUSP6 is >90%, this seems unlikely (**Fig. 3.12A**). Alternatively, sustained loss of DUSP6 in the DUSP6-null subclones may have caused compensatory mechanisms by other DUSPs which increase the sensitivity to ALK inhibition. If this were the case, the short-term loss of DUSP6 in the mixed population may not cause these alternations resulting in no difference in response to ALK inhibition. Further experiments are required to demonstrate the effect of sustained DUSP6-KO on other DUSPs.

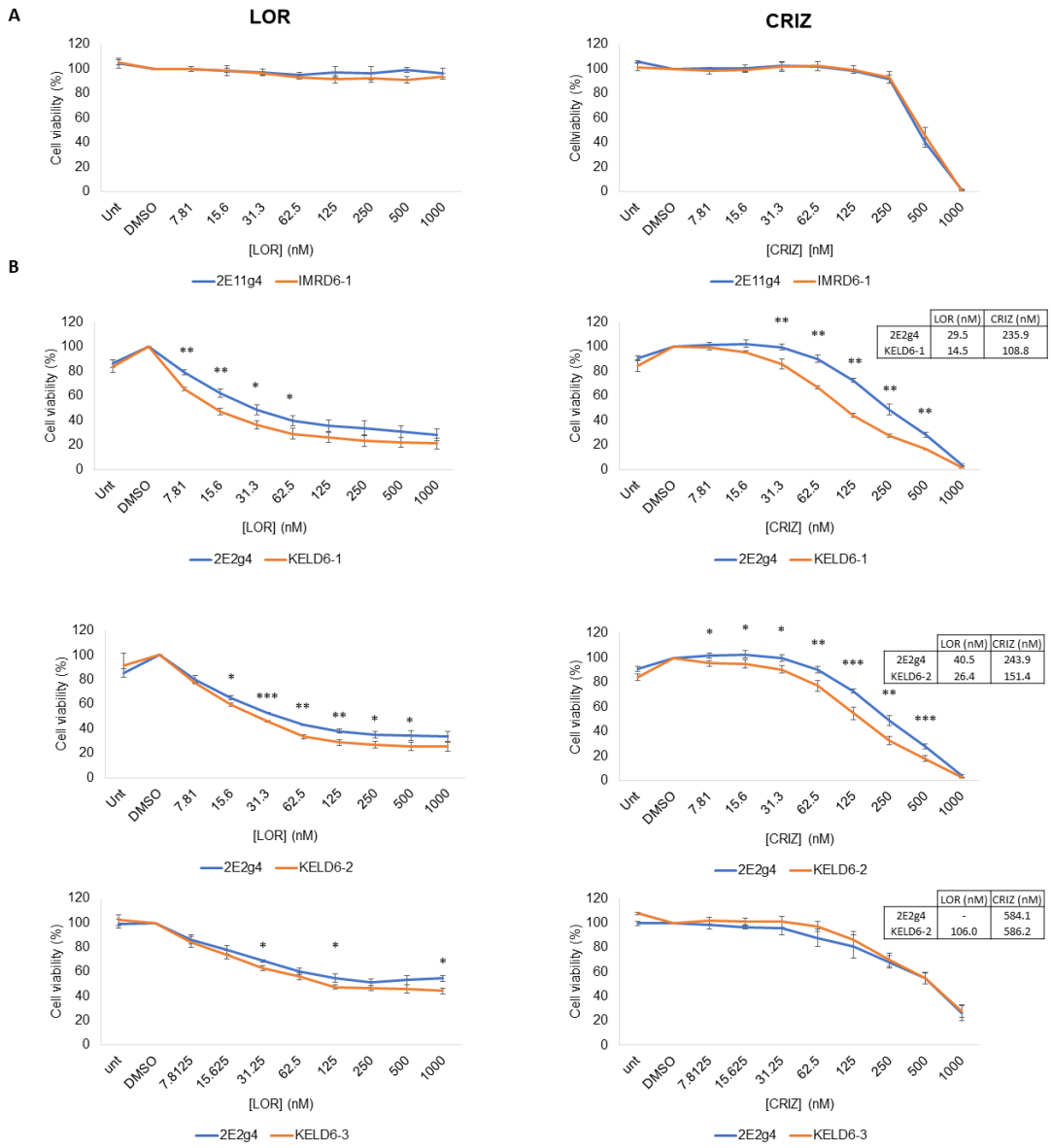

Figure 6.9 – Loss of DUSP6 sensitised KELLY cells to ALK inhibition. (A) IMR-32 and (B) KELLY WT and DUSP6-null subclones were treated with increasing doses of lorlatinib (LOR) and crizotinib (CRIZ) for 7 days and cell viability was measure using the resazurin assay (n ≥ 3). EC50 values presented in tables next to dose-response curves. Independent samples t-test comparing equivalent drug concentrations; *p ≤ 0.05; **p ≤ 0.005.

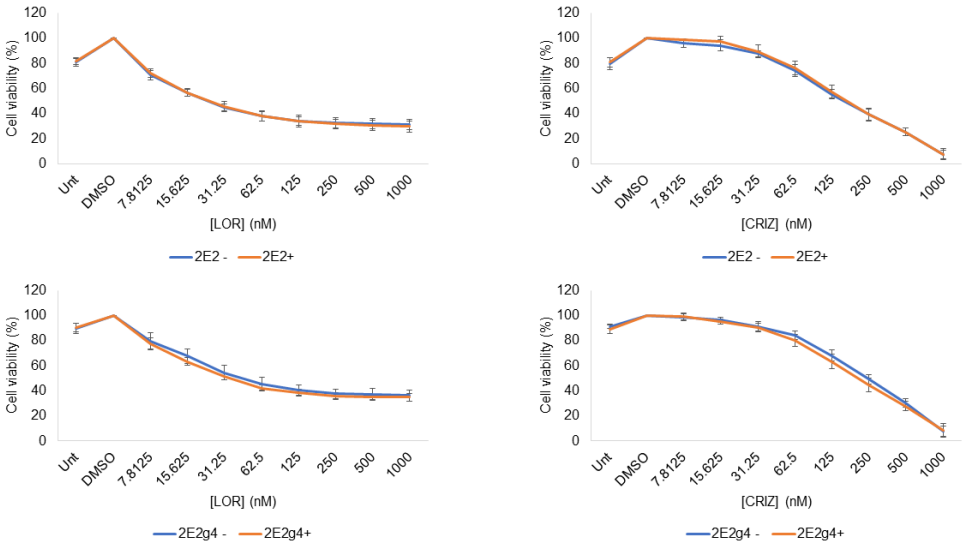

Figure 6.10 – Acute depletion of DUSP6 does not affect sensitivity to ALK inhibition. KELLY cells with and without the DUSP6 gRNA, termed 2E2 and 2E2g4 respectively, were incubated with 1 µg/ml Dox for 6 days and then treated with increasing doses of lorlatinib (LOR) and crizotinib (CRIZ) for 7 days. At the end point, cell viability was measure using the resazurin assay (n = 5). Independent samples t-test comparing equivalent drug concentrations did not identify any statistically significant differences.

These collective though somewhat conflicting results suggest that complete loss of DUSP6 may under some circumstances be involved in ALK inhibitor-mediated cell death. ALK upregulates a wide range of signalling pathways including the MAPK and AKT pathways (**Fig. 6.2**). To identify the pathway DUSP6 might be regulating downstream of ALK, we investigated whether a similar result would be observed if the MAPK or AKT pathways were inhibited. Dose-response assays were performed using an inhibitor for each pathway in KELLY (**Fig. 6.11A**) and IMR-32 cells (**Fig. 6.11B**). In KELLY cells, loss of DUSP6 did not increase the potency of any of these inhibitors suggesting ALK-mediated regulation of DUSP6 is unlikely to be via by any of these pathways (**Fig. 6.11A**). Furthermore, these results demonstrate the drug sensitisation is specific to ALK inhibition as opposed to an intrinsic difference to drug treatments between each cell population. As IMR-32 cell growth is ALK-independent (**Fig. 6.9A**), one would expect them to be less dependent on ERK signalling. Surprisingly, there was little difference in ERK inhibition on cell survival between KELLY and IMR-32 cells. Loss of DUSP6

appeared to marginally increase the potency of the MEK inhibition in IMR-32 cells, however this experiment was only performed once and so should be repeated before conclusions can be made.

An alternative approach to identifying a DUSP6 substrate is to compare phosphorylation changes of ALK signalling pathways in cells with and without DUSP6. I have previously demonstrated using siRNAs that DUSP6 does not appear to regulate the MAPK or AKT signalling pathways (**Fig. 3.15**). Nonetheless, as ERK is a well-documented substrate of DUSP6, it is possible DUSP6 may target ERK in the context of ALK inhibition. ALK was acutely inhibited by lorlatinib and an immunoblot was performed to probe the on the MAPK and AKT signalling pathways (**Fig. 6.11C**). A shorter lorlatinib treatment (30 minutes and 3 hours) was used so DUSP6 expression was not significantly depleted in control cells. Lorlatinib induced a significant downregulation of ERK signalling but did not alter the AKT, p38 or JNK pathways. This is surprising as previous studies demonstrate ALK tumorigenicity is partly driven by AKT signalling (Borenäs et al., 2021, Van den Eynden et al., 2018). As KELLY cells were not assayed in their system, it is likely that ALK signalling is wired differently between different cell lines. Consistent with previous data, loss of DUSP6 did not affect intracellular signalling via any of these pathways in response to ALK inhibition (**Fig. 6.11C**). Overall, although ALK maintains DUSP6 expression, it remains unclear whether DUSP6 targets part of the ALK pathway or an unrelated pathway.

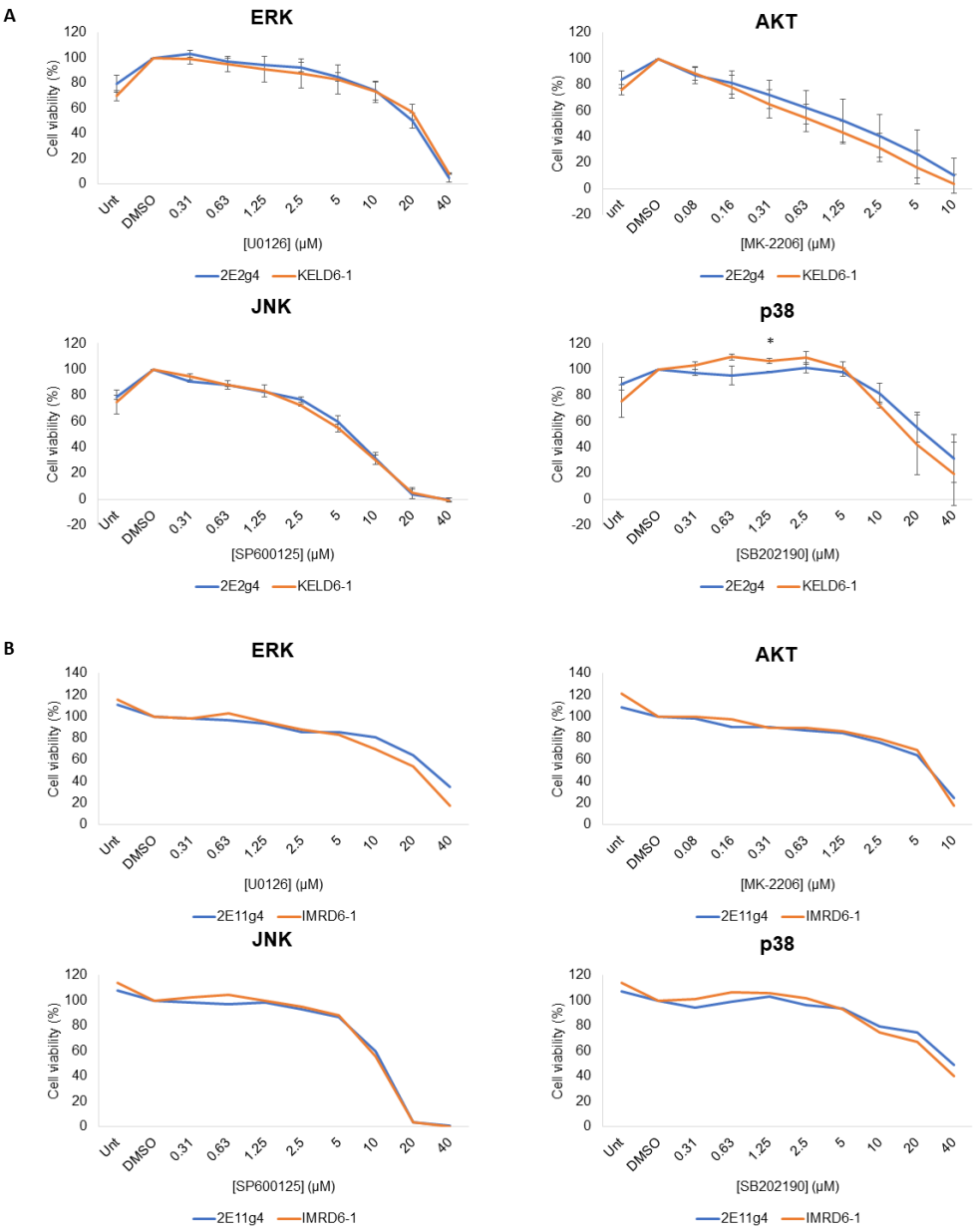
A
ERK
Cell viability (%)
[U0126] (μM)
2E2g4
KELD6-1
AKT
[MK-2206] (μM)
JNK
[SP600125] (μM)
p38
*
[SB202190] (μM)
B
2E11g4
IMRD6-1

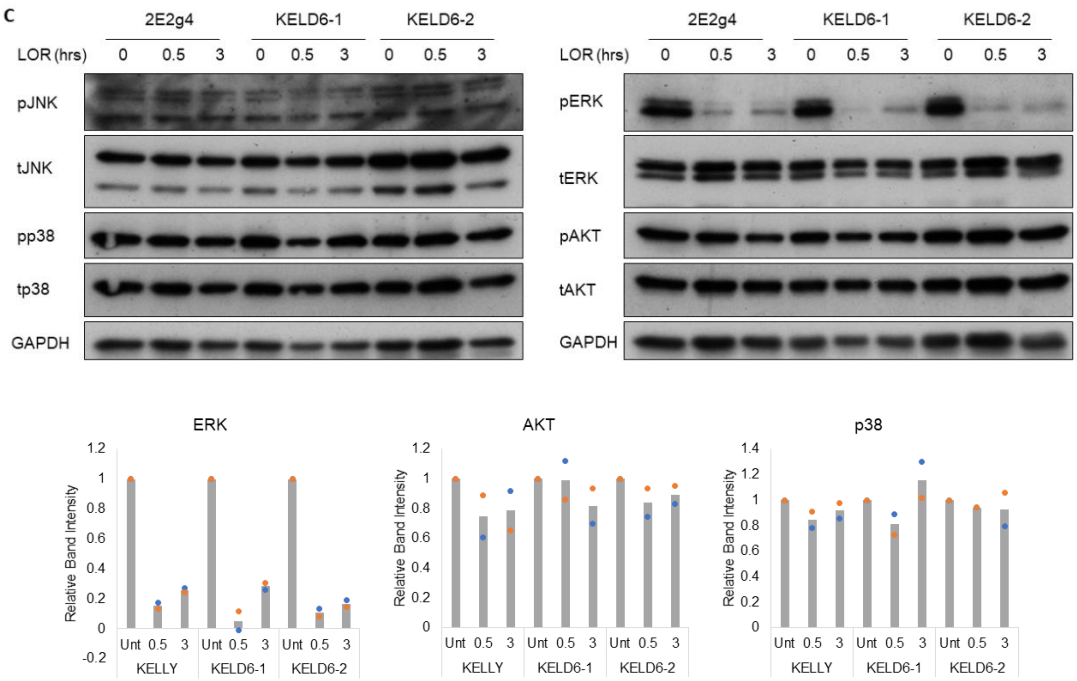

Figure 6.11 – ALK does not regulate DUSP6 via the MAPKs or AKT pathways. KELLY WT (2E2g4) and DUSP6-null subclone (KELD6-1) were treated with increasing doses of an ERK (U0126), AKT (MK-2206), JNK (SP600125) or p38 (SB202190) inhibitor for 7 days and cell viability was measure using the resazurin assay (n = 2). Independent samples t-test comparing equivalent drug concentrations; *p ≤ 0.05. (B) IMR-32 WT (2E11g4) and DUSP6-null subclone (IMRD6-1) were treated with increasing doses of an ERK, AKT, JNK or p38 inhibitor for 7 days and cell viability was measure using the resazurin assay (n = 1) (C) KELLY WT and DUSP6-null subclone were treated with 30nM lorlatinib for 0.5 or 3 hours followed by immunoblotting for the MAPKs. For quantification, each phosphoprotein was normalised to their respective total protein followed by a second normalisation to the untreated sample (n = 2). Data are expressed as a mean with individual experiments as overlaid dot plots.

These data demonstrate that loss of DUSP6 may decrease KELLY cell survival in response to ALK inhibition but does not influence ALK signalling via the AKT or MAPKs. It is possible that this effect on cell survival is not specific to DUSP6 as I previously demonstrated ALK also downregulates other DUSP genes such as *DUSP4* and *DUSP5* (**Fig. 6.4A**). Furthermore, ALK regulates DUSP4 at a transcriptional and post-translational level suggesting tight control of DUSP4 activity (Van den Eynden et al., 2018). Using the other DUSP-null subclones generated in **Chapter 5**, I sought to determine whether loss of any of DUSP3, DUSP4, DUSP10, DUSP12 or

DUSP26 could sensitise KELLY cells to lorlatinib treatment. It is evident from previous data that subclones generated using CRISPR-Cas9 are somewhat heterogeneous, demonstrated by their variable growth rates (**Fig. 5.6**). It is therefore unsurprising that they displayed a wide range of sensitivities to ALK inhibition (**Fig. 6.12**). None of the DUSPs displayed a pattern as consistent as the DUSP6-null subclones. KELD3-1 and KELD4-1 appeared more sensitive to lorlatinib than WT cells, however in the case of KELD3-1, DMSO alone also caused a growth effect which if normalised for, would remove the different sensitivity to lorlatinib. Interestingly, the KELD12-2 subclone was more resistant to lorlatinib demonstrating a potentially suppressive role of DUSP12 in NB cell growth. However, it is unfortunately difficult to conclude whether any of DUSP3, DUSP4 or DUSP12 are involved in ALK function as there was not a consistent pattern between subclones.

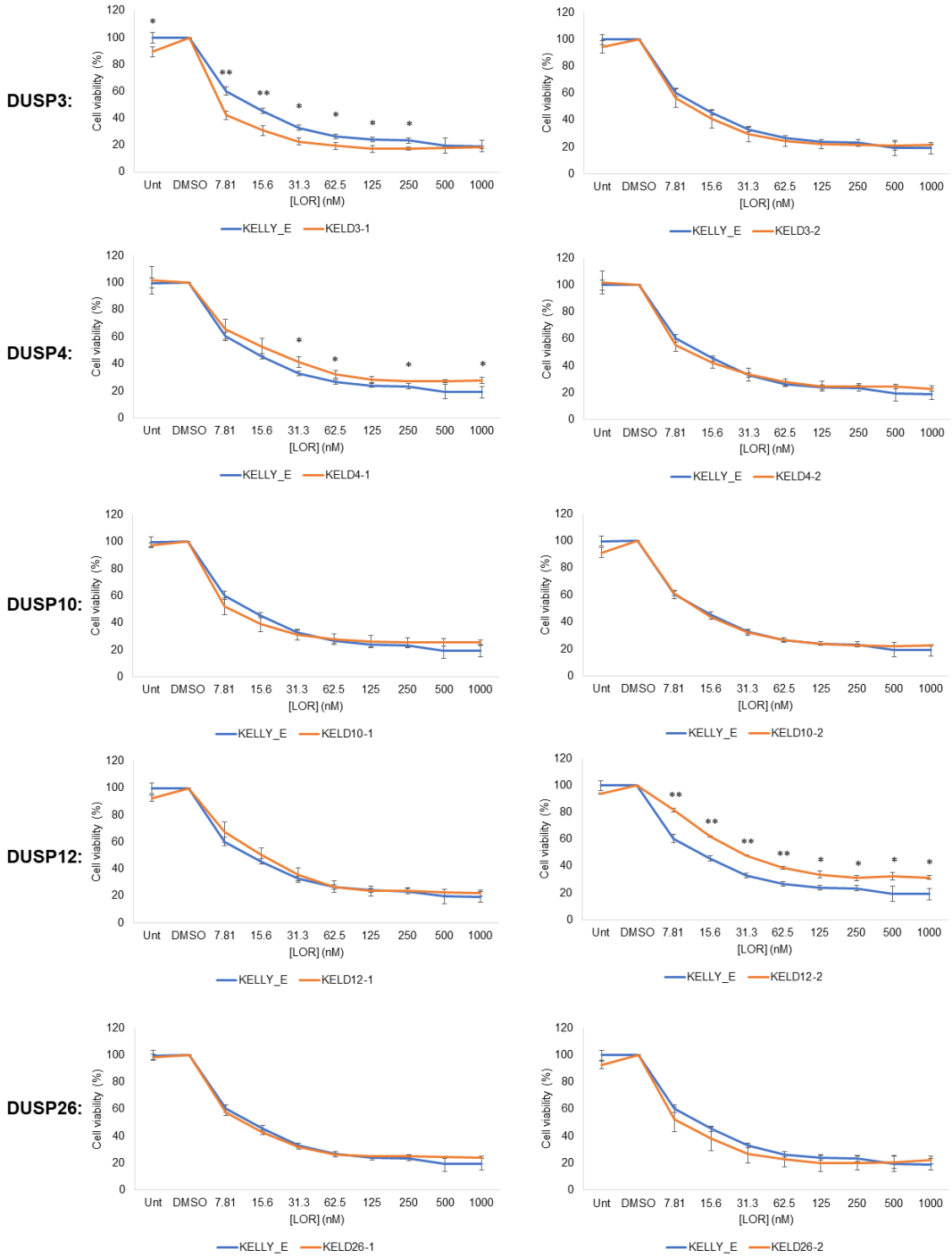

Figure 6.12 – Loss of other DUSP genes does not sensitise KELLY cells to ALK inhibition. KELLY WT (KELLY-E) and DUSP-null subclones were treated with increasing doses of lorlatinib (LOR) for 7 days and cell viability was measure using the resazurin assay (DUSP3, DUSP4, DUSP26, n = 3; DUSP10, DUSP12, n = 2). Independent samples t-test comparing equivalent drug concentrations; *$p \leq 0.05$.

Treating NB cells with lorlatinib and crizotinib *in vitro* can cause G1 cell cycle arrest or apoptotic cell death (Guan et al., 2016, Chen et al., 2016b). As loss

of DUSP6 sensitises the CRISPR knockout cells to ALK inhibition, we investigated whether this resulted in an increase in apoptotic cell death. Initially, KELLY cells were treated with 200 µM lorlatinib and monitored over 3 days to determine which timepoint apoptosis was initiated (**Fig. 6.13A**). Surprisingly, although there were far fewer cells in the plate, lorlatinib did not appear cytotoxic at 24 or 72 hours. Following this, cells were treated with 500 µM lorlatinib or crizotinib, a deliberately higher concentration than the EC50 values, to see whether cytotoxicity would be induced. Untreated cells were seeded at a lower density to compare cell morphology (**Fig. 6.13B**). Although ALK inhibition caused the cells to look unhealthy, few cells rounded up and detached suggesting lorlatinib is not cytotoxic. Unexpectedly, this suggested that in KELLY cells ALK inhibition is largely cytostatic as the cells are no longer able to proliferate.

It is possible that loss of DUSP6 increases the cytotoxic capacity of ALK inhibition resulting in a greater loss of cell viability. To investigate this, KELLY and DUSP6-null subclones were treated with lorlatinib and crizotinib for 3 days and cleavage of Cas3 (cCas3), a marker of apoptosis, was determined (**Fig. 6.13C-D**). LAN-5 cells were also included in the assay to determine whether the cytostatic effect of ALK inhibition is unique to KELLY cells. Loss of DUSP6 did not appear to alter cCas3, which remained low (<1.5%) in all samples (**Fig. 6.13D**). A one-way ANOVA was performed and there was no significant difference in cleavage of Cas3 within each cell group. Unfortunately, BCI was included as a positive control but did not induce a significant increase in cCas3 (**Fig 6.13D, orange bar**). Hence, I cannot conclude whether cCas3 is induced or whether the antibody is simply not working correctly. Nonetheless, together with the previous phase contrast images these data suggest that, as opposed to inducing cell death, the ALK inhibitor may instead reduce the rate of cell growth.

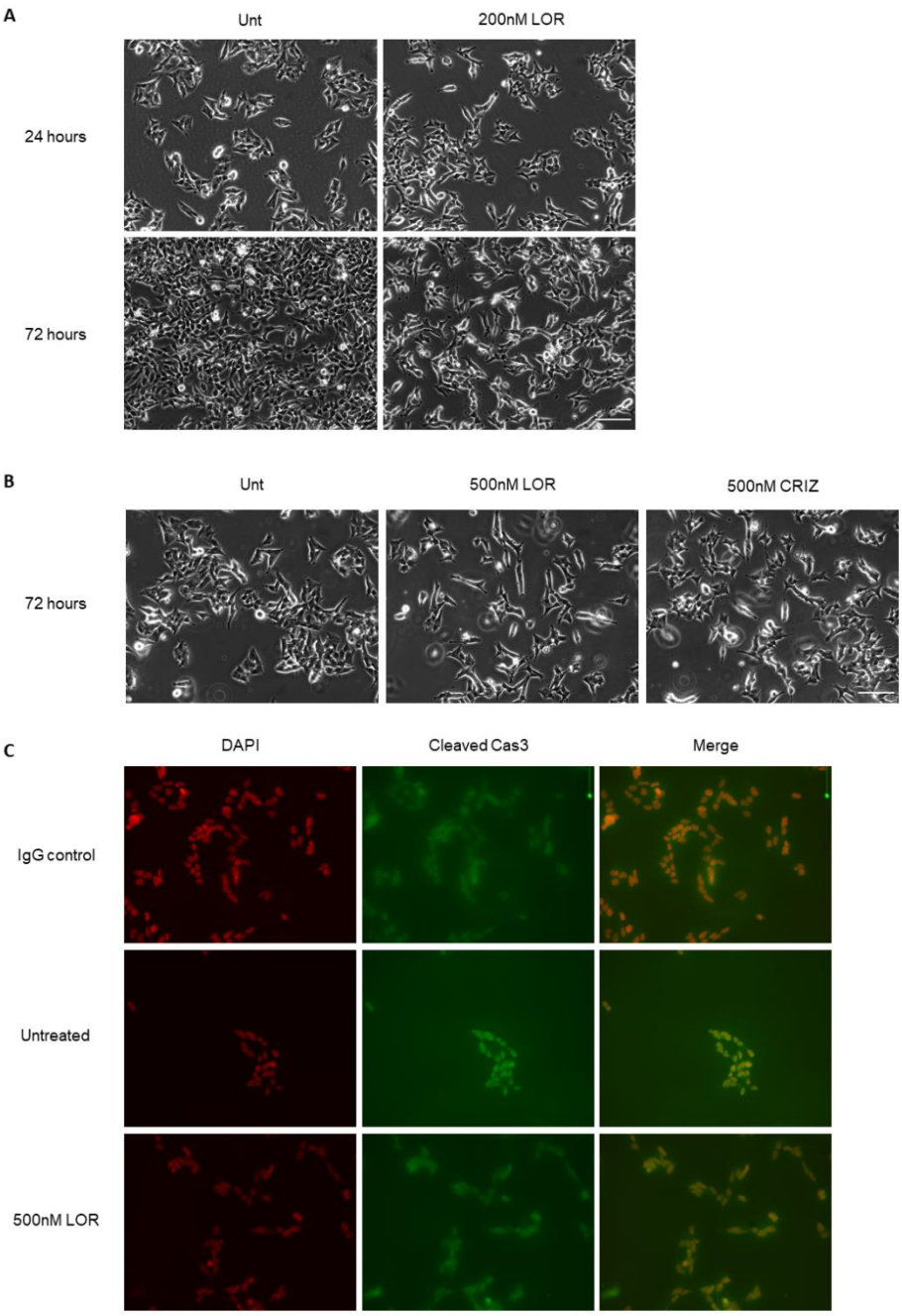
A
Unt
200nM LOR
24 hours
72 hours
B
Unt
500nM LOR
500nM CRIZ
72 hours
C
DAPI
Cleaved Cas3
Merge
IgG control
Untreated
500nM LOR

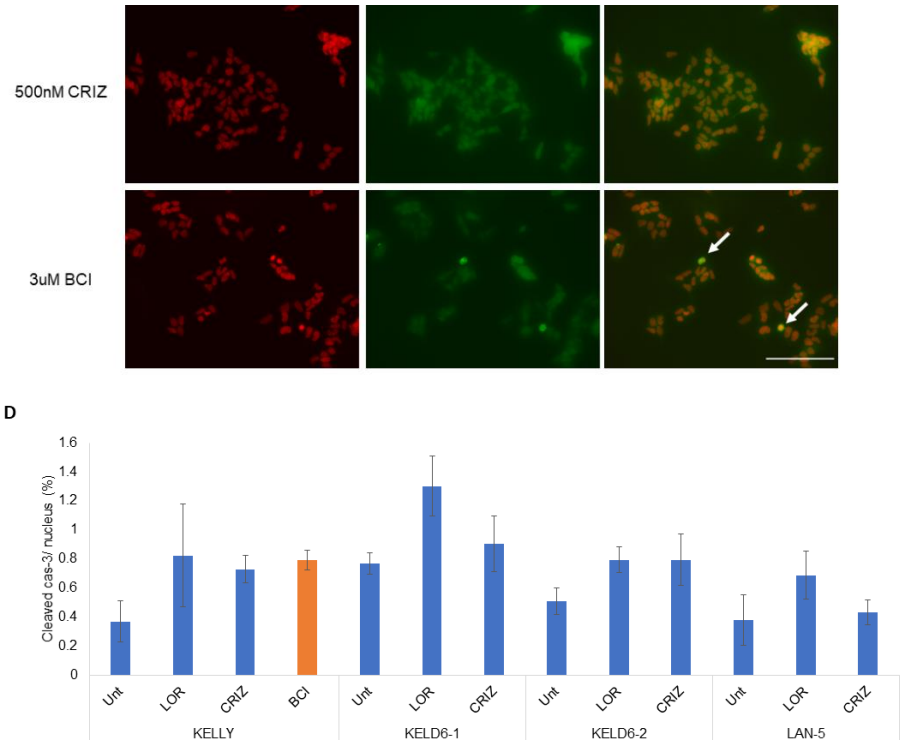

Figure 6.13 – ALK inhibition has a cytostatic effect on KELLY and LAN-5 cells. (A) KELLY cells were treated with 200 nM lorlatinib (LOR) for 24 and 72 hours followed by imaging (n = 1). (B) KELLY cells were treated with 500 nM lorlatinib (LOR) or crizotinib (CRIZ) for 72 hours followed by imaging (n = 1). KELLY, KELD6-1, KELD6-2 and LAN-1 cells were treated with 500 nM LOR or CRIZ or 3 µM BCI for 72 hours followed by immunofluorescence for cleaved Cas3 (n = 3). (C) Representative images for KELLY cells are presented where white arrows indicate cells with high cleavage of Cas3. (D) Quantified data are expressed as a mean ± SEM. Scale bar for all images = 100 µm. One-way ANOVA was performed but no significant differences were found within each cell population.

6.2.3. Re-introduction of DUSP6 does not rescue cell viability in response to ALK inhibition

It is possible that sensitisation to the ALK inhibitor by DUSP6-null subclones could simply be due to the heterogenous nature observed with the various DUSP-null subclones. With this in mind, the optimal way to confirm these results is to re-introduce DUSP6 into the DUSP6-null subclones and assess whether this returns cells to their original ALK inhibitor sensitivity. To this end, a vector was purchased which contained the WT DUSP6 open reading frame, including both start codons, with a C-terminal FLAG tag under a CMV

promoter (**Fig. 6.14**). KELD6-2 cells were transfected with the DUSP6-FLAG vector or an empty vector followed by selection with G418 over 4 weeks (**Fig. 6.14**). This generated a KELD6-2 cell population which contained either the DUSP6-FLAG or empty vector, termed KELD6-2-D6F and KELD6-2-E respectively.

To confirm that the exogenous DUSP6 was being expressed, an immunoblot was performed of the KELLY WT (2E2g4), KELD6-2-E and KELD6-2-D6F populations and probed for DUSP6. As expected, the cells containing the empty vector did not express DUSP6 whereas the KELD6-2-D6F population displayed a ~3-fold increase in DUSP6 expression (**Fig. 6.15A**). Unfortunately, when re-probing the membrane with the FLAG antibody, there was a poor signal with high background therefore a band for exogenous DUSP6 could not be identified (data not shown). Nonetheless the exogenous DUSP6 band is migrating slightly slower as a result of the C-terminal FLAG tag.

Interestingly, after treatment with lorlatinib, endogenous DUSP6 protein was abolished over 24 hours, but exogenous DUSP6 expression was unaffected (**Fig. 6.15A**). In agreement with CHX and MG132 experiments (**Fig. 6.8**), this strongly suggests that ALK regulates DUSP6 at a transcriptional level as it cannot regulate the exogenous DUSP6 promoter. There are two alternative possibilities as to why the exogenous DUSP6 is not degraded. Firstly, as there is an excess of DUSP6 protein, this may simply require a longer time frame to be targeted for proteasomal degradation. To investigate this, cells were treated for 48 hours with lorlatinib followed by an immunoblot for DUSP6 (**Fig. 6.15B**). Although endogenous DUSP6 protein was not depleted to the same extent as previously observed, it still displayed a downward trend. Conversely, exogenous DUSP6 protein remained unchanged. Secondly, the FLAG tag may abrogate part of the proteosome degradation process such as the addition of ubiquitin. To explore this possibility, WT cells and cells overexpressing DUSP6 were treated with CHX to compare the half life of DUSP6 (**Fig. 6.15C**). No significant difference was observed between the degradation of endogenous and exogenous DUSP6 suggesting proteasomal degradation of DUSP6 is

unaffected by the FLAG tag. It is worth mentioning that due to time constraints, these experiments were only performed once. Hence, robust conclusions cannot yet be made unless results are repeated.

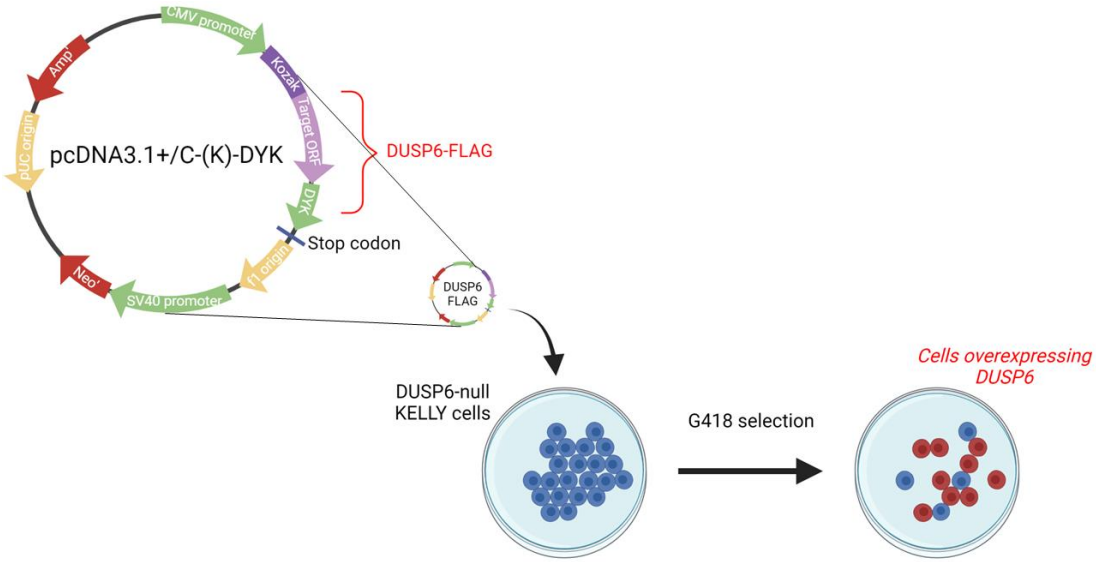

Figure 6.14 – Generation of KELLY cells expressing exogenous DUSP6 protein. The DUSP6-FLAG vector contains Ampicillin (Amp') and Neomycin (Neo') resistance markers used for selection and the DUSP6 open reading frame followed by a FLAG tag (DYK) under a CMV promoter. The KELD6-2 cell population was transfected with the DUSP6-FLAG vector or an Empty vector and selected for with G418 over 4 weeks. Antibiotic selection generated a mixed population of cells that overexpress DUSP6 protein.

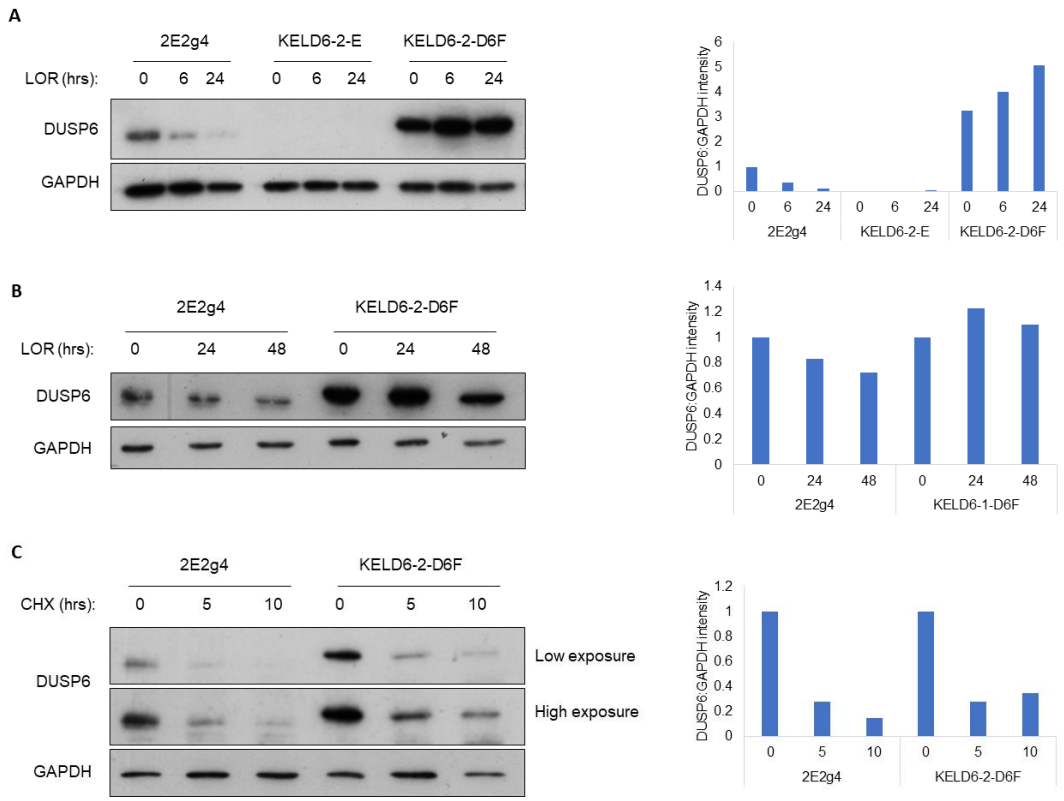

Figure 6.15 – Validation of DUSP6 overexpression. (A) Immunoblot of 2E2g4, KELD6-2-E (with empty vector) and KELD6-2-D6F (with DUSP6-FLAG vector) cells with an anti-DUSP6 antibody after treatment with 30 nM lorlatinib for 6 and 24 hours (n = 1). (B) Immunoblot of 2E2g4 and KELD6-2-D6F cells assessing DUSP6 expression after treatment with 30 nM lorlatinib for 24 and 48 hours (n = 1). (C) Immunoblot of 2E2g4 and KELD6-2-D6F cells assessing DUSP6 expression after treatment with 40 ug/ml CHX (n = 1). For each assay, DUSP6 was quantified to GAPDH.

To assess whether exogenous DUSP6 could rescue the cytostatic effect of the ALK inhibitor, dose response assays were performed in 2E2g4 cells, KELD6-2-D6F and KELD6-2-E cells (**Fig. 6.16**). Unfortunately, lorlatinib remained as potent in the cells with exogenous DUSP6 expression as the DUSP6-null cells. After treatment with crizotinib, there is a slight difference in cell viability in the DUSP6-null and DUSP6 overexpressing cells, however this is only a marginal effect. It is possible that a goldilocks effect is occurring, where inappropriate gene expression in either direction can have a detrimental cellular effect (Li et al., 2021, Spurlock et al., 2021, Wang et al., 2014b). Indeed, this has led to cell death in other cancer systems before (Wang et al., 2014b). Therefore, there is a possibility that significantly

reduced or increased levels of DUSP6 may reduce cell viability. Alternatively, as mentioned previously, sustained loss of DUSP6 may have induced compensatory mechanisms by other DUSP genes which cannot be reversed by exogenous DUSP6 protein. Nonetheless, if taken at face value, these data indicate that the increased sensitivity to lorlatinib treatment is not apparently due to loss of DUSP6.

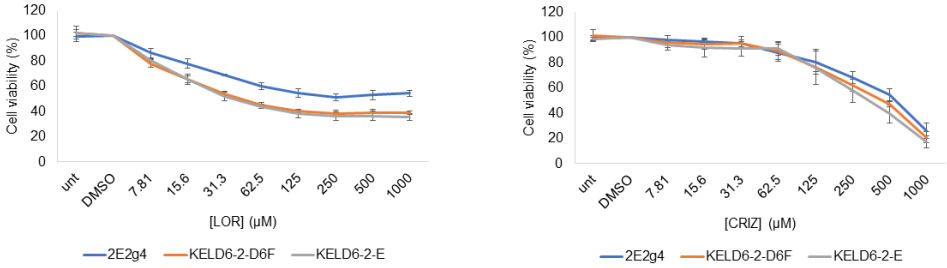

Figure 6.16 – Overexpression of DUSP6 does not rescue the incapacity to proliferate driven by the ALK inhibitor. 2E2g4, KELD6-2-D6F and KELD6-2-E cells were treated with increasing doses of lorlatinib (LOR) or crizotinib (CRIZ) for 7 days and cell viability was measure using the resazurin assay (n = 3). Independent samples t-test comparing equivalent drug concentrations between KELD6-2-D6F and KELD6-2-E did not identify any statistically significant differences.

6.2.4. Phosphoproteomic screen identifies potential roles of DUSP6 in ALK-mutated NB

A key question remaining from this study is what substrate(s) does DUSP6 have in NB cells? I have demonstrated a wide range of data that demonstrate, unexpectedly, that this is unlikely to be any of the MAPKs or AKT. The ALK receptor activates a myriad of intracellular signalling pathways which each have diverse and overlapping downstream effects (Hallberg and Palmer, 2016). As opposed to probing pathways individually, we sought to employ a phosphoproteomic approach to identify potential DUSP6 targets. Previous studies have performed phosphoproteomic screens successfully to identify ALK-mediated signalling pathways in NB cells (Borenäs et al., 2021, Van den Eynden et al., 2018, Chen et al., 2016a), hence the effect of DUSP6 depletion on ALK inhibitor treatment was

also investigated. Due to the concern of the heterogeneity of the DUSP-null subclones, I chose to use mixed populations of CRISPR-treated cells to investigate phosphoproteomic changes of loss of DUSP6. This should provide a more representative, averaged picture of the effect of DUSP6 deletion on intracellular signalling. Hence, iKELLY cells containing the DUSP6 gRNA (2E2g4) and the non-gRNA control (2E2) were treated with dox for 6 days to deplete DUSP6 protein (**Fig. 6.17A**). There is evidence that dox may influence the ERK and AKT signalling pathways, therefore cells were cultured without dox for 7 – 9 days prior to lorlatinib treatment (Chen et al., 2009a, Chang et al., 2014). Before samples were analysed by mass spectrometry, an immunoblot was run and probed for DUSP6 and pERK (**Fig. 6.17B**). It is evident that dox treatment abolished DUSP6 protein expression in the 2E2g4 cells. As expected, lorlatinib also significantly downregulated ERK phosphorylation. Surprisingly, there was also a statistically significant decrease in basal ERK phosphorylation levels in cells depleted of DUSP6 protein suggesting, contrary to previous studies above, ERK signalling was altered here in response to loss of DUSP6 (**Fig. 6.17B**).

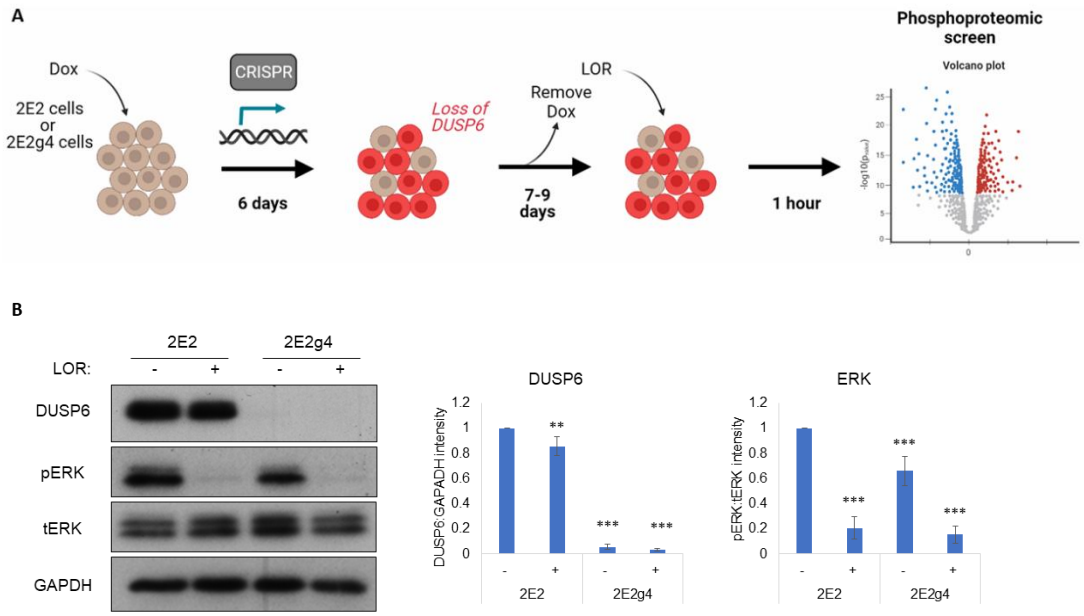

Figure 6.17 – Overview of phosphoproteomic screen. (A) 2E2 and 2E2g4 cells were treated with dox for 6 days. During this time, Cas9 will introduce indels into the DUSP6 gene. Following this, dox was removed for 7-9 days and cells then treated with lorlatinib (LOR) for 1 hour. A phosphoproteomic screen was then performed on lysates to identify proteins that demonstrate the most significant change in phosphorylation status (n = 4 biological replicates where each treatment and lysis was performed independently). (B) Table of the 4 samples for the phosphoproteomic analysis and the two key comparisons for analysis are displayed on the right-hand side. (C) Immunoblot for lysates sent for phosphoproteomic analysis probed for DUSP6 and pERK. For quantification, DUSP6 and pERK were normalised to GAPDH and tERK respectively, followed by a second normalisation to 2E2 - LOR. One-way ANOVA compared to 2E2 - LOR; **$p \leq 0.005$; ***$p \leq 0.0005$.

In total, the phosphoproteomic dataset contained 8250 phosphopeptides across 2503 unique proteins. The two main questions investigated in this study were (i) How does loss of DUSP6 affect the KELLY phosphoproteome and (ii) how does loss of DUSP6 affects intracellular ALK signalling? To answer these questions, pair-wise comparisons were made between the four treatment groups (**Table 6.1**). It is worth noting that for all the following analyses, the Log2-Fold Change and p-value of each comparison represents the phosphorylation change caused by the treatment. For example, the ERK1 Tyr204 phosphosite in the '2E2-LOR vs 2E2+LOR' comparison displayed a Log2-Fold Change of -1.82. This indicates lorlatinib

treatment in 2E2 cells caused a ~3.5-fold decrease of the ERK1 Tyr204 phosphosite. This data for this example is displayed in **Table A2** and **Table A3**.

Volcano plots were generated for each comparison, displayed in **Figure 6.18**. It is surprising that there were only 47 and 63 significantly upregulated and downregulated phosphopeptides after treatment with lorlatinib in 2E2 cells (**Fig. 6.18A-B** and **Fig. 6.19A**). Considering ALK is known to regulate a plethora of signalling cascades (Hallberg and Palmer, 2016) this was very unexpected. Conversely, lorlatinib treatment in the DUSP6 knockout cells caused a far greater effect on the intracellular phosphotome as 264 and 398 phosphopeptides were significantly upregulated and downregulated respectively. It is unlikely all of these phosphosites are altered solely by loss of DUSP6 and suggests the 2E2g4 population is biochemically somewhat different to the 2E2 population. This could potentially occur during puromycin selection of the gRNA in the 2E2g4 population or during treatment with dox, although dox is controlled for with the 2E2 cells. Loss of DUSP6 also caused a significant effect on the KELLY phosphoproteome (**Fig. 6.18C-D** and **Fig. 6.19B**). There are 66 and 100 significantly upregulated and downregulated phosphopeptides (relating to 57 and 80 proteins, respectively) after depletion of DUSP6. This suggests DUSP6 may influence many phosphoproteins in KELLY cells. Furthermore, there are significantly more peptides downregulated rather than upregulated by DUSP6 depletion after treatment with lorlatinib, suggesting that DUSP6 may be positively influencing the pathways regulated by ALK.

Following this, we then investigated whether the significantly altered phosphosites were the same for each lorlatinib comparison and DUSP6 depletion comparison. As displayed in **Figure 6.19A**, there were only a handful of common phosphopeptides upregulated and downregulated after lorlatinib treatment in both the 2E2 and 2E2g4 cells. Although we expected some differences due to the loss of DUSP6, this suggests loss of DUSP6 has a major effect on the biochemical response to lorlatinib treatment. Considering the number of phosphosites not in common between 2E2 and 2E2g4 cells, we were also now sceptical that this large variation is due to

inherent differences in the 2E2 and 2E2g4 cell populations. Loss of DUSP6 also caused a very different effect on the phosphoproteome in cells with and without lorlatinib treatment (**Fig. 6.19B**). Interestingly, the majority of overlapping, downregulated phosphopeptides from the ALK inhibitor comparisons are related to ERK signalling (**Fig. 6.19C, bold rows**). Considering ALK is hyperactive in KELLY cells, we expected ALK inhibition to downregulate a range of signalling pathways, however it appears that ALK predominantly activates the ERK signalling pathway. ERK appeared to function by phosphorylating two transcriptional repressors, CIC and ERF (le Gallic et al., 1999, Ren et al., 2020). Interestingly, a recent study demonstrates CIC directly represses DUSP6 expression until ERK-mediated phosphorylation of CIC induces its nuclear export (Ren et al., 2020).

Table 6.1 – Comparisons used for data analysis. Pair-wise comparisons of four treatment groups were used to analyse phosphoproteomic dataset. Comparisons can be split into two categories: effect of ALK inhibition or effect of DUSP6 depletion.

Comparison	Description
2E2-LOR vs 2E2+LOR	Effect of ALK inhibition in KELLY cells
2E2g4-LOR vs2E2g4+LOR	Effect of ALK inhibition in DUSP6-null KELLY cells
2E2-LOR vs 2E2g4-LOR	Effect of loss of DUSP6 in KELLY cells
2E2+LOR vs 2E2g4+LOR	Effect of loss of DUSP6 in KELLY cells treated with the ALK inhibitor

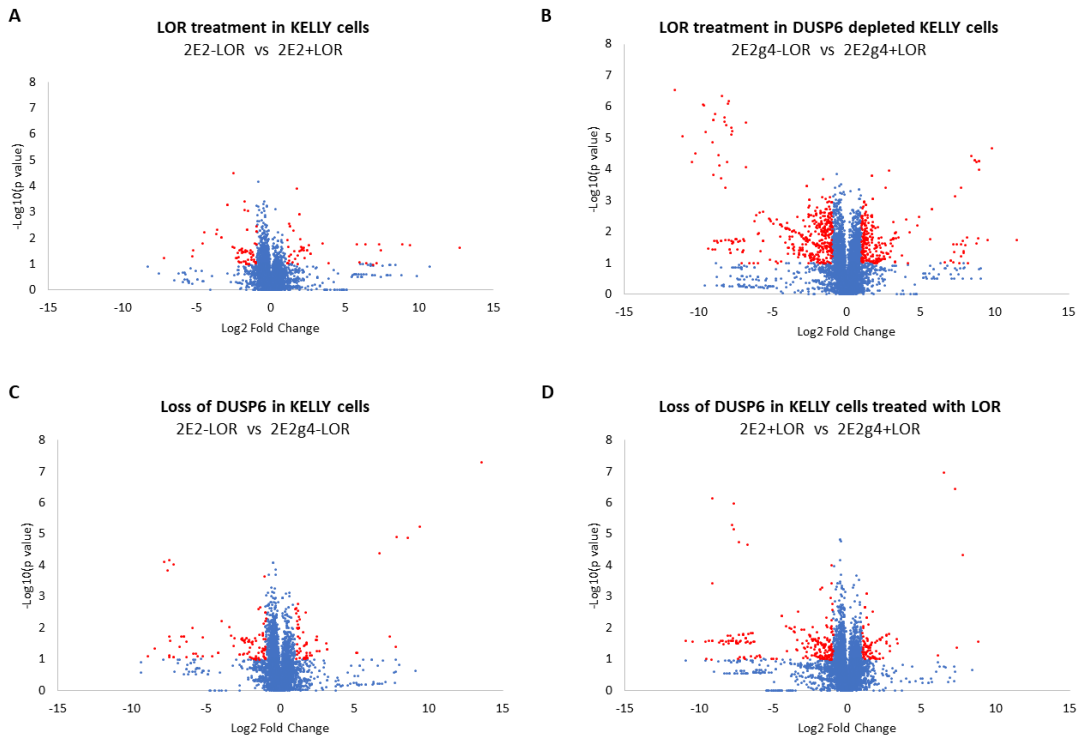

Figure 6.18 – Significant phosphopeptides after lorlatinib treatment and DUSP6 depletion. Volcano plots were generated for four pairwise comparisons: after treatment with 30 nM lorlatinib treatment in (A) 2E2 and (B) 2E2g4 cells and the effect of DUSP6 depletion in cells (C) without and (D) with 30 nM lorlatinib treatment (n = 4). Significant thresholds for differential phosphorylation were set as Log2-Fold Change > 1 and p value < 0.1 (red data points). P-value was generated by an independent samples t-test.

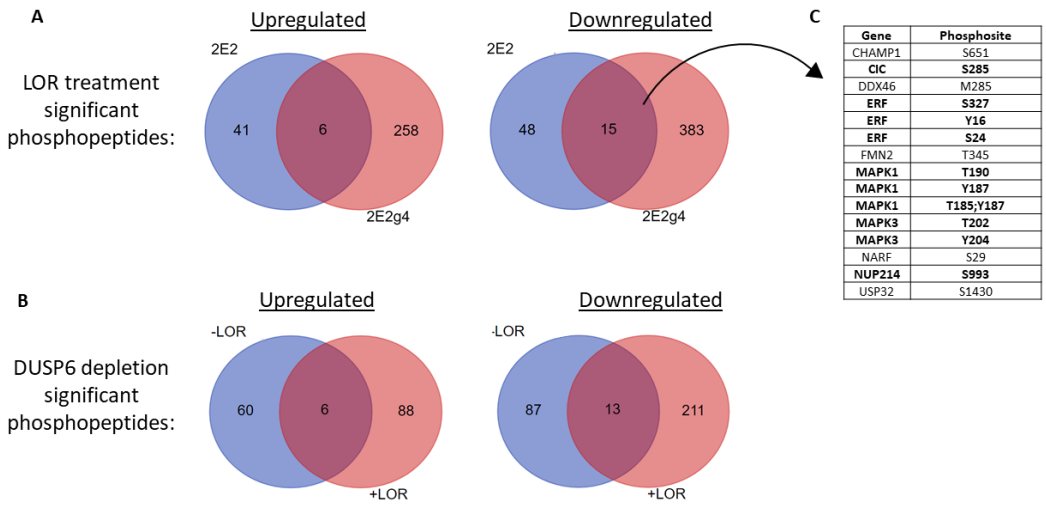

Gene	Phosphosite
CHAMP1	S651
CIC	**S285**
DDX46	M285
ERF	**S327**
ERF	**Y16**
ERF	**S24**
FMN2	T345
MAPK1	**T190**
MAPK1	**Y187**
MAPK1	**T185;Y187**
MAPK3	**T202**
MAPK3	**Y204**
NARF	S29
NUP214	**S993**
USP32	S1430

Figure 6.19 – There is a minor overlap in significant phosphopeptides between treatment comparisons. Venn diagrams of significant phosphopeptides between (A) the two ALK inhibitor comparisons (Fig. 6.16A-B) and (B) the two DUSP6 depletion comparisons. (C) The significant phosphopeptides that were downregulated in the ALK inhibitor comparisons.

For the phosphoproteomic dataset in **Chapter 4**, a biological pathway enrichment and KSEA were performed. Considering the biological pathway enrichment analysis does not incorporate phosphosite-specific data, we believed the KSEA was a more accurate measure of pathway activation. This method uses the phosphorylation changes on each protein in the dataset to determine kinase activity (Casado et al., 2013). A KSEA analysis was performed on the four treatment comparisons in **Table 6.1**. As expected, treatment with lorlatinib significantly downregulated the kinase activity of MAP2K1, JAK2 and RET kinases, all of which are related to ERK signalling (**Fig. 6.20**). Paradoxically, MAPK3 kinase (ERK1) activity appeared marginally upregulated in the KSEA after depletion of DUSP6 in lorlatinib treated cells. Nonetheless, due to the downregulation of MAPK1/3 phosphorylation demonstrated in **Figure 6.17B** and **Figure 6.19C**, it is unequivocal that ERK itself is not activated.

We expected loss of DUSP6 to activate at least one kinase pathway in KELLY cells. Surprisingly, only CSNK2A1, CDK1 and CDK2 were significantly altered and they were all downregulated (**Fig. 6.20, column 3**). Whereas DUSP6 is able to anchor ERK in the nucleus, a recent study

demonstrates that CSNK2A1 is able to drive ERK translocation to the nucleus (Plotnikov et al., 2019). One potential hypothesis is that by depleting KELLY cells of DUSP6, ERK is no longer restrained in the cytoplasm and no longer needs CSNK2A1 to aid its migration to the nucleus. There is a correlation between many of the kinases in the first two columns of the KSEA (**Fig. 6.20**), however the majority only gain statistical significance in the DUSP6 depleted cells. Importantly, this indicates that the pathways altered by lorlatinib are enhanced further after loss of DUSP6. These data suggest there is indeed a biochemical interaction between DUSP6 and ALK inhibition which merits further exploration.

Unsurprisingly, many of the kinases identified in the KSEA are involved in ALK signalling. For example, drug discovery against both mTOR and CDK4/6 have been investigated as potential combinations to ALK inhibition in NB (Moore et al., 2014, Wood et al., 2017). Furthermore, a recent study demonstrates GSK3 is regulated downstream of ALK in NB cells (Gonzalez Malagon et al., 2018). With this in mind, the kinase-related phosphosites related to MAPK1/3, CDK4/6, mTOR and GSK3 signalling are displayed in **Figure 6.21**. Many phosphoproteins relating to these pathways that were not identified in the KSEA were added to the heatmaps (**Fig. 6.21, curly brackets**). As expected, the phosphosites related to ERK signalling are significantly downregulated after treatment with lorlatinib (**Fig. 6.21A**). Interestingly, although loss of DUSP6 didn't affect pERK, the phosphorylation of one of its downstream targets, ERF, is significantly upregulated (le Gallic et al., 1999). This suggests ERF may be a DUSP6 substrate and is worth further investigation. The only statistically significant changes related to CDK4/6 signalling are present on RB1 (**Fig. 6.21B**). There appears to be a strong upregulation of RB1 phosphorylation after lorlatinib treatment in cells with depleted DUSP6, but not without. Interestingly, phosphorylation of RB1 at S807/S811 has been identified as an early event in neuronal cell death in SH-SY5Y cells (Hamdane et al., 2005). This provides a potential pathway for concurrent ALK inhibition and DUSP6 depletion to augment NB cell death.

There are a wide range of proteins involved in mTOR signalling that were differentially phosphorylated between cells with either lorlatinib treatment or DUSP6 depletion (columns 1 and 3) compared to both treatments combined (columns 2 and 4) (**Fig. 6.21C**). This appeared to be the case for: EEF2K, TSC2, EIF4B, 4E-BP1, PRAS40, p70S6K, among others. The KSEA result suggests, although marginal, loss of DUSP6 led to a downregulation of mTOR signalling (**Fig. 6.20**). These data are consistent with the phosphoproteomic analysis in **Chapter 4** where BCI treatment also downregulated mTOR signalling.

GSK3 is a global regulator of intracellular signalling and has a broad range of substrates involved in neurogenesis and neuronal differentiation (Hur and Zhou, 2010). Similar to mTOR signalling, many of these proteins, including GSK3α/β itself, are phosphorylated differently after lorlatinib treatment and DUSP6 depletion compared to both combined (**Fig. 6.21D**). This is most visible for GSK3α/β, Tau, β-catenin, NFATC2IP, UNG and CTPS1. Although many of these proteins are substrates of GSK3 (Hur and Zhou, 2010), in most cases their change in phosphorylation does not correlate with GSK3 suggesting their regulation is more complex than simply being targeted by GSK3. The broader effect on mTOR and GSK3 signalling could be indicative of an indirect consequence of DUSP6 depletion rather than identifying a direct target of DUSP6. Nonetheless, these data highlight the importance of DUSP6 in phosphorylation events downstream of ALK signalling and raises a number of interesting avenues worth exploring further.

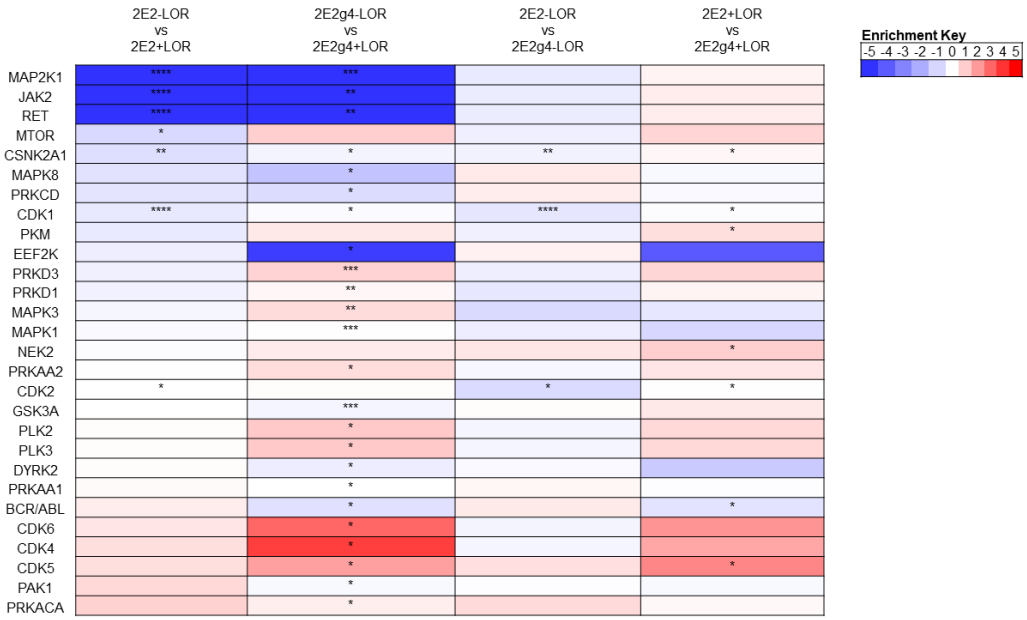

Figure 6.20 – KSEA heatmap of significantly enriched kinases. The enrichment key is based on the z-score value, a normalized score for each kinase. Red and blue indicate activation and inactivation of kinase, respectively. For example, MAP2K1 was significantly inactivated after LOR treatment (column 1). Only the statistically significant kinase substrates are displayed. The MAP2K1, JAK2 and RET z-scores were below -5. The p-value represents a statistical assessment of the z-score (previously described in Casado et al. (2013)) where *$p \leq 0.05$; **$p \leq 0.005$; ***$p \leq 0.0005$.

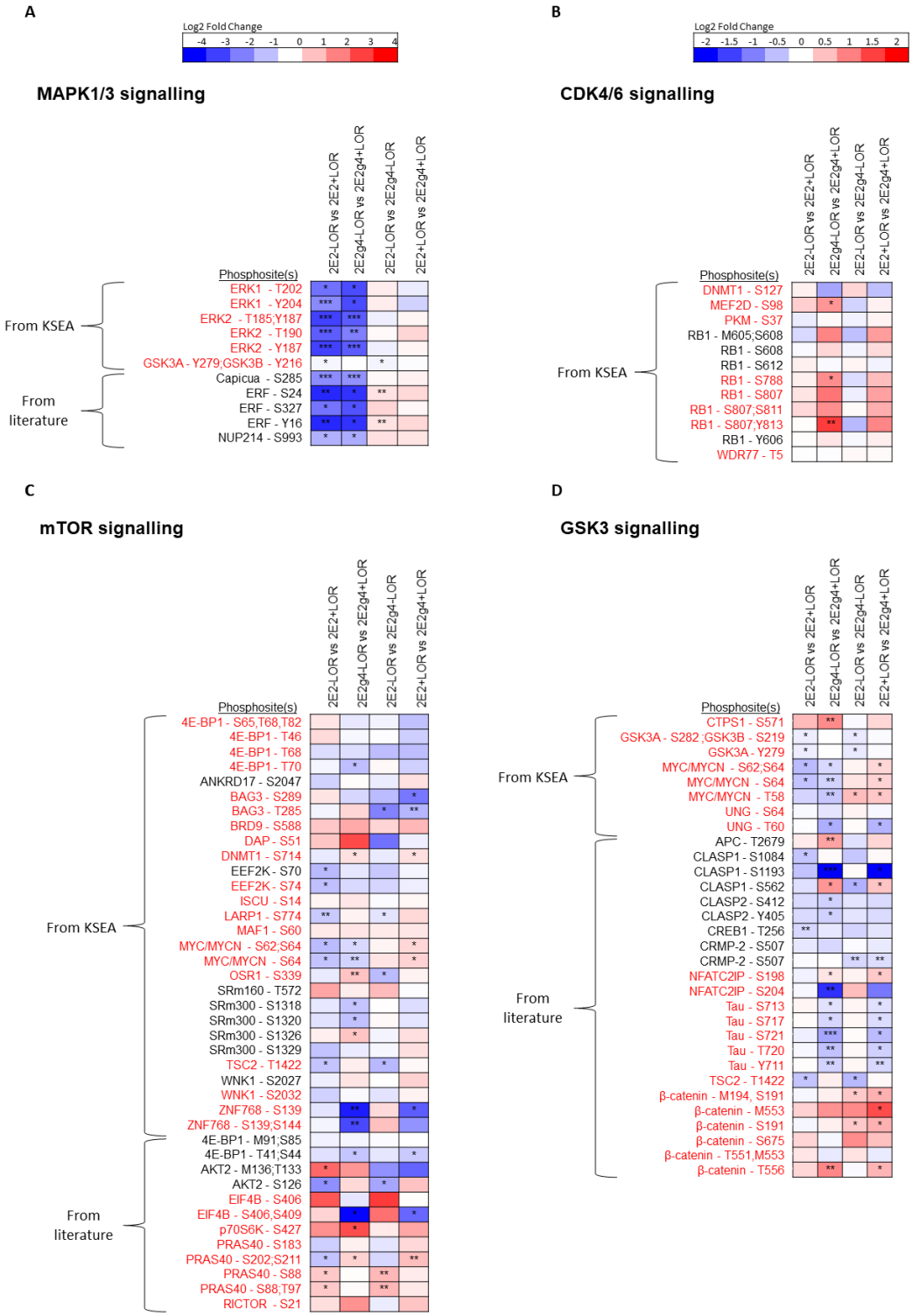

Figure 6.21 – Log2-Fold Changes for kinase-related phosphosites. The Log2-Fold Change for a range of phosphoproteins related to the (A) MAPK1/3, (B) CDK4/6, (C) mTOR and (D) GSK3 kinases. As indicated in the curly brackets, peptides were manually identified in the literature alongside substrates from the KSEA analysis. Phosphosites are presented as protein name followed by phosphosite. Phosphosites in red have been referenced multiple times in the Phosphositeplus resource (Hornbeck et al., 2015). Log2-Fold Change

key in (A) used for MAPK1/3 signalling and in (B) used for heatmaps in (B-D). Independent samples t-test; *p ≤ 0.05; **p ≤ 0.005; ***p ≤ 0.0005

To complement the findings from the KSEA, we sought to perform a separate pathway analysis. For this we used the Qiagen Ingenuity Pathway Analysis (IPA) software which allows you to map changes in phosphorylation onto well-known canonical pathways. We hoped this would allow us to get a better view on what pathways were differentially phosphorylated and whether they include the kinases from the KSEA. It is worth noting that this software uses one phosphosite with the greatest Log2-Fold Change per protein, therefore some phosphosites shown in my KSEA study are not included in the IPA analysis. The software recommends including 300 – 2000 phosphopeptides in the analysis so that relevant pathways are identified. Unfortunately, lorlatinib treatment generated a significantly smaller amount of changes than the other treatments and so a less stringent threshold of $p < 0.1$ was selected. This resulted in between ~500 – ~1000 phosphorylation changes across the four dataset comparisons.

The canonical pathways differentially regulated by each dataset comparison are presented in **Figure 6.22**. In this analysis, both lorlatinib treatment and DUSP6 knockout resulted in significantly more downregulated pathways than upregulated pathways. This is expected for lorlatinib treatment as there will be a clear inhibition of the pathways downstream of ALK. However, it is surprising that loss of DUSP6 suppresses of a wide range of signalling pathways. There are a subset of pathways of interest that are highlighted by the red arrows. The first question to ask is what pathway could DUSP6 be regulating? Similar to the KSEA, these data suggest ERK is not regulated by DUSP6. Rather than upregulation of ERK, loss of DUSP6 results in a clear downregulation of ERK signalling (**Fig. 6.17B** and **Fig. 6.19C**). Upon inspection of the pathway, there are various members upstream of ERK such as RAF1 that are downregulated (**Fig. 6.23A**). Although MEK1/2 does appear upregulated, this is due to phosphorylation of Ser30, a site not known to activate MEK1/2 in the literature.

Loss of DUSP6 also led to a significant downregulation of RhoA signalling (**Fig. 6.22** and **Fig. 6.23B**). The Rho family are a group of GTPases that act as molecular switches for a wide range of molecular signalling pathways (Hodge and Ridley, 2016). A previous report demonstrates that the downstream RhoA target, ROCK1/2, is associated with poor survival in NB and chemical inhibition of ROCK1/2 suppresses NB cell growth (Dyberg et al., 2017). Interestingly, in NB cells inhibition of ROCK1/2 downregulated GSK3β phosphorylation and promoted MYCN degradation via phosphorylation. This is consistent with our phosphoproteomic dataset where downregulation of RhoA in DUSP6-null cells is concomitant with an increase and decrease in MYCN and GSK3 phosphorylation, respectively (**Fig. 6.21D**). Unfortunately, the ROCK-MYCN/GSK3 relationship is not present in the IPA software and so is not displayed in **Figure 6.23B**, however a range of other downregulated proteins were identified. Together, these data suggests DUSP6 may be promoting RhoA signalling which potentially alters the GSK3/MYCN axis and promotes NB cell growth. Considering GSK3 signalling in the KSEA was significantly affected by lorlatinib treatment in DUSP6-null cells (**Fig. 6.20**), the regulation of RhoA signalling may be involved in ALK signalling.

Following this, we also investigated whether DUSP6 is influencing ALK signalling. To determine this, the effect of lorlatinib on canonical pathways was compared in WT and DUSP6-null cells (**Fig. 6.22, columns 1 and 2**). Interestingly, mTOR signalling displayed a similar pattern in the IPA to the KSEA where lorlatinib treatment significantly downregulated mTOR but this was reversed if lorlatinib treatment was performed in DUSP6-null cells. This also appeared to be the case and is more exaggerated for the PI3K/AKT signalling pathway which on closer inspection included part of the mTOR pathway (PI3K/AKT canonical pathway in **Figure A5**). The proteins which drove the change in PI3K/AKT signalling were: RPS6KB1, HSP90, 14-3-3, β-catenin, PDPK1 and TYK2. This provides many potential intracellular targets that could be regulated by DUSP6. However, considering the PI3K/ATK and mTOR pathways promote NB cell growth (Johnsen et al.,

2008, Opel et al., 2007), it is unclear how this role of DUSP6 could be of therapeutic value.

An alternative pathway that appears differentially regulated by lorlatinib in the absence of DUSP6 is the HIPPO pathway (**Fig. 6.22, columns 1 and 2**). The HIPPO pathway is a conserved signalling cascade driven by LATS1/2-mediated activation of YAP/TAZ (Misra and Irvine, 2018). YAP/TAZ is retained in the cytoplasm by 14-3-3 until dephosphorylated where it can translocate to the nucleus and transcriptionally regulate multiple genes (Moon et al., 2017)**.** Importantly, it is well documented that activation of YAP/TAZ can promote NB cell growth (Shim and Goldsmith, 2021). Furthermore, YAP1 promoted resistance to a MEK inhibitor in RAS-driven NB and to an ALK inhibitor in ALK-rearranged lung cancer suggesting there is crosstalk between the ALK-ERK and HIPPO signalling pathways (Coggins et al., 2019, Tsuji et al., 2020). In our study, loss of DUSP6 significantly downregulated a wide range of HIPPO pathway phosphoproteins in response to lorlatinib (**Fig. 6.24 green circles**). Furthermore, there was a concurrent increase in various 14-3-3 isoforms suggesting YAP/TAZ was no longer retained in the cytoplasm (**Fig. 6.24 red circles**). It is worth mentioning that the HIPPO pathway is interconnected to a wide range of other pathways, including RhoA signalling which is also potentially regulated by DUSP6 (Ohgushi et al., 2015). These data suggest that DUSP6 could promote signalling via the HIPPO pathway downstream of ALK which, when inhibited, would enhance lorlatinib-mediated cell death.

Figure 6.22 – IPA analysis reveals differentially regulated canonical pathways. A wide range of significantly regulated pathways were identified after treatment with lorlatinib and depletion of DUSP6. Pathways with red arrows are of interest and are analysed further in subsequent figures. Pathways were included if one of the dataset comparisons contained a z-score > 2 or < -2. Right-tailed Fishers Exact test performed with Benjamini-Hochberg correction; *p ≤ 0.1; **p ≤ 0.01; ***p ≤ 0.001.

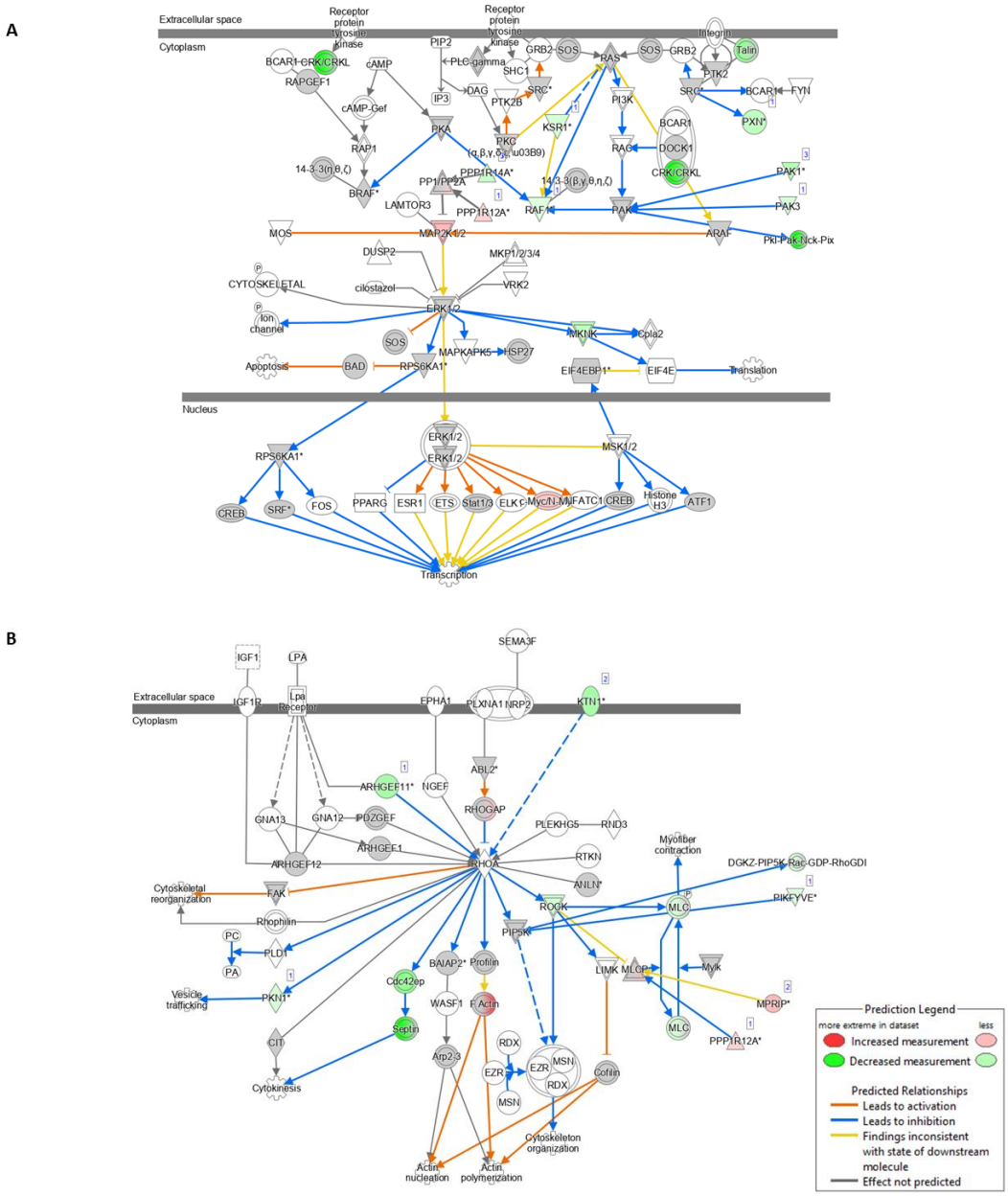

Figure 6.23 – ERK and RhoA signalling pathways are downregulated in DUSP6 KO cells. Loss of DUSP6 caused a downregulation of the (A) ERK and (B) RhoA canonical pathways. Proteins coloured red or green were identified in the dataset and satisfied the criteria Log2-Fold Change > 2 whereas proteins coloured grey were identified in the dataset but did not satisfy this criteria. Red or green colour gradients indicate proteins that represent multiple proteins/isoforms with differing phosphosites. Arrow colours indicate predicted activation or inactivation based on identified changes to phosphoproteins (see key). Canonical pathways were generated in the IPA software.

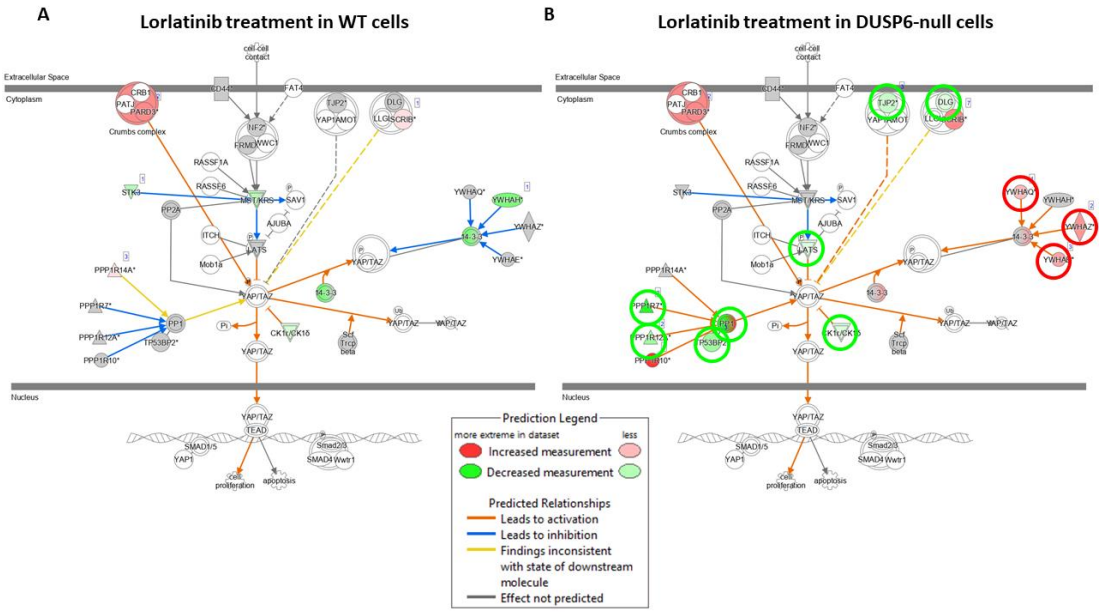

Figure 6.24 – HIPPO signalling is downregulated by lorlatinib in DUSP6-null cells. Signalling via the HIPPO pathway after treatment of lorlatinib in cells (A) with and (B) without DUSP6 protein. Proteins circled in green and red in (B) are downregulated and upregulated after loss of DUSP6, respectively. Proteins coloured red or green were identified in the dataset and satisfied the criteria Log2-Fold Change > 2 whereas proteins coloured grey were identified in the dataset but did not satisfy this criteria. Red or green colour gradients indicate proteins that represent multiple proteins/isoforms with differing phosphosites. Arrow colours indicate predicted activation or inactivation based on identified changes to phosphoproteins (see key). Canonical pathways were generated in the IPA software.

6.3. Discussion

A proportion of NB is characterised by hyperactive signalling via the ALK pathway. ALK can signal via multiple intracellular signalling pathways (**Fig 6.2**) (Trigg and Turner, 2018). In this chapter, we investigated how DUSPs are regulated by ALK and whether they can be manipulated to alter cell growth in response to ALK inhibition. Initial experiments demonstrated several MKPs were activated by ALK in KELLY cells. As DUSP6 expression was significantly depleted after ALK inhibition, the ALK-DUSP6 relationship was investigated further. In KELLY and LAN-5 cells, ALK regulated DUSP6 in both an ERK-dependent and -independent manner. Complete loss of DUSP6 appeared to sensitise KELLY cells to ALK inhibition, however re-

introduction of exogenous DUSP6 did not rescue cell viability. Lastly, a broader phosphoproteomic screen was performed to identify what the DUSP6 substrate(s) downstream of ALK may be in KELLY cells. Loss of DUSP6 appeared to significantly downregulate the RhoA/ROCK signalling pathway suggesting DUSP6 may target a member of that pathway. Interestingly, ALK inhibition caused a large number of phosphorylation changes only in DUSP6-null cells, for example the HIPPO pathway. This suggests DUSP6 indeed carries out a functional role downstream of ALK in KELLY cells.

Two recent RNA sequencing studies using different ALK inhibitors and different NB cell lines previously demonstrated DUSP gene expression is regulated downstream of ALK (**Fig. 6.3**) (Borenäs et al., 2021, Van den Eynden et al., 2018). The data presented above demonstrate that in KELLY and LAN-5 cells, *DUSP4*, *DUSP5* and *DUSP6* were significantly downregulated after treatment with lorlatinib. Considering all three are negative feedback regulators of ERK signalling, the downregulation of DUSP expression could simply be a knock-on effect of ERK inhibition. This transcriptional response was most pronounced for DUSP6 as lorlatinib treatment for 6 hours decreased *DUSP6* gene expression by >80%. Interestingly, I then demonstrated in KELLY and LAN-5 cells that DUSP6 was at least partly regulated independently of ERK. There is evidence that DUSP6 is regulated at a transcriptional and translational level and can undergo various post-translational changes (Reviewed in Ahmad et al. (2018) and Pérez-Sen et al. (2019)). Interestingly, ALK inhibition depleted DUSP6 protein in ALK-mutated cell lines, the higher molecular weight protein was lost first. Similarly, accumulation of DUSP6 after treatment with a proteasomal inhibitor resulted in the addition of a higher molecular weight band. Prior to protein degradation, DUSP6 is both phosphorylated and ubiquitinated, therefore this higher molecular weight band likely represents one of these modifications (Bermudez et al., 2008, Marchetti et al., 2005, Wu et al., 2021).

The stage at which DUSP6 is regulated by ALK was also investigated. In LAN-5 cells, these data suggested DUSP6 may be regulated partly by a

post-translational mechanism whereas in KELLY cells the data pointed towards a transcriptional mechanism. A model displaying this regulation in LAN-5 cells is presented in **Figure 6.25**. The *DUSP6* gene contains consensus binding sites for a number of transcription factors including β-catenin, NF-κB, Forkhead and ETS proteins (Ekerot et al., 2008). The best characterised of these are the ETS proteins as they are nuclear targets of ERK. Hence, both ETS1 and ETS2 form a major component of the DUSP6-ERK feedback loop (Ekerot et al., 2008, Furukawa et al., 2008). However, in NB cells it appears DUSP6 is transcriptionally regulated by an ERK-independent mechanism as well. This suggests that in NB cells, other transcription factors are also regulating the DUSP6 gene downstream of ALK. DUSP6 is also regulated post-transcriptionally by phosphorylation, sumoylation and ubiquitination (Marchetti et al., 2005, Wu et al., 2021, Ma et al., 2020). As well as upregulating DUSP6 transcriptionally, ERK can phosphorylate DUSP6 at Ser159 and Ser197 targeting it for proteasomal degradation (Marchetti et al., 2005). Phosphorylation of DUSP6 at Ser159 is also inhibited by rapamycin, implicating the PI3K/mTOR pathway in regulating DUSP6 (Bermudez et al., 2008). Interestingly, proteolysis of DUSP6 driven by mTOR occurred in both an ERK-dependent and -independent manner suggesting these pathways can cross-talk to mediate DUSP6 function. This is one possible route for ALK to regulate DUSP6, however in the phosphoproteomic dataset the IPA and KSEA analyses suggest loss of DUSP6 suppressed mTOR activity. Considering mTOR is known to drive NB cell growth (Johnsen et al., 2008), it is unclear how mTOR inhibition could improve lorlatinib efficacy. DUSP6 is also phosphorylated by CK2α which increases its phosphatase activity against ERK (Castelli et al., 2004). It is likely that this phosphorylation event is not at Ser159 or Ser197 as the functional consequence is very different. There are many E3 ubiquitin ligases, the majority of which are TRIM proteins, that have co-immunoprecipitated and ubiquitinated DUSP6 (Tong et al., 2020, Wu et al., 2021, Zhu et al., 2020). In LAN-5 cells, we hypothesise that ALK prevents DUSP6 phosphorylation and ubiquitination that precedes DUSP6

degradation (**Fig. 6.25**). Further studies are required to see whether this is directed via ERK.

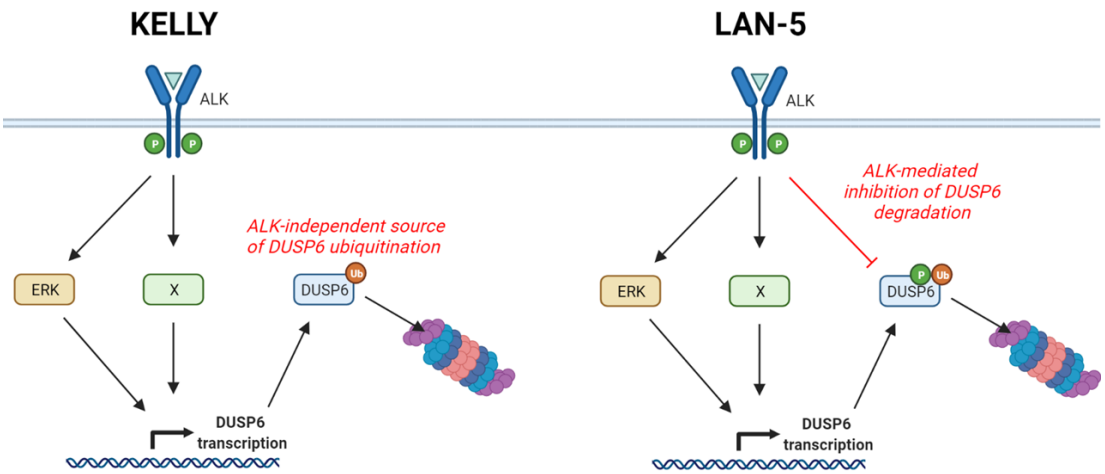

Figure 6.25 – Working model for how ALK regulates DUSP6 expression in KELLY and LAN-5 cells. In both cell lines, DUSP6 expression is tightly controlled by ALK signalling in an ERK-dependent and-independent manner, highlighted by the unidentified protein termed 'x'. Furthermore, DUSP6 is targeted for proteasomal degradation in both cell lines. However, in LAN-5 cells it appears DUSP6 can be regulated by ALK both transcriptionally and post-translationally. Whether these post-translational changes involve phosphorylation, ubiquitination or both is unknown.

It has been suggested that perturbing ERK feedback inhibitors may alter current ALK inhibitor therapies (Lambertz et al., 2015). Hence, we investigated whether suppressing DUSP6 expression could augment ALK inhibitor-mediated cell death. Indeed, complete loss of DUSP6 expression appeared to sensitise NB cells to lorlatinib treatment. This is a counter-intuitive concept because ALK inhibition itself reduces DUSP6 expression. This could suggest that complete loss of DUSP6 is required to see an effect. We investigated whether this effect was due to MAPK or AKT inhibition but increased sensation in DUSP6-null cells was not reproduced. Similarly, this also appeared unique to DUSP6 as knockout of other DUSPs did not result in the same lorlatinib sensitisation. There was also a surprising effect of DMSO on NB cell growth and frustratingly, this was different between cell populations. Treatment with DMSO can alter a host of physiological and morphological processes (Verheijen et al., 2019). Importantly, experiments in promyoblast cells demonstrated DMSO may promote ERK signalling (Yu

et al., 2008), a very relevant pathway to our system. Although all experiments were performed <1% DMSO, we recommend future experiments to use 0.02% DMSO as this was used in **Figure 6.9B** (KELD6-3 data) and removed the growth suppression observed by DMSO.

Unfortunately, re-introduction of exogenous DUSP6 did not rescue the sensitisation of ALK inhibition. Therefore, contrary to the previous data, it appears ALK inhibitor sensitisation is not due to loss of DUSP6 and instead results from clonal variation. However, there are various other potential explanations for this. Firstly, there is a possibility that these cells have adapted to not having DUSP6 protein. The DUSP-null subclones have been through multiple rounds of division therefore the functional role(s) of DUSP6 are likely to have been replaced. As mentioned previously, in thyroid cancer cells loss of DUSP5 resulted in an upregulation of DUSP6 and vice versa (Buffet et al., 2017). Considering DUSP5 and DUSP6 both target ERK in thyroid cancer, this is likely a compensatory mechanism to restrain ERK signalling. With this in mind, an assessment comparing DUSP expression in cells with and without DUSP6 would be beneficial. Alternatively, it is possible that DUSP6 overexpression is also able to increase lorlatinib efficacy. Wang et al. (2014b) demonstrated that both over- and under-expression of SRPK1, a splicing kinase, can lead to constitutive AKT activation and tumorigenesis in mice. Furthermore, there are other studies where gene expression must be fine-tuned to not perturb protein function (Spurlock et al., 2021, Li et al., 2021). It is well known that the spatiotemporal regulation of ERK by the MKPs is tightly regulated (Kidger and Keyse, 2016). Therefore, it is conceivable that disrupting the tight regulation of DUSP6 in either direction could significantly alter intracellular signalling. This idea is supported by the observation that both increased and decreased DUSP expression can be related to cancer progression (Caunt and Keyse, 2013). In the case of DUSP6, this is even more striking as it shows tumour-promoting and suppressing roles within the same tumour type (Li et al. 2012). Hence, overexpression of DUSP6 protein in NB could also display a pro-tumorigenic effect as it does in other cancer models. To investigate this, the consequence of DUSP6 overexpression on NB cell

survival should be explored further. Lastly, it is also worth mentioning that editing of off-target sites in these DUSP6-KO clones has not been determined. Therefore it is also possible that sensitisation to the ALK inhibitor is due to an off-target effect which would not be rescued by exogenous DUSP6. Nevertheless off-target effects of this CRISPR system have been assessed previously with other guides in our laboratory and we only found targeted editing of on-target sites (See **Chapter 3.2.5**). Considering these approaches only assessed potential off-target regions, to comprehensively assess off-target editing in this system, unbiased whole genome sequencing of DUSP6-null subclones is required (Zischewski et al., 2017).

There remains the question as to what DUSP6 could be targeting in NB cells. Considering the tight regulation of DUSP6 by ALK, one would expect a functional role of DUSP6 in NB cells. To assess this question, a phosphoproteomic screen was performed after loss of DUSP6 and treatment with lorlatinib. Consistent with previous experiments, DUSP6 did not appear to regulate ERK signalling. There were minor changes of other ERK-related proteins although ERK itself was not differentially phosphorylated. As suggested in **Chapter 3**, these data could indicate DUSP6 anchors ERK, preventing its function but not its phosphorylation. However, this is unlikely as the majority of ERK-related phosphopeptides were downregulated in the absence of DUSP6 rather than upregulated.

The majority of other pathways which were perturbed by loss of DUSP6 were downregulated. One pathway significantly downregulated in DUSP6-null cells was the RhoA/ROCK signalling pathway. RhoA is a member of the RAS superfamily of GTPases and activates a myriad of signalling pathways, including ROCK (Hodge and Ridley, 2016). Importantly, RhoA/ROCK signalling can promote NB cell proliferation (Dyberg et al., 2017). In this study, ROCK inhibition abolished NB cell proliferation in SK-N-BE(2) and SH-SY5Y cells and a xenograft model (Dyberg et al., 2017). Interestingly, suppression of ROCK signalling led to a decrease in GSK3 and increase in MYCN phosphorylation. Similarly, in the phosphoproteomic screen loss of DUSP6 downregulated phosphorylation of ROCK and GSK3 and increased

MYCN phosphorylation. These data suggest DUSP6 can influence NB cell survival via ROCK, as displayed in **Figure 6.26**. It is worth mentioning DUSP6 could also influence RhoA/ROCK signalling indirectly via ERK. In lung epithelial cells, ERK-mediated phosphorylation of RhoA targeted it for proteasomal degradation (Wei et al., 2013). However, our data currently does not support any interaction between ERK and DUSP6, hence it is not included in **Figure 6.26**. As mentioned in **Chapter 6.1**, ALK can also drive MYCN function and suppress GSK3 via PI3K/AKT (**Fig. 6.2**) (Chesler et al., 2006, Berry et al., 2012). Contractively, ALK is also believed to drive tumorigenesis via GSK3 activation (Gonzalez Malagon et al., 2018). As lorlatinib treatment suppressed ROCK, GSK3 and MYCN phosphorylation, it is conceivable that loss of DUSP6 perturbs this pathway to promote lorlatinib efficacy.

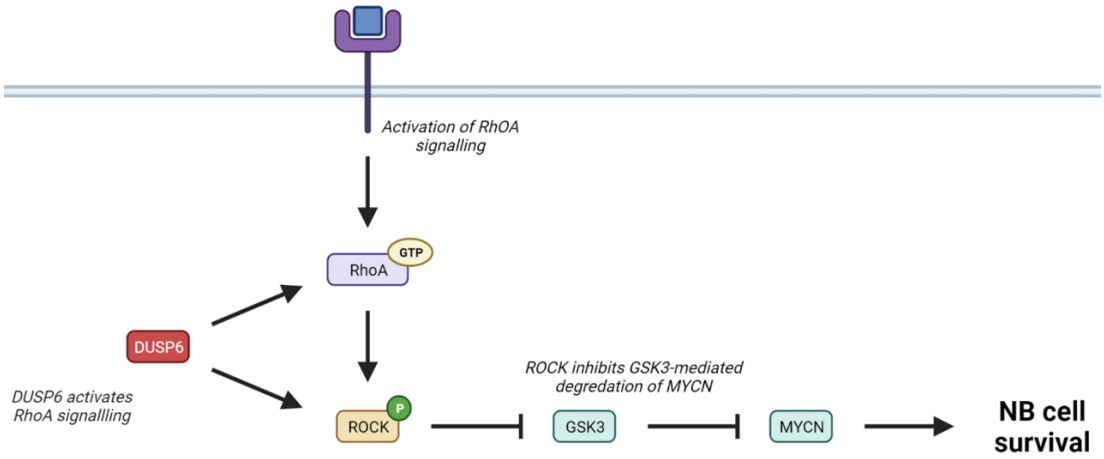

Figure 6.26 – Model speculating how DUSP6 could regulate RhoA signalling pathway. RhoA is activated by a myriad of extracellular signals and directly activates ROCK. ROCK subsequently inhibits GSK3-mediated degradation of MYCN which allows MYCN to drive NB cell survival. In this model, DUSP6 promotes RhoA signalling either via activation of ROCK or RhoA.

As demonstrated with the RhoA pathway, this analysis also helped me investigate how DUSP6 could influence ALK inhibition. Lorlatinib differentially regulated a wide range of signalling pathways in DUSP6-null cells compared to WT cells. One pathway of interest is the Hippo pathway. It appeared that HIPPO signalling was unaffected by lorlatinib treatment in WT cells but was significantly downregulated by lorlatinib treatment in

DUSP6-null cells. This suggests that removal of DUSP6 potentially introduces a vulnerability in the HIPPO pathway to lorlatinib treatment. YAP/HIPPO signalling has been deemed an important driver in high-risk NB and therapy resistance (Shim and Goldsmith, 2021). Interestingly, a previous report demonstrates YAP1 promotes resistance to MEK inhibition in RAS-driven NB (Coggins et al., 2019). Furthermore, in ALK-rearranged lung cancer, targeting YAP-TAZ appears to overcome acquired ALK-inhibitor resistance (Tsuji et al., 2020). Together this suggests that there is cross-talk between YAP/TAZ and ALK-ERK signalling. Our data suggest that loss of DUSP6 promotes ALK signalling via the HIPPO pathway. A model of this regulation is presented in **Figure 6.27**. In support of this model, the 14-3-3 complex, known to bind and sequester YAP/TAZ function (Moon et al., 2017), is significantly upregulated after ALK inhibition in DUSP6-null cells (**Fig 6.24**). Furthermore, a recent study demonstrated that the molecular chaperone BAG3 aids YAP/TAZ translocation to the nucleus and activity and BAG3 was also significantly downregulated after depletion of DUSP6 (**Fig. 6.21C**) (Baldan et al., 2021). However, a difficulty with this model is the fact neither lorlatinib treatment nor DUSP6 knockout alone suppressed YAP/TAZ signalling in the IPA. This suggests after removal of DUSP6, there are molecular changes in KELLY cells which promote ALK-HIPPO signalling, or that there is redundancy between DUSP6 and ALK signalling, however the details of this mechanism are unclear. Furthermore, considering YAP/TAZ have a large pool of transcriptional targets, it is hard to glean from this phosphoproteomic analysis which YAP/TAZ targets could promote NB cell growth. In future, an investigation into the YAP/TAZ transcriptional targets in NB cells, either by qPCR, RNA-Seq or Chip-Seq would be very beneficial.

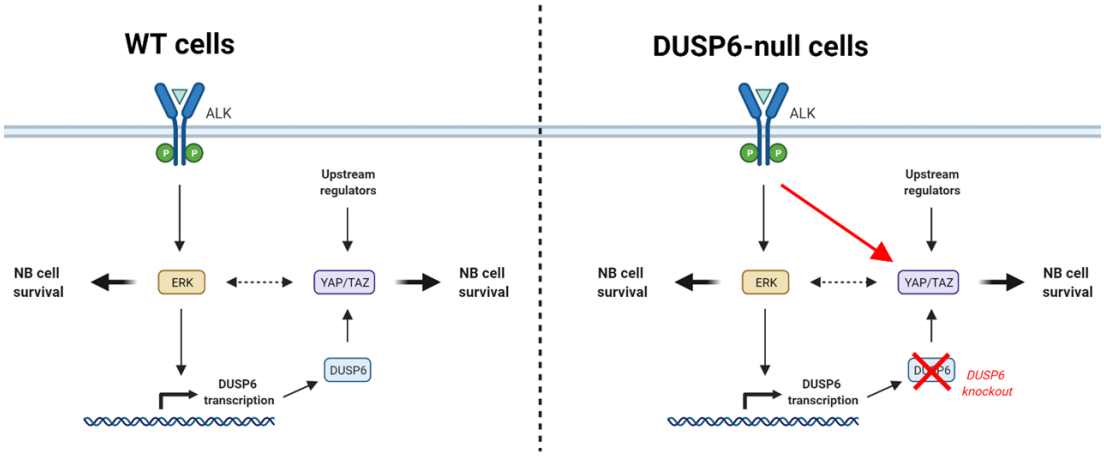

Figure 6.27 – Model speculating how loss of DUSP6 could promote ALK-HIPPO signalling. In this model, NB cell growth is driven independently via ALK and YAP/TAZ signalling. However, removal of DUSP6 promotes the ALK-HIPPO signalling pathway. Therefore lorlatinib treatment will be more effective as both pathways will be inhibited.

The goal of this chapter was to reveal the role of DUSPs in NB cells by manipulating signalling through the ALK oncoprotein. By targeting NB cells with ALK inhibitors, I hoped to identify DUSPs which were regulated by ALK. Furthermore, DUSPs that appeared part of the ALK-signalling pathway could be investigated further to determine whether they were important to ALK-mediated cell growth. It became evident that DUSP6 expression was under extremely tight control by ALK in ALK-mutated cell lines. We demonstrated that DUSP6 could be regulated by ALK in an ERK-dependent and -independent manner suggesting alternative pathways present within the same cell can regulate DUSP6 expression. CRISPR/Cas9-mediated inactivation of the *DUSP6* gene appeared to sensitise NB cell subclones to ALK inhibition, potentially revealing a co-dependency of NB cells to ALK and DUSP6 signalling. However, re-introduction of exogenous DUSP6 did not rescue the cell viability, putting this conclusion in doubt. Nevertheless, in the phosphoproteomic screen, loss of DUSP6 did indeed generate enhanced signalling changes when ALK is also inhibited (or vice versa) suggesting at least biochemically, DUSP6 is influencing ALK function. In the phosphoproteomic screen, loss of DUSP6 again did not affect ERK signalling, consistent with my previous findings, but a wide range of other pathways that were identified. For example, we demonstrated the RhoA and

HIPPO pathways are potentially regulated by DUSP6 downstream of ALK, as demonstrated by the models presented in **Figure 6.26** and **Figure 6.27**. Unfortunately, I have not had the time to test these hypotheses directly, but they serve as interesting starting points for future experiments. With resistance emerging to conventional ALK inhibitors, we hope that these current data reveal how these pathways are connected to ALK. This in turn could highlight new points of sensitivity in ALK signalling which could be targeted therapeutically.

Chapter 7. Concluding remarks

7.1. Summary of key findings

NB is an extracranial paediatric cancer that accounts for 7-10% of paediatric malignancies worldwide (Brodeur, 2003). A range of targeted molecular therapies are under investigation which seek to perturb signalling pathways believed to promote tumour progression (Greengard, 2018). Our group and others have demonstrated that PTP function is important to NB cell growth and that PTP inhibition can be detrimental to NB cell survival, or can promote neuronal differentiation (Clark et al., 2013, Clark et al., 2015, Boutterin et al., 2013, Tian et al., 2016). A previous shRNA screen performed in the laboratory had preliminarily evidence that several DUSP enzymes could potentially be growth-promoting (Dr. Ann Cichon, unpublished data). DUSPs are a family of PTPs that are implicated in a wide range of cancers (Low and Zhang, 2016, Gao et al., 2021). I hypothesised therefore that DUSPs may be an important class of enzymes that promote NB cell survival. Consequently, the overarching goal of this project was to investigate the role of DUSPs in NB cells and whether inhibition of DUSP function could be used to suppress NB cell growth.

Initially in **Chapter 3**, a large siRNA screen was performed across 4 NB cell lines to reveal 'oncogenic-like' DUSPs. In parallel, a cox regression analysis was performed to determine which DUSPs were independent predictors of NB cell survival. Together, these data identified a subset of DUSP candidates, namely DUSP3, DUSP4, DUSP6, DUSP10, DUSP12 and DUSP26, that merited further exploration. Considering there is significant literature surrounding the role of DUSP6 in cancer (reviewed in Ahmad et al. (2018)), I largely focussed on an investigation of how DUSP6 was involved in NB cell growth. Interestingly, DUSP6 siRNA pools also displayed cell specific effects which suggests the changes in cell viability are due to knockdown of the target. However, the DUSP6 siRNA pool was later demonstrated to be hampered with off-target toxicities. I created an efficient workflow to design effective gRNAs and this was employed to generate a range of DUSP6-null subclones. Loss of DUSP6 marginally reduced KELLY cell growth but not that of IMR-32 cells. Considering this correlates with the

cell ALK-status, the potential roles of DUSP6 downstream of ALK were investigated in **Chapter 6**. Loss of DUSP6 also did not appear to affect the MAPK signalling pathways, suggesting there are alternative DUSP6 substrates present in KELLY or IMR-32 cells. Furthermore, this suggested there were other DUSPs restraining ERK signalling in NB cells or that DUSPs cooperate to regulate ERK in a redundant fashion.

In parallel, the role of DUSP6 in NB was also investigated chemically in **Chapter 4** using a dual DUSP1/6 inhibitor, BCI. Initial results were promising as BCI and its analog BCI-215 displayed potent cytotoxicity in a range of NB cell lines. However, after careful analysis of these effects these inhibitors appeared to display major of-target toxicities, since BCI-mediated loss of cell viability was unaffected by depletion of DUSP1 and DUSP6 protein. Nonetheless, it is likely that biochemically both chemicals are still inhibiting DUSP1/6. A phosphoproteomic analysis demonstrated BCI triggers a strong JNK and mTOR response in KELLY and IMR-32 cells but it is unclear whether these result from DUSP1/6 inhibition or an off-target effect. It is therefore very unlikely that BCI could be considered as a therapeutic lead in NB until its targets and actions are fully defined.

In **Chapter 5** the remaining DUSP candidates identified in the siRNA screen were investigated further. For each gene, DUSP-null subclones were generated using CRISPR/Cas9. Unfortunately, the significant growth suppression by siRNA-mediated gene depletion was not reproduced by genetic deletion of each DUSP gene. However, the DUSP3 subclones showed reduced clonal growth capabilities compared with WT cells and one of the subclones displayed a reduced population growth rate. This might reflect reduced stem cell properties in the DUSP3-null cells.

Given the disparity between siRNA data and the DUSP-null clones, I became more concerned about siRNA off-targeting. Using these DUSP-null subclones, I went on to demonstrate that the siRNA pools from the siRNA screen indeed displayed significant off-target toxicities, similar to what was observed with the DUSP6 siRNA pool in **Chapter 3**. While the siRNA analysis in CRISPR clones was under way, I committed to a digenic study

by treating DUSP-null cells with DUSP siRNAs. These data suggested DUSP5 may promote IMR-32 cell growth in a DUSP6-dependent fashion, however due to the siRNA off-target effects, conclusions from the digenic study would need further validation.

Furthermore, we investigated whether the DUSPs individually target MAPK signalling. Surprisingly, very little difference in MAPK signalling was observed after knockdown of each MAPK phosphatase. This suggests that, similar to DUSP6, there are non-MAPK related pathways regulated by these phosphatase enzymes in NB cells. However, considering only individual DUSPs were knocked down, it is possible DUSPs still regulate ERK redundantly.

Lastly, in **Chapter 6** I investigated the role of DUSPs downstream of the ALK oncogene. I demonstrated ALK maintains the expression of a subset of DUSPs. As this was most pronounced for DUSP6, I decided to characterise the biochemical and phenotypic effect of DUSP6 depletion on ALK inhibition. ALK appeared to regulate DUSP6 gene expression in an ERK-dependent and -independent manner. Considering there are multiple transcription factor binding sites in the DUSP6 promoter region (Ekerot et al., 2008), there are various pathways through which ALK may alter DUSP6 transcription. Although loss of DUSP6 in certain instances sensitised cells to ALK inhibition, this was not rescued by re-introduction of exogenous DUSP6. Unfortunately, this suggests removing DUSP6 alone is unlikely to affect the potency of ALK-targeted therapies. Nonetheless, the biochemical effect of DUSP6 depletion was also investigated in a phosphoproteomic screen. There appeared to be significant co-dependency on DUSP6 and ALK signalling as inhibition of both produced numerous, novel phosphoproteomic changes that did not occur after independent pathway inhibition. Interestingly, these data demonstrated DUSP6 may promote RhoA or HIPPO signalling which could potentially influence ALK inhibition in NB cells.

7.2. Final discussion points

7.2.1. Comparing loss of function approaches

During this project, I sought to investigate the role of DUSPs using three loss-of-function approaches: chemical inhibition, siRNA-mediated gene knockdown and genetic disruption using CRISPR/Cas9. Unexpectedly, a common theme throughout the project was the identification of significant off-target effects. Treatment with BCI and siRNA pools caused off-target toxicities which were initially misinterpreted as genetic dependencies. These issues are discussed extensively in **Chapter 4.3** and **Chapter 5.3**. In both cases, experiments using the DUSP-null subclones were critical in characterising potential off-target toxicities. Indeed, previous reports have used CRISPR/Cas9 target KO to characterise off-target effects for small molecule inhibitors and RNAi chemicals (Huang et al., 2017, Niessen et al., 2017, Lin et al., 2019a). It appeared the CRISPR/Cas9 system did not display similar off-target effects, however unbiased whole genome sequencing and the use of additional independent gRNAs are required to confirm this (Zischewski et al., 2017). Unfortunately, these data revealed clear discrepancies from different LOF approaches, predominantly from false positives. In agreement with this, the Cancer Dependency Map (DepMap) portal also reveals discordance between CRISPR/Cas9 and RNAi-based gene disruption (Tsherniak et al., 2017). In the DepMap portal, RNAi and CRISPR screens performed on a wide range of cell lines have been systematically analysed to identify cellular dependencies. However, there are a number of genes which display different CRISPR and RNAi perturbation effects within the same cell line. For example, the perturbation effect of DUSP6 in various NB cell lines is plotted in **Figure 7.1** (KELLY cells highlighted grey). For each gene effect, the lower the score the higher the likelihood of dependency on that gene. Hence, similar to our data, the DepMap portal suggests KELLY cells are dependent on DUSP6 in the RNAi-based screen but not in the CRISPR/Cas9 screen. A disadvantage of the large-scale screens included in the DepMap portal is that they are based

on a phenotypic effect as opposed to a biochemical response. Nonetheless, the DEMETER2 analysis framework, used to generate the RNAi-based perturbation score (McFarland et al., 2018), is designed to segregate on- and off-target effects which should improve the reliability of the phenotypic response. It is also possible that the differences between CIRSPR/Cas9- and siRNA-mediated gene depletion stem not from off-target effects, but from the time taken to remove the DUSP protein. In my studies, siRNA treatments significantly depleted DUSP mRNA within 24 hours and cell viability was measured within 6 days. Conversely, the generation of the DUSP-null subclones and assessment of cell growth differences was a far longer process. The longer timeframe may result in intracellular changes not present after siRNA treatments. Alternatively, the cells may autoregulate to compensate for the changes in DUSP expression over the longer timeframe. Overall, these data demonstrate that results from RNAi-based gene knockdown or chemical inhibition should be validated using cells depleted of the target.

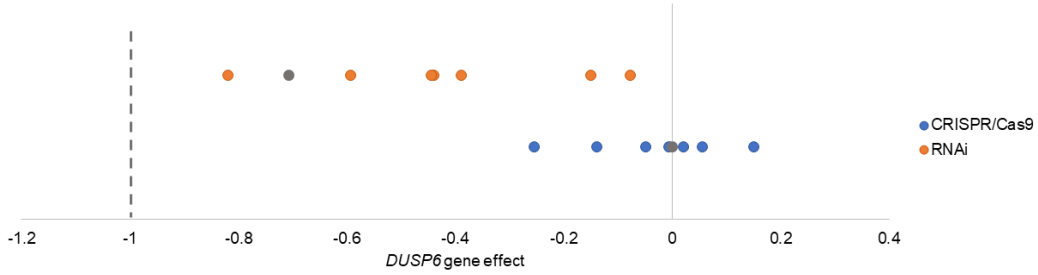

Figure 7.1 – Perturbation effect of *DUSP6* gene in a CRISPR/Cas9 or RNAi screen in NB cell lines. The closer a score is to -1 (grey dashed line), the more likely the cell line is dependent on the gene. KELLY cell line is in grey. RNAi and CRISPR/Cas9 score generated using the DEMETER2 (McFarland et al. 2018) and CHRONOS (Dempster et al., 2021) analytical framework, respectively. Data was downloaded from the DepMap portal (Tsherniak et al., 2017).

The alternative method which appeared to avoid these off-target toxicities was CRISPR/Cas9 gene editing. The DUSP-null subclones were useful tools to investigate protein function, however they often displayed disparate results within the same assay. As discussed in **Chapter 5**, this heterogeneity is averaged when using the inducible CRISPR system and is

why mixed populations containing indels in the *DUSP6* gene were used to determine the phenotypic and biochemical effect of DUSP6 depletion (**Chapter 3.2.6** and **Chapter 6.2.4**, respectively). Instead, subclones could be combined to form a pseudo mixed population. Or an alternative CRISPR/Cas9 technique such as CRISPR interference could be used (Gilbert et al., 2014). In this system, CRISPR/Cas9 targets the gene with a transcriptional repressor, leading to gene silencing with higher specificity than RNAi. Overall, CRISPR/Cas9 appears the most reliable tool to investigate protein LOF. However, there is some heterogeneity between clonal populations therefore multiple clones should be compared or mixed populations used.

7.2.2. The collective role of DUSPs in NB cells

The overarching aim of the project was to determine the function of DUSPs in NB cells and whether any are able to promote NB cell growth. Considering a small number of DUSPs appeared growth-promoting in a previous shRNA screen (Dr. Ann Cichon, unpublished data), I expected in my broad siRNA screen to find DUSPs that have a functional role in NB cells. Furthermore, hyper-activation of ERK signalling occurs frequently in NB, predominantly through mutation and amplification of the ALK gene, and DUSPs appear critical regulators of this pathway. This aim was split into two questions: (i) are DUSPs important to NB cell survival? And (ii) are DUSPs functionally important in regulating the MAPK and AKT signalling pathways in NB cells? Both of these questions were investigated using siRNA and genetic disruption in **Chapter 3** and **Chapter 5**.

Notwithstanding the aforementioned off-target toxicities using siRNAs, they still reduced target DUSP mRNA expression significantly. Hence, the DUSP genes that didn’t alter NB cell viability in that assay are likely unimportant to NB cell survival. It is worth noting that in a different assay or under different assay conditions DUSP gene dependencies could be revealed. Conclusions on which DUSPs could individually promote NB cell growth were taken from CRISPR/Cas9 studies. There were hints that a minority of

DUSPs could suppress NB cell growth. Within the mixed population, loss of DUSP6 mildly decreased NB cell growth, but only 1 out of 2 subclones displayed this effect. Similarly, 1 out of 2 DUSP3 subclones grew slower than WT cells and they also formed fewer and smaller colonies in a clonogenicity assay. Nonetheless, in both cases the growth effect appears marginal. Hence, there does not appear to be a DUSP that, at least individually, significantly regulates NB cell growth in these conditions.

The cox regression analysis demonstrated that *DUSP4* and *DUSP26* are independent predictors of cell survival in a tumour-promoting and -suppressing manner respectively. Considering both are able to dephosphorylate ERK, it was possible these DUSPs alter ERK signalling to regulate NB survival. However, the biochemical screen performed in the presence of FGF demonstrates it is unlikely any of the MKPs tested can individually regulate the MAPKs under basal conditions or after stimulation with FGF (although DUSP26 was not included in this screen and would be intriguing to investigate further). Loss of DUSP8 did induce a marginal increase in ERK signalling, however overall, there was not a statistically significant change by any of the DUSPs included. This was a surprising finding considering ERK signalling must be regulated somehow by dephosphorylation in NB cells. Previous reports demonstrate ERK can promote NB cell growth in both ALK-WT and ALK-mutated NB cells (Xie et al., 2019, Lopez-Delisle et al., 2018). Furthermore, RAF and MEK inhibition has been investigated in NB driven by ERK signalling with varying degrees of success (Coggins et al., 2019, Tanaka et al., 2016, Umapathy et al., 2017). This further reinforces that ERK signalling must be regulated in NB cells. One possible answer is that DUSPs function more as a network where they compensate for each other. I investigated this phenotypically in **Chapter 5**, where DUSPs were knocked down in cells already lacking DUSP4 or DUSP6 protein. Unfortunately, few obvious compensatory relationships, where loss of two DUSPs decreased cell viability more than each DUSP alone, were identified. There appeared a potential dependency of DUSP5 on DUSP6 in IMR-32 cells, a potential epistatic relationship. As mentioned in **Chapter 1.2**, DUSP5 and DUSP6 are believed to cooperate

to regulate ERK localisation and function (Caunt and Keyse, 2013). Indeed, loss of *DUSP6* can alter DUSP5 expression (and vice versa) in BRAF^{V600E} thyroid cancer cells. Furthermore, both the *DUSP5* and *DUSP6* promoters contain ETS-binding sites and can therefore potentially be regulated by similar ERK-related transcription factors (Buffet et al., 2015, Ekerot et al., 2008). Hence, it is possible DUSP6 expression is required at least partially for DUSP5 expression and function. This is supported by the fact that *DUSP5* and *DUSP6* gene expression display a strongly correlation in NB patients.

Nonetheless these data do not demonstrate how DUSPs could compensate for one another or act epistatically. There could potentially be a very high level of redundancy between DUSPs. To investigate this, sub-groups of DUSPs would have to be knocked down or removed genetically. A previous study by Caunt et al. (2008a) knocked down each DUSP sub family: nuclear inducible MKPs (DUSP1, -2, -4, and -5), cytoplasmic MKPs (DUSP6, -7, and -9), or the JNK/p38 MKPs (DUSP10 and -16) in HEK293 cells. They demonstrated that collectively, the nuclear inducible DUSPs inactivated and anchored ERK within the nucleus and suppressed ERK-mediated upregulation of EGR-1. Importantly, these effects were greater than that seen by knockdown of individual DUSPs. These data suggest a potential compensatory network of DUSPs could be revealed in NB cells if more DUSPs are targeted at once. Taken together, there are two important assays which should be performed in future. Firstly, the expression of DUSP genes should be investigated in DUSP KO cells. This would reveal likely candidates that are compensating for the targeted DUSP. Secondly, sub-families of DUSPs should be targeted in NB cells as this could reveal whether they collectively regulate MAPK signalling and NB cell growth. Given the off-target effect of siRNAs revealed here, a multiplexed CRISPR/Cas9 system would instead be a preferable approach. Indeed, a myriad of methods have recently been developed which allow multiple gRNA expression within the same cell (McCarty et al., 2020).

7.2.3. The function of DUSP6 in ALK-driven NB

DUSP6 has been implicated in tumorigenesis in a wide of cancers, with both tumour promoting and suppressing properties depending on the context (Reviewed in (Ahmad et al., 2018). Hence, a principle aim of the thesis was to investigate the biological and phenotypic consequence of targeting DUSP6 in NB cells. As mentioned previously, I demonstrated that loss of DUSP6 causes a marginal growth reduction in KELLY cells but not in IMR-32 cells (**Chapter 3**). This led me to hypothesise that DUSP6 is functionally important to cells with hyperactive ALK. I subsequently demonstrated that the expression of *DUSP4*, *DUSP5* and *DUSP6* were all maintained by ALK signalling (**Chapter 6**). This could be partly due to the ALK-ERK signalling axis. Indeed, treatment with a MEK inhibitor decreased DUSP6 expression. Furthermore, the level of pERK tracks with that of DUSP6 in four NB cell lines. Hence, it is likely that ERK regulates DUSP6 transcriptionally in NB cells. Nonetheless, at least in KELLY cells, I have shown for the first time that ALK can also regulate DUSP6 expression in an ERK-independent manner.

Having said this, all three LOF approaches (chemical inhibition, RNAi knockdown and genetic disruption) agree in that DUSP6 most likely does not regulate ERK in KELLY or IMR-32 cells, at least under basic culture conditions. In terms of chemical inhibition, BCI caused numerous changes in intracellular signalling (in immunoblots and the phosphoproteomic screen), but ERK signalling remained unaltered. Similarly, ERK signalling was unaffected after siRNA-mediated DUSP6 knockdown under both basal conditions and after stimulation with EGF. Furthermore, after genetic disruption of DUSP6 with CRISPR/Cas9, no convincing difference in ERK signalling was observed in DUSP6-null cells after ERK stimulation with EGF or inhibition with lorlatinib. As suggested in **Chapter 3**, it is still possible for DUSP6 to prevent ERK function by anchoring ERK in the cytoplasm (Karlsson et al., 2004). However, one would expect this to alter downstream targets of ERK in both the phosphoproteomic screens, which it does not.

Taken together, in KELLY and IMR-32 cells it is unlikely that DUSP6 regulates ERK.

It is worth mentioning that the only evidence suggesting DUSP6 does regulate ERK signalling is in AS cells. After treatment with cycloheximide and MG132, there was an inverse correlation between pERK and DUSP6. Interestingly, AS cells demonstrated the highest DUSP6 expression and DUSP6 protein is degraded the quickest after treatment with CHX (protein half life < 1hr). Therefore in this setting, DUSP6 may carry out fine-tuned regulation of ERK. Considering AS cells contain the gain of function $NRAS^{Q61K}$ mutation, further work is required to determine whether DUSP6 manipulation would suppress hyperactive RAS-ERK signalling.

Experiments performed in **Chapter 6.1** also revealed the sheer heterogeneity of intracellular signalling in different cell lines. Looking at the ALK-DUSP6 signalling axis alone, there were differences observed between each cell line (KELLY, IMR-32, AS, LAN-5, SH-SY5Y). Part of this is explained by their ALK-status. This is exemplified by a recent study that performed RNA-Sequencing, whole-exome sequencing and deep-targeted sequencing of up to 140 spatially and temporally distinct samples from 10 patients (Schmelz et al., 2021). Their data identified extensive heterogeneity between patients and within each tumour. This highlights the difficulty in generating molecular targeted therapies for NB as each tumour displays unique characteristics and is itself heterogenous in makeup.

The fact that ALK has such stringent regulation of DUSP6 expression suggests DUSP6 is functional in KELLY cells. Furthermore, sustained loss of DUSP6 clearly caused a wide range of intracellular changes, demonstrated in the phosphoproteomic screen, suggesting DUSP6 is a key regulator in the context of ALK signalling in KELLY cells. Although historically deemed an ERK-specific phosphatase, various other MAPK and non-MAPK targets have been identified (Lee et al., 2021, Ndong et al., 2014, Ma et al., 2020, Zhang et al., 2011, Hu et al., 2019). As discussed in **Chapter 3**, it is possible ERK could still interact with DUSP6 to promote DUSP6-mediated dephosphorylation of an alternative substrate (Zhang et

al., 2011). Interestingly, in the phosphoproteomic screen, either the loss of DUSP6 or ALK inhibition influenced many signalling pathways. However, importantly, ALK inhibition in the DUSP6-null cells either augmented or reversed many of these effects. For example, pGSK3 was downregulated by ALK inhibition and loss of DUSP6 but unaffected by ALK inhibition in DUSP6-null cells. This suggests there is a biochemical interaction between ALK and DUSP6 signalling. A model is presented in **Figure 7.2** as to how DUSP6 may function in ALK-mutated NB cells. Here, ALK and DUSP6 function in a cooperative and redundant fashion to regulate a myriad of pathways which in turn, promote NB cell growth. Loss of either DUSP6 or ALK signalling appears to suppress a combination of the pathways displayed (among others) and results in decreased NB cell growth. However, combined inhibition of both ALK and DUSP6 has a different effect on each of these pathways, which varies between pathway. Of course, the pathways and proteins highlighted in the model also regulate each other and are only a small subset of the pathways identified in the screen, therefore in reality there are likely many regulatory mechanisms at play. Nonetheless, suppression of DUSP6 and ALK together has a very different effect on these pathways than either treatment alone, suggesting DUSP6 is important to ALK signalling. The next step here is to identify the DUSP6 substrate(s) in KELLY cells. The phosphoproteomic dataset has identified numerous candidates which merit further exploration. Of particular interest are the pathways that are already implicated in NB cell growth, such as mTOR signalling (Segerström et al., 2011, Vaughan et al., 2016). Interestingly, BCI treatment also downregulated mTOR signalling, therefore further studies into how DUSP6 could regulate this pathway would be beneficial.

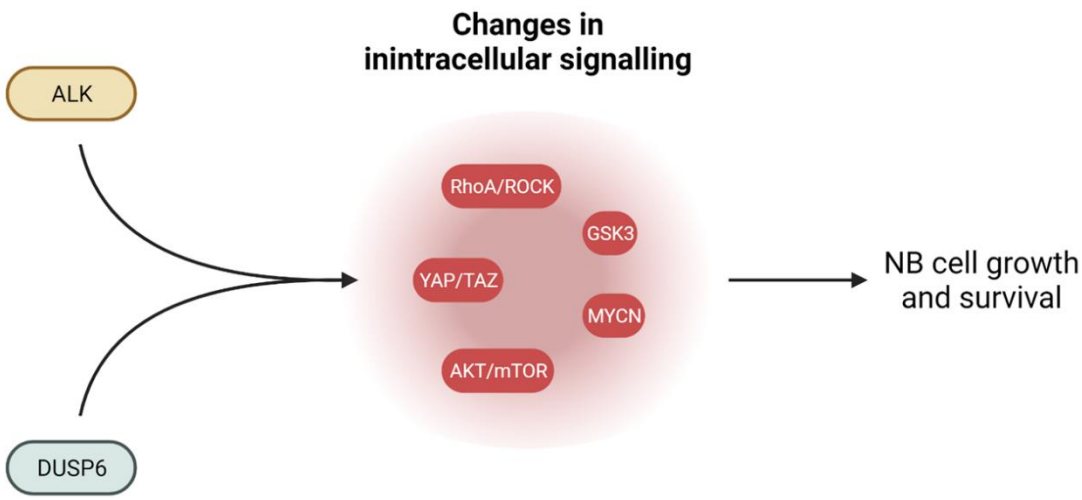

Figure 7.2 – Redundancy and cooperation of ALK and DUSP6 signalling promotes NB cell survival. In this model, DUSP6 and ALK promote NB cell growth and survival via a myriad of signalling pathways. Independently, ALK inhibition or loss of DUSP6 both affect many intracellular pathways (pathways of interest are presented in model). But crucially, ALK inhibition in DUSP6-null cells has a different effect on these pathways. Similarly, loss of DUSP6 or inhibition of ALK both suppress KELLY cell growth. ALK inhibition in the DUSP6-null subclones appears to augment NB cell death but this is potentially due to clonal variation.

Importantly, the data presented here identify a range of pathways that may be important to the ALK oncogene and could also be targeted therapeutically. There are a myriad of inhibitors which target distinct aspects of the RhoA/ROCK and YAP/TAZ signalling pathways (Shim and Goldsmith, 2021, Clayton and Ridley, 2020). I hope that these data will help identify alternative pathways, potentially regulated by DUSP6, that could serve as molecular targets in NB.

Overall, the number of DUSP substrates has significantly increased over the past decade. This has led to mounting evidence that DUSPs are important regulators of many cellular processes. Alongside this, many reports demonstrate deregulated DUSP function can have a detrimental role in a wide range of human cancers. Various reports highlight how DUSPs may influence pathways downstream of ALK, predominantly in *in vitro* models (reviewed in Nunes-Xavier et al. (2019b)). However, it is unclear what the DUSP targets are and whether DUSPs can be manipulated to suppress NB cell survival. My data suggest that individually, DUSPs do not

appear critical regulators of the MAPK pathways or of NB cell growth. However, there were hints that DUSPs may function more as a network in NB cells. Further experiments in 3D culture models or *in vivo* may uncover DUSP substrates could not be identified *in vitro*. Considering the broad range of known DUSP substrates (**Table 1.1**), testing other cancer properties such as cell invasiveness or migration may also reveal important DUSP functions. It will also be of significant interest to determine the role of DUSP6 downstream of ALK. Significant research is aimed at improving the efficacy of ALK inhibitors, by improved structural design or by testing combinations with other drugs. My data demonstrate ALK signalling is significantly affected in cells depleted of DUSP6 protein. Identifying what the molecular substrate(s) of DUSP6 are may reveal alternative pathways that could potentially be targeted in combination with ALK in future.

Appendices

Appendix 1 – Individual siRNA oligonucleotide sequences

Table A1 – Each individual siRNA sequence, its target name and source. Individual siRNAs used as pools were mixed at equimolar ratios.

Target gene	Sequence	Catalogue Number	Source
DUSP1	AGGAGGAUACGAAGCGUUU	J-003484-21	Dharmacon
DUSP1	UUUGUGAAGCAGAGGCGAA	J-003484-22	Dharmacon
DUSP1	GCUUACCUUAUGAGGACUA	J-003484-23	Dharmacon
DUSP1	CCAACCAUUUUGAGGGUCA	J-003484-24	Dharmacon
DUSP2	GGAGAUCAGUGCCUGGUUC	J-003565-06	Dharmacon
DUSP2	GUCCCGAUCUGUGCUCUGA	J-003565-07	Dharmacon
DUSP2	UCACAGCCGUCCUCAACGU	J-003565-08	Dharmacon
DUSP2	CGAGGCCUUUGACUUCGUU	J-003565-09	Dharmacon
DUSP4	GUACAUCGAUGCCGUGAAG	J-003963-07	Dharmacon
DUSP4	CAUCACGGCUCUGUUGAAU	J-003963-08	Dharmacon
DUSP4	GAAGGACACUAUCAGUACA	J-003963-09	Dharmacon
DUSP4	GGACUGCCCAAACCACUUU	J-003963-10	Dharmacon
DUSP5	GAGACUUUCUACUCGGAAU	J-003566-06	Dharmacon
DUSP5	UCACCUCGCUACUCGCUUG	J-003566-07	Dharmacon
DUSP5	AAACUGGGAUGGAGGAAUC	J-003566-08	Dharmacon
DUSP5	CCACUUUCAAGAAGCAAUA	J-003566-09	Dharmacon
DUSP6	GAACUGUGGUGUCUUGGUA	J-003964-06	Dharmacon
DUSP6	GACUGUGGCUUACCUUAUG	J-003964-07	Dharmacon
DUSP6	GGCAUUAGCCGCUCAGUCA	J-003964-08	Dharmacon
DUSP6	GAAAUGGCGAUCAGCAAGA	J-003964-09	Dharmacon
DUSP7	CAAGGUGGUUUCAACAAGU	J-003567-07	Dharmacon
DUSP7	GGACGUGCUCGGCAAGUAU	J-003567-08	Dharmacon
DUSP7	CAACGACGCCUACGACUUU	J-003567-09	Dharmacon
DUSP7	CUAAGCAGCCCGUGCGACA	J-003567-10	Dharmacon
DUSP8	CGACGACGCCUACAGGUUC	J-003568-05	Dharmacon
DUSP8	AACGACAACUACUGUGAAA	J-003568-06	Dharmacon
DUSP8	AAACAAGGAUCUGAUGACG	J-003568-07	Dharmacon
DUSP8	GUUCAUCGAUAAAGCCAAG	J-003568-08	Dharmacon
DUSP9	CGACUGCUCUGAUGCGGAA	J-003569-09	Dharmacon
DUSP9	CGAGAAGAAUGGUGACUUU	J-003569-10	Dharmacon
DUSP9	CAGGGAGGCUUCAGCAGAU	J-003569-11	Dharmacon
DUSP9	CCACCUCUCUCUCAACGAU	J-003569-12	Dharmacon
DUSP10	CAAAGGCAAACGACCAAUU	J-003965-06	Dharmacon

DUSP10	UGGAGACGGUUGUGUGACA	J-003965-07	Dharmacon
DUSP10	CGAGAAUCCUUACACCAAA	J-003965-08	Dharmacon
DUSP10	CAUGACUGAUGCUUAUAAA	J-003965-09	Dharmacon
DUSP16	GGUUGUAGUUUACGAUCAA	J-007890-05	Dharmacon
DUSP16	UGGGAUUGGUUAUGUGUUA	J-007890-06	Dharmacon
DUSP16	GGAGCGUGGAGGACAAUUA	J-007890-07	Dharmacon
DUSP16	GACAAAGUGUUAAUUACAG	J-007890-08	Dharmacon
DUSP3	UCACAUACCUGGGCAUCAA	J-007894-05	Dharmacon
DUSP3	UGAAAGGGCUGCCGACUUC	J-007894-06	Dharmacon
DUSP3	CAACACCAAUGCCAACUUC	J-007894-07	Dharmacon
DUSP3	GCUCUUAGUUCUUCAAGUA	J-007894-08	Dharmacon
DUSP11	GGUGGUAUCCUUAUAAUUA	J-007885-09	Dharmacon
DUSP11	GUACCCAGGUCAAGUGAUU	J-007885-10	Dharmacon
DUSP11	CCACUGUACCCAUGGUUUA	J-007885-11	Dharmacon
DUSP11	GGACCUAGGUAUAAUCUAC	J-007885-12	Dharmacon
DUSP12	CGAAGUGUGGCCAUAAUAA	J-007886-06	Dharmacon
DUSP12	GGGUUUGAGUGGCAACUGA	J-007886-07	Dharmacon
DUSP12	CAUGAAGACUGACCAACUU	J-007886-08	Dharmacon
DUSP12	GCACUGUCAUGCAGGAGUC	J-007886-09	Dharmacon
DUSP13	GUGCAGGCCCACCGCAAUA	J-007887-05	Dharmacon
DUSP13	GGACACAGGUGCCAAAUUC	J-007887-06	Dharmacon
DUSP13	GAAUGUCCCUGGAGUACUA	J-007887-07	Dharmacon
DUSP13	GGGCGGUUCUGAUCUGGCA	J-007887-08	Dharmacon
DUSP14	CCAUUGAGAUCCCUAAUUU	J-007888-09	Dharmacon
DUSP14	UUUGGGAAGUCGACAGUUA	J-007888-10	Dharmacon
DUSP14	GGCAUCACCUGCAUUGUUA	J-007888-11	Dharmacon
DUSP14	CCCGACACCUGAUGCCUUA	J-007888-12	Dharmacon
DUSP15	CGGCAAGUGAGGAUGCAGU	J-008484-07	Dharmacon
DUSP15	GCUUUAGGCAGCAGCUUGA	J-008484-08	Dharmacon
DUSP15	GGGCCAGUUCCCAGAAGCU	J-008484-09	Dharmacon
DUSP15	GUAUUAAAGAGACACAGAA	J-008484-10	Dharmacon
DUSP18	ACUAUGAGUUCCAAUUGUU	J-007891-05	Dharmacon
DUSP18	GAAUGAUCCCUGACAUCUA	J-007891-06	Dharmacon
DUSP18	GGAAGUCCGUUUGAUGAUU	J-007891-07	Dharmacon
DUSP18	CAAGAACACUGUGCACAUG	J-007891-08	Dharmacon
DUSP19	CAAUAAGUGUGACAGAAUA	J-007892-06	Dharmacon
DUSP19	CCAACAUCCUGUCUUAUUU	J-007892-07	Dharmacon
DUSP19	GAACAAACCUCAUUUACCA	J-007892-08	Dharmacon
DUSP19	UGACAACGCUAACUGGAAA	J-007892-09	Dharmacon
DUSP21	UUGCGUACCUCAUGAAAUA	J-007893-06	Dharmacon
DUSP21	UCAACUCGCCGGUAGGUAA	J-007893-07	Dharmacon
DUSP21	CUACAGCUUCUCCCAAAUA	J-007893-08	Dharmacon
DUSP21	GGAAGUGGUCAACGUAUUC	J-007893-09	Dharmacon
DUSP22	GCAUGAGGUCCAUCAGUAU	J-004517-09	Dharmacon
DUSP22	UGUUGGAGGGAGUUAAAUA	J-004517-10	Dharmacon
DUSP22	UGACACUGGUGAUCGCAUA	J-004517-11	Dharmacon
DUSP22	GCGGAACAAUUGAGCAAGA	J-004517-12	Dharmacon

DUSP23	AAGCAGUCUUCCAGUUCUA	J-007909-05	Dharmacon
DUSP23	GCACCAUGCUGGCCUGUUA	J-007909-06	Dharmacon
DUSP23	CCGACCAGAUCGACCGCUU	J-007909-07	Dharmacon
DUSP23	UGAAAUCCGACGACUACGA	J-007909-08	Dharmacon
DUSP26	GUAACUGGCUUUGGGCUUC	J-008027-09	Dharmacon
DUSP26	GGAAGAUCCUGGUGCAUUG	J-008027-10	Dharmacon
DUSP26	GGACAUGGCUAACAACCGC	J-008027-11	Dharmacon
DUSP26	CAACAUCCUUUCCUCAAUG	J-008027-12	Dharmacon
DUSP27	GCAUAGAGGUUGGCAGGUU	J-022081-05	Dharmacon
DUSP27	AUGAGGCGCUGCUGACUUA	J-022081-06	Dharmacon
DUSP27	GAGUCUAAAUCCUCCAGUU	J-022081-07	Dharmacon
DUSP27	ACACCAGCCUCUAUAAUAC	J-022081-08	Dharmacon
DUSP28	CGGAUUAGAUGUUGCUAUA	J-023179-17	Dharmacon
DUSP28	GCCUGAAAUCAUAAGAAUA	J-023179-18	Dharmacon
DUSP28	GGAUGUCCCUGCACUGAUA	J-023179-19	Dharmacon
DUSP28	CAUCAAAGGCAAGAGGGUU	J-023179-20	Dharmacon
Scrambled	UGGUUUACAUGUCGACUAA	D-001810-01	Dharmacon
Scrambled	UGGUUUACAUGUUGUGUGA	D-001810-02	Dharmacon
Scrambled	UGGUUUACAUGUUUUCUGA	D-001810-03	Dharmacon
Scrambled	UGGUUUACAUGUUUUCCUA	D-001810-04	Dharmacon
GAPDH	GUCAACGGAUUUGGUCGUA	D-001830-01	Dharmacon
GAPDH	CAACGGAUUUGGUCGUAUU	D-001830-12	Dharmacon
GAPDH	GACCUCAACUACAUGGUUU	D-001830-13	Dharmacon
GAPDH	UGGUUUACAUGUUCCAAUA	D-001830-14	Dharmacon
KIF11	UUCAGUUCUUACCAGUGUUGAUGGG	AM4639	Invitrogen

Appendix 2 – Phosphoproteomic analysis output

Two phosphoproteomic datasets were analysed in **Chapter 4** and **Chapter 6**. The raw mass spectrometry output was analysed consistently for both datasets by Dr. Vinothini Rajeeve and Prof. Pedro Cutillas at the Barts Cancer Institute (**Chapter 2.4.1**). This analysis resulted in a peptide intensity for each sample corresponding to a protein phosphorylation site. An example of this output from the DUSP6 depletion and ALK inhibition study in **Chapter 6.2.4** is presented in **Table A2** for the ERK1 Tyr204 phosphorylation site. Peptide intensities were then averaged and used to generate Log2-Fold Changes and a p-value for each pairwise comparison. P-values were generated by an independent samples t-test. The resulting Log2-Fold Change and p-value for the ERK1 Tyr204 phosphorylation site are presented in **Table A3**.

Table A2 – Peptide intensities for the ERK1 Tyr204 phosphopeptide. Example peptide intensity for the four replicates in each treatment condition for the p03928 peptide. This peptide corresponds to the ERK1 Tyr204 phosphorylation site.

Peptide ID	**2E2- (1)**	**2E2- (2)**	**2E2- (3)**	**2E2- (4)**	**2E2g4- (1)**	**2E2g4- (2)**	**2E2g4- (3)**	**2E2g4- (4)**
p03928	17.4	18.4	17.6	16.7	29	17.4	18.7	21.9
Peptide ID	**2E2+ (1)**	**2E2+ (2)**	**2E2+ (3)**	**2E2+ (4)**	**2E2g4+ (1)**	**2E2g4+ (2)**	**2E2g4+ (3)**	**2E2g4+ (4)**
p03928	3.92	2.77	7.07	6.08	4.05	3.61	0.0302	4.54

Table A3 – Log2-Fold Change and p-value for peptide p03928. An example output from the phosphoproteomic dataset where the Log2-Fold Change and p-value was calculated for peptide p03928 which corresponds to the ER1 Tyr204 phosphorylation site. Data was generated using the peptide intensities from **Table A2**. P-values were generated by an independent samples t-test.

	2E2- vs 2E2+	**2E2- vs 2E2g4-**	**2E2+ vs 2E2g4+**	**2E2g4- vs 2E2g4+**
Log2-Fold Change	-1.821	0.312	-2.519	-2.831
p-value	0.001	0.138	0.071	0.057

Appendix 3 – DUSP27 expression across NB cell lines

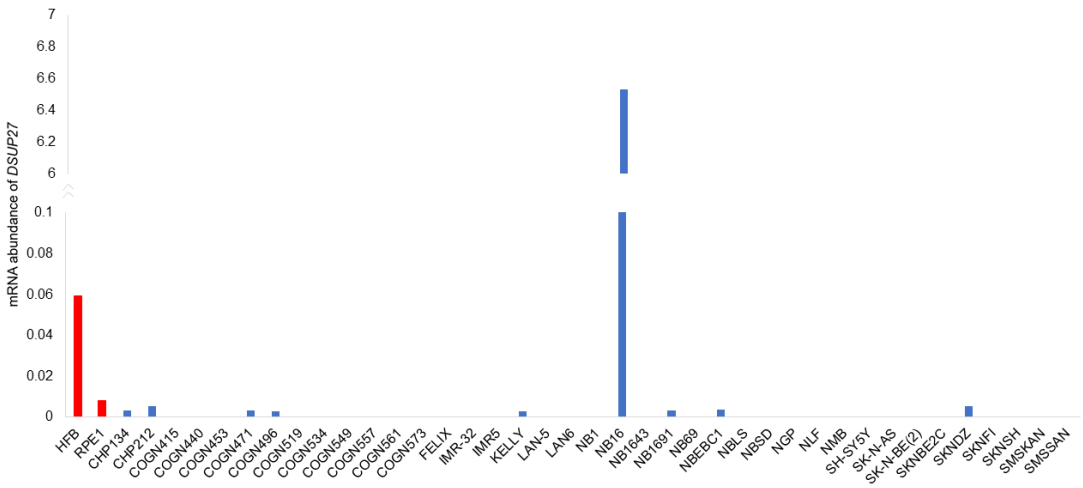

Figure A1 – MRNA expression of *DUSP27* across NB cell lines. Transcriptomic profiling of 39 commonly used NB cell lines, including many used within this project (IMR-32, KELLY, LAN-5, NB1, SK-N-AS, SK-N-BE(2) and SH-SY5Y). Control lines used were human fetal brain (HFB) and hTERT-immortalized retinal pigment epithelial cells (RPE-1), depicted in red. *DUSP27* mRNA is either not detected or very lowly expressed in the majority of cell lines assayed (Harenza et al., 2017).

Appendix 4 – Cell populations that derive from NB cell lines

iIMR-32	IMR-32 cells transfected with an inducible CRISPR-Cas9 vector
iKELLY	KELLY cells transfected with an inducible CRISPR-Cas9 vector
2E11	iIMR-32 cells treated with dox and single cell cloned for high Cas9 expression
2E2	iKELLY cells treated with dox and single cell cloned for high Cas9 expression
2E11g1	2E11 cells transfected with the DUSP6 g1 vector and selected with puromycin
2E11g3	2E11 cells transfected with the DUSP6 g3 vector and selected with puromycin
2E11g4	2E11 cells transfected with the DUSP6 g4 vector and selected with puromycin
2E2g1	2E2 cells transfected with the DUSP6 g1 vector and selected with puromycin
2E2g3	2E2 cells transfected with the DUSP6 g3 vector and selected with puromycin
2E2g4	2E2 cells transfected with the DUSP6 g4 vector and selected with puromycin
2F8	Subclone of 2E2g3 after dox treatment
3E9	Subclone of 2E2g3 after dox treatment
KELD3-1	KELLY cell subclone after transfection with the DUSP3 gRNA-Cas9 vector
KELD3-2	KELLY cell subclone after transfection with the DUSP3 gRNA-Cas9 vector
KELD4-1	KELLY cell subclone after co-transfection with a DUSP4 gRNA and Cas9 vector
KELD4-2	KELLY cell subclone after co-transfection with a DUSP4 gRNA and Cas9 vector
KELD6-1	Subclone of 2E2g4 after dox treatment
KELD6-2	Subclone of 2E2g4 after dox treatment
KELD6-3	Subclone of 2E2g4 after dox treatment

IMRD6-1 Subclone of 2E11g4 after dox treatment

KELD10-1 KELLY cell subclone after transfection with the DUSP10 gRNA-Cas9 vector

KELD10-2 KELLY cell subclone after transfection with the DUSP10 gRNA-Cas9 vector

KELD12-1 KELLY cell subclone after transfection with the DUSP12 gRNA-Cas9 vector

KELD12-2 KELLY cell subclone after transfection with the DUSP12 gRNA-Cas9 vector

KELD26-1 KELLY cell subclone after transfection with the DUSP26 gRNA-Cas9 vector

KELD26-2 KELLY cell subclone after transfection with the DUSP26 gRNA-Cas9 vector

KELD6-E KELLY cell subclone after transfection with the empty gRNA-Cas9 vector

KELD6-2-E KELD6-2 mixed population after transfection with the empty gRNA-Cas9 vector

KELD6-2-D6F KELD6-2 mixed population after transfection with the DUSP1 gRNA-Cas9 vector

Appendix 5 – Synergy maps for Bliss and Loewe models

A

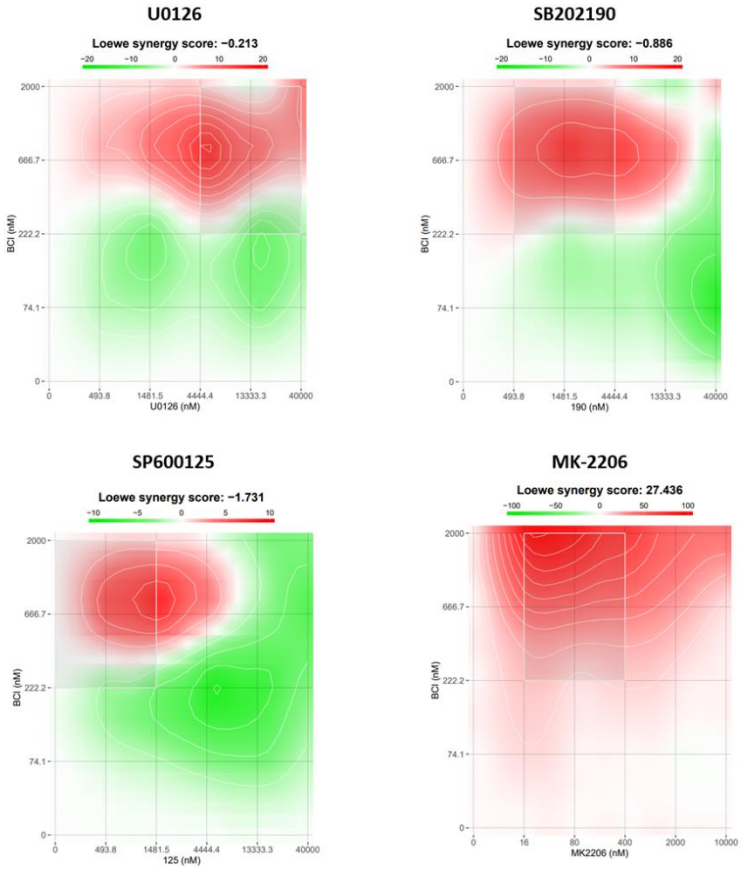

B

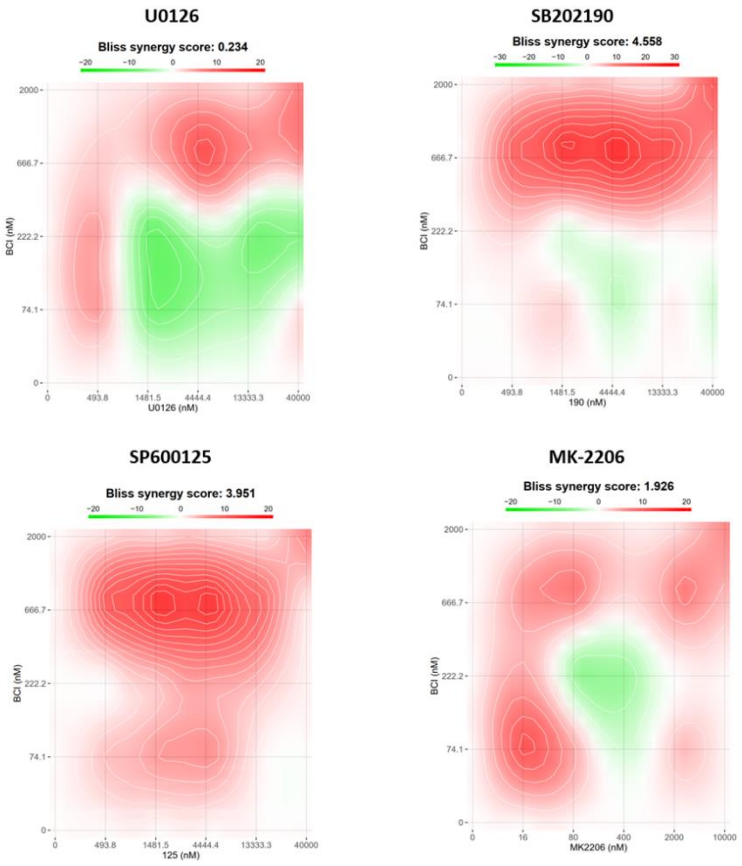

Figure A2 – A 2D synergy map using the Loewe and Bliss reference models. KELLY cells were treated with increasing concentrations of BCI concurrently with an ERK (U0126), AKT (MK-2206), JNK (SP600125) p38 (SB202190) inhibitor and cell survival was measured after 6 days using a resazurin assay. Data are presented in synergy maps using the (A) Loewe and (B) Bliss reference models. Data were normalised to cells treated with DMSO and then expressed as a mean ± SD (n = 3). Red regions depict synergy and green regions depict antagonism. A synergy score of >10 and <-10 is deemed synergistic and antagonistic respectively. Data generated using the SynergyFinder 2.0 tool (Ianevski et al., 2020).

Appendix 6 – Indels present in candidate DUSP-null subclones

```
A
DUSP3_WT        CTCACGCGTTGCCCACGTAGAT-CCGCGGGGTGACCTCGTTGCAGGGCTGGCTCG
KELD3_1         CTCACGCGTTGCCCACGTAGATCCCGCGGGGTGACCTCGTTGCAGGGCTGGCTCG
                ********************** ******************************

DUSP3_WT        CTCACGCGTTGCCCACGTAGAT-CCGCGGGGTGACCTCGTTGCAGGGCTGGCTCG
KELD3_2_alle_2  CTCACGCGTTGCCCACGTAGATCCCGCGGGGTGACCTCGTTGCAGGGCTGGCTCG
KELD3_2_alle_1  CTCACGCGTTGCCCACGTAGAT--CGCGGGGTGACCTCGTTGCAGGGCTGGCTCG
                **********************  *******************************

B
DUSP4_WT        GCACAGCGCGGGCTACATCCTAGGTTCGGTCAACGTGCGCTGTAACACCATCGTGC
KELD4_1         GCACAGCGCGGGCTACAT--AAGGTTCGGTCAACGTGCGCTGTAACACCATCGTGC
                ******************   **********************************

DUSP4_WT        GCACAGCGCGGGCTACATCCTAGGTTCGGTCAACGTGCGCTGTAACACCATCGTGC
KELD4_2         GCACAGCGCGGGCTACAT----GGTTCGGTCAACGTGCGCTGTAACACCATCGTGC
                *******************    **********************************

C
DUSP10_WT       AGGCTGCGAATCTGACGTATATGCCCTCATC-CAGCGGCTCTGCCCGCTCGCTGAATTGT
KELD10_1        AGGCTGCGAATCTGACGTATATGCCCTCATCGCAGCGGCTCTGCCCGCTCGCTGAATTGT
                ****************************** ****************************

DUSP10_WT       AGGCTGCGAATCTGACGTATATGCCCTCATCCAGCGGCTCTGCCCGCTCGCTGAATTGT
KELD10_2        AGGCTGCGAATCTGACGTATATGCCCTCAT-CAGCGGCTCTGCCCGCTCGCTGAATTGT
                ****************************** ****************************

D
DUSP12_WT       GAGGGCCGTGCGGTGTTGGTGCACTGGTGAGTGGCCGGGTCAGTGGGTGACGTGCCCC
KELD12_1_alle2  GAGGGCCGTGC----TTGGTGCACTGGTGAGTGGCCGGGTCAGTGGGTGACGTGCCCC
KELD12_1_alle1  GAGGGCCGTGC-----TGGTGCACTGGTGAGTGGCCGGGTCAGTGGGTGACGTGCCCC
                ***********     ****************************************

DUSP12_WT       GAGGGCCGTGC-GGTGTTGGTGCACTGGTGAGTGGCCGGGTCAGTGGGTGACGTGCCCC
KELD12_2_alle2  GAGGGCCGTGCGGGTGTTGGTGCACTGGTGAGTGGCCGGGTCAGTGGGTGACGTGCCCC
KELD12_2_alle1  GAGGGCCGTGC--GTGTTGGTGCACTGGTGAGTGGCCGGGTCAGTGGGTGACGTGCCCC
                ***********  *********************************************

E
DUSP26_WT       CACAGGCAAGACAGCCTGTAACCATGC--CGACGAGGTCTGGCCAGGCCTCTATCTCGG
KELD26_1_alle2  CACAGGCAAGACAGCCTGTAACCATGCCGCGACGAGGTCTGGCCAGGCCTCTATCTCGG
KELD26_1_alle1  CACAGGCAAGACAGCCTGTAAC---------ACGAGGTCTGGCCAGGCCTCTATCTCGG
                **********************         ****************************

DUSP26_WT       CACAGGCAAGACAGCCTGTAACCATGCCGACGAGGTCTGGCCAGGCCTCTATCTCGG
KELD26_2        CACAGGCAAGACAGCCTGTAACCATGC--ACGAGGTCTGGCCAGGCCTCTATCTCGG
                **************************  **************************
```

Figure A3 – Sequence alignment of the gRNA region of KELLY cells and the DUSP-null subclones. Sequencing of the gRNA region for the (A) DUSP3, (B) DUSP4, (C) DUSP10, (D) DUSP12 and (E) DUSP26 gene. For homozygous mutations only one sequence is shown whereas for hemizygous mutations both alleles are displayed.

Appendix 7 – Inverse correlations of pERK levels and DUSP6 expression in SK-N-AS cells

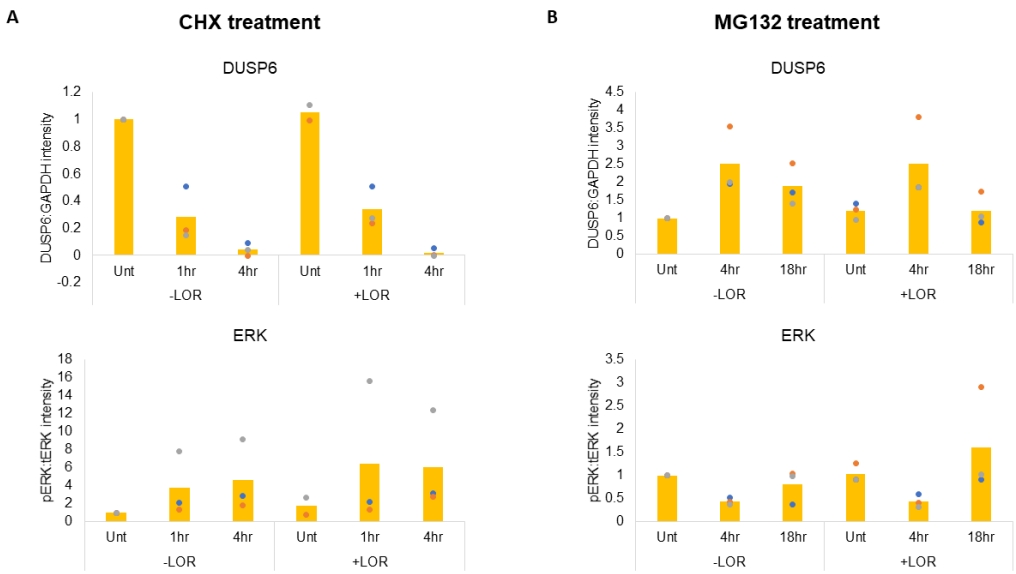

Figure A4 – Quantification of pERK levels and DUSP6 expression in SK-N-AS cells after CHX and MG132 treatment. (A) AS cells were treated with 40 µg/ml CHX for (A) 1 and 4 hours in the presence or absence of 30 nM lorlatinib (LOR) followed by immunoblotting for DUSP6 and pERK (n ≥ 2). (B) SK-N-AS cells were treated with 10 mM MG132 for 4 and 18 hours in the presence or absence of 30 nM lorlatinib (LOR) followed by immunoblotting for DUSP6 and pERK (n ≥ 3). pERK and DUSP6 were normalised to GAPDH and tERK respectively, followed by a second normalisation to untreated.

Appendix 8 – PI3K/AKT canonical pathway from IPA analysis

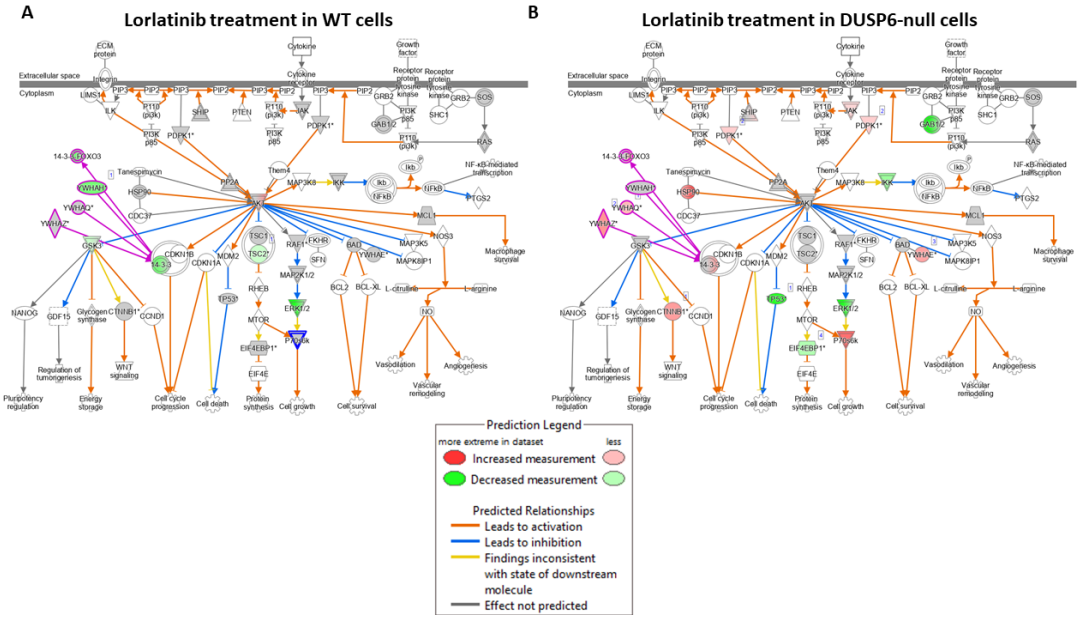

Figure A5 – PI3K/AKT signalling is downregulated by lorlatinib in DUSP6-null cells. Signalling via the PI3K/AKT pathway after treatment of lorlatinib in cells (A) with and (B) without DUSP6 protein. There is a downregulation of many proteins in DUSP6-null cells after treatment with lorlatinib. Arrow colours indicate predicted activation or inactivation based on identified changes to phosphoproteins (see key). Purple lines represent proteins within a protein family. Canonical pathways were generated in the IPA software.

References

ABDOLLAHI, P., VANDSEMB, E. N., HJORT, M. A., MISUND, K., HOLIEN, T., SPONAAS, A.-M., RØ, T. B., SLØRDAHL, T. S. & BØRSET, M. 2017. Src family kinases are regulated in multiple myeloma cells by phosphatase of regenerating liver-3. *Molecular Cancer Research,* 15**,** 69-77.

ADAMEYKO, I. & ERNFORS, P. 2014. Nerves transport stem-like cells generating parasympathetic neurons. *Cell Cycle,* 13**,** 2805-2806.

AHMAD, M. K., ABDOLLAH, N. A., SHAFIE, N. H., YUSOF, N. M. & RAZAK, S. R. A. 2018. Dual-specificity phosphatase 6 (DUSP6): a review of its molecular characteristics and clinical relevance in cancer. *Cancer Biol Med,* 15**,** 14-28.

AHMED, Z., LIN, C.-C., SUEN, K. M., MELO, F. A., LEVITT, J. A., SUHLING, K. & LADBURY, J. E. 2013. Grb2 controls phosphorylation of FGFR2 by inhibiting receptor kinase and Shp2 phosphatase activity. *Journal of Cell Biology,* 200**,** 493-504.

AKSAMITIENE, E., KHOLODENKO, B. N., KOLCH, W., HOEK, J. B. & KIYATKIN, A. 2010. PI3K/Akt-sensitive MEK-independent compensatory circuit of ERK activation in ER-positive PI3K-mutant T47D breast cancer cells. *Cellular signalling,* 22**,** 1369-1378.

AL-MUTAIRI, M. S., CADALBERT, L. C., MCGACHY, H. A., SHWEASH, M., SCHROEDER, J., KURNIK, M., SLOSS, C. M., BRYANT, C. E., ALEXANDER, J. & PLEVIN, R. 2010. MAP kinase phosphatase-2 plays a critical role in response to infection by Leishmania mexicana. *PLoS pathogens,* 6**,** e1001192.

ALCOLEA, M. P., CASADO, P., RODRÍGUEZ-PRADOS, J.-C., VANHAESEBROECK, B. & CUTILLAS, P. R. 2012. Phosphoproteomic analysis of leukemia cells under basal and drug-treated conditions identifies markers of kinase pathway activation and mechanisms of resistance. *Molecular & Cellular Proteomics,* 11**,** 453-466.

ALONSO, A., RAHMOUNI, S., WILLIAMS, S., VAN STIPDONK, M., JAROSZEWSKI, L., GODZIK, A., ABRAHAM, R. T., SCHOENBERGER, S. P. & MUSTELIN, T. 2003. Tyrosine phosphorylation of VHR phosphatase by ZAP-70. *Nature immunology,* 4**,** 44-48.

ALONSO, A., SASIN, J., BOTTINI, N., FRIEDBERG, I., FRIEDBERG, I., OSTERMAN, A., GODZIK, A., HUNTER, T., DIXON, J. & MUSTELIN, T. 2004. Protein tyrosine phosphatases in the human genome. *Cell,* 117**,** 699-711.

ALONSO, A., SAXENA, M., WILLIAMS, S. & MUSTELIN, T. 2001. Inhibitory role for dual specificity phosphatase VHR in T cell antigen receptor and CD28-induced Erk and Jnk activation. *Journal of Biological Chemistry,* 276**,** 4766-4771.

AMAND, M., ERPICUM, C., BAJOU, K., CERIGNOLI, F., BLACHER, S., MARTIN, M., DEQUIEDT, F., DRION, P., SINGH, P. & ZURASHVILI, T. 2014. DUSP3/VHR is a pro-angiogenic atypical dual-specificity phosphatase. *Molecular cancer,* 13**,** 1-18.

ANNENKOV, A. 2014. Receptor tyrosine kinase (RTK) signalling in the control of neural stem and progenitor cell (NSPC) development. *Molecular neurobiology,* 49**,** 440-471.

ANTTILA, J. V., SHUBIN, M., CAIRNS, J., BORSE, F., GUO, Q., MONONEN, T., VÁZQUEZ-GARCÍA, I., PULKKINEN, O. & MUSTONEN, V. 2019. Contrasting the impact of cytotoxic and cytostatic drug therapies on tumour progression. *PLoS computational biology,* 15**,** e1007493.

ARNOLDUSSEN, Y. J., LORENZO, P. I., PRETORIUS, M. E., WÆHRE, H., RISBERG, B., MÆLANDSMO, G. M., DANIELSEN, H. E. & SAATCIOGLU, F. 2008. The Mitogen-Activated Protein Kinase Phosphatase Vaccinia H1–Related Protein Inhibits Apoptosis in Prostate Cancer Cells and Is Overexpressed in Prostate Cancer. *Cancer research,* 68**,** 9255-9264.

ATTIYEH, E. F., LONDON, W. B., MOSSÉ, Y. P., WANG, Q., WINTER, C., KHAZI, D., MCGRADY, P. W., SEEGER, R. C., LOOK, A. T. & SHIMADA, H. 2005. Chromosome 1p and 11q deletions and outcome in neuroblastoma. *New England Journal of Medicine,* 353**,** 2243-2253.

AURTENETXE, O., ZALDUMBIDE, L., ERRAMUZPE, A., LÓPEZ, R., LÓPEZ, J. I., CORTÉS, J. M., PULIDO, R. & NUNES-XAVIER, C. E. 2018. DUSP5 expression associates with poor prognosis in human neuroblastoma. *Experimental and molecular pathology,* 105**,** 272-278.

BAKER, D. L., SCHMIDT, M. L., COHN, S. L., MARIS, J. M., LONDON, W. B., BUXTON, A., STRAM, D., CASTLEBERRY, R. P., SHIMADA, H. & SANDLER, A. 2010. Outcome after reduced chemotherapy for intermediate-risk neuroblastoma. *New England Journal of Medicine,* 363**,** 1313-1323.

BALDAN, S., MERIIN, A. B., YAGLOM, J., ALEXANDROV, I., VARELAS, X., XIAO, Z.-X. J. & SHERMAN, M. Y. 2021. The Hsp70–Bag3 complex modulates the phosphorylation and nuclear translocation of Hippo pathway protein Yap. *Journal of Cell Science,* 134**,** jcs259107.

BAR-SEVER, Z., BIASSONI, L., SHULKIN, B., KONG, G., HOFMAN, M. S., LOPCI, E., MANEA, I., KOZIOROWSKI, J., CASTELLANI, R. & BOUBAKER, A. 2018. Guidelines on nuclear medicine imaging in neuroblastoma. *European journal of nuclear medicine and molecular imaging,* 45**,** 2009-2024.

BARR, A. J. 2010. Protein tyrosine phosphatases as drug targets: strategies and challenges of inhibitor development. *Future medicinal chemistry,* 2**,** 1563-1576.

BARTOSZEWSKI, R. & SIKORSKI, A. F. 2019. Editorial focus: understanding off-target effects as the key to successful RNAi therapy. *Cellular & molecular biology letters,* 24**,** 1-23.

BAYÓN, Y. & ALONSO, A. 2010. Atypical DUSPs: 19 phosphatases in search of a role (Chap. 9). *Emerging Signaling Pathways in Tumor Biology. Transworld Research Network, Kerala, India*.

BEIERLE, E. A., MASSOLL, N. A., HARTWICH, J., KURENOVA, E. V., GOLUBOVSKAYA, V. M., CANCE, W. G., MCGRADY, P. & LONDON, W. B. 2008. Focal adhesion kinase expression in human neuroblastoma: immunohistochemical and real-time PCR analyses. *Clinical Cancer Research,* 14**,** 3299-3305.

BEISKE, K., BURCHILL, S., CHEUNG, I., HIYAMA, E., SEEGER, R., COHN, S., PEARSON, A. & MATTHAY, K. 2009. Consensus criteria for sensitive detection of

minimal neuroblastoma cells in bone marrow, blood and stem cell preparations by immunocytology and QRT-PCR: recommendations by the International Neuroblastoma Risk Group Task Force. *British journal of cancer,* 100**,** 1627-1637.

BELL, E., LUNEC, J. & TWEDDLE, D. 2007. Cell cycle regulation targets of MYCN identified by gene expression microarrays. *Cell cycle,* 6**,** 1249-1256.

BELL, E., PREMKUMAR, R., CARR, J., LU, X., LOVAT, P. E., KEES, U. R., LUNEC, J. & TWEDDLE, D. 2006. The role of MYCN in the failure of MYCN amplified neuroblastoma cell lines to G1 arrest after DNA damage. *Cell Cycle,* 5**,** 2639-2647.

BENTIRES-ALJ, M., PAEZ, J. G., DAVID, F. S., KEILHACK, H., HALMOS, B., NAOKI, K., MARIS, J. M., RICHARDSON, A., BARDELLI, A. & SUGARBAKER, D. J. 2004. Activating mutations of the noonan syndrome-associated SHP2/PTPN11 gene in human solid tumors and adult acute myelogenous leukemia. *Cancer research,* 64**,** 8816-8820.

BERMINGHAM JR, J. R., SHUMAS, S., WHISENHUNT, T., ROSENFELD, M. G. & SCHERER, S. S. 2001. Modification of representational difference analysis applied to the isolation of forskolin-regulated genes from Schwann cells. *Journal of neuroscience research,* 63**,** 516-524.

BERMUDEZ, O., MARCHETTI, S. & GIMOND, C. 2008. Post-translational regulation of the ERK phosphatase DUSP6/MKP3 by the mTOR pathway. *Oncogene,* 27**,** 3685-3691.

BERNARD-PIERROT, I., GRUEL, N., STRANSKY, N., VINCENT-SALOMON, A., REYAL, F., RAYNAL, V., VALLOT, C., PIERRON, G., RADVANYI, F. & DELATTRE, O. 2008. Characterization of the recurrent 8p11-12 amplicon identifies PPAPDC1B, a phosphatase protein, as a new therapeutic target in breast cancer. *Cancer research,* 68**,** 7165-7175.

BERRY, T., LUTHER, W., BHATNAGAR, N., JAMIN, Y., POON, E., SANDA, T., PEI, D., SHARMA, B., VETHAROY, W. R., HALLSWORTH, A., AHMAD, Z., BARKER, K., MOREAU, L., WEBBER, H., WANG, W., LIU, Q., PEREZ-ATAYDE, A., RODIG, S., CHEUNG, N. K., RAYNAUD, F., HALLBERG, B., ROBINSON, S. P., GRAY, N. S., PEARSON, A. D., ECCLES, S. A., CHESLER, L. & GEORGE, R. E. 2012. The ALK(F1174L) mutation potentiates the oncogenic activity of MYCN in neuroblastoma. *Cancer Cell,* 22**,** 117-30.

BLEEKER, G., TYTGAT, G. A., ADAM, J. A., CARON, H. N., KREMER, L. C., HOOFT, L. & VAN DALEN, E. C. 2015. 123I-MIBG scintigraphy and 18F-FDG-PET imaging for diagnosing neuroblastoma. *Cochrane Database of Systematic Reviews*.

BLEVINS, M. A., KOUZNETSOVA, J., KRUEGER, A. B., KING, R., GRINER, L. M., HU, X., SOUTHALL, N., MARUGAN, J. J., ZHANG, Q. & FERRER, M. 2015. Small molecule, NSC95397, inhibits the CtBP1-protein partner interaction and CtBP1-mediated transcriptional repression. *Journal of biomolecular screening,* 20**,** 663-672.

BLUME-JENSEN, P. & HUNTER, T. 2001. Oncogenic kinase signalling. *Nature,* 411**,** 355-365.

BOETTCHER, M., COVARRUBIAS, S., BITON, A., BLAU, J., WANG, H., ZAITLEN, N. & MCMANUS, M. T. 2019. Tracing cellular heterogeneity in pooled genetic screens via multi-level barcoding. *BMC genomics,* 20**,** 1-9.

BOLLU, L. R., MAZUMDAR, A., SAVAGE, M. I. & BROWN, P. H. 2017. Molecular pathways: targeting protein tyrosine phosphatases in cancer. *Clinical Cancer Research,* 23**,** 2136-2142.

BONHAM, C. A. & VACRATSIS, P. O. 2009. Redox regulation of the human dual specificity phosphatase YVH1 through disulfide bond formation. *Journal of Biological Chemistry,* 284**,** 22853-22864.

BONNEAU, D. & LONGY, M. 2000. Mutations of the human PTEN gene. *Human mutation,* 16**,** 109-122.

BORENÄS, M., UMAPATHY, G., LAI, W. Y., LIND, D. E., WITEK, B., GUAN, J., MENDOZA-GARCIA, P., MASUDI, T., CLAEYS, A. & CHUANG, T. P. 2021. ALK ligand ALKAL2 potentiates MYCN-driven neuroblastoma in the absence of ALK mutation. *The EMBO journal,* 40**,** e105784.

BOULDING, T., WU, F., MCCUAIG, R., DUNN, J., SUTTON, C. R., HARDY, K., TU, W., BULLMAN, A., YIP, D. & DAHLSTROM, J. E. 2016. Differential roles for DUSP family members in epithelial-to-mesenchymal transition and cancer stem cell regulation in breast cancer. *PloS one,* 11**,** e0148065.

BOUTTERIN, M., MAZOT, P., FAURE, C., DOLY, S., GERVASI, N., TREMBLAY, M. & VIGNY, M. 2013. Control of ALK (wild type and mutated forms) phosphorylation: specific role of the phosphatase PTP1B. *Cellular signalling,* 25**,** 1505-1513.

BOWES, J., BROWN, A. J., HAMON, J., JAROLIMEK, W., SRIDHAR, A., WALDRON, G. & WHITEBREAD, S. 2012. Reducing safety-related drug attrition: the use of in vitro pharmacological profiling. *Nature reviews Drug discovery,* 11**,** 909-922.

BOWN, N., COTTERILL, S., ŁASTOWSKA, M., O'NEILL, S., PEARSON, A. D., PLANTAZ, D., MEDDEB, M., DANGLOT, G., BRINKSCHMIDT, C. & CHRISTIANSEN, H. 1999. Gain of chromosome arm 17q and adverse outcome in patients with neuroblastoma. *New England Journal of Medicine,* 340**,** 1954-1961.

BRENNER, A. K. & GUNNES, M. W. 2021. Therapeutic Targeting of the Anaplastic Lymphoma Kinase (ALK) in Neuroblastoma—A Comprehensive Update. *Pharmaceutics,* 13**,** 1427.

BRESLER, S. C., WEISER, D. A., HUWE, P. J., PARK, J. H., KRYTSKA, K., RYLES, H., LAUDENSLAGER, M., RAPPAPORT, E. F., WOOD, A. C. & MCGRADY, P. W. 2014. ALK mutations confer differential oncogenic activation and sensitivity to ALK inhibition therapy in neuroblastoma. *Cancer cell,* 26**,** 682-694.

BRESLER, S. C., WOOD, A. C., HAGLUND, E. A., COURTRIGHT, J., BELCASTRO, L. T., PLEGARIA, J. S., COLE, K., TOPOROVSKAYA, Y., ZHAO, H. & CARPENTER, E. L. 2011. Differential inhibitor sensitivity of anaplastic lymphoma kinase variants found in neuroblastoma. *Science translational medicine,* 3**,** 108ra114-108ra114.

BRODEUR, G. M. 2003. Neuroblastoma: biological insights into a clinical enigma. *Nature reviews cancer,* 3**,** 203.

BRODEUR, G. M. & BAGATELL, R. 2014. Mechanisms of neuroblastoma regression. *Nature reviews Clinical oncology,* 11**,** 704-713.

BRODEUR, G. M., PRITCHARD, J., BERTHOLD, F., CARLSEN, N., CASTEL, V., CASTELBERRY, R., DE BERNARDI, B., EVANS, A. E., FAVROT, M. & HEDBORG, F. 1993. Revisions of the international criteria for neuroblastoma diagnosis, staging, and response to treatment. *Journal of clinical oncology,* 11**,** 1466-1477.

BRODEUR, G. M., SEEGER, R. C., SCHWAB, M., VARMUS, H. E. & BISHOP, J. M. 1984. Amplification of N-myc in untreated human neuroblastomas correlates with advanced disease stage. *Science,* 224**,** 1121-1124.

BRYNCZKA, C., LABHART, P. & MERRICK, B. A. 2007. NGF-mediated transcriptional targets of p53 in PC12 neuronal differentiation. *BMC genomics,* 8**,** 1-17.

BUFFET, C., CATELLI, M.-G., HECALE-PERLEMOINE, K., BRICAIRE, L., GARCIA, C., GALLET-DIERICK, A., RODRIGUEZ, S., CORMIER, F. & GROUSSIN, L. 2015. Dual specificity phosphatase 5, a specific negative regulator of ERK signaling, is induced by serum response factor and Elk-1 transcription factor. *PloS one,* 10**,** e0145484.

BUFFET, C., HECALE-PERLEMOINE, K., BRICAIRE, L., DUMONT, F., BAUDRY, C., TISSIER, F., BERTHERAT, J., COCHAND-PRIOLLET, B., RAFFIN-SANSON, M.-L. & CORMIER, F. 2017. DUSP5 and DUSP6, two ERK specific phosphatases, are markers of a higher MAPK signaling activation in BRAF mutated thyroid cancers. *PloS one,* 12.

BUNONE, G., BORRELLO, M. G., PICETTI, R., BONGARZONE, I., PEVERALI, F. A., DE FRANCISCIS, V., DELLA VALLE, G. & PIEROTTI, M. A. 1995. Induction of RET proto-oncogene expression in neuroblastoma cells precedes neuronal differentiation and is not mediated by protein synthesis. *Experimental cell research,* 217**,** 92-99.

CAI, C., HU, W., ZHANG, Y., HU, X., YANG, S., QIU, H., WANG, R., MA, M., QIU, Y. & CHU, T. 2021. BCI Suppresses RANKL-Mediated Osteoclastogenesis and Alleviates Ovariectomy-Induced Bone Loss. *Frontiers in pharmacology,* 12.

CAIN, E. L. & BEESER, A. 2013. Emerging Roles of Atypical Dual Specificity Phosphatases in Cancer. *Oncogene and Cancer-From Bench to Clinic,* 93.

CAMPS, M., NICHOLS, A., GILLIERON, C., ANTONSSON, B., MUDA, M., CHABERT, C., BOSCHERT, U. & ARKINSTALL, S. 1998. Catalytic activation of the phosphatase MKP-3 by ERK2 mitogen-activated protein kinase. *Science,* 280**,** 1262-1265.

CAO, S., MURPHY, B. T., FOSTER, C., LAZO, J. S. & KINGSTON, D. G. 2009. Bioactivities of simplified adociaquinone B and naphthoquinone derivatives against Cdc25B, MKP-1, and MKP-3 phosphatases. *Bioorganic & medicinal chemistry,* 17**,** 2276-2281.

CAPASSO, M., DISKIN, S. J., TOTARO, F., LONGO, L., MARIANO, M. D., RUSSO, R., CIMMINO, F., HAKONARSON, H., TONINI, G. P. & DEVOTO, M. 2013. Replication of GWAS-identified neuroblastoma risk loci strengthens the role of BARD1 and affirms the cumulative effect of genetic variations on disease susceptibility. *Carcinogenesis,* 34**,** 605-611.

CARÉN, H., ABEL, F., KOGNER, P. & MARTINSSON, T. 2008. High incidence of DNA mutations and gene amplifications of the ALK gene in advanced sporadic neuroblastoma tumours. *Biochemical Journal,* 416**,** 153-159.

CARÉN, H., DJOS, A., NETHANDER, M., SJÖBERG, R.-M., KOGNER, P., ENSTRÖM, C., NILSSON, S. & MARTINSSON, T. 2011. Identification of epigenetically regulated genes that predict patient outcome in neuroblastoma. *BMC cancer,* 11**,** 1-11.

CARR-WILKINSON, J., O'TOOLE, K., WOOD, K. M., CHALLEN, C. C., BAKER, A. G., BOARD, J. R., EVANS, L., COLE, M., CHEUNG, N.-K. V. & BOOS, J. 2010. High frequency of p53/MDM2/p14ARF pathway abnormalities in relapsed neuroblastoma. *Clinical cancer research,* 16**,** 1108-1118.

CARRACEDO, A., MA, L., TERUYA-FELDSTEIN, J., ROJO, F., SALMENA, L., ALIMONTI, A., EGIA, A., SASAKI, A. T., THOMAS, G. & KOZMA, S. C. 2008. Inhibition of mTORC1 leads to MAPK pathway activation through a PI3K-dependent feedback loop in human cancer. *The Journal of clinical investigation,* 118**,** 3065-3074.

CASADO, P., RODRIGUEZ-PRADOS, J.-C., COSULICH, S. C., GUICHARD, S., VANHAESEBROECK, B., JOEL, S. & CUTILLAS, P. R. 2013. Kinase-substrate enrichment analysis provides insights into the heterogeneity of signaling pathway activation in leukemia cells. *Science signaling,* 6**,** rs6-rs6.

CASTEL, V., VILLAMÓN, E., CAÑETE, A., NAVARRO, S., RUIZ, A., MELERO, C., HERRERO, A., YÁÑEZ, Y. & NOGUERA, R. 2010. Neuroblastoma in adolescents: genetic and clinical characterisation. *Clinical and Translational Oncology,* 12**,** 49-54.

CASTELLI, M., CAMPS, M., GILLIERON, C., LEROY, D., ARKINSTALL, S., ROMMEL, C. & NICHOLS, A. 2004. MAP kinase phosphatase 3 (MKP3) interacts with and is phosphorylated by protein kinase CK2α. *Journal of Biological Chemistry,* 279**,** 44731-44739.

CAUNT, C. J., ARMSTRONG, S. P., RIVERS, C. A., NORMAN, M. R. & MCARDLE, C. A. 2008a. Spatiotemporal regulation of ERK2 by dual specificity phosphatases. *Journal of Biological Chemistry,* 283**,** 26612-26623.

CAUNT, C. J. & KEYSE, S. M. 2013. Dual-specificity MAP kinase phosphatases (MKPs): shaping the outcome of MAP kinase signalling. *FEBS J,* 280**,** 489-504.

CAUNT, C. J., RIVERS, C. A., CONWAY-CAMPBELL, B. L., NORMAN, M. R. & MCARDLE, C. A. 2008b. Epidermal Growth Factor Receptor and Protein Kinase C Signaling to ERK2 SPATIOTEMPORAL REGULATION OF ERK2 BY DUAL SPECIFICITY PHOSPHATASES. *Journal of Biological Chemistry,* 283**,** 6241-6252.

CAZES, A., LOPEZ-DELISLE, L., TSAROVINA, K., PIERRE-EUGÈNE, C., DE PRETER, K., PEUCHMAUR, M., NICOLAS, A., PROVOST, C., LOUIS-BRENNETOT, C. & DAVEAU, R. 2014. Activated Alk triggers prolonged neurogenesis and Ret upregulation providing a therapeutic target in ALK-mutated neuroblastoma. *Oncotarget,* 5**,** 2688.

CHAKRABARTI, A. M., HENSER-BROWNHILL, T., MONSERRAT, J., POETSCH, A. R., LUSCOMBE, N. M. & SCAFFIDI, P. 2019. Target-specific precision of CRISPR-mediated genome editing. *Molecular cell,* 73**,** 699-713. e6.

CHAN, D. W., LIU, V. W., TSAO, G. S., YAO, K.-M., FURUKAWA, T., CHAN, K. K. & NGAN, H. Y. 2008. Loss of MKP3 mediated by oxidative stress enhances tumorigenicity and chemoresistance of ovarian cancer cells. *Carcinogenesis,* 29**,** 1742-1750.

CHANG, H.-H., LU, M.-Y., YANG, Y.-L., CHOU, S.-W., LIN, D.-T., LIN, K.-H., HSU, W.-M., JENG, Y.-M. & JOU, S.-T. 2019. The prognostic roles of and correlation between ALK and MYCN protein expression in neuroblastoma. *Journal of clinical pathology***,** jclinpath-2019-206063.

CHANG, J. H., MELLON, E., SCHANEN, N. C. & TWISS, J. L. 2003. Persistent TrkA activity is necessary to maintain transcription in neuronally differentiated PC12 cells. *Journal of Biological Chemistry,* 278**,** 42877-42885.

CHANG, M.-Y., RHEE, Y.-H., YI, S.-H., LEE, S.-J., KIM, R.-K., KIM, H., PARK, C.-H. & LEE, S.-H. 2014. Doxycycline enhances survival and self-renewal of human pluripotent stem cells. *Stem cell reports,* 3**,** 353-364.

CHANTHERY, Y. H., GUSTAFSON, W. C., ITSARA, M., PERSSON, A., HACKETT, C. S., GRIMMER, M., CHARRON, E., YAKOVENKO, S., KIM, G. & MATTHAY, K. K. 2012. Paracrine signaling through MYCN enhances tumor-vascular interactions in neuroblastoma. *Science translational medicine,* 4**,** 115ra3-115ra3.

CHEN, H.-F., CHUANG, H.-C. & TAN, T.-H. 2019. Regulation of dual-specificity phosphatase (DUSP) ubiquitination and protein stability. *International journal of molecular sciences,* 20**,** 2668.

CHEN, H.-H., LUCHE, R., WEI, B. & TONKS, N. K. 2004. Characterization of two distinct dual specificity phosphatases encoded in alternative open reading frames of a single gene located on human chromosome 10q22. 2. *Journal of Biological Chemistry,* 279**,** 41404-41413.

CHEN, K., LV, F., XU, G., ZHANG, M., WU, Y. & WU, Z. 2016a. Phosphoproteomics reveals ALK promote cell progress via RAS/JNK pathway in neuroblastoma. *Oncotarget,* 7**,** 75968.

CHEN, L., HUMPHREYS, A., TURNBULL, L., BELLINI, A., SCHLEIERMACHER, G., SALWEN, H., COHN, S. L., BOWN, N. & TWEDDLE, D. A. 2016b. Identification of different ALK mutations in a pair of neuroblastoma cell lines established at diagnosis and relapse. *Oncotarget,* 7**,** 87301.

CHEN, X., XIA, S., LI, R., LIU, H., HUANG, Y., QIAN, X., XIAO, X., XU, X., LIN, X. & TIAN, Y. 2009a. Doxycycline enhances the Ras-MAPK signaling and proliferation of mouse thymic epithelial cells. *Journal of cellular biochemistry,* 107**,** 494-503.

CHEN, Y.-N. P., LAMARCHE, M. J., CHAN, H. M., FEKKES, P., GARCIA-FORTANET, J., ACKER, M. G., ANTONAKOS, B., CHEN, C. H.-T., CHEN, Z. & COOKE, V. G. 2016c. Allosteric inhibition of SHP2 phosphatase inhibits cancers driven by receptor tyrosine kinases. *Nature,* 535**,** 148-152.

CHEN, Y., CHOU, H., YANG, C., CHEN, H., LIU, Y., LIN, T., YEH, C., CHAO, W., TSOU, H. & CHUANG, H. 2017. Deficiency in VHR/DUSP3, a suppressor of focal adhesion kinase, reveals its role in regulating cell adhesion and migration. *Oncogene,* 36**,** 6509-6517.

CHEN, Y., TAKITA, J., CHOI, Y. L., KATO, M., OHIRA, M., SANADA, M., WANG, L., SODA, M., KIKUCHI, A. & IGARASHI, T. 2008. Oncogenic mutations of ALK kinase in neuroblastoma. *Nature,* 455**,** 971.

CHEN, Y., TAKITA, J., HIWATARI, M., IGARASHI, T., HANADA, R., KIKUCHI, A., HONGO, T., TAKI, T., OGASAWARA, M. & SHIMADA, A. 2006. Mutations of the PTPN11 and RAS genes in rhabdomyosarcoma and pediatric hematological malignancies. *Genes, Chromosomes and Cancer,* 45**,** 583-591.

CHEN, Z., LIN, Y., BARBIERI, E., BURLINGAME, S., HICKS, J., LUDWIG, A. & SHOHET, J. M. 2009b. Mdm2 deficiency suppresses MYCN-Driven neuroblastoma tumorigenesis in vivo. *Neoplasia,* 11**,** 753-762.

CHESLER, L., GOLDENBERG, D. D., COLLINS, R., GRIMMER, M., KIM, G. E., TIHAN, T., NGUYEN, K., YAKOVENKO, S., MATTHAY, K. K. & WEISS, W. A. 2008. Chemotherapy-induced apoptosis in a transgenic model of neuroblastoma proceeds through p53 induction. *Neoplasia,* 10**,** 1268-IN34.

CHESLER, L., SCHLIEVE, C., GOLDENBERG, D. D., KENNEY, A., KIM, G., MCMILLAN, A., MATTHAY, K. K., ROWITCH, D. & WEISS, W. A. 2006. Inhibition of phosphatidylinositol 3-kinase destabilizes Mycn protein and blocks malignant progression in neuroblastoma. *Cancer research,* 66**,** 8139-8146.

CHEUNG, N.-K. V., CHEUNG, I. Y., KUSHNER, B. H., OSTROVNAYA, I., CHAMBERLAIN, E., KRAMER, K. & MODAK, S. 2012a. Murine anti-GD2 monoclonal antibody 3F8 combined with granulocyte-macrophage colony-stimulating factor and 13-cis-retinoic acid in high-risk patients with stage 4 neuroblastoma in first remission. *Journal of clinical oncology,* 30**,** 3264.

CHEUNG, N.-K. V., ZHANG, J., LU, C., PARKER, M., BAHRAMI, A., TICKOO, S. K., HEGUY, A., PAPPO, A. S., FEDERICO, S. & DALTON, J. 2012b. Association of age at diagnosis and genetic mutations in patients with neuroblastoma. *Jama,* 307**,** 1062-1071.

CHITALE, D., GONG, Y., TAYLOR, B. S., BRODERICK, S., BRENNAN, C., SOMWAR, R., GOLAS, B., WANG, L., MOTOI, N. & SZOKE, J. 2009. An integrated genomic analysis of lung cancer reveals loss of DUSP4 in EGFR-mutant tumors. *Oncogene,* 28**,** 2773-2783.

CHITRANSHI, N., DHEER, Y., GUPTA, V., ABBASI, M., MIRZAEI, M., YOU, Y., CHUNG, R., GRAHAM, S. L. & GUPTA, V. 2017. PTPN11 induces endoplasmic stress and apoptosis in SH-SY5Y cells. *Neuroscience,* 364**,** 175-189.

CHOI, Y. L., SODA, M., YAMASHITA, Y., UENO, T., TAKASHIMA, J., NAKAJIMA, T., YATABE, Y., TAKEUCHI, K., HAMADA, T. & HARUTA, H. 2010. EML4-ALK mutations in lung cancer that confer resistance to ALK inhibitors. *New England Journal of Medicine,* 363**,** 1734-1739.

CHU, C., RASALKAR, D., HU, Y., CHENG, F., LI, C. & CHU, W. 2011. Clinical presentations and imaging findings of neuroblastoma beyond abdominal mass and a review of imaging algorithm. *The British journal of radiology,* 84**,** 81-91.

CLAEYS, S., DENECKER, G., DURINCK, K., DECAESTEKER, B., MUS, L. M., LOONTIENS, S., VANHAUWAERT, S., ALTHOFF, K., WIGERUP, C. & BEXELL, D. 2019. ALK positively regulates MYCN activity through repression of HBP1 expression. *Oncogene,* 38**,** 2690.

CLARK, O., DAGA, S. & STOKER, A. W. 2013. Tyrosine phosphatase inhibitors combined with retinoic acid can enhance differentiation of neuroblastoma cells and trigger ERK-and AKT-dependent, p53-independent senescence. *Cancer letters,* 328**,** 44-54.

CLARK, O., PARK, I., DI FLORIO, A., CICHON, A.-C., RUSTIN, S., JUGOV, R., MAESHIMA, R. & STOKER, A. W. 2015. Oxovanadium-based inhibitors can drive redox-sensitive cytotoxicity in neuroblastoma cells and synergise strongly with buthionine sulfoximine. *Cancer letters,* 357**,** 316-327.

CLAYTON, N. S. & RIDLEY, A. J. 2020. Targeting Rho GTPase signaling networks in cancer. *Frontiers in Cell and Developmental Biology,* 8**,** 222.

COGGINS, G. E., FARREL, A., RATHI, K. S., HAYES, C. M., SCOLARO, L., ROKITA, J. L. & MARIS, J. M. 2019. YAP1 mediates resistance to MEK1/2 inhibition in neuroblastomas with hyperactivated RAS signaling. *Cancer research,* 79**,** 6204-6214.

COHN, S. L., PEARSON, A. D., LONDON, W. B., MONCLAIR, T., AMBROS, P. F., BRODEUR, G. M., FALDUM, A., HERO, B., IEHARA, T. & MACHIN, D. 2009. The International Neuroblastoma Risk Group (INRG) classification system: an INRG task force report. *Journal of clinical oncology,* 27**,** 289.

COOK, J., PASS, H., RUSSO, A., IYPE, S. & MITCHELL, J. 1989. Use of monochlorobimane for glutathione measurements in hamster and human tumor cell lines. *International Journal of Radiation Oncology* Biology* Physics,* 16**,** 1321-1324.

COTTERMAN, R. & KNOEPFLER, P. S. 2009. N-Myc regulates expression of pluripotency genes in neuroblastoma including lif, klf2, klf4, and lin28b. *PloS one,* 4**,** e5799.

COX, D. R. 1972. Regression models and life-tables. *Journal of the Royal Statistical Society: Series B (Methodological),* 34**,** 187-202.

CSANAKY, K., HESS, M. W. & KLIMASCHEWSKI, L. 2019. Membrane-associated, not cytoplasmic or nuclear, fgfr1 induces neuronal differentiation. *Cells,* 8**,** 243.

CZARNEK, M., SARAD, K., KARAŚ, A., KOCHAN, J. & BERETA, J. 2021. Non-targeting control for MISSION shRNA library silences SNRPD3 leading to cell death or permanent growth arrest. *Molecular Therapy-Nucleic Acids,* 26**,** 711-731.

CZEKANSKA, E. M. 2011. Assessment of cell proliferation with resazurin-based fluorescent dye. *Mammalian cell viability.* Springer.

DAYEM, A. A., KIM, B., GURUNATHAN, S., CHOI, H. Y., YANG, G., SAHA, S. K., HAN, D., HAN, J., KIM, K. & KIM, J. H. 2014. Biologically synthesized silver nanoparticles induce neuronal differentiation of SH-SY5Y cells via modulation of reactive oxygen species, phosphatases, and kinase signaling pathways. *Biotechnology journal,* 9**,** 934-943.

DE BERNARDI, B., PIANCA, C., PISTAMIGLIO, P., VENESELLI, E., VISCARDI, E., PESSION, A., ALVISI, P., CARLI, M., DONFRANCESCO, A. & CASALE, F. 2001. Neuroblastoma with symptomatic spinal cord compression at diagnosis: treatment and results with 76 cases. *Journal of clinical oncology,* 19**,** 183-190.

DE BROUWER, S., DE PRETER, K., KUMPS, C., ZABROCKI, P., PORCU, M., WESTERHOUT, E. M., LAKEMAN, A., VANDESOMPELE, J., HOEBEECK, J. & VAN MAERKEN, T. 2010. Meta-analysis of neuroblastomas reveals a

skewed ALK mutation spectrum in tumors with MYCN amplification. *Clinical cancer research,* 16**,** 4353-4362.

DEMPSTER, J. M., BOYLE, I., VAZQUEZ, F., ROOT, D. E., BOEHM, J. S., HAHN, W. C., TSHERNIAK, A. & MCFARLAND, J. M. 2021. Chronos: a cell population dynamics model of CRISPR experiments that improves inference of gene fitness effects. *Genome biology,* 22**,** 1-23.

DENU, J. M. & DIXON, J. E. 1998. Protein tyrosine phosphatases: mechanisms of catalysis and regulation. *Current opinion in chemical biology,* 2**,** 633-641.

DENU, J. M., STUCKEY, J. A., SAPER, M. A. & DIXON, J. E. 1996. Form and function in protein dephosphorylation. *Cell,* 87**,** 361-364.

DICKINSON, R. J. & KEYSE, S. M. 2006. Diverse physiological functions for dual-specificity MAP kinase phosphatases. *J Cell Sci,* 119**,** 4607-4615.

DOENCH, J. G., FUSI, N., SULLENDER, M., HEGDE, M., VAIMBERG, E. W., DONOVAN, K. F., SMITH, I., TOTHOVA, Z., WILEN, C. & ORCHARD, R. 2016. Optimized sgRNA design to maximize activity and minimize off-target effects of CRISPR-Cas9. *Nature biotechnology,* 34**,** 184-191.

DONCHEVA, N. T., MORRIS, J. H., GORODKIN, J. & JENSEN, L. J. 2018. Cytoscape StringApp: network analysis and visualization of proteomics data. *Journal of proteome research,* 18**,** 623-632.

DOWD, S., SNEDDON, A. A. & KEYSE, S. M. 1998. Isolation of the human genes encoding the pyst1 and Pyst2 phosphatases: characterisation of Pyst2 as a cytosolic dual-specificity MAP kinase phosphatase and its catalytic activation by both MAP and SAP kinases. *Journal of cell science,* 111**,** 3389-3399.

DU, Z. & LOVLY, C. M. 2018. Mechanisms of receptor tyrosine kinase activation in cancer. *Molecular cancer,* 17**,** 1-13.

DUBOIS, S. G., KALIKA, Y., LUKENS, J. N., BRODEUR, G. M., SEEGER, R. C., ATKINSON, J. B., HAASE, G. M., BLACK, C. T., PEREZ, C. & SHIMADA, H. 1999. Metastatic sites in stage IV and IVS neuroblastoma correlate with age, tumor biology, and survival. *Journal of pediatric hematology/oncology,* 21**,** 181-189.

DUBOIS, S. G., MOSSE, Y. P., FOX, E., KUDGUS, R. A., REID, J. M., MCGOVERN, R., GROSHEN, S., BAGATELL, R., MARIS, J. M. & TWIST, C. J. 2018. Phase II trial of alisertib in combination with irinotecan and temozolomide for patients with relapsed or refractory neuroblastoma. *Clinical Cancer Research,* 24**,** 6142-6149.

DULYANINOVA, N. G., HITE, K. M., ZENCHECK, W. D., SCUDIERO, D. A., ALMO, S. C., SHOEMAKER, R. H. & BRESNICK, A. R. 2011. Cysteine 81 is critical for the interaction of S100A4 and myosin-IIA. *Biochemistry,* 50**,** 7218-7227.

DUMBA, M., JAWAD, N. & MCHUGH, K. 2015. Neuroblastoma and nephroblastoma: a radiological review. *Cancer Imaging,* 15**,** 1-14.

DYBERG, C., FRANSSON, S., ANDONOVA, T., SVEINBJÖRNSSON, B., LÄNNERHOLM-PALM, J., OLSEN, T. K., FORSBERG, D., HERLENIUS, E., MARTINSSON, T. & BRODIN, B. 2017. Rho-associated kinase is a therapeutic target in neuroblastoma. *Proceedings of the National Academy of Sciences,* 114**,** E6603-E6612.

EASTON, J. B., ROYER, A. R. & MIDDLEMAS, D. S. 2006. The protein tyrosine phosphatase, Shp2, is required for the complete activation of the RAS/MAPK pathway by brain-derived neurotrophic factor. *Journal of neurochemistry,* 97**,** 834-845.

ECHEVERRI, C. J., BEACHY, P. A., BAUM, B., BOUTROS, M., BUCHHOLZ, F., CHANDA, S. K., DOWNWARD, J., ELLENBERG, J., FRASER, A. G. & HACOHEN, N. 2006. Minimizing the risk of reporting false positives in large-scale RNAi screens. *Nature methods,* 3**,** 777-779.

ECKSCHLAGER, T., PILÁT, D., KODET, R., DAHBIOVA, R., STANKOVA, J., JASINSKA, J. & HRUSAK, O. 1996. DNA ploidy in neuroblastoma. *Neoplasma,* 43**,** 23-26.

EKEROT, M., STAVRIDIS, M. P., DELAVAINE, L., MITCHELL, M. P., STAPLES, C., OWENS, D. M., KEENAN, I. D., DICKINSON, R. J., STOREY, K. G. & KEYSE, S. M. 2008. Negative-feedback regulation of FGF signalling by DUSP6/MKP-3 is driven by ERK1/2 and mediated by Ets factor binding to a conserved site within the DUSP6/MKP-3 gene promoter. *Biochemical Journal,* 412**,** 287-298.

ELEVELD, T. F., OLDRIDGE, D. A., BERNARD, V., KOSTER, J., DAAGE, L. C., DISKIN, S. J., SCHILD, L., BENTAHAR, N. B., BELLINI, A. & CHICARD, M. 2015. Relapsed neuroblastomas show frequent RAS-MAPK pathway mutations. *Nature genetics,* 47**,** 864.

ELSON, A. 2018. Stepping out of the shadows: Oncogenic and tumor-promoting protein tyrosine phosphatases. *Int J Biochem Cell Biol,* 96**,** 135-147.

ENGEDAL, N., KORKMAZ, C. G. & SAATCIOGLU, F. 2002. C-Jun N-terminal kinase is required for phorbol ester-and thapsigargin-induced apoptosis in the androgen responsive prostate cancer cell line LNCaP. *Oncogene,* 21**,** 1017-1027.

ESPADA, L., MEO-EVOLI, N., SANCHO, P., REAL, S., FABREGAT, I., AMBROSIO, S. & TAULER, A. 2012. ROS production is essential for the apoptotic function of E2F1 in pheochromocytoma and neuroblastoma cell lines. *PloS one,* 7**,** e51544.

ESPOSITO, C. L., D'ALESSIO, A., DE FRANCISCIS, V. & CERCHIA, L. 2008. A cross-talk between TrkB and Ret tyrosine kinases receptors mediates neuroblastoma cells differentiation. *PloS one,* 3**,** e1643.

FANTAUZZO, K. A. & SORIANO, P. 2015. Receptor tyrosine kinase signaling: regulating neural crest development one phosphate at a time. *Current topics in developmental biology,* 111**,** 135-182.

FEDR, R., PERNICOVÁ, Z., SLABÁKOVÁ, E., STRAKOVÁ, N., BOUCHAL, J., GREPL, M., KOZUBÍK, A. & SOUČEK, K. 2013. Automatic cell cloning assay for determining the clonogenic capacity of cancer and cancer stem-like cells. *Cytometry Part A,* 83**,** 472-482.

FLETCHER, J. I., ZIEGLER, D. S., TRAHAIR, T. N., MARSHALL, G. M., HABER, M. & NORRIS, M. D. 2018. Too many targets, not enough patients: rethinking neuroblastoma clinical trials. *Nat Rev Cancer,* 18**,** 389-400.

FOUCQUIER, J. & GUEDJ, M. 2015. Analysis of drug combinations: current methodological landscape. *Pharmacology research & perspectives,* 3**,** e00149.

FRANKEN, N. A., RODERMOND, H. M., STAP, J., HAVEMAN, J. & VAN BREE, C. 2006. Clonogenic assay of cells in vitro. *Nature protocols,* 1**,** 2315-2319.

FRIEDBERG, I., NIKA, K., TAUTZ, L., SAITO, K., CERIGNOLI, F., FRIEDBERG, I., GODZIK, A. & MUSTELIN, T. 2007. Identification and characterization of DUSP27, a novel dual-specific protein phosphatase. *FEBS letters,* 581**,** 2527-2533.

FURCHT, C. M., BUONATO, J. M. & LAZZARA, M. J. 2015. EGFR-activated Src family kinases maintain GAB1-SHP2 complexes distal from EGFR. *Science signaling,* 8**,** ra46-ra46.

FURLAN, A., DYACHUK, V., KASTRITI, M. E., CALVO-ENRIQUE, L., ABDO, H., HADJAB, S., CHONTOROTZEA, T., AKKURATOVA, N., USOSKIN, D. & KAMENEV, D. 2017. Multipotent peripheral glial cells generate neuroendocrine cells of the adrenal medulla. *Science,* 357**,** eaal3753.

FURUKAWA, T., FUJISAKI, R., YOSHIDA, Y., KANAI, N., SUNAMURA, M., ABE, T., TAKEDA, K., MATSUNO, S. & HORII, A. 2005. Distinct progression pathways involving the dysfunction of DUSP6/MKP-3 in pancreatic intraepithelial neoplasia and intraductal papillary-mucinous neoplasms of the pancreas. *Modern Pathology,* 18**,** 1034-1042.

FURUKAWA, T., TANJI, E., XU, S. & HORII, A. 2008. Feedback regulation of DUSP6 transcription responding to MAPK1 via ETS2 in human cells. *Biochemical and biophysical research communications,* 377**,** 317-320.

FUSCO, P., ESPOSITO, M. R. & TONINI, G. P. 2018. Chromosome instability in neuroblastoma. *Oncology letters,* 16**,** 6887-6894.

GABAY, M., LI, Y. & FELSHER, D. W. 2014. MYC activation is a hallmark of cancer initiation and maintenance. *Cold Spring Harbor perspectives in medicine,* 4**,** a014241.

GAMBLE, L. D., KEES, U. R., TWEDDLE, D. A. & LUNEC, J. 2012. MYCN sensitizes neuroblastoma to the MDM2-p53 antagonists Nutlin-3 and MI-63. *Oncogene,* 31**,** 752-763.

GAO, P.-P., QI, X.-W., SUN, N., SUN, Y.-Y., ZHANG, Y., TAN, X.-N., DING, J., HAN, F. & ZHANG, Y. 2021. The emerging roles of dual-specificity phosphatases and their specific characteristics in human cancer. *Biochimica et Biophysica Acta (BBA)-Reviews on Cancer,* 1876**,** 188562.

GARCIA FORTANET, J., CHEN, C. H.-T., CHEN, Y.-N. P., CHEN, Z., DENG, Z., FIRESTONE, B., FEKKES, P., FODOR, M., FORTIN, P. D. & FRIDRICH, C. 2016. Allosteric inhibition of SHP2: identification of a potent, selective, and orally efficacious phosphatase inhibitor. *Journal of medicinal chemistry,* 59**,** 7773-7782.

GARDNER, S., GROSS, S. M., DAVID, L. L., KLIMEK, J. E. & ROTWEIN, P. 2015. Separating myoblast differentiation from muscle cell fusion using IGF-I and the p38 MAP kinase inhibitor SB202190. *American Journal of Physiology-Cell Physiology,* 309**,** C491-C500.

GARNER, E. F. & BEIERLE, E. A. 2016. Cancer stem cells and their interaction with the tumor microenvironment in neuroblastoma. *Cancers,* 8**,** 5.

GAUGUET, J. M., PACE-EMERSON, T., GRANT, F. D., SHUSTERMAN, S., DUBOIS, S. G., FRAZIER, A. L. & VOSS, S. D. 2017. Evaluation of the utility of 99mTc-MDP bone scintigraphy versus MIBG scintigraphy and cross-sectional

imaging for staging patients with neuroblastoma. *Pediatric Blood & Cancer,* 64**,** e26601.

GENG, Q., XHABIJA, B., KNUCKLE, C., BONHAM, C. A. & VACRATSIS, P. O. 2017. The atypical dual specificity phosphatase hYVH1 associates with multiple ribonucleoprotein particles. *Journal of Biological Chemistry,* 292**,** 539-550.

GEORGE, R. E., LONDON, W. B., COHN, S. L., MARIS, J. M., KRETSCHMAR, C., DILLER, L., BRODEUR, G. M., CASTLEBERRY, R. P. & LOOK, A. T. 2005. Hyperdiploidy plus nonamplified MYCN confers a favorable prognosis in children 12 to 18 months old with disseminated neuroblastoma: a Pediatric Oncology Group study. *J Clin Oncol,* 23**,** 6466-6473.

GEORGE, R. E., SANDA, T., HANNA, M., FRÖHLING, S., LUTHER II, W., ZHANG, J., AHN, Y., ZHOU, W., LONDON, W. B. & MCGRADY, P. 2008. Activating mutations in ALK provide a therapeutic target in neuroblastoma. *Nature,* 455**,** 975.

GHERARDI, S., VALLI, E., ERRIQUEZ, D. & PERINI, G. 2013. MYCN-mediated transcriptional repression in neuroblastoma: the other side of the coin. *Frontiers in oncology,* 3**,** 42.

GHOSH, N., DAS, A., CHAFFEE, S., ROY, S. & SEN, C. K. 2018. Reactive oxygen species, oxidative damage and cell death. *Immunity and inflammation in health and disease.* Elsevier.

GILBERT, L. A., HORLBECK, M. A., ADAMSON, B., VILLALTA, J. E., CHEN, Y., WHITEHEAD, E. H., GUIMARAES, C., PANNING, B., PLOEGH, H. L. & BASSIK, M. C. 2014. Genome-scale CRISPR-mediated control of gene repression and activation. *Cell,* 159**,** 647-661.

GLEASON, A. C., GHADGE, G., CHEN, J., SONOBE, Y. & ROOS, R. P. 2021. Machine learning predicts translation initiation sites in neurologic diseases with expanded repeats. *bioRxiv*.

GOLDSMITH, K. C., KAYSER, K., GROSHEN, S. G., CHIODA, M., THURM, H. C., CHEN, J., PELTZ, G., GRANGER, M., MARIS, J. & MATTHAY, K. K. 2020. Phase I trial of lorlatinib in patients with ALK-driven refractory or relapsed neuroblastoma: A New Approaches to Neuroblastoma Consortium study. American Society of Clinical Oncology.

GONZALEZ MALAGON, S. G., LOPEZ MUÑOZ, A. M., DORO, D., BOLGER, T. G., POON, E., TUCKER, E. R., ADEL AL-LAMI, H., KRAUSE, M., PHIEL, C. J. & CHESLER, L. 2018. Glycogen synthase kinase 3 controls migration of the neural crest lineage in mouse and Xenopus. *Nature communications,* 9**,** 1-15.

GRAMMER, T. C. & BLENIS, J. 1997. Evidence for MEK-independent pathways regulating the prolonged activation of the ERK-MAP kinases. *Oncogene,* 14**,** 1635-1642.

GREENGARD, E. G. 2018. Molecularly targeted therapy for neuroblastoma. *Children,* 5**,** 142.

GROOM, L. A., SNEDDON, A. A., ALESSI, D. R., DOWD, S. & KEYSE, S. M. 1996. Differential regulation of the MAP, SAP and RK/p38 kinases by Pyst1, a novel cytosolic dual-specificity phosphatase. *The EMBO journal,* 15**,** 3621-3632.

GROSSMANN, K. S., WENDE, H., PAUL, F. E., CHERET, C., GARRATT, A. N., ZURBORG, S., FEINBERG, K., BESSER, D., SCHULZ, H. & PELES, E. 2009. The tyrosine phosphatase Shp2 (PTPN11) directs Neuregulin-1/ErbB signaling throughout Schwann cell development. *Proceedings of the National Academy of Sciences,* 106**,** 16704-16709.

GUAN, J., TUCKER, E., WAN, H., CHAND, D., DANIELSON, L., RUUTH, K., EL WAKIL, A., WITEK, B., JAMIN, Y. & UMAPATHY, G. 2016. The ALK inhibitor PF-06463922 is effective as a single agent in neuroblastoma driven by expression of ALK and MYCN. *Disease models & mechanisms,* 9**,** 941-952.

GUAN, J., UMAPATHY, G., YAMAZAKI, Y., WOLFSTETTER, G., MENDOZA, P., PFEIFER, K., MOHAMMED, A., HUGOSSON, F., ZHANG, H. & HSU, A. W. 2015. FAM150A and FAM150B are activating ligands for anaplastic lymphoma kinase. *elife,* 4**,** e09811.

GUAN, K., BROYLES, S. S. & DIXON, J. E. 1991. A Tyr/Ser protein phosphatase encoded by vaccinia virus. *Nature,* 350**,** 359-362.

HAAGENSON, K. K. & WU, G. S. 2010. The role of MAP kinases and MAP kinase phosphatase-1 in resistance to breast cancer treatment. *Cancer and Metastasis Reviews,* 29**,** 143-149.

HALLBERG, B. & PALMER, R. 2016. The role of the ALK receptor in cancer biology. *Annals of Oncology,* 27**,** iii4-iii15.

HAMDANE, M., BRETTEVILLE, A., SAMBO, A.-V., SCHINDOWSKI, K., BÉGARD, S., DELACOURTE, A., BERTRAND, P. & BUÉE, L. 2005. p25/Cdk5-mediated retinoblastoma phosphorylation is an early event in neuronal cell death. *Journal of cell science,* 118**,** 1291-1298.

HANN, H.-W. L., EVANS, A. E., SIEGEL, S. E., WONG, K. Y., SATHER, H., DALTON, A., HAMMOND, D. & SEEGER, R. C. 1985. Prognostic importance of serum ferritin in patients with Stages III and IV neuroblastoma: the Childrens Cancer Study Group experience. *Cancer research,* 45**,** 2843-2848.

HANNUS, M., BEITZINGER, M., ENGELMANN, J. C., WEICKERT, M.-T., SPANG, R., HANNUS, S. & MEISTER, G. 2014. siPools: highly complex but accurately defined siRNA pools eliminate off-target effects. *Nucleic acids research,* 42**,** 8049-8061.

HANSFORD, L. M., MCKEE, A. E., ZHANG, L., GEORGE, R. E., GERSTLE, J. T., THORNER, P. S., SMITH, K. M., LOOK, A. T., YEGER, H. & MILLER, F. D. 2007. Neuroblastoma cells isolated from bone marrow metastases contain a naturally enriched tumor-initiating cell. *Cancer research,* 67**,** 11234-11243.

HAO, L. & ELSHAMY, W. M. 2007. BRCA1-IRIS activates cyclin D1 expression in breast cancer cells by downregulating the JNK phosphatase DUSP3/VHR. *International journal of cancer,* 121**,** 39-46.

HARENZA, J. L., DIAMOND, M. A., ADAMS, R. N., SONG, M. M., DAVIDSON, H. L., HART, L. S., DENT, M. H., FORTINA, P., REYNOLDS, C. P. & MARIS, J. M. 2017. Transcriptomic profiling of 39 commonly-used neuroblastoma cell lines. *Scientific Data,* 4**,** 1-9.

HART, L. S., RADER, J., RAMAN, P., BATRA, V., RUSSELL, M. R., TSANG, M., GAGLIARDI, M., CHEN, L., MARTINEZ, D. & LI, Y. 2017. Preclinical therapeutic synergy of MEK1/2 and CDK4/6 inhibition in neuroblastoma. *Clinical Cancer Research,* 23**,** 1785-1796.

HECHT, M., BROMBERG, Y. & ROST, B. 2015. Better prediction of functional effects for sequence variants. *BMC genomics,* 16**,** S1.

HENKEL, L., RAUSCHER, B., SCHMITT, B., WINTER, J. & BOUTROS, M. 2020. Genome-scale CRISPR screening at high sensitivity with an empirically designed sgRNA library. *BMC biology,* 18**,** 1-21.

HENKENS, R., DELVENNE, P., ARAFA, M., MOUTSCHEN, M., ZEDDOU, M., TAUTZ, L., BONIVER, J., MUSTELIN, T. & RAHMOUNI, S. 2008. Cervix carcinoma is associated with an up-regulation and nuclear localization of the dual-specificity protein phosphatase VHR. *BMC cancer,* 8**,** 1-9.

HERTOG, J. D., ÖSTMAN, A. & BÖHMER, F. D. 2008. Protein tyrosine phosphatases: regulatory mechanisms. *The FEBS journal,* 275**,** 831-847.

HIJAZI, M., SMITH, R., RAJEEVE, V., BESSANT, C. & CUTILLAS, P. R. 2020. Reconstructing kinase network topologies from phosphoproteomics data reveals cancer-associated rewiring. *Nature Biotechnology,* 38**,** 493-502.

HILDESHEIM, J., AWWAD, R. T. & FORNACE JR, A. J. 2004. p38 Mitogen-activated protein kinase inhibitor protects the epidermis against the acute damaging effects of ultraviolet irradiation by blocking apoptosis and inflammatory responses. *Journal of Investigative Dermatology,* 122**,** 497-502.

HODGE, R. G. & RIDLEY, A. J. 2016. Regulating Rho GTPases and their regulators. *Nature reviews Molecular cell biology,* 17**,** 496-510.

HORNBECK, P. V., ZHANG, B., MURRAY, B., KORNHAUSER, J. M., LATHAM, V. & SKRZYPEK, E. 2015. PhosphoSitePlus, 2014: mutations, PTMs and recalibrations. *Nucleic acids research,* 43**,** D512-D520.

HOYT, R., ZHU, W., CERIGNOLI, F., ALONSO, A., MUSTELIN, T. & DAVID, M. 2007. Cutting edge: selective tyrosine dephosphorylation of interferon-activated nuclear STAT5 by the VHR phosphatase. *The Journal of Immunology,* 179**,** 3402-3406.

HU, X., TANG, Z., MA, S., YU, Y., CHEN, X. & ZANG, G. 2019. Tripartite motif-containing protein 7 regulates hepatocellular carcinoma cell proliferation via the DUSP6/p38 pathway. *Biochemical and biophysical research communications,* 511**,** 889-895.

HU, Y. & MIVECHI, N. F. 2006. Association and regulation of heat shock transcription factor 4b with both extracellular signal-regulated kinase mitogen-activated protein kinase and dual-specificity tyrosine phosphatase DUSP26. *Molecular and cellular biology,* 26**,** 3282-3294.

HUANG, H.-T., SEO, H.-S., ZHANG, T., WANG, Y., JIANG, B., LI, Q., BUCKLEY, D. L., NABET, B., ROBERTS, J. M. & PAULK, J. 2017. MELK is not necessary for the proliferation of basal-like breast cancer cells. *Elife,* 6**,** e26693.

HUANG, M. & WEISS, W. A. 2013. Neuroblastoma and MYCN. *Cold Spring Harbor perspectives in medicine,* 3**,** a014415.

HÜBNER, N. C., WANG, L. H.-C., KAULICH, M., DESCOMBES, P., POSER, I. & NIGG, E. A. 2010. Re-examination of siRNA specificity questions role of PICH and Tao1 in the spindle checkpoint and identifies Mad2 as a sensitive target for small RNAs. *Chromosoma,* 119**,** 149-165.

HUNTER, T. 2014. The genesis of tyrosine phosphorylation. *Cold Spring Harbor perspectives in biology,* 6**,** a020644.

HUR, E.-M. & ZHOU, F.-Q. 2010. GSK3 signalling in neural development. *Nature Reviews Neuroscience,* 11**,** 539-551.

IANEVSKI, A., GIRI, A. K. & AITTOKALLIO, T. 2020. SynergyFinder 2.0: visual analytics of multi-drug combination synergies. *Nucleic acids research,* 48**,** W488-W493.

IMAJO, M., TSUCHIYA, Y. & NISHIDA, E. 2006. Regulatory mechanisms and functions of MAP kinase signaling pathways. *IUBMB life,* 58**,** 312-317.

INFARINATO, N. R., PARK, J. H., KRYTSKA, K., RYLES, H. T., SANO, R., SZIGETY, K. M., LI, Y., ZOU, H. Y., LEE, N. V. & SMEAL, T. 2016. The ALK/ROS1 inhibitor PF-06463922 overcomes primary resistance to crizotinib in ALK-driven neuroblastoma. *Cancer discovery,* 6**,** 96-107.

IRBY, R. B. & YEATMAN, T. J. 2000. Role of Src expression and activation in human cancer. *Oncogene,* 19**,** 5636-5642.

ITO, T., YOUNG, M. J., LI, R., JAIN, S., WERNITZNIG, A., KRILL-BURGER, J. M., LEMKE, C. T., MONDUCCI, D., RODRIGUEZ, D. J. & CHANG, L. 2021. Paralog knockout profiling identifies DUSP4 and DUSP6 as a digenic dependence in MAPK pathway-driven cancers. *Nature genetics,* 53**,** 1664-1672.

IZUMI, H. & KANEKO, Y. 2012. Evidence of asymmetric cell division and centrosome inheritance in human neuroblastoma cells. *Proceedings of the National Academy of Sciences,* 109**,** 18048-18053.

JACKSON, A. L. & LINSLEY, P. S. 2010. Recognizing and avoiding siRNA off-target effects for target identification and therapeutic application. *Nature reviews Drug discovery,* 9**,** 57-67.

JAMES, S. J., JIAO, H., TEH, H.-Y., TAKAHASHI, H., PNG, C. W., PHOON, M. C., SUZUKI, Y., SAWASAKI, T., XIAO, H. & CHOW, V. T. 2015. MAPK phosphatase 5 expression induced by influenza and other RNA virus infection negatively regulates IRF3 activation and type I interferon response. *Cell reports,* 10**,** 1722-1734.

JANOUEIX-LEROSEY, I., LEQUIN, D., BRUGIÈRES, L., RIBEIRO, A., DE PONTUAL, L., COMBARET, V., RAYNAL, V., PUISIEUX, A., SCHLEIERMACHER, G. & PIERRON, G. 2008. Somatic and germline activating mutations of the ALK kinase receptor in neuroblastoma. *Nature,* 455**,** 967.

JEON, Y.-M., LEE, S., KIM, S., KWON, Y., KIM, K., CHUNG, C. G., LEE, S., LEE, S. B. & KIM, H.-J. 2017. Neuroprotective effects of protein tyrosine phosphatase 1B inhibition against ER stress-induced toxicity. *Molecules and cells,* 40**,** 280.

JIANG, J., JIN, M.-S., KONG, F., WANG, Y.-P., JIA, Z.-F., CAO, D.-H., MA, H.-X., SUO, J. & CAO, X.-Y. 2013. Increased expression of tyrosine phosphatase SHP-2 in Helicobacter pylori-infected gastric cancer. *World journal of gastroenterology: WJG,* 19**,** 575.

JIMÉNEZ-MARTÍNEZ, M., OSTALÉ, C. M., VAN DER BURG, L. R., GALÁN-MARTÍNEZ, J., HARDWICK, J. C., LÓPEZ-PÉREZ, R., HAWINKELS, L. J., STAMATAKIS, K. & FRESNO, M. 2019a. DUSP10 is a regulator of YAP1 activity promoting cell proliferation and colorectal cancer progression. *Cancers,* 11**,** 1767.

JIMÉNEZ-MARTÍNEZ, M., STAMATAKIS, K. & FRESNO, M. 2019b. The dual-specificity phosphatase 10 (DUSP10): its role in cancer, inflammation, and immunity. *International journal of molecular sciences,* 20**,** 1626.

JOHNSEN, J., SEGERSTRÖM, L., ORREGO, A., ELFMAN, L., HENRIKSSON, M., KÅGEDAL, B., EKSBORG, S., SVEINBJÖRNSSON, B. & KOGNER, P. 2008. Inhibitors of mammalian target of rapamycin downregulate MYCN protein expression and inhibit neuroblastoma growth in vitro and in vivo. *Oncogene,* 27**,** 2910-2922.

KALTENMEIER, C. T., VOLLMER, L. L., VERNETTI, L. A., CAPRIO, L., DAVIS, K., KOROTCHENKO, V. N., DAY, B. W., TSANG, M., HULKOWER, K. I. & LOTZE, M. T. 2017. A tumor cell-selective inhibitor of mitogen-activated protein kinase phosphatases sensitizes breast cancer cells to lymphokine-activated killer cell activity. *Journal of Pharmacology and Experimental Therapeutics,* 361**,** 39-50.

KAMEL, H. F. M. & AL-AMODI, H. S. A. B. 2017. Exploitation of gene expression and cancer biomarkers in paving the path to era of personalized medicine. *Genomics, proteomics & bioinformatics,* 15**,** 220-235.

KANDA, Y., MIZUNO, A., TAKASAKI, T., SATOH, R., HAGIHARA, K., MASUKO, T., ENDO, Y., TANABE, G. & SUGIURA, R. 2021. Down-regulation of dual-specificity phosphatase 6, a negative regulator of oncogenic ERK signaling, by ACA-28 induces apoptosis in NIH/3T3 cells overexpressing HER2/ErbB2. *Genes to Cells,* 26**,** 109-116.

KANEKO, Y., KANDA, N., MASEKI, N., SAKURAI, M., TSUCHIDA, Y., TAKEDA, T., OKABE, I. & SAKURAI, M. 1987. Different karyotypic patterns in early and advanced stage neuroblastomas. *Cancer research,* 47**,** 311-318.

KANG, T.-H. & KIM, K.-T. 2006. Negative regulation of ERK activity by VRK3-mediated activation of VHR phosphatase. *Nature cell biology,* 8**,** 863.

KARLSSON, M., MATHERS, J., DICKINSON, R. J., MANDL, M. & KEYSE, S. M. 2004. Both nuclear-cytoplasmic shuttling of the dual specificity phosphatase MKP-3 and its ability to anchor MAP kinase in the cytoplasm are mediated by a conserved nuclear export signal. *Journal of Biological Chemistry,* 279**,** 41882-41891.

KAUFMANN, S. H., DESNOYERS, S., OTTAVIANO, Y., DAVIDSON, N. E. & POIRIER, G. G. 1993. Specific proteolytic cleavage of poly (ADP-ribose) polymerase: an early marker of chemotherapy-induced apoptosis. *Cancer research,* 53**,** 3976-3985.

KEYSE, S. M. 2008. Dual-specificity MAP kinase phosphatases (MKPs) and cancer. *Cancer and Metastasis Reviews,* 27**,** 253-261.

KHOLODENKO, I. V., KALINOVSKY, D. V., DORONIN, I. I., DEYEV, S. M. & KHOLODENKO, R. V. 2018. Neuroblastoma origin and therapeutic targets for immunotherapy. *Journal of immunology research,* 2018.

KIDGER, A. M. & KEYSE, S. M. The regulation of oncogenic Ras/ERK signalling by dual-specificity mitogen activated protein kinase phosphatases (MKPs). Seminars in cell & developmental biology, 2016. Elsevier, 125-132.

KIM, B. R., HA, J., KANG, E. & CHO, S. 2020. Regulation of signal transducer and activator of transcription 3 activation by dual-specificity phosphatase 3. *BMB reports,* 53**,** 335.

KIM, G. S., CHOI, Y. K., SONG, S. S., KIM, W.-K. & HAN, B. H. 2005. MKP-1 contributes to oxidative stress-induced apoptosis via inactivation of

ERK1/2 in SH-SY5Y cells. *Biochemical and biophysical research communications,* 338**,** 1732-1738.

KIM, H., LEE, H.-J., OH, Y., CHOI, S.-G., HONG, S.-H., KIM, H.-J., LEE, S.-Y., CHOI, J.-W., HWANG, D. S. & KIM, K.-S. 2014. The DUSP26 phosphatase activator adenylate kinase 2 regulates FADD phosphorylation and cell growth. *Nature communications,* 5**,** 1-11.

KIM, S. J. & RYU, S. E. 2012. Structure and catalytic mechanism of human protein tyrosine phosphatome. *BMB Reports,* 45**,** 693-699.

KIM, S. Y., OH, M., LEE, K.-S., KIM, W.-K., OH, K.-J., LEE, S. C., BAE, K.-H. & HAN, B.-S. 2016. Profiling analysis of protein tyrosine phosphatases during neuronal differentiation. *Neuroscience letters,* 612**,** 219-224.

KITTLER, R., SURENDRANATH, V., HENINGER, A.-K., SLABICKI, M., THEIS, M., PUTZ, G., FRANKE, K., CALDARELLI, A., GRABNER, H. & KOZAK, K. 2007. Genome-wide resources of endoribonuclease-prepared short interfering RNAs for specific loss-of-function studies. *Nature methods,* 4**,** 337-344.

KOCAK, H., ACKERMANN, S., HERO, B., KAHLERT, Y., OBERTHUER, A., JURAEVA, D., ROELS, F., THEISSEN, J., WESTERMANN, F. & DEUBZER, H. 2013. Hox-C9 activates the intrinsic pathway of apoptosis and is associated with spontaneous regression in neuroblastoma. *Cell death & disease,* 4**,** e586-e586.

KOGA, S., KOJIMA, S., KISHIMOTO, T., KUWABARA, S. & YAMAGUCHI, A. 2012. Over-expression of map kinase phosphatase-1 (MKP-1) suppresses neuronal death through regulating JNK signaling in hypoxia/re-oxygenation. *Brain research,* 1436**,** 137-146.

KOHLER, J., RUBIE, H., CASTEL, V., BEISKE, K., HOLMES, K., GAMBINI, C., CASALE, F., MUNZER, C., ERMINIO, G. & PARODI, S. 2013. Treatment of children over the age of one year with unresectable localised neuroblastoma without MYCN amplification: results of the SIOPEN study. *European journal of cancer,* 49**,** 3671-3679.

KOROTCHENKO, V. N., SAYDMOHAMMED, M., VOLLMER, L. L., BAKAN, A., SHEETZ, K., DEBIEC, K. T., GREENE, K. A., AGLIORI, C. S., BAHAR, I. & DAY, B. W. 2014. In vivo structure–activity relationship studies support allosteric targeting of a dual specificity phosphatase. *ChemBioChem,* 15**,** 1436-1445.

KOZAROVA, A., HUDSON, J. W. & VACRATSIS, P. O. 2011. The dual-specificity phosphatase hYVH1 (DUSP12) is a novel modulator of cellular DNA content. *Cell Cycle,* 10**,** 1669-1678.

KRISHNAN, N., KONIDARIS, K. F., GASSER, G. & TONKS, N. K. 2018. A potent, selective, and orally bioavailable inhibitor of the protein-tyrosine phosphatase PTP1B improves insulin and leptin signaling in animal models. *Journal of Biological Chemistry,* 293**,** 1517-1525.

KUCHARSKA, A., RUSHWORTH, L. K., STAPLES, C., MORRICE, N. A. & KEYSE, S. M. 2009. Regulation of the inducible nuclear dual-specificity phosphatase DUSP5 by ERK MAPK. *Cellular signalling,* 21**,** 1794-1805.

KUMMAR, S., GUTIERREZ, M., DOROSHOW, J. H. & MURGO, A. J. 2006. Drug development in oncology: classical cytotoxics and molecularly targeted agents. *British journal of clinical pharmacology,* 62**,** 15-26.

LAMBERTZ, I., KUMPS, C., CLAEYS, S., LINDNER, S., BECKERS, A., JANSSENS, E., CARTER, D. R., CAZES, A., CHEUNG, B. B. & DE MARIANO, M. 2015. Upregulation of MAPK negative feedback regulators and RET in mutant ALK neuroblastoma: implications for targeted treatment. *Clinical Cancer Research,* 21**,** 3327-3339.

LARSEN, M. R., THINGHOLM, T. E., JENSEN, O. N., ROEPSTORFF, P. & JØRGENSEN, T. J. 2005. Highly selective enrichment of phosphorylated peptides from peptide mixtures using titanium dioxide microcolumns. *Molecular & cellular proteomics,* 4**,** 873-886.

LASORELLA, A., BOLDRINI, R., DOMINICI, C., DONFRANCESCO, A., YOKOTA, Y., INSERRA, A. & IAVARONE, A. 2002. Id2 is critical for cellular proliferation and is the oncogenic effector of N-myc in human neuroblastoma. *Cancer research,* 62**,** 301-306.

LASORELLA, A., NOSEDA, M., BEYNA, M. & IAVARONE, A. 2000. Id2 is a retinoblastoma protein target and mediates signalling by Myc oncoproteins. *Nature,* 407**,** 592-598.

LAZO, J. S., NEMOTO, K., PESTELL, K. E., COOLEY, K., SOUTHWICK, E. C., MITCHELL, D. A., FUREY, W., GUSSIO, R., ZAHAREVITZ, D. W. & JOO, B. 2002. Identification of a potent and selective pharmacophore for Cdc25 dual specificity phosphatase inhibitors. *Molecular pharmacology,* 61**,** 720-728.

LAZO, J. S., NUNES, R., SKOKO, J. J., DE OLIVEIRA, P. E. Q., VOGT, A. & WIPF, P. 2006. Novel benzofuran inhibitors of human mitogen-activated protein kinase phosphatase-1. *Bioorganic & medicinal chemistry,* 14**,** 5643-5650.

LE GALLIC, L., SGOURAS, D., BEAL JR, G. & MAVROTHALASSITIS, G. 1999. Transcriptional repressor ERF is a Ras/mitogen-activated protein kinase target that regulates cellular proliferation. *Molecular and cellular biology,* 19**,** 4121-4133.

LEBEDEV, T. D., VAGAPOVA, E. R., POPENKO, V. I., LEONOVA, O. G., SPIRIN, P. V. & PRASSOLOV, V. S. 2019. Two receptors, two isoforms, two cancers: comprehensive analysis of KIT and TrkA expression in neuroblastoma and acute myeloid leukemia. *Frontiers in Oncology***,** 1046.

LEE, B., SAHOO, A., SAWADA, J., MARCHICA, J., SAHOO, S., LAYNG, F. I., FINLAY, D., MAZAR, J., JOSHI, P. & KOMATSU, M. 2021. MicroRNA-211 modulates the DUSP6-ERK5 signaling axis to promote BRAFV600E-driven melanoma growth in vivo and BRAF/MEK inhibitor resistance. *Journal of Investigative Dermatology,* 141**,** 385-394.

LEGEAY, M., DONCHEVA, N. T., MORRIS, J. H. & JENSEN, L. J. 2020. Visualize omics data on networks with Omics Visualizer, a Cytoscape App. *F1000Research,* 9.

LI, J., YEN, C., LIAW, D., PODSYPANINA, K., BOSE, S., WANG, S. I., PUC, J., MILIARESIS, C., RODGERS, L. & MCCOMBIE, R. 1997. PTEN, a putative protein tyrosine phosphatase gene mutated in human brain, breast, and prostate cancer. *science,* 275**,** 1943-1947.

LI, W., CHEN, Z., ZONG, Y., GONG, F., ZHU, Y., ZHU, Y., LV, J., ZHANG, J., XIE, L. & SUN, Y. 2011. PP2A inhibitors induce apoptosis in pancreatic cancer cell line PANC-1 through persistent phosphorylation of IKKα and sustained activation of the NF-κB pathway. *Cancer letters,* 304**,** 117-127.

LI, W., SONG, L., RITCHIE, A. M. & MELTON, D. W. 2012. Increased levels of DUSP6 phosphatase stimulate tumourigenesis in a molecularly distinct melanoma subtype. *Pigment cell & melanoma research,* 25**,** 188-199.

LI, X., GOOBIE, G. C., GREGORY, A. D., KASS, D. J. & ZHANG, Y. 2021. Toll-Interacting Protein in Pulmonary Diseases. Abiding by the Goldilocks Principle. *American journal of respiratory cell and molecular biology,* 64**,** 536-546.

LIN, A., GIULIANO, C. J., PALLADINO, A., JOHN, K. M., ABRAMOWICZ, C., YUAN, M. L., SAUSVILLE, E. L., LUKOW, D. A., LIU, L. & CHAIT, A. R. 2019a. Off-target toxicity is a common mechanism of action of cancer drugs undergoing clinical trials. *Science translational medicine,* 11**,** eaaw8412.

LIN, H. P., HO, H. M., CHANG, C. W., YEH, S. D., SU, Y. W., TAN, T. H. & LIN, W. J. 2019b. DUSP22 suppresses prostate cancer proliferation by targeting the EGFR-AR axis. *The FASEB Journal,* 33**,** 14653-14667.

LIU, M., QIN, Y., HU, Q., LIU, W., JI, S., XU, W., FAN, G., YE, Z., ZHANG, Z. & XU, X. 2021. SETD8 potentiates constitutive ERK1/2 activation via epigenetically silencing DUSP10 expression in pancreatic cancer. *Cancer Letters,* 499**,** 265-278.

LIU, R., VAN BERLO, J. H., YORK, A. J., VAGNOZZI, R. J., MAILLET, M. & MOLKENTIN, J. D. 2016. DUSP8 regulates cardiac ventricular remodeling by altering ERK1/2 signaling. *Circulation research,* 119**,** 249-260.

LIU, S., SUN, J.-P., ZHOU, B. & ZHANG, Z.-Y. 2006. Structural basis of docking interactions between ERK2 and MAP kinase phosphatase 3. *Proceedings of the National Academy of Sciences,* 103**,** 5326-5331.

LIU, T., BOHLKEN, A., KULJACA, S., LEE, M., NGUYEN, T., SMITH, S., CHEUNG, B., NORRIS, M., HABER, M. & HOLLOWAY, A. 2005. The retinoid anticancer signal: mechanisms of target gene regulation. *British journal of cancer,* 93**,** 310.

LIU, Y., GOROSPE, M., YANG, C. & HOLBROOK, N. J. 1995. Role of mitogen-activated protein kinase phosphatase during the cellular response to genotoxic stress: inhibition of c-Jun N-terminal kinase activity and AP-1-dependent gene activation. *Journal of Biological Chemistry,* 270**,** 8377-8380.

LODA, M., CAPODIECI, P., MISHRA, R., YAO, H., CORLESS, C., GRIGIONI, W., WANG, Y., MAGI-GALLUZZI, C. & STORK, P. 1996. Expression of mitogen-activated protein kinase phosphatase-1 in the early phases of human epithelial carcinogenesis. *The American journal of pathology,* 149**,** 1553.

LOOK, A. T., HAYES, F. A., SHUSTER, J. J., DOUGLASS, E. C., CASTLEBERRY, R. P., BOWMAN, L., SMITH, E. & BRODEUR, G. 1991. Clinical relevance of tumor cell ploidy and N-myc gene amplification in childhood neuroblastoma: a Pediatric Oncology Group study. *Journal of Clinical Oncology,* 9**,** 581-591.

LOPEZ-DELISLE, L., PIERRE-EUGÈNE, C., LOUIS-BRENNETOT, C., SURDEZ, D., RAYNAL, V., BAULANDE, S., BOEVA, V., GROSSETÊTE-LALAMI, S., COMBARET, V. & PEUCHMAUR, M. 2018. Activated ALK signals through the ERK–ETV5–RET pathway to drive neuroblastoma oncogenesis. *Oncogene,* 37**,** 1417.

LOW, H. B. & ZHANG, Y. 2016. Regulatory roles of MAPK phosphatases in cancer. *Immune network,* 16**,** 85-98.

MA, R., MA, L., WENG, W., WANG, Y., LIU, H., GUO, R., GAO, Y., TU, J., XU, T.-L., CHENG, J., ZHU, M. X., ZHOU, A. & LI, Y. 2020. DUSP6 SUMOylation protects cells from oxidative damage via direct regulation of Drp1 dephosphorylation. *Science Advances,* 6**,** eaaz0361.

MAGI-GALLUZZI, C., MISHRA, R., FIORENTINO, M., MONTIRONI, R., YAO, H., CAPODIECI, P., WISHNOW, K., KAPLAN, I., STORK, P. & LODA, M. 1997. Mitogen-activated protein kinase phosphatase 1 is overexpressed in prostate cancers and is inversely related to apoptosis. *Laboratory investigation; a journal of technical methods and pathology,* 76**,** 37-51.

MANDL, M., SLACK, D. N. & KEYSE, S. M. 2005. Specific inactivation and nuclear anchoring of extracellular signal-regulated kinase 2 by the inducible dual-specificity protein phosphatase DUSP5. *Molecular and cellular biology,* 25**,** 1830-1845.

MARCHETTI, S., GIMOND, C., CHAMBARD, J.-C., TOUBOUL, T., ROUX, D., POUYSSÉGUR, J. & PAGÈS, G. 2005. Extracellular signal-regulated kinases phosphorylate mitogen-activated protein kinase phosphatase 3/DUSP6 at serines 159 and 197, two sites critical for its proteasomal degradation. *Molecular and cellular biology,* 25**,** 854-864.

MARENGO, B., DE CIUCIS, C., RICCIARELLI, R., FURFARO, A., COLLA, R., CANEPA, E., TRAVERSO, N., MARINARI, U. M., PRONZATO, M. A. & DOMENICOTTI, C. 2013. p38MAPK inhibition: a new combined approach to reduce neuroblastoma resistance under etoposide treatment. *Cell death & disease,* 4**,** e589-e589.

MARÍN-RUBIO, J. L., DE ARRIBA, M. C., COBOS-FERNÁNDEZ, M. A., GONZÁLEZ-SÁNCHEZ, L., ORS, I., SASTRE, I., FERNÁNDEZ-PIQUERAS, J. & VILLA-MORALES, M. 2016. Deregulated FADD expression and phosphorylation in T-cell lymphoblastic lymphoma. *Oncotarget,* 7**,** 61485.

MARIS, J. M., HOGARTY, M. D., BAGATELL, R. & COHN, S. L. 2007. Neuroblastoma. *The Lancet,* 369**,** 2106-2120.

MARIS, J. M., WHITE, P. S., BELTINGER, C. P., SULMAN, E. P., CASTLEBERRY, R. P., SHUSTER, J. J., LOOK, A. T. & BRODEUR, G. M. 1995. Significance of chromosome 1p loss of heterozygosity in neuroblastoma. *Cancer research,* 55**,** 4664-4669.

MARSH-ARMSTRONG, B., FAJNZYLBER, J. M., KORNTNER, S., PLAMAN, B. A. & BISHOP, A. C. 2018. The allosteric site on SHP2's protein tyrosine phosphatase domain is targetable with druglike small molecules. *ACS omega,* 3**,** 15763-15770.

MARSHALL, G. M., LIU, P. Y., GHERARDI, S., SCARLETT, C. J., BEDALOV, A., XU, N., IRACI, N., VALLI, E., LING, D. & THOMAS, W. 2011. SIRT1 promotes N-Myc oncogenesis through a positive feedback loop involving the effects of MKP3 and ERK on N-Myc protein stability. *PLoS genetics,* 7**,** e1002135.

MATHSYARAJA, H. & EISENMAN, R. N. 2016. Parsing Myc paralogs in oncogenesis. *Cancer Cell,* 29**,** 1-2.

MATTHAY, K. K., MARIS, J. M., SCHLEIERMACHER, G., NAKAGAWARA, A., MACKALL, C. L., DILLER, L. & WEISS, W. A. 2016. Neuroblastoma. *Nat Rev Dis Primers,* 2**,** 16078.

MATTHAY, K. K., VILLABLANCA, J. G., SEEGER, R. C., STRAM, D. O., HARRIS, R. E., RAMSAY, N. K., SWIFT, P., SHIMADA, H., BLACK, C. T. & BRODEUR, G. M. 1999. Treatment of high-risk neuroblastoma with intensive chemotherapy, radiotherapy, autologous bone marrow transplantation, and 13-cis-retinoic acid. *New England Journal of Medicine,* 341**,** 1165-1173.

MAYOR, R. & THEVENEAU, E. 2013. The neural crest. *Development,* 140**,** 2247-2251.

MCCARTY, N. S., GRAHAM, A. E., STUDENÁ, L. & LEDESMA-AMARO, R. 2020. Multiplexed CRISPR technologies for gene editing and transcriptional regulation. *Nature communications,* 11**,** 1-13.

MCFARLAND, J. M., HO, Z. V., KUGENER, G., DEMPSTER, J. M., MONTGOMERY, P. G., BRYAN, J. G., KRILL-BURGER, J. M., GREEN, T. M., VAZQUEZ, F. & BOEHM, J. S. 2018. Improved estimation of cancer dependencies from large-scale RNAi screens using model-based normalization and data integration. *Nature communications,* 9**,** 1-13.

MEGISON, M. L., STEWART, J. E., NABERS, H. C., GILLORY, L. A. & BEIERLE, E. A. 2013. FAK inhibition decreases cell invasion, migration and metastasis in MYCN amplified neuroblastoma. *Clinical & experimental metastasis,* 30**,** 555-568.

MENDELL, A. L. & MACLUSKY, N. J. 2019. The testosterone metabolite 3α-androstanediol inhibits oxidative stress-induced ERK phosphorylation and neurotoxicity in SH-SY5Y cells through an MKP3/DUSP6-dependent mechanism. *Neuroscience Letters,* 696**,** 60-66.

MESSINA, S., FRATI, L., LEONETTI, C., ZUCHEGNA, C., DI ZAZZO, E., CALOGERO, A. & PORCELLINI, A. 2011. Dual-specificity phosphatase DUSP6 has tumor-promoting properties in human glioblastomas. *Oncogene,* 30**,** 3813-3820.

MILELLA, M., FALCONE, I., CONCIATORI, F., CESTA INCANI, U., DEL CURATOLO, A., INZERILLI, N., NUZZO, C., VACCARO, V., VARI, S. & COGNETTI, F. 2015. PTEN: multiple functions in human malignant tumors. *Frontiers in oncology,* 5**,** 24.

MISRA-PRESS, A., RIM, C. S., YAO, H., ROBERSON, M. S. & STORK, P. J. 1995. A Novel Mitogen-activated Protein Kinase Phosphatase. STRUCTURE, EXPRESSION, AND REGULATION∗. *Journal of Biological Chemistry,* 270**,** 14587-14596.

MISRA, J. R. & IRVINE, K. D. 2018. The Hippo signaling network and its biological functions. *Annual review of genetics,* 52**,** 65-87.

MIYAMOTO, D., MIYAMOTO, M., TAKAHASHI, A., YOMOGITA, Y., HIGASHI, H., KONDO, S. & HATAKEYAMA, M. 2008. Isolation of a distinct class of gain-of-function SHP-2 mutants with oncogenic RAS-like transforming activity from solid tumors. *Oncogene,* 27**,** 3508-3515.

MOELANS, C. B., VAN MALDEGEM, C. M., VAN DER WALL, E. & VAN DIEST, P. J. 2018. Copy number changes at 8p11-12 predict adverse clinical outcome and chemo-and radiotherapy response in breast cancer. *Oncotarget,* 9**,** 17078.

MOLENAAR, J. J., KOSTER, J., ZWIJNENBURG, D. A., VAN SLUIS, P., VALENTIJN, L. J., VAN DER PLOEG, I., HAMDI, M., VAN NES, J., WESTERMAN, B. A. & VAN ARKEL, J. 2012. Sequencing of neuroblastoma identifies chromothripsis and defects in neuritogenesis genes. *Nature,* 483**,** 589.

MOLINA, G., VOGT, A., BAKAN, A., DAI, W., QUEIROZ DE OLIVEIRA, P., ZNOSKO, W., SMITHGALL, T. E., BAHAR, I., LAZO, J. S., DAY, B. W. & TSANG, M. 2009. Zebrafish chemical screening reveals an inhibitor of Dusp6 that expands cardiac cell lineages. *Nat Chem Biol,* 5**,** 680-7.

MONCLAIR, T., BRODEUR, G. M., AMBROS, P. F., BRISSE, H. J., CECCHETTO, G., HOLMES, K., KANEKO, M., LONDON, W. B., MATTHAY, K. K. & NUCHTERN, J. G. 2009. The international neuroblastoma risk group (INRG) staging system: an INRG task force report. *Journal of clinical oncology,* 27**,** 298.

MONTEIRO, L. F., FERRUZO, P. Y. M., RUSSO, L. C., FARIAS, J. O. & FORTI, F. L. 2018. DUSP3/VHR: a druggable dual phosphatase for human diseases. *Reviews of Physiology, Biochemistry and Pharmacology 176.* Springer.

MONTOYA, A., BELTRAN, L., CASADO, P., RODRÍGUEZ-PRADOS, J.-C. & CUTILLAS, P. R. 2011. Characterization of a TiO2 enrichment method for label-free quantitative phosphoproteomics. *Methods,* 54**,** 370-378.

MOON, S., KIM, W., KIM, S., KIM, Y., SONG, Y., BILOUSOV, O., KIM, J., LEE, T., CHA, B. & KIM, M. 2017. Phosphorylation by NLK inhibits YAP-14-3-3-interactions and induces its nuclear localization. *EMBO reports,* 18**,** 61-71.

MOORE, N. F., AZAROVA, A. M., BHATNAGAR, N., ROSS, K. N., DRAKE, L. E., FRUMM, S., LIU, Q. S., CHRISTIE, A. L., SANDA, T. & CHESLER, L. 2014. Molecular rationale for the use of PI3K/AKT/mTOR pathway inhibitors in combination with crizotinib in ALK-mutated neuroblastoma. *Oncotarget,* 5**,** 8737.

MOROZOVA, O., VOJVODIC, M., GRINSHTEIN, N., HANSFORD, L. M., BLAKELY, K. M., MASLOVA, A., HIRST, M., CEZARD, T., MORIN, R. D. & MOORE, R. 2010. System-level analysis of neuroblastoma tumor–initiating cells implicates AURKB as a novel drug target for neuroblastoma. *Clinical Cancer Research,* 16**,** 4572-4582.

MOSSÉ, Y. P., DEYELL, R. J., BERTHOLD, F., NAGAKAWARA, A., AMBROS, P. F., MONCLAIR, T., COHN, S. L., PEARSON, A. D., LONDON, W. B. & MATTHAY, K. K. 2014. Neuroblastoma in older children, adolescents and young adults: a report from the International Neuroblastoma Risk Group project. *Pediatric blood & cancer,* 61**,** 627-635.

MOSSE, Y. P., LAUDENSLAGER, M., KHAZI, D., CARLISLE, A. J., WINTER, C. L., RAPPAPORT, E. & MARIS, J. M. 2004. Germline PHOX2B mutation in hereditary neuroblastoma. *The American Journal of Human Genetics,* 75**,** 727-730.

MOSSÉ, Y. P., LAUDENSLAGER, M., LONGO, L., COLE, K. A., WOOD, A., ATTIYEH, E. F., LAQUAGLIA, M. J., SENNETT, R., LYNCH, J. E. & PERRI, P. 2008. Identification of ALK as a major familial neuroblastoma predisposition gene. *Nature,* 455**,** 930.

MUDA, M., MANNING, E. R., ORTH, K. & DIXON, J. E. 1999. Identification of the human YVH1 protein-tyrosine phosphatase orthologue reveals a novel zinc binding domain essential for in vivo function. *Journal of Biological Chemistry,* 274**,** 23991-23995.

MUNIYAPPA, H. & DAS, K. C. 2008. Activation of c-Jun N-terminal kinase (JNK) by widely used specific p38 MAPK inhibitors SB202190 and SB203580: a MLK-3-MKK7-dependent mechanism. *Cellular signalling,* 20**,** 675-683.

NAKAGAWARA, A., ARIMA-NAKAGAWARA, M., SCAVARDA, N. J., AZAR, C. G., CANTOR, A. B. & BRODEUR, G. M. 1993. Association between high levels of expression of the TRK gene and favorable outcome in human neuroblastoma. *New England Journal of Medicine,* 328**,** 847-854.

NAKAGAWARA, A., AZAR, C. G., SCAVARDA, N. J. & BRODEUR, G. M. 1994. Expression and function of TRK-B and BDNF in human neuroblastomas. *Molecular and cellular biology,* 14**,** 759-767.

NAU, M. M., BROOKS, B. J., BATTEY, J., SAUSVILLE, E., GAZDAR, A. F., KIRSCH, I. R., MCBRIDE, O., BERTNESS, V., HOLLIS, G. F. & MINNA, J. D. 1985. L-myc, a new myc-related gene amplified and expressed in human small cell lung cancer. *Nature,* 318**,** 69-73.

NDONG, C., LANDRY, R. P., SAHA, M. & ROMERO-SANDOVAL, E. A. 2014. Mitogen-activated protein kinase (MAPK) phosphatase-3 (MKP-3) displays a p-JNK-MAPK substrate preference in astrocytes in vitro. *Neuroscience letters,* 575**,** 13-18.

NGAN, E. S.-W. 2015. Heterogeneity of neuroblastoma. *Oncoscience,* 2**,** 837.

NGUYỄN, L. B., DISKIN, S. J., CAPASSO, M., WANG, K., DIAMOND, M. A., GLESSNER, J., KIM, C., ATTIYEH, E. F., MOSSE, Y. P. & COLE, K. 2011. Phenotype restricted genome-wide association study using a gene-centric approach identifies three low-risk neuroblastoma susceptibility Loci. *PLoS genetics,* 7**,** e1002026.

NICHOLS, A., CAMPS, M., GILLIERON, C., CHABERT, C., BRUNET, A., WILSBACHER, J., COBB, M., POUYSSEGUR, J., SHAW, J. P. & ARKINSTALL, S. 2000. Substrate recognition domains within extracellular signal-regulated kinase mediate binding and catalytic activation of mitogen-activated protein kinase phosphatase-3. *Journal of Biological Chemistry,* 275**,** 24613-24621.

NIESSEN, S., DIX, M. M., BARBAS, S., POTTER, Z. E., LU, S., BRODSKY, O., PLANKEN, S., BEHENNA, D., ALMADEN, C. & GAJIWALA, K. S. 2017. Proteome-wide map of targets of T790M-EGFR-directed covalent inhibitors. *Cell chemical biology,* 24**,** 1388-1400. e7.

NOMURA, M., SHIIBA, K.-I., KATAGIRI, C., KASUGAI, I., MASUDA, K., SATO, I., SATO, M., KAKUGAWA, Y., NOMURA, E. & HAYASHI, K. 2012. Novel function of MKP-5/DUSP10, a phosphatase of stress-activated kinases, on ERK-dependent gene expression, and upregulation of its gene expression in colon carcinomas. *Oncology reports,* 28**,** 931-936.

NUCHTERN, J. G., LONDON, W. B., BARNEWOLT, C. E., NARANJO, A., MCGRADY, P. W., GEIGER, J. D., DILLER, L., SCHMIDT, M. L., MARIS, J. M. & COHN, S. L. 2012. A prospective study of expectant observation as primary therapy for neuroblastoma in young infants, a children's oncology group study. *Annals of surgery,* 256**,** 573.

NUNES-XAVIER, C., ROMA-MATEO, C., RIOS, P., TARREGA, C., CEJUDO-MARIN, R., TABERNERO, L. & PULIDO, R. 2011. Dual-specificity MAP kinase phosphatases as targets of cancer treatment. *Anti-Cancer Agents in Medicinal Chemistry (Formerly Current Medicinal Chemistry-Anti-Cancer Agents),* 11**,** 109-132.

NUNES-XAVIER, C. E., AURTENETXE, O., ZALDUMBIDE, L., LÓPEZ-ALMARAZ, R., ERRAMUZPE, A., CORTÉS, J. M., LÓPEZ, J. I. & PULIDO, R. 2019a. Protein

tyrosine phosphatase PTPN1 modulates cell growth and associates with poor outcome in human neuroblastoma. *Diagnostic Pathology,* 14**,** 1-8.

NUNES-XAVIER, C. E., TÁRREGA, C., CEJUDO-MARÍN, R., FRIJHOFF, J., SANDIN, Å., ÖSTMAN, A. & PULIDO, R. 2010. Differential up-regulation of MAP kinase phosphatases MKP3/DUSP6 and DUSP5 by Ets2 and c-Jun converge in the control of the growth arrest versus proliferation response of MCF-7 breast cancer cells to phorbol ester. *Journal of Biological Chemistry,* 285**,** 26417-26430.

NUNES-XAVIER, C. E., ZALDUMBIDE, L., AURTENETXE, O., LÓPEZ-ALMARAZ, R., LÓPEZ, J. I. & PULIDO, R. 2019b. Dual-Specificity Phosphatases in Neuroblastoma Cell Growth and Differentiation. *International journal of molecular sciences,* 20**,** 1170.

OCHIAI, H., TAKENOBU, H., NAKAGAWA, A., YAMAGUCHI, Y., KIMURA, M., OHIRA, M., OKIMOTO, Y., FUJIMURA, Y., KOSEKI, H. & KOHNO, Y. 2010. Bmi1 is a MYCN target gene that regulates tumorigenesis through repression of KIF1B β and TSLC1 in neuroblastoma. *Oncogene,* 29**,** 2681-2690.

OHGUSHI, M., MINAGUCHI, M. & SASAI, Y. 2015. Rho-signaling-directed YAP/TAZ activity underlies the long-term survival and expansion of human embryonic stem cells. *Cell stem cell,* 17**,** 448-461.

OKUDELA, K., YAZAWA, T., WOO, T., SAKAEDA, M., ISHII, J., MITSUI, H., SHIMOYAMADA, H., SATO, H., TAJIRI, M. & OGAWA, N. 2009. Down-regulation of DUSP6 expression in lung cancer: its mechanism and potential role in carcinogenesis. *The American journal of pathology,* 175**,** 867-881.

OLSEN, J. V., BLAGOEV, B., GNAD, F., MACEK, B., KUMAR, C., MORTENSEN, P. & MANN, M. 2006. Global, in vivo, and site-specific phosphorylation dynamics in signaling networks. *Cell,* 127**,** 635-648.

OPEL, D., POREMBA, C., SIMON, T., DEBATIN, K.-M. & FULDA, S. 2007. Activation of Akt predicts poor outcome in neuroblastoma. *Cancer research,* 67**,** 735-745.

ÖSTMAN, A., HELLBERG, C. & BÖHMER, F. D. 2006. Protein-tyrosine phosphatases and cancer. *Nature Reviews Cancer,* 6**,** 307-320.

OZEK, C., KANOSKI, S. E., ZHANG, Z.-Y., GRILL, H. J. & BENCE, K. K. 2014. Protein-tyrosine phosphatase 1B (PTP1B) is a novel regulator of central brain-derived neurotrophic factor and tropomyosin receptor kinase B (TrkB) signaling. *Journal of Biological Chemistry,* 289**,** 31682-31692.

PALACIOS-MORENO, J., FOLTZ, L., GUO, A., STOKES, M. P., KUEHN, E. D., GEORGE, L., COMB, M. & GRIMES, M. L. 2015. Neuroblastoma tyrosine kinase signaling networks involve FYN and LYN in endosomes and lipid rafts. *PLoS computational biology,* 11**,** e1004130.

PARK, J.-W., WOLLMANN, G., URBIOLA, C., FOGLI, B., FLORIO, T., GELEY, S. & KLIMASCHEWSKI, L. 2018. Sprouty2 enhances the tumorigenic potential of glioblastoma cells. *Neuro-oncology,* 20**,** 1044-1054.

PARK, J. R., BAGATELL, R., LONDON, W. B., MARIS, J. M., COHN, S. L., MATTAY, K. M., HOGARTY, M. & COMMITTEE, C. N. 2013. Children's Oncology Group's 2013 blueprint for research: neuroblastoma. *Pediatric blood & cancer,* 60**,** 985-993.

PARMAR, R., WADIA, F., YASSA, R. & ZENIOS, M. 2013. Neuroblastoma: a rare cause of a limping child. How to avoid a delayed diagnosis? *Journal of Pediatric Orthopaedics,* 33**,** e45-e51.

PATHAN, M., KEERTHIKUMAR, S., ANG, C. S., GANGODA, L., QUEK, C. Y., WILLIAMSON, N. A., MOURADOV, D., SIEBER, O. M., SIMPSON, R. J. & SALIM, A. 2015. FunRich: An open access standalone functional enrichment and interaction network analysis tool. *Proteomics,* 15**,** 2597-2601.

PATTERSON, K. I., BRUMMER, T., O'BRIEN, P. M. & DALY, R. J. 2009. Dual-specificity phosphatases: critical regulators with diverse cellular targets. *Biochem J,* 418**,** 475-89.

PAULSSON, K., HORVAT, A., STRÖMBECK, B., NILSSON, F., HELDRUP, J., BEHRENDTZ, M., FORESTIER, E., ANDERSSON, A., FIORETOS, T. & JOHANSSON, B. 2008. Mutations of FLT3, NRAS, KRAS, and PTPN11 are frequent and possibly mutually exclusive in high hyperdiploid childhood acute lymphoblastic leukemia. *Genes, Chromosomes and Cancer,* 47**,** 26-33.

PAVIC, K., DUAN, G. & KÖHN, M. 2015. VHR/DUSP3 phosphatase: structure, function and regulation. *The FEBS journal,* 282**,** 1871-1890.

PAVIC, K., RIOS, P., DZEYK, K., KOEHLER, C., LEMKE, E. A. & KÖHN, M. 2014. Unnatural amino acid mutagenesis reveals dimerization as a negative regulatory mechanism of VHR's phosphatase activity. *ACS chemical biology,* 9**,** 1451-1459.

PERDIGUERO, E., RUIZ-BONILLA, V., GRESH, L., HUI, L., BALLESTAR, E., SOUSA-VICTOR, P., BAEZA-RAJA, B., JARDÍ, M., BOSCH-COMAS, A. & ESTELLER, M. 2007. Genetic analysis of p38 MAP kinases in myogenesis: fundamental role of p38α in abrogating myoblast proliferation. *The EMBO journal,* 26**,** 1245-1256.

PÉREZ-SEN, R., QUEIPO, M. J., GIL-REDONDO, J. C., ORTEGA, F., GÓMEZ-VILLAFUERTES, R., MIRAS-PORTUGAL, M. T. & DELICADO, E. G. 2019. Dual-specificity phosphatase regulation in neurons and glial cells. *International Journal of Molecular Sciences,* 20**,** 1999.

PINTO, N. R., APPLEBAUM, M. A., VOLCHENBOUM, S. L., MATTHAY, K. K., LONDON, W. B., AMBROS, P. F., NAKAGAWARA, A., BERTHOLD, F., SCHLEIERMACHER, G. & PARK, J. R. 2015. Advances in risk classification and treatment strategies for neuroblastoma. *Journal of clinical oncology,* 33**,** 3008.

PIYA, S., KIM, J. Y., BAE, J., SEOL, D.-W., MOON, A. R. & KIM, T.-H. 2012. DUSP6 is a novel transcriptional target of p53 and regulates p53-mediated apoptosis by modulating expression levels of Bcl-2 family proteins. *FEBS letters,* 586**,** 4233-4240.

PLOTNIKOV, A., CHUDERLAND, D., KARAMANSHA, Y., LIVNAH, O. & SEGER, R. 2019. Nuclear ERK translocation is mediated by protein kinase CK2 and accelerated by autophosphorylation. *Cell. Physiol. Biochem,* 53**,** 366-387.

POTTIER, C., FRESNAIS, M., GILON, M., JÉRUSALEM, G., LONGUESPÉE, R. & SOUNNI, N. E. 2020. Tyrosine kinase inhibitors in cancer: breakthrough and challenges of targeted therapy. *Cancers,* 12**,** 731.

PRAHALLAD, A., HEYNEN, G. J., GERMANO, G., WILLEMS, S. M., EVERS, B., VECCHIONE, L., GAMBINO, V., LIEFTINK, C., BEIJERSBERGEN, R. L. & DI

NICOLANTONIO, F. 2015. PTPN11 is a central node in intrinsic and acquired resistance to targeted cancer drugs. *Cell reports,* 12**,** 1978-1985.

PUGH, T. J., MOROZOVA, O., ATTIYEH, E. F., ASGHARZADEH, S., WEI, J. S., AUCLAIR, D., CARTER, S. L., CIBULSKIS, K., HANNA, M. & KIEZUN, A. 2013. The genetic landscape of high-risk neuroblastoma. *Nature genetics,* 45**,** 279.

PUISSANT, A., FRUMM, S. M., ALEXE, G., BASSIL, C. F., QI, J., CHANTHERY, Y. H., NEKRITZ, E. A., ZEID, R., GUSTAFSON, W. C. & GRENINGER, P. 2013. Targeting MYCN in neuroblastoma by BET bromodomain inhibition. *Cancer discovery,* 3**,** 308-323.

RAHMOUNI, S., CERIGNOLI, F., ALONSO, A., TSUTJI, T., HENKENS, R., ZHU, C., LOUIS-DIT-SULLY, C., MOUTSCHEN, M., JIANG, W. & MUSTELIN, T. 2006. Loss of the VHR dual-specific phosphatase causescell-cycle arrest and senescence. *Nature cell biology,* 8**,** 524-531.

RAJBHANDARI, P., LOPEZ, G., CAPDEVILA, C., SALVATORI, B., YU, J., RODRIGUEZ-BARRUECO, R., MARTINEZ, D., YARMARKOVICH, M., WEICHERT-LEAHEY, N. & ABRAHAM, B. J. 2018. Cross-cohort analysis identifies a TEAD4–MYCN positive feedback loop as the core regulatory element of high-risk neuroblastoma. *Cancer discovery,* 8**,** 582-599.

RAMAN, P., ZIMMERMAN, S., RATHI, K. S., DE TORRENTÉ, L., SARMADY, M., WU, C., LEIPZIG, J., TAYLOR, D. M., TOZEREN, A. & MAR, J. C. 2019. A comparison of survival analysis methods for cancer gene expression RNA-Sequencing data. *Cancer Genetics,* 235**,** 1-12.

RAMKISSOON, A., CHANEY, K. E., MILEWSKI, D., WILLIAMS, K. B., WILLIAMS, R. L., CHOI, K., MILLER, A. A., KALIN, T. V., PRESSEY, J. G. & SZABO, S. 2019. Targeted inhibition of the dual specificity phosphatases DUSP1 and DUSP6 suppress MPNST growth via JNK. *Clinical Cancer Research***,** clincanres. 3224.2018.

RAN, F., HSU, P. D., WRIGHT, J., AGARWALA, V., SCOTT, D. A. & ZHANG, F. 2013. Genome engineering using the CRISPR-Cas9 system. *Nature protocols,* 8**,** 2281-2308.

RASTOGI, P., NASEEM, S., VARMA, N., DAS, R., AHLUWALIA, J., SACHDEVA, M. U. S., SHARMA, P., KUMAR, N. & MARWAHA, R. K. 2015. Bone marrow involvement in neuroblastoma: a study of hemato-morphological features. *Indian Journal of Hematology and Blood Transfusion,* 31**,** 57-60.

REDAELLI, S., CECCON, M., ZAPPA, M., SHARMA, G. G., MASTINI, C., MAURI, M., NIGOGHOSSIAN, M., MASSIMINO, L., CORDANI, N. & FARINA, F. 2018. Lorlatinib treatment elicits multiple on-and off-target mechanisms of resistance in ALK-driven cancer. *Cancer Research,* 78**,** 6866-6880.

REDZA-DUTORDOIR, M. & AVERILL-BATES, D. A. 2016. Activation of apoptosis signalling pathways by reactive oxygen species. *Biochimica et Biophysica Acta (BBA)-Molecular Cell Research,* 1863**,** 2977-2992.

REFFAS, S. & SCHLEGEL, W. 2000. Compartment-specific regulation of extracellular signal-regulated kinase (ERK) and c-Jun N-terminal kinase (JNK) mitogen-activated protein kinases (MAPKs) by ERK-dependent and non-ERK-dependent inductions of MAPK phosphatase (MKP)-3 and MKP-1 in differentiating P19 cells. *Biochemical Journal,* 352**,** 701-708.

REGAD, T. 2015. Targeting RTK signaling pathways in cancer. *Cancers,* 7**,** 1758-1784.

REITERER, V., EYERS, P. A. & FARHAN, H. 2014. Day of the dead: pseudokinases and pseudophosphatases in physiology and disease. *Trends in cell biology,* 24**,** 489-505.

REN, Y., OUYANG, Z., HOU, Z., YAN, Y., ZHI, Z., SHI, M., DU, M., LIU, H., WEN, Y. & SHAO, Y. 2020. CIC is a mediator of the ERK1/2-DUSP6 negative feedback loop. *IScience,* 23**,** 101635.

RIBATTI, D., RAFFAGHELLO, L., PASTORINO, F., NICO, B., BRIGNOLE, C., VACCA, A. & PONZONI, M. 2002. In vivo angiogenic activity of neuroblastoma correlates with MYCN oncogene overexpression. *International journal of cancer,* 102**,** 351-354.

RICHARDS, M. W., BURGESS, S. G., POON, E., CARSTENSEN, A., EILERS, M., CHESLER, L. & BAYLISS, R. 2016. Structural basis of N-Myc binding by Aurora-A and its destabilization by kinase inhibitors. *Proceedings of the National Academy of Sciences,* 113**,** 13726-13731.

ROZEN, E. J. & SHOHET, J. M. 2021. Systematic review of the receptor tyrosine kinase superfamily in neuroblastoma pathophysiology. *Cancer and Metastasis Reviews***,** 1-20.

RUIZ-PÉREZ, M. V., HENLEY, A. B. & ARSENIAN-HENRIKSSON, M. 2017. The MYCN protein in health and disease. *Genes,* 8**,** 113.

RUSHWORTH, L. K., KIDGER, A. M., DELAVAINE, L., STEWART, G., VAN SCHELVEN, S., DAVIDSON, J., BRYANT, C. J., CADDYE, E., EAST, P. & CAUNT, C. J. 2014. Dual-specificity phosphatase 5 regulates nuclear ERK activity and suppresses skin cancer by inhibiting mutant Harvey-Ras (HRasQ61L)-driven SerpinB2 expression. *Proceedings of the National Academy of Sciences,* 111**,** 18267-18272.

RUSSO, L. C., FARIAS, J. O. & FORTI, F. L. 2020. DUSP3 maintains genomic stability and cell proliferation by modulating NER pathway and cell cycle regulatory proteins. *Cell Cycle,* 19**,** 1545-1561.

SALMEEN, A., ANDERSEN, J. N., MYERS, M. P., MENG, T.-C., HINKS, J. A., TONKS, N. K. & BARFORD, D. 2003. Redox regulation of protein tyrosine phosphatase 1B involves a sulphenyl-amide intermediate. *Nature,* 423**,** 769-773.

SARBASSOV, D. D., GUERTIN, D. A., ALI, S. M. & SABATINI, D. M. 2005. Phosphorylation and regulation of Akt/PKB by the rictor-mTOR complex. *Science,* 307**,** 1098-1101.

SATTU, K., HOCHGRÄFE, F., WU, J., UMAPATHY, G., SCHÖNHERR, C., RUUTH, K., CHAND, D., WITEK, B., FUCHS, J. & LI, P. K. 2013. Phosphoproteomic analysis of anaplastic lymphoma kinase (ALK) downstream signaling pathways identifies signal transducer and activator of transcription 3 as a functional target of activated ALK in neuroblastoma cells. *The FEBS journal,* 280**,** 5269-5282.

SAUSEN, M., LEARY, R. J., JONES, S., WU, J., REYNOLDS, C. P., LIU, X., BLACKFORD, A., PARMIGIANI, G., DIAZ JR, L. A. & PAPADOPOULOS, N. 2013. Integrated genomic analyses identify ARID1A and ARID1B alterations in the childhood cancer neuroblastoma. *Nature genetics,* 45**,** 12.

SCHINDELIN, J., ARGANDA-CARRERAS, I., FRISE, E., KAYNIG, V., LONGAIR, M., PIETZSCH, T., PREIBISCH, S., RUEDEN, C., SAALFELD, S. & SCHMID, B. 2012. Fiji: an open-source platform for biological-image analysis. *Nature methods,* 9**,** 676-682.

SCHLEIERMACHER, G., MICHON, J., RIBEIRO, A., PIERRON, G., MOSSERI, V., RUBIE, H., MUNZER, C., BÉNARD, J., AUGER, N. & COMBARET, V. 2011. Segmental chromosomal alterations lead to a higher risk of relapse in infants with MYCN-non-amplified localised unresectable/disseminated neuroblastoma (a SIOPEN collaborative study). *British journal of cancer,* 105**,** 1940-1948.

SCHLESSINGER, J. 2014. Receptor tyrosine kinases: legacy of the first two decades. *Cold Spring Harb Perspect Biol,* 6.

SCHMELZ, K., TOEDLING, J., HUSKA, M., CWIKLA, M. C., KRUETZFELDT, L.-M., PROBA, J., AMBROS, P. F., AMBROS, I. M., BORAL, S. & LODRINI, M. 2021. Spatial and temporal intratumour heterogeneity has potential consequences for single biopsy-based neuroblastoma treatment decisions. *Nature communications,* 12**,** 1-13.

SCHMID, C. A., ROBINSON, M. D., SCHEIFINGER, N. A., MÜLLER, S., COGLIATTI, S., TZANKOV, A. & MÜLLER, A. 2015. DUSP4 deficiency caused by promoter hypermethylation drives JNK signaling and tumor cell survival in diffuse large B cell lymphoma. *Journal of Experimental Medicine,* 212**,** 775-792.

SCHMITTGEN, T. D. & LIVAK, K. J. 2008. Analyzing real-time PCR data by the comparative CT method. *Nature protocols,* 3**,** 1101-1108.

SCHNEEBERGER, V. E., LUETTEKE, N., REN, Y., BERNS, H., CHEN, L., FOROUTAN, P., MARTINEZ, G. V., HAURA, E. B., CHEN, J. & COPPOLA, D. 2014. SHP2E76K mutant promotes lung tumorigenesis in transgenic mice. *Carcinogenesis,* 35**,** 1717-1725.

SCHNEIDER, C. A., RASBAND, W. S. & ELICEIRI, K. W. 2012. NIH Image to ImageJ: 25 years of image analysis. *Nature methods,* 9**,** 671-675.

SCHNEIDERMAN, J., LONDON, W. B., BRODEUR, G. M., CASTLEBERRY, R. P., LOOK, A. T. & COHN, S. L. 2008. Clinical significance of MYCN amplification and ploidy in favorable-stage neuroblastoma: a report from the Children's Oncology Group. *Journal of clinical oncology,* 26**,** 913-918.

SCHÖNHERR, C., RUUTH, K., KAMARAJ, S., WANG, C.-L., YANG, H.-L., COMBARET, V., DJOS, A., MARTINSSON, T., CHRISTENSEN, J. G. & PALMER, R. H. 2012. Anaplastic Lymphoma Kinase (ALK) regulates initiation of transcription of MYCN in neuroblastoma cells. *Oncogene,* 31**,** 5193-5200.

SEEGER, R. C., BRODEUR, G. M., SATHER, H., DALTON, A., SIEGEL, S. E., WONG, K. Y. & HAMMOND, D. 1985. Association of multiple copies of the N-myc oncogene with rapid progression of neuroblastomas. *New England Journal of Medicine,* 313**,** 1111-1116.

SEGERSTRÖM, L., BARYAWNO, N., SVEINBJÖRNSSON, B., WICKSTRÖM, M., ELFMAN, L., KOGNER, P. & JOHNSEN, J. I. 2011. Effects of small molecule inhibitors of PI3K/Akt/mTOR signaling on neuroblastoma growth in vitro and in vivo. *International journal of cancer,* 129**,** 2958-2965.

SEKINE, Y., IKEDA, O., HAYAKAWA, Y., TSUJI, S., IMOTO, S., AOKI, N., SUGIYAMA, K. & MATSUDA, T. 2007. DUSP22/LMW-DSP2 regulates estrogen receptor-α-

mediated signaling through dephosphorylation of Ser-118. *Oncogene,* 26**,** 6038-6049.

SENTMANAT, M. F., PETERS, S. T., FLORIAN, C. P., CONNELLY, J. P. & PRUETT-MILLER, S. M. 2018. A survey of validation strategies for CRISPR-Cas9 editing. *Scientific reports,* 8**,** 1-8.

SETERNES, O.-M., KIDGER, A. M. & KEYSE, S. M. 2019. Dual-specificity MAP kinase phosphatases in health and disease. *Biochimica et Biophysica Acta (BBA)-Molecular Cell Research,* 1866**,** 124-143.

SHANG, X., BURLINGAME, S. M., OKCU, M. F., GE, N., RUSSELL, H. V., EGLER, R. A., DAVID, R. D., VASUDEVAN, S. A., YANG, J. & NUCHTERN, J. G. 2009. Aurora A is a negative prognostic factor and a new therapeutic target in human neuroblastoma. *Molecular cancer therapeutics,* 8**,** 2461-2469.

SHANG, X., VASUDEVAN, S., YU, Y., GE, N., LUDWIG, A., WESSON, C., WANG, K., BURLINGAME, S., ZHAO, Y. & RAO, P. 2010. Dual-specificity phosphatase 26 is a novel p53 phosphatase and inhibits p53 tumor suppressor functions in human neuroblastoma. *Oncogene,* 29**,** 4938-4946.

SHANNON, P., MARKIEL, A., OZIER, O., BALIGA, N. S., WANG, J. T., RAMAGE, D., AMIN, N., SCHWIKOWSKI, B. & IDEKER, T. 2003. Cytoscape: a software environment for integrated models of biomolecular interaction networks. *Genome research,* 13**,** 2498-2504.

SHAW, A. T., FRIBOULET, L., LESHCHINER, I., GAINOR, J. F., BERGQVIST, S., BROOUN, A., BURKE, B. J., DENG, Y.-L., LIU, W. & DARDAEI, L. 2016. Resensitization to crizotinib by the lorlatinib ALK resistance mutation L1198F. *New England Journal of Medicine,* 374**,** 54-61.

SHEN, J., ZHOU, S., SHI, L., LIU, X., LIN, H. & YU, H. 2017. DUSP1 inhibits cell proliferation, metastasis and invasion and angiogenesis in gallbladder cancer. *Oncotarget,* 8**,** 12133.

SHEN, W. H., BALAJEE, A. S., WANG, J., WU, H., ENG, C., PANDOLFI, P. P. & YIN, Y. 2007. Essential role for nuclear PTEN in maintaining chromosomal integrity. *Cell,* 128**,** 157-170.

SHI, Y. 2002. Mechanisms of caspase activation and inhibition during apoptosis. *Molecular cell,* 9**,** 459-470.

SHI, Y., MA, I. T., PATEL, R. H., SHANG, X., CHEN, Z., ZHAO, Y., CHENG, J., FAN, Y., ROJAS, Y., BARBIERI, E., CHEN, Z., YU, Y., JIN, J., KIM, E. S., SHOHET, J. M., VASUDEVAN, S. A. & YANG, J. 2015. NSC-87877 inhibits DUSP26 function in neuroblastoma resulting in p53-mediated apoptosis. *Cell Death Dis,* 6**,** e1841.

SHIM, J. & GOLDSMITH, K. C. 2021. A New Player in Neuroblastoma: YAP and Its Role in the Neuroblastoma Microenvironment. *Cancers,* 13**,** 4650.

SHIMADA, H., UMEHARA, S., MONOBE, Y., HACHITANDA, Y., NAKAGAWA, A., GOTO, S., GERBING, R. B., STRAM, D. O., LUKENS, J. N. & MATTHAY, K. K. 2001. International neuroblastoma pathology classification for prognostic evaluation of patients with peripheral neuroblastic tumors: a report from the Children's Cancer Group. *Cancer,* 92**,** 2451-2461.

SHIN, J.-W., KWON, S.-B., BAK, Y., LEE, S.-K. & YOON, D.-Y. 2018. BCI induces apoptosis via generation of reactive oxygen species and activation of

intrinsic mitochondrial pathway in H1299 lung cancer cells. *Science China Life Sciences,* 61**,** 1243-1253.

SHOJAEE, S., CAESER, R., BUCHNER, M., PARK, E., SWAMINATHAN, S., HURTZ, C., GENG, H., CHAN, L. N., KLEMM, L. & HOFMANN, W.-K. 2015. Erk negative feedback control enables pre-B cell transformation and represents a therapeutic target in acute lymphoblastic leukemia. *Cancer cell,* 28**,** 114-128.

SHUSTER, J. J., MCWILLIAMS, N. B., CASTLEBERRY, R., NITSCHKE, R., SMITH, E. I., ALTSHULER, G., KUN, L., BRODEUR, G., JOSHI, V. & VIETTI, T. 1992. Serum lactate dehydrogenase in childhood neuroblastoma. A Pediatric Oncology Group recursive partitioning study. *American journal of clinical oncology,* 15**,** 295-303.

SLACK, A. & SHOHET, J. M. 2005. MDM2 as a critical effector of the MYCN oncogene in tumorigenesis. *Cell Cycle,* 4**,** 857-860.

SMITH, S. J., DIEHL, N., LEAVITT, J. A. & MOHNEY, B. G. 2010. Incidence of pediatric Horner syndrome and the risk of neuroblastoma: a population-based study. *Archives of ophthalmology,* 128**,** 324-329.

SONG, H., WU, C., WEI, C., LI, D., HUA, K., SONG, J., XU, H., CHEN, L. & FANG, L. 2015. Silencing of DUSP6 gene by RNAi-mediation inhibits proliferation and growth in MDA-MB-231 breast cancer cells: an in vitro study. *International journal of clinical and experimental medicine,* 8**,** 10481.

SONG, M. S., CARRACEDO, A., SALMENA, L., SONG, S. J., EGIA, A., MALUMBRES, M. & PANDOLFI, P. P. 2011. Nuclear PTEN regulates the APC-CDH1 tumor-suppressive complex in a phosphatase-independent manner. *Cell,* 144**,** 187-199.

SONG, M. S., SALMENA, L. & PANDOLFI, P. P. 2012. The functions and regulation of the PTEN tumour suppressor. *Nature reviews Molecular cell biology,* 13**,** 283-296.

SOULSBY, M. & BENNETT, A. M. 2009. Physiological signaling specificity by protein tyrosine phosphatases. *Physiology,* 24**,** 281-289.

SPITZ, R., HERO, B., ERNESTUS, K. & BERTHOLD, F. 2003. Deletions in chromosome arms 3p and 11q are new prognostic markers in localized and 4s neuroblastoma. *Clinical cancer research,* 9**,** 52-58.

SPURLOCK, B., PARKER, D., BASU, M. K., HJELMELAND, A., SAJINA, G., LIU, S., SIEGAL, G. P., GUNTER, A., MORAN, A. & MITRA, K. 2021. Fine-tuned repression of Drp1-driven mitochondrial fission primes a 'stem/progenitor-like state'to support neoplastic transformation. *Elife,* 10**,** e68394.

ST-DENIS, N., GUPTA, G. D., LIN, Z. Y., GONZALEZ-BADILLO, B., VERI, A. O., KNIGHT, J. D. R., RAJENDRAN, D., COUZENS, A. L., CURRIE, K. W., TKACH, J. M., CHEUNG, S. W. T., PELLETIER, L. & GINGRAS, A. C. 2016. Phenotypic and Interaction Profiling of the Human Phosphatases Identifies Diverse Mitotic Regulators. *Cell Rep,* 17**,** 2488-2501.

STANFORD, S. M. & BOTTINI, N. 2017. Targeting Tyrosine Phosphatases: Time to End the Stigma. *Trends Pharmacol Sci,* 38**,** 524-540.

STECK, P. A., PERSHOUSE, M. A., JASSER, S. A., YUNG, W., LIN, H., LIGON, A. H., LANGFORD, L. A., BAUMGARD, M. L., HATTIER, T. & DAVIS, T. 1997. Identification of a candidate tumour suppressor gene, MMAC1, at

chromosome 10q23. 3 that is mutated in multiple advanced cancers. *Nature genetics,* 15**,** 356-362.

SUGIURA, R., SATOH, R. & TAKASAKI, T. 2021. ERK: A double-edged sword in cancer. ERK-dependent apoptosis as a potential therapeutic Strategy for cancer. *Cells,* 10**,** 2509.

SUNG, H., FERLAY, J., SIEGEL, R. L., LAVERSANNE, M., SOERJOMATARAM, I., JEMAL, A. & BRAY, F. 2021. Global cancer statistics 2020: GLOBOCAN estimates of incidence and mortality worldwide for 36 cancers in 185 countries. *CA: a cancer journal for clinicians,* 71**,** 209-249.

TANAKA, N. & FUKUZAWA, M. 2008. MYCN downregulates integrin α1 to promote invasion of human neuroblastoma cells. *International journal of oncology,* 33**,** 815-821.

TANAKA, T., HIGASHI, M., KIMURA, K., WAKAO, J., FUMINO, S., IEHARA, T., HOSOI, H., SAKAI, T. & TAJIRI, T. 2016. MEK inhibitors as a novel therapy for neuroblastoma: Their in vitro effects and predicting their efficacy. *Journal of pediatric surgery,* 51**,** 2074-2079.

TANG, J. P., TAN, C. P., LI, J., SIDDIQUE, M. M., GUO, K., CHAN, S. W., PARK, J. E., TAY, W. N., HUANG, Z. Y. & LI, W. C. 2010. VHZ is a novel centrosomal phosphatase associated with cell growth and human primary cancers. *Molecular cancer,* 9**,** 1-9.

TANOUE, T., MORIGUCHI, T. & NISHIDA, E. 1999. Molecular cloning and characterization of a novel dual specificity phosphatase, MKP-5. *Journal of Biological Chemistry,* 274**,** 19949-19956.

TANUMA, N., NOMURA, M., IKEDA, M., KASUGAI, I., TSUBAKI, Y., TAKAGAKI, K., KAWAMURA, T., YAMASHITA, Y., SATO, I. & SATO, M. 2009. Protein phosphatase Dusp26 associates with KIF3 motor and promotes N-cadherin-mediated cell–cell adhesion. *Oncogene,* 28**,** 752-761.

TARTAGLIA, M., NIEMEYER, C. M., FRAGALE, A., SONG, X., BUECHNER, J., JUNG, A., HÄHLEN, K., HASLE, H., LICHT, J. D. & GELB, B. D. 2003. Somatic mutations in PTPN11 in juvenile myelomonocytic leukemia, myelodysplastic syndromes and acute myeloid leukemia. *Nature genetics,* 34**,** 148-150.

TAUTZ, L., PELLECCHIA, M. & MUSTELIN, T. 2006. Targeting the PTPome in human disease. *Expert opinion on therapeutic targets,* 10**,** 157-177.

THIELE, C. 1998. Neuroblastoma: In (Ed.) Masters. *J. Human Cell Culture. Lancaster, UK: Kluwer Academic Publishers,* 1**,** 21-53.

THOMPSON, E. M. & STOKER, A. W. 2021. A Review of DUSP26: Structure, Regulation and Relevance in Human Disease. *International Journal of Molecular Sciences,* 22**,** 776.

TIAN, X., FAN, J., HOU, W., BAI, S., AO, Q. & TONG, H. 2016. Sodium orthovanadate induces the apoptosis of SH-SY5Y cells by inhibiting PIWIL2. *Molecular medicine reports,* 13**,** 874-880.

TOLBERT, V. P. & MATTHAY, K. K. 2018. Neuroblastoma: clinical and biological approach to risk stratification and treatment. *Cell and tissue research,* 372**,** 195-209.

TOLEDANO-KATCHALSKI, H., KRAUT, J., SINES, T., GRANOT-ATTAS, S., SHOHAT, G., GIL-HENN, H., YUNG, Y. & ELSON, A. 2003. Protein Tyrosine Phosphatase ε Inhibits Signaling by Mitogen-Activated Protein Kinases11The Israel

Science Foundation, founded by The Israel Academy of Sciences and Humanities, and by a research grant from Mr. and Mrs. Lon Morton. *Molecular cancer research,* 1**,** 541-550.

TONG, X., MU, P., ZHANG, Y., ZHAO, J. & WANG, X. 2020. TRIM59, amplified in ovarian cancer, promotes tumorigenesis through the MKP3/ERK pathway. *Journal of Cellular Physiology,* 235**,** 8236-8245.

TONKS, N. K. 2006. Protein tyrosine phosphatases: from genes, to function, to disease. *Nature reviews Molecular cell biology,* 7**,** 833-846.

TORRES, T. E., RUSSO, L. C., SANTOS, A., MARQUES, G. R., MAGALHAES, Y. T., TABASSUM, S. & FORTI, F. L. 2017. Loss of DUSP3 activity radiosensitizes human tumor cell lines via attenuation of DNA repair pathways. *Biochimica et Biophysica Acta (BBA)-General Subjects,* 1861**,** 1879-1894.

TRIGG, R. M. & TURNER, S. D. 2018. ALK in neuroblastoma: biological and therapeutic implications. *Cancers,* 10**,** 113.

TROCHET, D., BOURDEAUT, F., JANOUEIX-LEROSEY, I., DEVILLE, A., DE PONTUAL, L., SCHLEIERMACHER, G., COZE, C., PHILIP, N., FRÉBOURG, T. & MUNNICH, A. 2004. Germline mutations of the paired–like homeobox 2B (PHOX2B) gene in neuroblastoma. *The American Journal of Human Genetics,* 74**,** 761-764.

TSHERNIAK, A., VAZQUEZ, F., MONTGOMERY, P. G., WEIR, B. A., KRYUKOV, G., COWLEY, G. S., GILL, S., HARRINGTON, W. F., PANTEL, S. & KRILL-BURGER, J. M. 2017. Defining a cancer dependency map. *Cell,* 170**,** 564-576. e16.

TSUJI, T., OZASA, H., AOKI, W., ABURAYA, S., YAMAMOTO FUNAZO, T., FURUGAKI, K., YOSHIMURA, Y., YAMAZOE, M., AJIMIZU, H. & YASUDA, Y. 2020. YAP1 mediates survival of ALK-rearranged lung cancer cells treated with alectinib via pro-apoptotic protein regulation. *Nature communications,* 11**,** 1-16.

TSUTSUMI, R., RAN, H. & NEEL, B. G. 2018. Off-target inhibition by active site-targeting SHP 2 inhibitors. *FEBS open bio,* 8**,** 1405-1411.

UEDA, K., ARAKAWA, H. & NAKAMURA, Y. 2003. Dual-specificity phosphatase 5 (DUSP5) as a direct transcriptional target of tumor suppressor p53. *Oncogene,* 22**,** 5586-5591.

UMAPATHY, G., GUAN, J., GUSTAFSSON, D. E., JAVANMARDI, N., CERVANTES-MADRID, D., DJOS, A., MARTINSSON, T., PALMER, R. H. & HALLBERG, B. 2017. MEK inhibitor trametinib does not prevent the growth of anaplastic lymphoma kinase (ALK)–addicted neuroblastomas. *Science signaling,* 10**,** eaam7550.

VAN DEN EYNDEN, J., UMAPATHY, G., ASHOURI, A., CERVANTES-MADRID, D., SZYDZIK, J., RUUTH, K., KOSTER, J., LARSSON, E., GUAN, J. & PALMER, R. H. 2018. Phosphoproteome and gene expression profiling of ALK inhibition in neuroblastoma cell lines reveals conserved oncogenic pathways. *Sci. Signal.,* 11**,** eaar5680.

VAN GOLEN, C. M., SOULES, M. E., GRAUMAN, A. R. & FELDMAN, E. L. 2003. N-Myc overexpression leads to decreased β1 integrin expression and increased apoptosis in human neuroblastoma cells. *Oncogene,* 22**,** 2664-2673.

VAN OVERBEEK, M., CAPURSO, D., CARTER, M. M., THOMPSON, M. S., FRIAS, E., RUSS, C., REECE-HOYES, J. S., NYE, C., GRADIA, S. & VIDAL, B. 2016. DNA

repair profiling reveals nonrandom outcomes at Cas9-mediated breaks. *Molecular cell,* 63**,** 633-646.

VAN VLIET, C., BUKCZYNSKA, P. E., PURYER, M. A., SADEK, C. M., SHIELDS, B. J., TREMBLAY, M. L. & TIGANIS, T. 2005. Selective regulation of tumor necrosis factor–induced Erk signaling by Src family kinases and the T cell protein tyrosine phosphatase. *Nature immunology,* 6**,** 253-260.

VANGIPURAM, S. D., WANG, Z. J. & LYMAN, W. D. 2010. Resistance of stem-like cells from neuroblastoma cell lines to commonly used chemotherapeutic agents. *Pediatric blood & cancer,* 54**,** 361-368.

VASUDEVAN, S. A., SKOKO, J., WANG, K., BURLINGAME, S. M., PATEL, P. N., LAZO, J. S., NUCHTERN, J. G. & YANG, J. 2005. MKP-8, a novel MAPK phosphatase that inhibits p38 kinase. *Biochemical and biophysical research communications,* 330**,** 511-518.

VAUGHAN, L., CLARKE, P. A., BARKER, K., CHANTHERY, Y., GUSTAFSON, C. W., TUCKER, E., RENSHAW, J., RAYNAUD, F., LI, X. & BURKE, R. 2016. Inhibition of mTOR-kinase destabilizes MYCN and is a potential therapy for MYCN-dependent tumors. *Oncotarget,* 7**,** 57525.

VEGA-LOPEZ, G. A., CERRIZUELA, S. & AYBAR, M. J. 2017. Trunk neural crest cells: formation, migration and beyond. *International Journal of Developmental Biology,* 61**,** 5-15.

VERHEIJEN, M., LIENHARD, M., SCHROODERS, Y., CLAYTON, O., NUDISCHER, R., BOERNO, S., TIMMERMANN, B., SELEVSEK, N., SCHLAPBACH, R. & GMUENDER, H. 2019. DMSO induces drastic changes in human cellular processes and epigenetic landscape in vitro. *Scientific reports,* 9**,** 1-12.

VILLA-MORALES, M., COBOS, M., GONZÁLEZ-GUGEL, E., ÁLVAREZ-IGLESIAS, V., MARTÍNEZ, B., PIRIS, M., CARRACEDO, A., BENÍTEZ, J. & FERNÁNDEZ-PIQUERAS, J. 2014. FAS system deregulation in T-cell lymphoblastic lymphoma. *Cell death & disease,* 5**,** e1110-e1110.

VO, K. T., MATTHAY, K. K., NEUHAUS, J., LONDON, W. B., HERO, B., AMBROS, P. F., NAKAGAWARA, A., MINIATI, D., WHEELER, K. & PEARSON, A. D. 2014. Clinical, biologic, and prognostic differences on the basis of primary tumor site in neuroblastoma: a report from the international neuroblastoma risk group project. *Journal of clinical oncology,* 32**,** 3169.

VOGT, A., COOLEY, K. A., BRISSON, M., TARPLEY, M. G., WIPF, P. & LAZO, J. S. 2003. Cell-active dual specificity phosphatase inhibitors identified by high-content screening. *Chemistry & biology,* 10**,** 733-742.

VOGT, A., MCDONALD, P. R., TAMEWITZ, A., SIKORSKI, R. P., WIPF, P., SKOKO, J. J. & LAZO, J. S. 2008. A cell-active inhibitor of mitogen-activated protein kinase phosphatases restores paclitaxel-induced apoptosis in dexamethasone-protected cancer cells. *Molecular cancer therapeutics,* 7**,** 330-340.

WAGNER, E. F. & NEBREDA, Á. R. 2009. Signal integration by JNK and p38 MAPK pathways in cancer development. *Nature Reviews Cancer,* 9**,** 537-549.

WAHA, A., FELSBERG, J., HARTMANN, W., VON DEM KNESEBECK, A., MIKESKA, T., JOOS, S., WOLTER, M., KOCH, A., YAN, P. S. & ENDL, E. 2010. Epigenetic downregulation of mitogen-activated protein kinase phosphatase MKP-2

relieves its growth suppressive activity in glioma cells. *Cancer research,* 70**,** 1689-1699.

WANG, C., GONG, B., BUSHEL, P. R., THIERRY-MIEG, J., THIERRY-MIEG, D., XU, J., FANG, H., HONG, H., SHEN, J. & SU, Z. 2014a. The concordance between RNA-seq and microarray data depends on chemical treatment and transcript abundance. *Nature biotechnology,* 32**,** 926-932.

WANG, H.-Y., CHENG, Z. & MALBON, C. C. 2003. Overexpression of mitogen-activated protein kinase phosphatases MKP1, MKP2 in human breast cancer. *Cancer letters,* 191**,** 229-237.

WANG, J.-Y., YEH, C.-L., CHOU, H.-C., YANG, C.-H., FU, Y.-N., CHEN, Y.-T., CHENG, H.-W., HUANG, C.-Y. F., LIU, H.-P. & HUANG, S.-F. 2011. Vaccinia H1-related phosphatase is a phosphatase of ErbB receptors and is down-regulated in non-small cell lung cancer. *Journal of Biological Chemistry,* 286**,** 10177-10184.

WANG, J. Y., LIN, C. H., YANG, C. H., TAN, T. H. & CHEN, Y. R. 2006. Biochemical and biological characterization of a neuroendocrine-associated phosphatase. *Journal of neurochemistry,* 98**,** 89-101.

WANG, J. Y., YANG, C. H., YEH, C. L., LIN, C. H. & CHEN, Y. R. 2008. NEAP causes down-regulation of EGFR, subsequently induces the suppression of NGF-induced differentiation in PC12 cells. *Journal of neurochemistry,* 107**,** 1544-1555.

WANG, P., ZHOU, Z., HU, A., DE ALBUQUERQUE, C. P., ZHOU, Y., HONG, L., SIERECKI, E., AJIRO, M., KRUHLAK, M. & HARRIS, C. 2014b. Both decreased and increased SRPK1 levels promote cancer by interfering with PHLPP-mediated dephosphorylation of Akt. *Molecular cell,* 54**,** 378-391.

WANG, W., WANG, X., RAJAEI, M., YOUN, J. Y., ZAFAR, A., DEOKAR, H., BUOLAMWINI, J. K., YANG, J., FOSTER, J. H. & ZHOU, J. 2020. Targeting MDM2 for neuroblastoma therapy: in vitro and in vivo anticancer activity and mechanism of action. *Cancers,* 12**,** 3651.

WEE, P. & WANG, Z. 2017. Epidermal growth factor receptor cell proliferation signaling pathways. *Cancers,* 9**,** 52.

WEI, J., MIALKI, R. K., DONG, S., KHOO, A., MALLAMPALLI, R. K., ZHAO, Y. & ZHAO, J. 2013. A new mechanism of RhoA ubiquitination and degradation: Roles of SCFFBXL19 E3 ligase and Erk2. *Biochimica et Biophysica Acta (BBA)-Molecular Cell Research,* 1833**,** 2757-2764.

WESTERMANN, F., MUTH, D., BENNER, A., BAUER, T., HENRICH, K.-O., OBERTHUER, A., BRORS, B., BEISSBARTH, T., VANDESOMPELE, J. & PATTYN, F. 2008. Distinct transcriptional MYCN/c-MYC activities are associated with spontaneous regression or malignant progression in neuroblastomas. *Genome biology,* 9**,** 1-14.

WILSON, K. P., MCCAFFREY, P. G., HSIAO, K., PAZHANISAMY, S., GALULLO, V., BEMIS, G. W., FITZGIBBON, M. J., CARON, P. R., MURCKO, M. A. & SU, M. S. 1997. The structural basis for the specificity of pyridinylimidazole inhibitors of p38 MAP kinase. *Chemistry & biology,* 4**,** 423-431.

WISHART, M. J. & DIXON, J. E. 1998. Gathering STYX: phosphatase-like form predicts functions for unique protein-interaction domains. *Trends in biochemical sciences,* 23**,** 301-306.

WISHART, M. J. & DIXON, J. E. 2002. PTEN and myotubularin phosphatases: from 3-phosphoinositide dephosphorylation to disease. *Trends in cell biology,* 12**,** 579-585.

WITTIG-BLAICH, S., WITTIG, R., SCHMIDT, S., LYER, S., BEWERUNGE-HUDLER, M., GRONERT-SUM, S., STROBEL-FREIDEKIND, O., MÜLLER, C., LIST, M. & JASKOT, A. 2017. Systematic screening of isogenic cancer cells identifies DUSP6 as context-specific synthetic lethal target in melanoma. *Oncotarget,* 8**,** 23760.

WOOD, A. C., KRYTSKA, K., RYLES, H. T., INFARINATO, N. R., SANO, R., HANSEL, T. D., HART, L. S., KING, F. J., SMITH, T. R. & AINSCOW, E. 2017. Dual ALK and CDK4/6 inhibition demonstrates synergy against neuroblastoma. *Clinical Cancer Research,* 23**,** 2856-2868.

WU, D. & YOTNDA, P. 2011. Production and detection of reactive oxygen species (ROS) in cancers. *JoVE (Journal of Visualized Experiments)***,** e3357.

WU, Q. N., LIAO, Y. F., LU, Y. X., WANG, Y., LU, J. H., ZENG, Z. L., HUANG, Q. T., SHENG, H., YUN, J. P., XIE, D., JU, H. Q. & XU, R. H. 2018. Pharmacological inhibition of DUSP6 suppresses gastric cancer growth and metastasis and overcomes cisplatin resistance. *Cancer Lett,* 412**,** 243-255.

WU, Y.-T., MA, S.-Y., SUN, W.-Q., SHEN, W.-W., ZHU, H.-T., ZHANG, Q. & CHEN, H.-F. 2021. TRIM65 promotes invasion of endometrial stromal cells by activating ERK1/2/C-myc signaling via ubiquitination of DUSP6. *The Journal of Clinical Endocrinology & Metabolism,* 106**,** 526-538.

WU, Z.-L., SCHWARTZ, E., SEEGER, R. & LADISCH, S. 1986. Expression of GD2 ganglioside by untreated primary human neuroblastomas. *Cancer research,* 46**,** 440-443.

XIE, G., WU, H., CAI, W., CHEN, M., HUANG, W., YAN, W. & CHANG, Y. 2019. RDM 1 promotes neuroblastoma growth through the RAS–Raf–MEK–ERK pathway. *FEBS Open bio,* 9**,** 490-497.

XU, S., FURUKAWA, T., KANAI, N., SUNAMURA, M. & HORII, A. 2005. Abrogation of DUSP6 by hypermethylation in human pancreatic cancer. *Journal of human genetics,* 50**,** 159-167.

XU, Y. & FISHER, G. J. 2012. Receptor type protein tyrosine phosphatases (RPTPs)–roles in signal transduction and human disease. *Journal of cell communication and signaling,* 6**,** 125-138.

YADAV, B., WENNERBERG, K., AITTOKALLIO, T. & TANG, J. 2015. Searching for drug synergy in complex dose–response landscapes using an interaction potency model. *Computational and structural biotechnology journal,* 13**,** 504-513.

YAMASHIRO, D. J., NAKAGAWARA, A., IKEGAKI, N., LIU, X. & BRODEUR, G. M. 1996. Expression of TrkC in favorable human neuroblastomas. *Oncogene,* 12**,** 37-41.

YANG, C.-H., YEH, Y.-J., WANG, J.-Y., LIU, Y.-W., CHEN, Y.-L., CHENG, H.-W., CHENG, C.-M., CHUANG, Y.-J., YUH, C.-H. & CHEN, Y.-R. 2017. NEAP/DUSP26 suppresses receptor tyrosine kinases and regulates neuronal development in zebrafish. *Scientific reports,* 7**,** 1-9.

YANG, Y., YANG, W. S., YU, T., YI, Y.-S., PARK, J. G., JEONG, D., KIM, J. H., OH, J. S., YOON, K. & KIM, J.-H. 2014. Novel anti-inflammatory function of NSC95397

by the suppression of multiple kinases. *Biochemical pharmacology,* 88**,** 201-215.

YARDEN, Y. & PINES, G. 2012. The ERBB network: at last, cancer therapy meets systems biology. *Nature Reviews Cancer,* 12**,** 553-563.

YIP, S.-C., SAHA, S. & CHERNOFF, J. 2010. PTP1B: a double agent in metabolism and oncogenesis. *Trends in biochemical sciences,* 35**,** 442-449.

YOKOYAMA, A., KARASAKI, H., URUSHIBARA, N., NOMOTO, K., IMAI, Y., NAKAMURA, K., MIZUNO, Y., OGAWA, K. & KIKUCHI, K. 1997. The characteristic gene expressions of MAPK phosphatases 1 and 2 in hepatocarcinogenesis, rat ascites hepatoma cells, and regenerating rat liver. *Biochemical and biophysical research communications,* 239**,** 746-751.

YOSHIDA, G. J. 2018. Emerging roles of Myc in stem cell biology and novel tumor therapies. *Journal of Experimental & Clinical Cancer Research,* 37**,** 1-20.

YU, A. L., GILMAN, A. L., OZKAYNAK, M. F., LONDON, W. B., KREISSMAN, S. G., CHEN, H. X., SMITH, M., ANDERSON, B., VILLABLANCA, J. G., MATTHAY, K. K., SHIMADA, H., GRUPP, S. A., SEEGER, R., REYNOLDS, C. P., BUXTON, A., REISFELD, R. A., GILLIES, S. D., COHN, S. L., MARIS, J. M. & SONDEL, P. M. 2010. Anti-GD2 Antibody with GM-CSF, Interleukin-2, and Isotretinoin for Neuroblastoma. *New England Journal of Medicine,* 363**,** 1324-1334.

YU, H.-N., LEE, Y.-R., NOH, E.-M., LEE, K.-S., SONG, E.-K., HAN, M.-K., LEE, Y.-C., YIM, C.-Y., PARK, J. & KIM, B.-S. 2008. Tumor necrosis factor-α enhances DMSO-induced differentiation of HL-60 cells through the activation of ERK/MAPK pathway. *International journal of hematology,* 87**,** 189-194.

YUAN, X., BU, H., ZHOU, J., YANG, C.-Y. & ZHANG, H. 2020. Recent advances of SHP2 inhibitors in cancer therapy: Current development and clinical application. *Journal of medicinal chemistry,* 63**,** 11368-11396.

ZAFAR, A., WANG, W., LIU, G., WANG, X., XIAN, W., MCKEON, F., FOSTER, J., ZHOU, J. & ZHANG, R. 2021. Molecular targeting therapies for neuroblastoma: Progress and challenges. *Medicinal Research Reviews,* 41**,** 961-1021.

ZAGE, P. E., WHITTLE, S. B. & SHOHET, J. M. 2017. CD114: A new member of the neural Crest-Derived cancer stem cell marker family. *Journal of Cellular Biochemistry,* 118**,** 221-231.

ZEINELDIN, M., FEDERICO, S., CHEN, X., FAN, Y., XU, B., STEWART, E., ZHOU, X., JEON, J., GRIFFITHS, L. & NGUYEN, R. 2020. MYCN amplification and ATRX mutations are incompatible in neuroblastoma. *Nature communications,* 11**,** 1-20.

ZENG, L.-F., ZHANG, R.-Y., YU, Z.-H., LI, S., WU, L., GUNAWAN, A. M., LANE, B. S., MALI, R. S., LI, X. & CHAN, R. J. 2014. Therapeutic potential of targeting the oncogenic SHP2 phosphatase. *Journal of medicinal chemistry,* 57**,** 6594-6609.

ZENG, X., ZHU, C. & ZHU, X. 2021. DUSP4 promotes the carcinogenesis of CCRCC via negative regulation of autophagic death. *Bioscience, Biotechnology, and Biochemistry,* 85**,** 1839-1845.

ZHANG, J., ZHANG, F. & NIU, R. 2015. Functions of Shp2 in cancer. *Journal of cellular and molecular medicine,* 19**,** 2075-2083.

ZHANG, R.-Y., YU, Z.-H., ZENG, L., ZHANG, S., BAI, Y., MIAO, J., CHEN, L., XIE, J. & ZHANG, Z.-Y. 2016. SHP2 phosphatase as a novel therapeutic target for melanoma treatment. *Oncotarget,* 7**,** 73817.

ZHANG, X., DONG, Z., ZHANG, C., UNG, C. Y., HE, S., TAO, T., OLIVEIRA, A. M., MEVES, A., JI, B. & LOOK, A. T. 2017. Critical role for GAB2 in neuroblastoma pathogenesis through the promotion of SHP2/MYCN cooperation. *Cell reports,* 18**,** 2932-2942.

ZHANG, Y.-Y., WU, J.-W. & WANG, Z.-X. 2011. Mitogen-activated protein kinase (MAPK) phosphatase 3-mediated cross-talk between MAPKs ERK2 and p38α. *Journal of Biological Chemistry,* 286**,** 16150-16162.

ZHANG, Z.-Y. 2002. Protein tyrosine phosphatases: structure and function, substrate specificity, and inhibitor development. *Annual review of pharmacology and toxicology,* 42**,** 209-234.

ZHANG, Z., KOBAYASHI, S., BORCZUK, A. C., LEIDNER, R. S., LAFRAMBOISE, T., LEVINE, A. D. & HALMOS, B. 2010. Dual specificity phosphatase 6 (DUSP6) is an ETS-regulated negative feedback mediator of oncogenic ERK signaling in lung cancer cells. *Carcinogenesis,* 31**,** 577-586.

ZHANG, Z. Y. 2017. Drugging the Undruggable: Therapeutic Potential of Targeting Protein Tyrosine Phosphatases. *Acc Chem Res,* 50**,** 122-129.

ZHENG, X. M., WANG, Y. & FALLEN, C. J. 1992. Cell transformation and activation of pp60c-src by overexpression of a protein tyrosine phosphatase. *Nature,* 359**,** 336-339.

ZHOU, X., COAD, J., DUCATMAN, B. & AGAZIE, Y. 2008. SHP2 is up-regulated in breast cancer cells and in infiltrating ductal carcinoma of the breast, implying its involvement in breast oncogenesis. *Histopathology,* 53**,** 389-402.

ZHU, H., CHEN, Y., ZHANG, J., QIAN, C., QIU, W., SHEN, H. & SHEN, Z. 2020. Knockdown of TRIM37 promotes apoptosis and suppresses tumor growth in gastric Cancer by inactivation of the ERK1/2 pathway. *OncoTargets and therapy,* 13**,** 5479.

ZHU, S., LEE, J.-S., GUO, F., SHIN, J., PEREZ-ATAYDE, A. R., KUTOK, J. L., RODIG, S. J., NEUBERG, D. S., HELMAN, D. & FENG, H. 2012. Activated ALK collaborates with MYCN in neuroblastoma pathogenesis. *Cancer cell,* 21**,** 362-373.

ZISCHEWSKI, J., FISCHER, R. & BORTESI, L. 2017. Detection of on-target and off-target mutations generated by CRISPR/Cas9 and other sequence-specific nucleases. *Biotechnology advances,* 35**,** 95-104.